Effect of multipass welds and pores on residual stresses in butt-welded joints

Analyzing the Interplay: Investigating the Influence of Defects and Welding Passes on Thin and Thick Plates

MSc Thesis

Dhomenico Roberto Cascella

Delft University of Technology

TU Delft

Effect of multipass welds and pores on residual stresses in butt-welded joints

Analyzing the Interplay: Investigating the Influence of Defects and Welding Passes on Thin and Thick Plates

by

Dhomenico Roberto Cascella

Student Name	Student Number
Dhomenico Roberto Cascella	5362865

Thesis submitted to Delft University of Technology for the degree of
Master of Science
in Civil Engineering
to be publicly defended on 22/08/2023

Committee members:	Prof. Dr. Ir. Milan Veljkovic	TUDelft, Chair
	Prof. Dr. Ir. Johan Maljaars	TNO, Supervisor
	Dr. Ir. Frans van der Meer	TUDelft, Supervisor
	Ir. David Malschaert	TUDelft, Daily supervisor

Institution:	Delft University of Technology
Place:	Faculty of Civil Engineering, Delft
Project Duration:	May, 2022 - August, 2023

TU Delft

Acknowledgements

I would like to express my sincere appreciation to my graduation committee for their invaluable support and guidance during the course of my thesis. Without their assistance, this achievement would not have been possible.

First and foremost, I extend my heartfelt gratitude to Prof. Milan Veljkovic for his exceptional mentorship, insightful advice, and understanding in navigating challenging circumstances encountered during the thesis. His expertise and direction played a vital role in shaping the outcome of this research.

I would also like to express my profound gratitude to Prof. Johan Maljaars for his support throughout my thesis. His patience, guidance, and consistent encouragement steered me toward the right path and significantly contributed to the overall success of this study.

Additionally, I extend my gratitude to Dr. Frans van der Meer for his valuable insights and contributions to this research. His expertise and perspectives were instrumental in enhancing the quality of my work.

Furthermore, I would like to express my profound appreciation to my daily supervisor, Ph.D. candidate David Malschaert. Our regular meetings every Thursday morning since May 2022 have been invaluable to the progress and success of my thesis. David's dedication, expertise, and support have had a profound impact on my research journey. His insightful input and guidance have shaped the direction and methodology of my thesis, pushing me to think critically and refine my arguments. His patience and attentiveness in addressing my questions and concerns have greatly enhanced my understanding of the subject matter. I am truly grateful for David's support, motivation, and genuine interest in my academic growth.

In addition to my academic advisors, I would like to express my sincere appreciation to my girlfriend, Virginia. Her unwavering support and motivation have been essential in my thesis journey. Her belief in my abilities, constant encouragement, and understanding have given me strength during challenging times. I am incredibly lucky to have her by my side, and I deeply treasure her support and love.

Finally, I want to take a moment to express my sincere appreciation to my mother Rosa, father Francesco, and sister Mariagrazia. Their presence and contributions have shaped who I am today.

I am eternally thankful to my mother, Rosa, for her boundless affection. Her nurturing demeanor has served as the driving influence propelling my educational journey. Her selflessness and sacrifices have laid the foundation for the beginning of my successes, and I am deeply indebted to her dedication.

To my father, Francesco, I am profoundly thankful for his guidance and steadfast support. His strength has been a constant source of inspiration. His work ethic and determination have instilled in me the values of perseverance and resilience, and I am forever grateful for his presence in my life.

To my beloved sister, Mariagrazia. Her genuine enthusiasm has been a pillar throughout my academic journey, touching my heart in ways words cannot fully capture. Her presence brings immeasurable joy and comfort to my life. Again, I will always be by your side.

Together, my mother, father, and sister have formed an unbreakable support system that has nurtured and propelled me forward. Their love, sacrifices, and belief in my abilities have given me the strength to overcome any obstacle. I am forever grateful for their presence, understanding, and encouragement. To my dear mother, father, and sister, Rosa, Francesco, and Mariagrazia, words cannot adequately express the depth of my gratitude. Thank you for being the pillars of strength in my life, for your love, and for supporting me in every step of my academic journey. I am eternally grateful for the immeasurable impact you have had on my life, and I cherish the moments we have shared together.

Abstract

Welding is a widely used process in various industries for joining materials, but it can introduce several complexities that affect the mechanical properties of the welded components. In particular, the presence of pores within the welded material can have significant implications for fatigue resistance, residual stresses, and overall structural integrity.

The primary objective of this thesis is to develop and analyze thermal and mechanical models to understand how various parameters, including geometry, mesh, material properties, boundary conditions, and heat input, influence the behavior of a welded thick plate containing pores. The simulations are conducted with different pore configurations and multiple welding passes to comprehensively explore their impact.

Two Finite Element (FE) models were designed. In the first model (Model 1), the objective was to replicate the experimental setup detailed by Qiang et al. in their work "Through-thickness welding residual stress and its effect on stress intensity factors for semi-elliptical surface cracks in a butt-welded steel plate" [41]. This endeavor was accomplished utilizing Abaqus as software. A Dflux subroutine, written in Fortran, was incorporated to effectively emulate the welding procedure. The model was constructed to account for multiple welding passes (up to 7). By extrapolating transverse and longitudinal stresses, a comparative analysis was conducted across five distinct models and the experimental data [41]. The intention was to elucidate variations and similarities in the results.

Subsequently, the second model (Model 2) was conceived to exploit the more favorable boundary conditions present in Zhang's model as described in "Effect of Welding Sequence and Constraint on the Residual Stress and Deformation of Thick Welded Butt Joint Made of Q345qD Steel" [58], when contrasted with the initial experiment. Following a similar procedure, the FE model was developed, with the added feature of an increased number of welding passes (up to 12). Distortions along three distinct paths and transverse and longitudinal residual stresses within two specific regions were extrapolated and subsequently compared. The investigation then progressed to the introduction of pores into Model 2, in the simulation characterized by the lowest number of passes. The aim was to assess the impact of these pores on temperatures, distortions, and residual stresses. By comparing the outcomes of the models both with and without defects, valuable insights were gained into the effect of pores during welding processes.

The main findings of this research can be summarized as follows:

- Thermal data extracted from a welding experiment conducted at four distinct positions within a 250mm x 200mm x 32mm plate, as documented in Zhang et al.'s publication [58], exhibited inconsistencies when compared to the results obtained through Abaqus simulations in this thesis. These disparities predominantly stem from the absence of accurately specified thermocouple placements in the reference paper [58]. Despite conscientious endeavors to pinpoint the precise thermocouple coordinates, discernible variations of 100 ℃ and a maximum divergence of 25% between the outcomes of the simulations and the reference findings were identified.
- Residual stresses obtained in Abaqus (Model 1) trying to replicate Qiang et al. paper [41] in a 700mm x 400mm x30 mm showed good agreement with the reference simulation but deviated from the experimental data. The obtained numerical values peaked around 150 MPa, while the experimental values reached more than double that magnitude (305 MPa), for specific simulations. The number of welding passes significantly influenced the compression at the sides of the plate, with an increasing trend as the number of passes increased.
- The simulations (Model 2) created to replicate Zhang et al. experiments [58] demonstrated better agreement with the experimental data for both longitudinal and transverse residual stresses. The number of passes played a crucial role in the results, with the eight to twelve passes simulation showing the closest match to the experimental data.
- The presence of the studied configuration of pores in the material did not affect significantly the shrinkage, distortions, and residual stresses in the simulations. Closer to the pores, higher values for residual stresses were found.

Based on the findings of this thesis, several recommendations for future research can be made. Laboratory experiments should be conducted to validate the numerical results obtained in this study. Sensitivity analysis considering modifications in the dimensions, boundary conditions, and pores locations of the model can provide further insights. Additionally, incorporating thermally independent properties can reduce the computational time of the simulations.

Overall, this thesis contributes to understanding the impact of pores on the thermal and mechanical behavior of thin and thick plates and provides a foundation for future research in this area.

Contents

List of Figures

List of Tables

1

Introduction

1.1 Research motivation

The driving force behind this research stems from the critical necessity of safeguarding the safety, durability, and structural robustness of buildings and bridges, particularly considering the widespread use of the steel under investigation in Chinese bridge construction. Ensuring the structural integrity of these bridges is of utmost importance to prevent potential failures and ensure the long-term reliability of vital infrastructure. Welded structures play a crucial role in various industries, and the performance of these structures depends significantly on the control of residual stresses. Residual stresses can cause distortion, cracking, and premature failure in welded joints, which may have severe consequences for the safety of infrastructure and the people who use them.

However, the presence of pores in butt steel welds poses a significant challenge to achieving optimal structural integrity. Pores are common defects that can form during the welding process, leading to stress concentration points and reduced mechanical properties in the welds. As a result, understanding the influence of pores on residual stresses in butt welds becomes imperative to address and mitigate potential structural failures.

By conducting research on how pores affect residual stresses, engineers and researchers can develop strategies to minimize pore formation during welding processes. This, in turn, will enhance the quality and reliability of welded joints, ensuring they can withstand the complex and dynamic loads experienced by buildings and bridges over their service lives.

In addition to addressing the impact of pores on residual stresses, the research also recognizes the vital role of fatigue performance in the structural integrity of buildings and bridges. Fatigue failure is a common failure mode in welded structures subjected to repeated or cyclic loading, such as the traffic loads on bridges or the dynamic forces experienced during seismic events. Reducing residual stresses induced by pores can improve the fatigue performance of welded structures, making them more resilient to cyclic loading and environmental conditions. Enhanced fatigue performance is particularly critical for structures like bridges, which experience repetitive vehicular loads and temperature fluctuations over time.

Fatigue failure occurs due to the accumulation of damage caused by cyclic loading, even when the applied stress is below the material's yield strength. In the presence of pores, the localized stress concentrations can act as stress raisers, accelerating the initiation and propagation of fatigue cracks. As a result, welded joints with pores are more susceptible to fatigue failure, significantly reducing the fatigue life of the structure.

Understanding how pores affect residual stresses in butt welds is closely linked to the fatigue performance of welded structures. Residual stresses can act as additional loading in the presence of cyclic loads, further influencing the initiation and growth of fatigue cracks. Therefore, investigating the interplay between pores, residual stresses, and fatigue performance is essential for predicting the durability and safe operation of welded structures over their design life.

The research aims to provide valuable insights into how the presence of pores alters the fatigue behavior of welded joints. By developing accurate finite element models that incorporate the effects of

pores and residual stresses, the behavior of welded structures under cyclic loading conditions can be simulated. These simulations will shed light on how pores influence the formation and growth of fatigue cracks, guiding the development of strategies to enhance fatigue resistance in welded structures.

Improving the fatigue performance of welded joints is crucial for ensuring the long-term reliability of buildings and bridges, especially in critical infrastructure applications. By gaining a comprehensive understanding of how pores affect both residual stresses and fatigue behavior, engineers and designers can implement measures to reduce pore formation during welding processes and optimize welding techniques to enhance the fatigue resistance of welded structures.

In conclusion, considering fatigue performance in conjunction with residual stresses and pore effects is vital to comprehensively assess the structural integrity of welded joints. The research's findings are expected to pave the way for improved design guidelines, welding procedures, and maintenance practices that will ultimately contribute to safer and more durable buildings and bridges, safeguarding public welfare and infrastructure investment.

1.2 Problem statement

Researching and modeling pores in butt steel welds can present several challenges. In terms of researching, identifying and measuring the pores can be difficult as they can be small and hard to detect. Additionally, the butt steel welds may be located in hard-to-reach areas, making it difficult to collect samples and perform research. The welding process itself is complex and can lead to variations in the micro-structure of the welds, making it difficult to understand the causes of pores.

When it comes to modeling pores in finite element programs, the complexity of the geometry of the pores can make it difficult to represent them accurately in the model. The pores can affect the mechanical properties of the material, making it difficult to predict the behavior of the weld under load. Discretization of the geometry can lead to errors if the pores are not properly represented, and the results of the analysis can depend on the mesh size and quality. Additionally, there is uncertainty in the input data as the pores can be affected by the welding process and environmental conditions. Modeling pores can also be computationally expensive and require advanced software and hardware. The results of the analysis can depend on the mesh size and quality, and the accuracy of the input data can be affected by the number of passes and the conditions of each pass.

Multiple weld passes in butt welds can also present additional challenges when researching and modeling pores. Each pass of the welding process can have an effect on the microstructure of the weld and the formation of pores. This can make it more difficult to understand the causes of pores and predict their behavior, as the properties of the weld can vary depending on the number of passes and the conditions of each pass.

In terms of research, it may be more difficult to collect samples and perform tests on multi-pass welds due to the complexity of the micro-structure and the potential for variations in the pores. In addition, it may be difficult to standardize the research methods used to study multi-pass welds, making it harder to compare results from different studies.

1.3 Research objectives

The research objectives are to investigate the residual stresses in a butt weld that includes pores. This will be achieved by developing two Finite Element (FE) models. The first model will be used to replicate the experiments and analyze how the number of welding passes influences the residual stress results. The second model will focus on replicating the results with the lowest number of passes while including the presence of pores in the welding process.

To validate the results obtained from the FE models, the study will analyze relevant literature and papers on temperature variations, distortions, and longitudinal and transverse residual stresses on multiple paths. The study will ensure that the FE models provide reliable and accurate results by comparing them with the results from previous studies.

Overall, the research aims to contribute to the understanding of the impact of welding passes and pores on residual stresses in butt welds. Developing accurate and reliable FE models will provide

insights into the control of pore formation during welding processes, ultimately improving the quality and integrity of welded structures.

The primary inquiry of the research is:

- "**How do the welding passes and pores affect the distortions and residual stresses induced by welding in a butt welded joint?**"

The primary research inquiry will be addressed through the following secondary questions.

- What aspects need to be considered during the numerical simulations?
- How are distortions influenced by varying numbers of passes?
- What is the correlation between the number of welding passes and the temperature variation in the weldment?
- What is the influence of the welding sequence on the residual stress distribution?
- How do the size, number, and location of pores influence the outcomes of the study?

1.4 Methodology

The methodology for the thesis involved the development of two Finite Element (FE) models to investigate the impact of welding passes and pores on residual stresses. The first model aimed to replicate Qiang et al.'s [41] experiment with Abaqus, utilizing a Dflux subroutine coded in Fortran to recreate the welding procedure. A FE model for multiple welding passes was modeled. The transverse and longitudinal stresses were then extrapolated, and the results were compared among the 5 models and the experimental data.

The second model was developed due to the easier boundaries offered in Zhang's model [58] compared to the first experiment. The same procedure was followed but with the addition of more welding passes. The distortions at three different paths and the transverse and longitudinal residual stresses at two different regions were extrapolated, and the results were compared. Pores were then added to the model with the lowest number of passes with comparable results to investigate their effect on temperatures, distortions, and residual stresses. The results of the models with and without defects will be compared to provide insights into the control of pore formation during welding processes and improve the quality and integrity of welded structures.

1.5 Scope

The scope of the thesis is to investigate the impact of welding passes and pores on residual stresses in butt welds. This will be achieved by developing three Finite Element (FE) models. The first two models aim to replicate previous experiments to analyze how the number of welding passes influences the residual stress results. The third model focuses on the impact of pores on residual stresses by using the lowest number of passes with comparable results.

The validation of the FE models will be done by analyzing relevant literature and papers on temperature variations, distortions, and longitudinal and transverse residual stresses on multiple paths. The study aims to provide insights into the control of pore formation during welding processes to improve the quality and integrity of welded structures.

Overall, the research aims to contribute to the understanding of the factors affecting residual stresses in butt welds, and to provide recommendations for improving the welding process to mitigate the impact of pores on residual stresses.

1.6 Structure of the research

Chapter 1: Introduction

The first chapter presents the research background, objective, and significance of the numerical simulation of an X-welded butt joint. It explains the need for the research and the advantages that the results may provide to the manufacturing industry.

Chapter 2: Literature review

The literature review chapter provides the necessary background knowledge to understand the welding process and its effects on welded joints. This chapter discusses the welding history and fundamentals, weldability of steel, electricity in welding, and discontinuities in welds. Moreover, this chapter analyzes welding residual stresses and distortions.

Chapter 3: Numerical simulation of an X-welded butt joint

The third chapter focuses on the numerical simulation of an X-welded butt joint. It provides two reference models, Qiang et al. [41] and Zhang et al. [58], that are used to analyze the behavior of the welded joint. This chapter also discusses the thermal model, including its assumptions, units, geometry and mesh, thermal properties, thermal boundary conditions, heat input, and steps. Finally, it presents the results of the numerical simulation in terms of residual stresses and distortions.

Chapter 4: Numerical simulation - Pores

The fourth chapter of this study is dedicated to investigating the impact of pores on a thick plate. The chosen model for analysis is Model 2, which was initially introduced in Chapter 3 and subsequently modified to incorporate the presence of pores. This chapter provides a detailed description of the thermal and mechanical model, encompassing aspects such as geometry, meshing techniques, material properties, boundary conditions, heat input, and computational steps employed.

Furthermore, the chapter presents the outcomes obtained from the numerical simulation, specifically focusing on the characterization of residual stresses and distortions. The results offer valuable insights into how the presence of pores influences the structural response of the thick plate, shedding light on the underlying phenomena and contributing to the overall understanding of the system's behavior.

Chapter 5: Conclusion and Recommendations

The final chapter summarizes the research findings and draws conclusions regarding the numerical simulation of an X-welded butt joint. Additionally, it suggests recommendations for future research that could improve the accuracy and reliability of the numerical simulation results. Finally, it discusses the significance of this research and its potential benefits to the manufacturing industry.

2

Literature review

2.1 Welding history and fundamentals

The development of welding technology has been a gradual process over time, starting with Sir Humphry Davy's discovery of the electric arc in 1800. This was followed by the discovery of carbon arc welding by Auguste De Meritens and Nikolai N. Benardos in 1881. C.L. Coffin was awarded the first US patent for an arc welding process using a metal electrode in 1890, while Strohmenger introduced a coated metal electrode in Great Britain around 1900. During this period, resistance welding processes were also developed, including spot welding, seam welding, projection welding, and flash butt welding. The production of oxygen and later the liquefying of air helped the development of gas welding and cutting, with acetylene torches being developed in the early 1900s. World War I led to a demand for armament production, leading to the establishment of welding companies to meet the requirements. The American Welding Society was founded by 20 members of the Wartime Welding Committee of the Emergency Fleet Corporation in 1919. In 1920, automatic welding was introduced by P.O. Nobel of the General Electric Company. During the 1920s, various types of welding electrodes were developed, including heavy-coated rods and light-coated rods. The research was also done into shielding the arc and weld area by externally applied gases, leading to the development of the atomic hydrogen welding process and the gas tungsten arc welding process. In the late 1920s and early 1930s, various forms of arc welding continued to develop. Shielding the arc and weld area with externally applied gases was a significant area of research. Alexander and Langmuir worked with hydrogen as a welding atmosphere, which resulted in the atomic hydrogen welding process. H.M. Hobart and P.K. Devers worked with atmospheres of argon and helium, resulting in the forerunner of the gas tungsten arc welding process.

During World War II, the demand for welding in armament production again increased. This led to the further development of welding technology and processes, including the growth of automatic welding. In the post-war years, welding continued to develop and grow in importance in various industries, including construction, transportation, and manufacturing.

In summary, the history of welding can be traced back to the discovery of acetylene in 1836 and the invention of the arc welding process in the late 1800s. From there, various forms of welding continued to develop and evolve, including gas welding, resistance welding, and automatic welding. The demand for welding during World Wars I and II played a significant role in advancing the technology and processes of welding. Today, welding is a critical process in many industries and continues to evolve and improve [22].

2.1.1 Weldability of steel

Weldability explains how well the materials impacted by the weld keep their original strength, corrosion resistance, oxidation resistance, and so on after welding. The properties of the weld metal are largely determined by the filler material used, the type of base material used, the welding method, and the welding methodology. In contrast, the composition of the base material primarily determines

the properties of the HAZ and the amount of thermal energy delivered during welding [45]. The names of the various portions of the material impacted by the weld are shown in Figure 2.1.

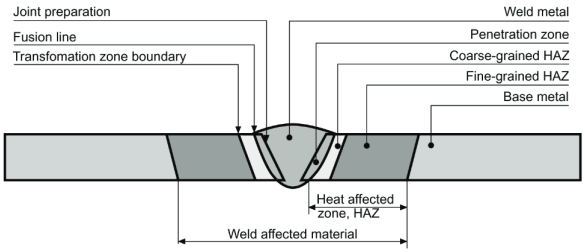

Figure 2.1: Weld affected zones [28]

Plain carbon steel is classified into five quality classes, from A to E, by the International Institute of Welding (IIW) [45] based on its manufacturing technique and impact strength. The European standard for general-purpose structural steel, EN 10025 [7], classifies steels differently based on their impact strength at various (low) temperatures. Carbon steels will be the steel classes analyzed in this thesis. The word 'carbon steels' as used here refers to plain carbon steel, carbon-manganese steel, and micro-alloyed steel. Plain carbon steels are distinguished by the addition of up to 0.20-0.25% carbon to boost strength. These were primarily designed as structural materials for welded constructions. Carbon-manganese steels may also include up to 1.5% manganese, with a maximum carbon concentration of 0.25%. According to the European steel standard EN 10025-2 [7], examples of such steels are S235JR and S275JR. The Chinese steel Q345qD can be considered part of this definition as it is allocated in the percentages given.

The carbon content in welded steel can significantly influence the likelihood of cracking during and after welding. This is because carbon affects the microstructure and mechanical properties of steel, which can impact its resistance to cracking. When carbon is added to steel, it increases its strength and hardness. However, it also decreases the material's ductility and toughness, which can make it more susceptible to cracking. This is particularly true if the steel is welded and then exposed to high stresses, such as those caused by thermal expansion or contraction, or mechanical loads. In addition, the cooling rate during welding can also affect the formation of microstructures in the weld and heat-affected zone. High-carbon steels tend to form harder and more brittle microstructures, such as martensite if they are cooled too rapidly, which can increase the risk of cracking. Furthermore, if the carbon content is too high, it can also cause the formation of carbides, which are hard, brittle, and prone to cracking. This is particularly true in the heat-affected zone, where the carbon content can become elevated due to the heat input from the welding process [30, 29].

To minimize the risk of cracking, it is important to select a steel with a carbon content appropriate for the intended application and to carefully control the welding process to avoid rapid cooling rates and the formation of undesirable microstructures. Post-weld heat treatment can also be used to relieve residual stresses and improve the ductility of the weld and heat-affected zone. By considering the carbon content of the steel and carefully managing the welding process, it is possible to reduce the likelihood of cracking and ensure a successful weld [30]. To some extent, the risk of problems can be determined by calculating the material's equivalent carbon content (CE):

$$\mathrm{CE} = \mathrm{C} + \frac{\mathrm{Mn}}{6} + \frac{\mathrm{Cr} + \mathrm{Mo} + \mathrm{V}}{5} + \frac{\mathrm{Cu} + \mathrm{Ni}}{6} \tag{2.1}$$

A steel is considered entirely weldable if its CE does not exceed 0.41 [28]. It is deemed weldable to a limited extent at higher levels, which in general means that welding is performed on the workpiece at a certain temperature in order to slow the rate of cooling (see [11]). Even if CE does not exceed these limitations, workpiece heating may be necessary at times. This means that preheating is necessary for steels in the minimum strength group for metal thicknesses larger than 50 mm, but not for steels in the maximum strength groups for metal thicknesses higher than 30 mm. Simple carbon steels are unlikely to require preheating temperatures exceeding 200 °C [45].

Because basic carbon steels were designed for use in welded constructions, there should be no problems if welding is done properly. However, if the material contains higher quantities of contaminating

components, there is a danger of thermal cracking in 'non-standard' steels, particularly unkilled steels (steel that has been inadequately deoxidized and evolves gas during solidification with the creation of pores). Furthermore, if a material with no demonstrated impact toughness is used where such toughness is required, there is a risk of brittle fractures in the HAZ. Brittle failure can occur when tensions in the material continue after welding, when combined with stress concentrations near a weld defect, or when the temperature falls below the material's transition point [28].

Some important parameters that should be taken into account are the deposition rate, the deposition efficiency, and the operation factor. The **deposition rate** of weld metal melted into the joint per unit of time (while the arc is striking) is commonly given in kg/h. Because the deposition rate is proportional to the current, it may be represented in a simplified form for a given current value as:

$$\text{Actual deposition rate} = \frac{\text{Maximum deposition rate} \cdot \text{Welding current}}{\text{Welding current at maximum deposition rate}} \tag{2.2}$$

The current is determined by the welding location, whether the pass is a root pass or a filler pass, and so on. For MIG welding, at the same current value, for a thicker wire the deposition rate will be lower [45]. It has to be considered that a thicker wire will also mean that a higher current value can be applied therefore the deposition rate can be increased (e.g. 1mm wire maximum deposition rate at 280A of 70 g/min and a 1.6 mm at the same amperage deposits 60 g/min but can reach 140 g/min at 500A [28]).

The **deposition efficiency** is the percentage of the total weight of filler material utilized that is transformed to usable weld metal [10]. This value should be combined with the 'duty cycle' or '**operation factor**' that is a critical component in determining the time required by the welder [28]. This is a percentage number that compares the length of time the arc is burning and weld metal is being deposited to the entire amount of time the welder is operating. Typical deposition efficiency and operator factors are provided below.

Table 2.1: Some values for comparative cost calculations [10, 44]

	Operator factor	Deposition efficiency
Manual metal arc welding	0.3	0.6
MIG/MAG, solid wire	0.45	0.95
MAG, flux cored wire	0.4	0.85
Submerged arc welding	0.8	0.98

2.1.2 Electricity in welding

2.1.2.1 Voltage and current

A flow of electrically charged particles is referred to as an electric current. When the amount of free electrons in a conductor grows or decreases, an electric charge, or potential, is created. Because electrons have a negative charge, an excess of them results in a negative potential, while a shortage results in a positive potential. The difference in potential is referred to as voltage, and it is what drives the flow of electrons. Pressure and flow in a gas or liquid are excellent analogies. Voltage is measured in volts [V], whereas the current is measured in ampères [A] (usually referred to simply as amps).

EN 60974 [8] defines a standard load line that indicates the voltage at which the power source must be verified and labeled for each amount of rated current.

MMA and SAW:	$U = 20 + 0.04 \cdot I$	For currents above 600 A: U = 44 V
TIG:	$U = 10 + 0.04 \cdot I$	For currents above 600 A: U = 34 V
MIG/MAG:	$U = 14 + 0.05 \cdot I$	For currents above 600 A: U = 44 V

Figure 2.2: Voltage and current[28]

2.1.2.2 Direct current and alternating current

A power source can deliver either direct current (DC) or alternating current (AC). A battery generates direct current, whereas a simple generator generates alternating current. An alternating current is distinguished by the fact that the current changes direction at a predetermined frequency. In Europe, electricity is supplied at 50 cycles per second, sometimes known as 50 hertz [Hz]. The benefit of alternating current is that its voltage may be readily adjusted or lowered in a transformer. When transporting energy over long distances, it is desirable to use a high voltage since the current is lowered proportionately, and so the losses in the power lines are minimized.

2.1.2.3 Resistance

The capacity of different conductors to carry electricity varies. A long and thin conductor, such as a wire, has an electrical resistance that is proportional to its length (L), cross-sectional area (A), and material resistivity (ρ). Resistance is measured in ohms (Ω), and it is easy to calculate:

$$\mathrm{R} = \frac{\rho \cdot L}{A} \tag{2.3}$$

Temperature affects resistivity: for most metals, it rises by around 0.4% per degree Celsius.

2.1.2.4 Ohm's law

Ohm's Law may be used to determine the voltage drop (V) of a wire or resistor if we know its resistance (R) and current (I):

$$\mathrm{V} = \mathrm{R} \cdot \mathrm{I} \tag{2.4}$$

2.1.2.5 Power

When a current travels through an electrical resistor, it produces not just a voltage drop but also heat. The power (P) of this heat may be simply determined using the formula:

$$\mathrm{P} = \mathrm{V} \cdot \mathrm{I} \tag{2.5}$$

or

$$\mathrm{P} = \mathrm{R} \cdot \mathrm{I}^2 \tag{2.6}$$

Ohm's Law wheel is a tool used in electrical engineering and electronics to calculate the values of voltage, current, resistance, and power in a circuit based on Ohm's Law. The Ohm's Law wheel is essentially a circular diagram that shows the relationships between these four variables. To use the Ohm's Law wheel, you simply select the variable you want to calculate (voltage, current, resistance, or power), and then follow the path around the circle to find the formula that relates the known variables to the unknown variable. The Ohm's Law wheel is a handy tool for quickly and easily calculating values in an electrical circuit without having to remember the formulas.

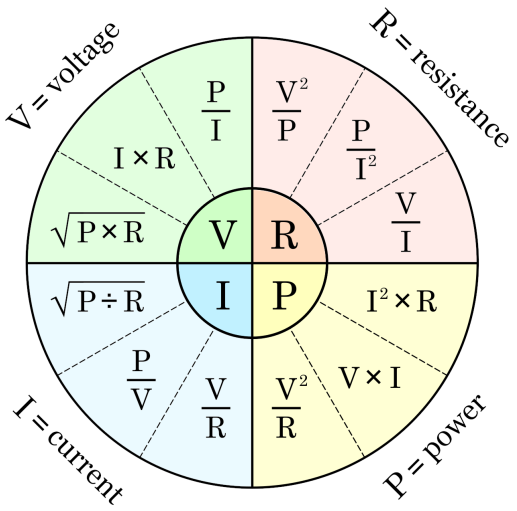

Figure 2.3: Ohm's Law wheel

2.1.2.6 Efficiency

The percentage of input power that makes it through to the welding process is referred to as efficiency. If the efficiency is 75%, this indicates that 25% of the input power is lost due to heat losses in the power source. If the efficiency is known, the real power demand may be calculated:

$$\text{Input power (Q)} = \text{Welding current (I)} \cdot \text{Welding voltage (V)} \cdot \text{Efficiency } (\eta) \tag{2.7}$$

The typical power source efficiency is in the range of 0.75-0.85. Here below are listed some values for the most common processes:

- MMA: 0.8
- MIG/MAG: 0.8
- SAW: 0.9-1.0
- TIG: 0.6

*(Efficiencies according to [9])

2.1.2.7 Welding power sources

Electric welding technologies were not developed until the end of the nineteenth century due to a lack of sufficient power sources. In 1905, AEG in Germany invented a welding generator. It was powered by a three-phase asynchronous motor and featured welding capabilities. It weighed 1000 kg and produced 250 A. DC current was often utilized for arc welding until the 1920s. The introduction of stick electrodes enabled the use of alternating current (AC). Because it was less expensive and consumed less energy, the welding transformer quickly gained popularity. Static welding rectifiers were launched around the end of the 1950s. Initially, selenium rectifiers were used, followed by silicone rectifiers. Thyristor rectifiers, which appeared later, enabled electronic control of the welding current. This sort of rectifier is now fairly widespread, at least for bigger welding power sources. However, the most notable advancement in welding power supply was in 1980, with the introduction of the welding inverter [28].

2.2 Discontinuities in welds

The American Welding Society publication [25] defines the term discontinuity as a break in the usual structure of a material, which can lead to non-uniform mechanical, metallurgical, or physical characteristics. It is important to note that a discontinuity does not always indicate a defect, as a defect

is defined as one or more discontinuities that cause a product or part to be unable to meet the minimum applicable acceptance standards or specifications. A flaw is also considered an undesirable type of discontinuity.

The AWS categorizes discontinuities into three major groups: technique and process, design, and metallurgical behavior. They all change the stress distribution in the weld or HAZ, but the latter can also affect mechanical characteristics and corrosion resistance.

Discontinuities diminish the resistive cross-section area and operate as stress concentrators, both of which are damaging to the structure's stability. The severity of discontinuity effects is determined by their form, size, placement in the joint, and direction relative to the maximum tensile stress.

The table below shows the various types of defects and their categorization according to AWS. It should be noted that some of the defects described in the table and grouped under a certain category can also be found in other groupings.

Table 2.2: Discontinuities in fusion welded joints: classification and characteristics

WELDING PROCESS OR PROCEDURE RELATED		METALLURGICAL			DESIGN RELATED	
Geometric	**Other**	**Cracks**	**Porosity**	**Microstructure alteration**	**Changes in sections**	**Weld joint type**
Misalignment	Arc strikes	Hot	Spherical	HAZ	Different thickness	Restraint
Undercut	Slag inclusions	Reheat, stress relief or strain-age	Elongated	Weld Metal and HAZ segregation	Partial penetration joints	Accessibility
Concavity/Convexity	Tungsten inclusions	Cold or delayed	Worm-hole	Base Metal laminations		
Excessive reinforcement	Oxide films	Lamellar tearing				
Improper reinforcement	Spatter					
Overlap	Arc craters					
Burn-through						
Backing left on						
Incomplete penetration						
Lack of fusion						
Shrinkage						
Surface irregularity						
Notes: For further information on this topic refer to [23, 25]						

Metallurgical discontinuities refer to alterations in the properties of both the base and weld metals. The majority of these discontinuities are closely associated with the welding process and the design of the welded structure. For instance, certain welding processes that employ high heat input may cause the separation of alloying elements in some metals, while the joining of dissimilar materials can result in significant embrittlement. The presence of metallurgical discontinuities is often the cause of crack formation. Specifically, cold cracks can result from localized embrittlement due to metallurgical discontinuities. These discontinuities may also occur in the base metal before fabrication, such as lamination defects, which are characterized by separation or weakness generally aligned parallel to the worked surface of a metal. This can result from piping blisters, seams, inclusions, or segregations that have been elongated and made directional by working processes like rolling, forging, or drawing.

Certain flaws that are detected in welded joints may result from decisions made during the **design** process. Proper design of the weldment is important in ensuring that the performance of the weldment is not adversely impacted by stress concentrations that may cause failure. For instance, a sudden change in the shape or cross-sectional area of a weldment can result in stress concentration, thereby causing a discontinuity. The design of the weldment can also influence the occurrence of mechanical and metallurgical discontinuities. Partial penetration, which is a recognized flaw, must be avoided in certain types of weldments. Furthermore, weldments that are designed with limited access for welding may make it difficult for the welder to produce a sound weld, thereby increasing the possibility of welder performance or process-related discontinuities. High restraint conditions can also increase the likelihood of hot or cold cracks that may arise in the weld metal or heat-affected zone.

For a double V groove, the possible discontinuities are given in Figure 2.4. Starting with the porosity, identified as (1b) in the figure cited above, it can only be found in the weld metal. Similarly, incomplete joint penetration (4) and an underfill (6) can be spotted in the same zone. Differently, inclusions (2a) and locations not completely melted (Incomplete fusion, 3) can be also found in the weld interface. In this position, the discontinuities that can be detected are undercuts (5) and overlaps (7). In addition, we can have other imperfections in the base material as laminations (8), delaminations (9), and laps/seams (10). Lastly, multiple types of cracks can be located in various areas of the plate (12 a-g).

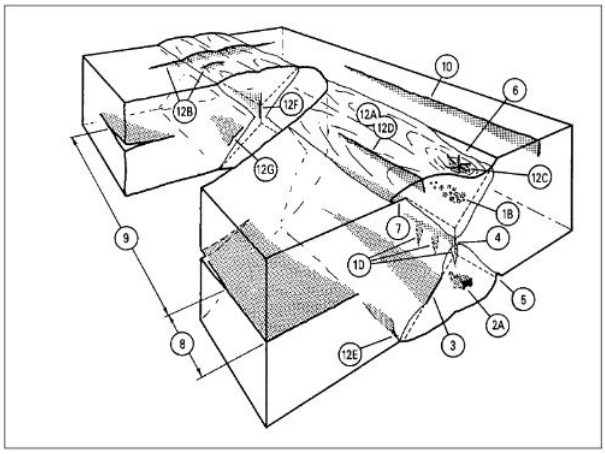

Figure 2.4: Discontinuities in a Double-V-Groove Weld in a Butt Joint [25]

2.2.0.1 Defects in geometry and other procedures

There are several problems that might be identified as a result of welding process flaws. These discontinuities are hazardous since they can all serve as locations for crack nucleation. Slag inclusions are non-metallic solid elements trapped beneath weld metal surfaces, in the root, or between beads in multipass welds. An erroneous arc or poor electrode use might cause slag to leak ahead of the arc and be covered by the weld pool. It is critical in multipass weldments to properly clean the beads after each pass, eliminating all slag that has developed.

The causes of lack of fusion (LOF) and lack of penetration (LOP) are often the poor selection of welding parameters and joint design, wrong electrode manipulation, and insufficient cleaning prior to welding. LOP is the quantity of base material that has been fused and resolidified to lead to a deeper throat than was initially established before welding. LOF, on the other hand, considers how effectively the base metal was melted and combined with the filler. The former are often found in roots, whereas the latter are located on joint surfaces.

Excessive convective forces, inappropriate welding settings, and poor electrode management can all result in unwanted mass flow. Weld metal can spread unevenly throughout the joint, resulting in overlaps, undercuts, underfill, and concavity or convexity, among other issues. Undercuts and overlaps can create severe mechanical notches that contribute to the formation of fatigue cracks. In order to avoid the production of such faults, the welding technique should be carefully designed. When welding multiple groove welds, for example, back gouging the root of the first weld can be utilized to ensure that there are no areas of insufficient penetration.

Although the degree of the faults displayed varies from weld to weld, their role as stress raisers must be reduced after welding using appropriate non-destructive procedures. Before the component is put into operation, any harmful discontinuities should be removed. Postweld grinding and TIG remelting, for example, can eliminate undercuts and overlaps, lowering the chance of fracture development.

2.2.0.2 Porosity

Due to excessive moisture on the base or filler material, or poor cleaning of the surfaces forming the joint, gas can become trapped in the weld pool during welding. If poor shielding is applied, the environment might potentially contaminate the weld pool. If the dissolved gas quantity in molten metal exceeds the solubility limit in solid metal at the solidification temperature, the liquid will experience a local increase in dissolved gas content due to rejection to the solid-liquid surface [25]. Bubbles develop when this value surpasses the solubility limit in molten metal. These bubbles tend to rise in the weld pool due to their buoyancy, but they are also vulnerable to convection. Bubbles will be swept in one direction or another depending on the specific force that dominates convection. Typically, gas is maintained in the pool, and following solidification, pores develop [28]. When welding non-killed steels, carbon dioxide can cause porosity. While nitrogen is typically the origin of pore development in ferritic steels and nickel alloys that do not contain nitride-producing components, hydrogen is the cause of porosity in aluminum

alloys and austenitic stainless steel. It is worth noting that, in addition to being the source of porosity, dissolved gases such as nitrogen, hydrogen, and oxygen can chemically react with molten metal to generate non-metallic brittle compounds. Hydrogen may also permeate to the metal around the pore, causing embrittlement due to a decrease in cohesive energy and lattice strength.

The main types of porosity are described below and most of them are given in Figure 2.5.

Scattered porosity, as the name suggests, appears as isolated or scattered voids throughout the weld bead. It can occur in any type of welding process, such as gas tungsten arc welding (GTAW), gas metal arc welding (GMAW), and shielded metal arc welding (SMAW), and is often attributed to poor gas coverage, incorrect welding parameters, or contaminated base metal.

Uniformly distributed porosity is a type of porosity that appears evenly dispersed throughout the weld metal or the heat-affected zone (HAZ). It can occur in any type of welding process and is often attributed to inadequate gas shielding, incorrect welding parameters, or contaminated base metal. In uniform porosity, the voids are usually small and evenly spaced apart, creating a uniform pattern throughout the weld. This type of porosity can weaken the weld and make it more susceptible to cracking and other types of failure.

Cluster porosity, on the other hand, appears as a group of small voids clustered together in a localized area. It is usually caused by poor arc stability or insufficient shielding gas coverage, which can lead to the entrapment of gas bubbles in the weld metal.

Wormhole is a type of porosity that appears as a tunnel-like void in the welded metal. It is often associated with gas tungsten arc welding (GTAW) and gas metal arc welding (GMAW) processes, where it can occur due to a combination of factors, such as high welding currents, slow travel speeds, and inadequate gas shielding.

Piping porosity (a in Figure 2.5) is characterized by pores that are longer than they are wide and lie approximately perpendicular to the weld face. Piping porosity can occur in fillet welds, where elongated porosity typically extends from the root of the weld toward the face. Elongated porosity is a type of porosity that is similar to piping porosity, but it lies approximately parallel to the weld axis. This type of porosity can be caused by a variety of factors, such as gas entrapment, improper electrode placement, or inadequate shielding gas. Elongated porosity (b in Figure 2.5) is typically longer than it is wide and can weaken the weld joint. In some cases, elongated porosity can lead to piping porosity if the pores are allowed to grow and spread. Both elongated and piping porosity can be caused by similar factors, such as gas entrapment, inadequate shielding gas, or improper welding technique.

Aligned (or linear) porosity appears as a series of small voids aligned along a specific direction, usually parallel or perpendicular to the weld axis. It is often caused by the presence of contaminants, such as oil, grease, or moisture, on the surface of the base metal or the filler metal [25].

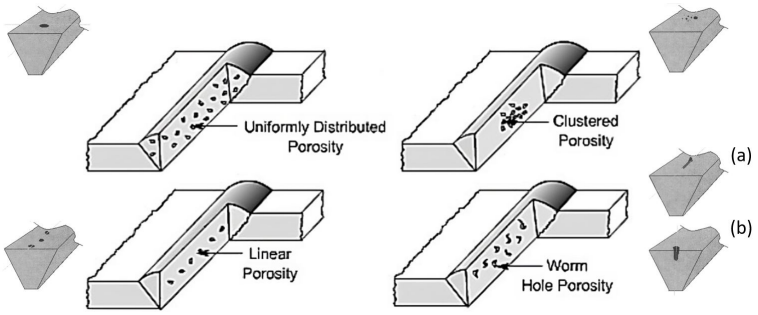

Figure 2.5: Porosity in a V-groove weld [21, 4]

The welding technique and practice are inextricably linked to porosity. It can be evenly distributed or isolated in clusters of pores, for example, in the crater or at the beginning of the bead, as a result of inappropriate arc initiation or termination. Linear porosity, on the other hand, can occur at a welded contact, the root bead, or a border between weld passes. It is the result of gas evolution caused by pollutants in boundaries. Pores are usually spherical, however, they can have sharp tips. It is also possible to come across extended porosity oriented toward the direction of welding, or beneath a wormlike form and texture. The latter is caused by the creation of pores between developing dendrites during solidification. When pores form in the face of a weld bead as a result of poor shielding, high

current, or incorrect polarity, they should be removed. Otherwise, they might operate as slag entrapment locations during successive passes. It has been found that an amount less than 3% by volume of porosity has almost no remarkable effect on static tensile or yield strength [25]. Although there are some cases where pores can arrest a propagating crack due to blunting of its tip, this is not a justification for accepting porosity. On the other hand, pores behave as stress raisers and therefore can promote crack nucleation during cyclic loading. From this point of view, surface porosity is more dangerous than bulk or internal porosity. The effect of the latter on fillet and butt welds with reinforcement is overshadowed by stress concentration on the weld toes. However, studies have shown that removing the weld reinforcement of butt joints causes exposed porosity to affect negatively their fatigue resistance.

The permissible limits for porosity in butt welds in Europe are defined by various standards, but the most important was written in 2014 by the International Organization for Standardization (ISO). The permissible limits for porosity in butt welds depend on the type of weld, the weld quality level, and the intended application of the welded component.

According to ISO 5817:2014 [24], which specifies in Table 1 the quality levels for imperfections in fusion-welded joints, the maximum permissible size and density of pores in butt welds are determined by the quality level of the weld. For a level B quality, which is typically required for structural welds, the maximum permissible pore size is 3 mm, and the maximum allowable density is 10 pores per linear meter. For a level C quality, which is typically required for non-structural welds, the maximum permissible pore size is 5 mm, and the maximum allowable density is 100 pores per linear meter. In order to account for fatigue loading in welded structures, Table 1 must be expanded upon with additional criteria as specified in Table C.1. For steel bridges decks some additional requirements are given in table C.5 of the Eurocode 3 part 2 [17]. The AWS D1.1 Structural Welding Code - Steel [5] is a widely used standard in North America, which specifies the permissible limits for porosity in butt welds based on the weld quality level and the intended application of the welded component. For a category B weld typically used for structural applications, the maximum allowable pore size is 3/16 inch (4.8 mm) and the maximum allowable pore density is 5 pores per linear inch (2 pores per linear centimeter). For a category C weld typically used for non-structural applications, the maximum allowable pore size is 1/8 inch (3.2 mm) and the maximum allowable pore density is 20 pores per linear inch (8 pores per linear centimeter).

Other international standards, such as those developed by the British Standards Institution (BSI), the Deutsches Institut für Normung (DIN) in Germany, and the Japan Welding Engineering Society (JWES), also specify permissible limits for porosity in butt welds, which are similar to those specified in the ISO and AWS standards.

In general, the permissible limits for porosity in butt welds in different parts of the world are typically based on similar principles and considerations, such as the weld quality level, the intended application of the welded component, and the size and density of the pores. However, there may be some variations in the specific limits and criteria used in different welding codes and standards.

2.3 Welding Residual Stresses and Distortions

2.3.1 Residual stresses

Stress refers to the average force per unit area experienced in a body. In materials, stress can be understood as the internal distribution of forces that counteract and respond to external loads. Stress can be categorized into two types: primary (load-controlled) and secondary (displacement-controlled) stress. Primary stress is the stress induced by external loads, while secondary stress is caused by thermal factors [56]. There is consensus among researchers that residual stress can be classified as a form of secondary stress, resulting from internal displacements within components in the absence of external loads. [54]

The occurrence of thermally induced residual stresses can be explained by the concept of heating and cooling under constraint. In Figure 2.6 is presented with three identical metal bars connected to two rigid blocks. Initially, all three bars are at room temperature. The middle bar is heated up while the side bars restrain its thermal expansion. As a result, compressive stresses are generated in the middle bar, which increases with increasing temperature until reaching the yield stress in compression. The yield stress denotes the maximum stress level in a material, beyond which plastic deformation occurs.

When heating ceases and the middle bar cools off, its thermal contraction is confined by the side bars. Consequently, the compressive stresses in the middle bar drop sharply, transform to tensile stresses, and increase with decreasing temperature until reaching the yield stress in tension. Thus, a residual tensile stress equivalent to the yield stress at room temperature is established in the middle bar after it cools down to room temperature. The residual stresses in the side bars are compressive stresses and amount to half of the tensile stress in the middle bar [30].

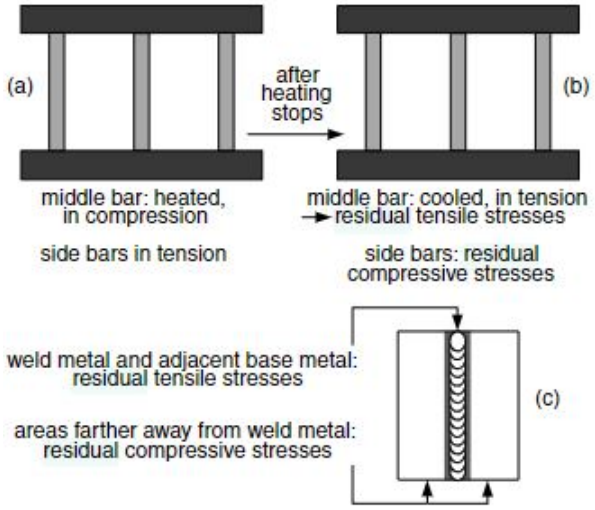

Figure 2.6: (a) stresses generated during heating, (b) stresses generated during cooling, and (c) residual stresses that persist in the weld after cooling. [30]

The impact of residual stress on components can vary and is dependent on the type of stress present. Typically, tensile residual stress has a detrimental effect, whereas compressive residual stress can enhance the quality of the component [47]. Both tensile and compressive residual stress are commonly found in manufactured components, including those produced through welding. While it is widely acknowledged that tensile residual stress is present in weld metal, the distribution of compressive residual stress is more complex and can vary based on factors such as welding parameters, type, sequence, component type, material, and size. [3]

Generally, in welding these type of stresses are caused by the following phenomena:

1. **Thermal variations**: Thermal variations, also referred to as thermal gradients, refer to the changes in temperature within an object, particularly in welded joints, where intense heat is utilized for joining. The intense heat used during the welding process leads to a significant difference in the cooling rate throughout the object, resulting in localized variations in both the surface and interior of the material. This differential in thermal contraction results in the creation of non-uniform stresses within the object[54, 43, 42].
2. **Mechanical deformation**: Residual stresses that arise from plastic deformation are a result of mechanical processing. They occur when the plastic deformation is non-uniform across the cross-section of a material undergoing a manufacturing process, such as bending, drawing, extruding, and rolling. During the deformation process, one portion of the material experiences elastic deformation while the other experiences plastic deformation. Upon removal of the load, the material endeavors to recover the elastic deformation, however, it is hindered from fully doing so by the adjacent plastically deformed material[54, 43, 42].
3. **Phase transformation**: Another mechanism by which residual stress can be induced is through phase transformation. This occurs when a material undergoes a phase transition, which results in a volume discrepancy between the newly formed phase and the surrounding material that has yet to undergo the phase transition. This volume discrepancy leads to expansion or contraction within the material, thus resulting in the generation of residual stress[54, 43].

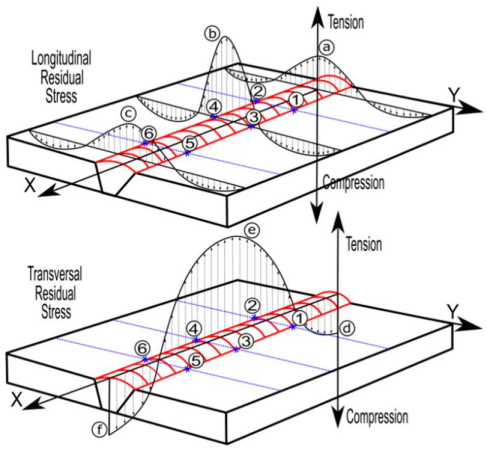

Figure 2.7: Usual patterns of longitudinal and transverse residual stresses in a butt weld [34]

Residual stress can be categorized into two levels: macro and micro residual stress. Macro residual stress refers to stresses that occur over extended distances within a material, while micro residual stress encompasses stresses that are present either between grains or within a grain [54]. The latter is often the result of different phases forming within a material following the application of thermal, loading, transformation, and intergranular stress [55]. There are three types of residual stress scales: type I (macro residual stress or macro stress), type II (micro residual stress or intergranular stress), and type III (micro residual stress or atomic-scale stress). Type I is stress that exists within a component on a larger scale than the grain size of the material and can result from misfits caused by nitriding, peening, cold hole expansion, and welding[55]. This type of stress can be observed in plastically deformed materials, such as shot-peened surfaces and welded materials. Type II stress is variable and dependent on the scale of an individual grain, resulting from the transformation of grains with differing orientations. Type III stress exists within a few atomic distances of a single grain and is due to coherence at interfaces, crystalline defects, and dislocation stress fields [19].

Therefore, the magnitude of residual stresses is largely influenced by several factors, including the material properties of the weld and parent materials, such as composition, micro-structure, thermal properties, and mechanical properties.

2.3.1.1 Material properties

Residual stresses in welded steel are influenced by a number of material properties. These properties include the coefficient of thermal expansion (CTE), which measures a material's response to changes in temperature, the elastic modulus, which measures a material's stiffness or resistance to deformation, and the yield strength, which measures the amount of stress a material can withstand before it begins to deform plastically. If these properties between the base metal and the welding material are significantly different, this can lead to residual stresses [45].

When using a filler material, its composition has a significant impact on the weld metal's properties. The weld metal's properties are further affected by extensive penetration into the base material. When welding without a filler, the suitability of the base material for welding determines the characteristics and quality of the weld. The changes in the properties of the base material in the HAZ are determined by the base material's composition as well as the heat input [28].

The microstructure of the base metal and the welding material can also play a role in the development of residual stresses, particularly if the material has a fine-grained microstructure. The iron-carbon diagram, also known as the Fe-C diagram, is a graphical representation of the various phases and transformations that occur when iron (Fe) is alloyed with carbon (C). It is a fundamental tool for understanding the behavior of steel, which is an iron-carbon alloy. The diagram is a plot of the percent carbon content on the x-axis and temperature on the y-axis. The diagram shows the various phases of iron and steel that exist at different carbon concentrations and temperatures, including austenite, ferrite, cementite, and pearlite. At low carbon concentrations and high temperatures, iron exists in the form of ferrite, which is a soft and ductile phase. As the carbon concentration increases, the ferrite

phase becomes unstable, and the material transforms into austenite, which is a high-temperature, face-centered cubic (FCC) phase. As the temperature decreases, the austenite phase can transform into other phases, depending on the carbon concentration. At a carbon concentration of about 0.8%, the austenite phase transforms into pearlite, which is a mixture of ferrite and cementite. Pearlite is a hard and strong phase that forms the basis of many steels. At higher carbon concentrations, the austenite phase can transform into other phases such as martensite and bainite, which are harder and stronger than pearlite. Martensite is a very hard phase that can be formed by quenching austenite at a high rate, while bainite is a hard but ductile phase that forms by cooling austenite at a slower rate [28]. This diagram allows engineers to design and manufacture steels with specific properties and performance characteristics. It is related to residual stresses in welding because the choice of steel composition and welding parameters can affect the phase transformations that occur during welding, which in turn can lead to the development of residual stresses. During welding, the high temperatures and rapid cooling rates can cause the material to undergo phase transformations, as indicated by the iron-carbon diagram. For example, if a high-carbon steel is welded and the cooling rate is too rapid, the austenite phase may transform into martensite, which is a very hard and brittle phase. This can lead to residual stresses in the weld area due to the differential contraction between the hard and brittle martensite phase and the surrounding softer material. Similarly, if the steel has a high carbon content and the cooling rate is too slow, the austenite phase may transform into a softer phase like pearlite, which may not have the strength required for the application. This can also lead to residual stresses due to the mismatch between the thermal expansion coefficients of the weld metal and the base metal. In the case of an austenitic structure, if it is cooled too quickly, ferrite and pearlite do not form, allowing for the emergence of alternate microstructures with higher hardness but poorer ductility. This is because martensite is formed, which is very hard and brittle, making the material harder as carbon content increases. If the heat input is minimal compared to the thickness of the surrounding metal, cooling will be rapid and martensite may form. Hardness will increase as a result, and hydrogen cracking and embrittlement may ensue. Wet flux or wet electrodes, damp or rusted metal surfaces or organic impurities such as oil, paint, or dirt can all cause hydrogen to escape into the weld metal (pores). As the substance cools and its solubility drops, it diffuses from the weld pool into the surrounding base material, causing cracks [28, 45].

Therefore, understanding the phase transformations that occur during welding and how they can lead to residual stresses is important for selecting the appropriate steel composition and welding parameters to minimize the development of residual stresses. The iron-carbon diagram provides a framework for predicting these phase transformations and can be used to inform the selection of welding parameters and steel composition for a given application.

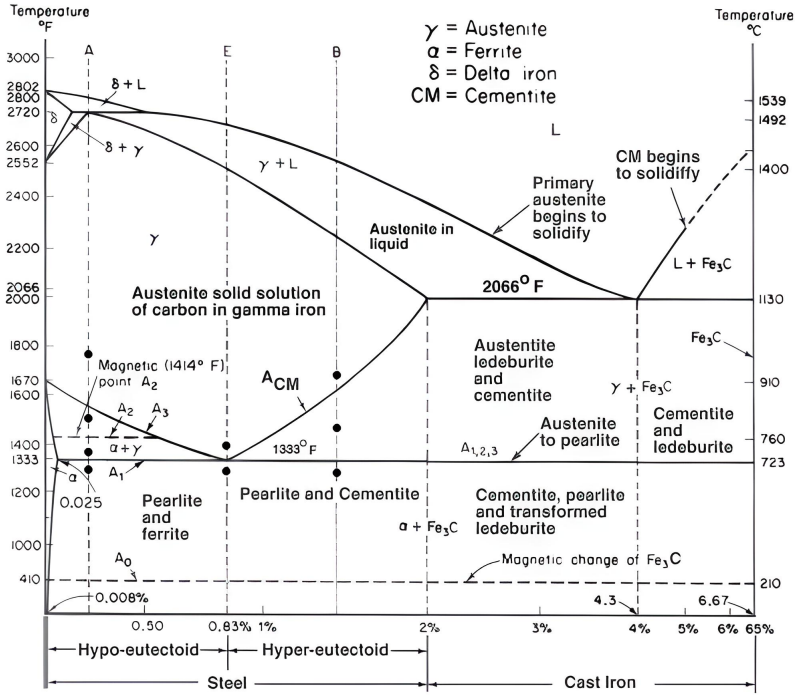

Figure 2.8: Iron-Carbon Phase Diagram [2]

Additionally, the specific welding process used can influence residual stresses, as different techniques have different thermal profiles and can result in different levels of residual stresses. Understanding the interplay between these material properties is important for welders to effectively manage residual stresses and prevent deformation and failure in the finished product.

2.3.1.2 Geometry

The geometry of the components being joined also plays a role, as does the restraints applied to the parts during the welding process, whether through the use of external fixtures or through attachment to other component parts of the structure [32]. The welding procedure itself, including the preparation, conditions, and pass sequence in the case of multi-pass welds, also contributes to the magnitude of residual stresses. Finally, residual stresses can be generated or relaxed through subsequent manufacturing operations after welding or through thermal or mechanical loading during the component's service life [49].

Within the fusion zone and heat-affected zone (HAZ), where the thermal softening and strains resulting from the heat flow during welding are sufficient to cause yielding, the residual stress field will be primarily influenced by the weld-induced residual stresses[58]. At greater distances from the weld, the residual stresses will be a combination of the weld-induced residual stresses and any pre-existing residual stresses in the parts being joined [32]. The extent to which these residual stresses superimpose on one another may vary, ranging from linear elastic to nonlinear elastic plastic or creep, depending on the magnitude of the residual stresses and the mechanical properties of the parent material. [32, 16, 19]

The principal axes of residual stress in a weld are longitudinal, transverse, and short transverse. Residual stresses in the weld in the longitudinal direction frequently equal or are slightly below the yield strength of the material [35]. The stresses in the weld are more depending on the clamping state of the pieces in the transverse direction [1].

Tensile residual stresses are critical in welding butt welds because they can potentially cause failures in the welded structure. If the magnitude of the tensile residual stresses exceeds the yield strength of the material, it can cause plastic deformation and lead to cracking, warping, and distortion [49]. Moreover, high tensile residual stresses can increase the susceptibility of the welded structure to fatigue cracking and decrease the overall fatigue life [52]. Hence, controlling and mitigating tensile residual stresses are essential for ensuring the structural integrity and durability of butt welds.

The magnitude of these tensile residual stresses is determined by the fulfillment of two conditions: the presence of constraints that restrict the free thermal contraction of the heated material and the thermal contraction strain that exceeds the yield strain of the material. The former is dependent upon the geometry and rigidity of the joined parts, while the latter is dependent on the properties of the material. Therefore, plasticity in the numerical simulations can be avoided if the two previous conditions are met. [32]

Tensile residual stresses of yield magnitude may occur if the thermal contraction strain during cooling post-welding exceeds the yield strain of the material, i.e. if the strain generated due to the cooling of the weld and adjacent heated parent surpasses the material's yield point. This is the case if:

$$\alpha(T_s - T_0) \geq \frac{\sigma_Y}{E} \tag{2.8}$$

where *a* is the coefficient of thermal expansion; T_s the softening temperature, defined here as the temperature at which the yield strength drops to 10% of its value at ambient temperature; T_0 the ambient or uniform pre-heat temperature; *E* the Young's modulus; s_Y the yield strength at ambient or pre-heat temperature [15].

2.3.1.3 Boundary conditions

The resistance to the thermal expansion and contraction of the heated material at a welded joint is known as restraint or boundary [14]. Despite its apparent simplicity, the concept of restraint is quite complex and varies in accordance with direction and position within the weld, and changes continuously during the fabrication process. A wide range of factors, including the geometry of the components being joined, the use of fabrication aids such as tacks, cleats, and jigs, the pass sequence in multipass welds, and the welding sequence in structures with multiple welds, can affect the restraint [36].

Longitudinal shrinkage of the weld is strongly opposed by the components being joined, leading to the generation of high tensile residual stresses throughout the thickness of the weld. On the other hand, the transverse shrinkage of the final weld passes on the upper surface of the plate is opposed by the previously deposited passes, generating tensile residual stresses near the upper face, which are balanced by compression at mid-thickness and tension at the lower surface. This results in a mean transverse stress through the thickness that is tensile, which is typically the case in butt-welded plates with similar length and width. The reduced transverse shrinkage at the ends of the welds leads to mean transverse compressive stresses at the ends of the weld and mean tensile stresses at mid-length. Meanwhile, the through-thickness residual stresses are entirely compressive. Each pass is free to shrink in the through-thickness direction during deposition, thus no residual stresses are generated in that direction initially. However, when the central region is compressed in the transverse direction due to the shrinkage of the near-surface passes, compressive stresses in the through-thickness direction are generated. [32]

2.3.1.4 Welding passes

In Figure 2.9 the fundamental structure of a single-pass weld is depicted. Heat travels quickly from the weld to the base material through the surface represented by the line ABC, whereas the surface ADC on the top of the weld loses heat more slowly. The primary grains form perpendicular to the surface that loses the most heat the fastest, i.e. the molten face when the metal solidifies. This will create residual stresses.

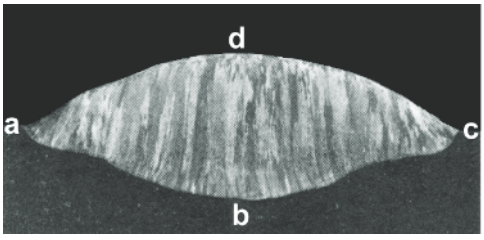

Figure 2.9: Structure of a single pass weld [28]

The residual stresses in butt welds can be significantly influenced by the welding passes used. These stresses are the remaining stresses in the material after welding and can have a notable impact on the strength and endurance of welded structures. The following are some ways in which welding passes can affect residual stresses in butt welds:

One of the significant factors affecting residual stresses is the **welding sequence**, as the order in which the welding passes are made can cause the material to expand or contract, resulting in residual stresses that can cause cracking and failure [25].

The **welding speed** is another factor that affects residual stresses. If the welding is performed too quickly, the heat input may not be adequate to penetrate the material fully, leading to incomplete fusion and residual stresses. In contrast, welding that is performed too slowly can cause excessive heat input, leading to material warping and distortion and resulting in residual stresses [30].

The **welding technique** utilized can also affect residual stresses. Welding techniques with a high heat input, such as gas tungsten arc welding (GTAW), can cause higher residual stresses than those with a lower heat input, such as gas metal arc welding (GMAW). Other examples can be shielded metal arc welding (SMAW) and gas metal arc welding (GMAW). SMAW involves the use of a consumable electrode coated in flux, which melts and forms a protective gas shield around the weld. This process typically results in slower welding speeds and higher heat input, which can lead to higher residual stresses in the welded material. SMAW is often used in industries such as construction and shipbuilding, where high strength and durability are required. GMAW, on the other hand, uses a continuous wire electrode and a shielding gas to protect the weld from atmospheric contamination. This process typically results in higher welding speeds and lower heat input, which can help to reduce residual stresses in the welded material. GMAW is often used in industries such as automotive and aerospace, where high precision and aesthetic quality are required. It is important to note that the choice of welding process should be carefully considered based on the specific requirements of the welded structure, as each process has its own advantages and limitations. In addition, proper welding techniques, such as maintaining proper electrode angle and travel speed, can also help to minimize residual stresses and improve the quality of the weld [31].

Post-weld heat treatment (PWHT) can help relieve residual stresses in butt welds by heating the welded material to a specific temperature and holding it there for a certain time. PWHT can help redistribute residual stresses and reduce the risk of failure [25, 30].

Some examples of residual stress curves with different parameters will be given below.

In [51] Vasantharaja et al. analyzed the residual stress and distortion in a 250mm x 240mm x 16mm 316LN stainless steel weld joint made by TIG welding in the middle of the plate, perpendicularly to the weld. For the double V groove joint made with 17 passes, the results are displayed in Figure 2.10

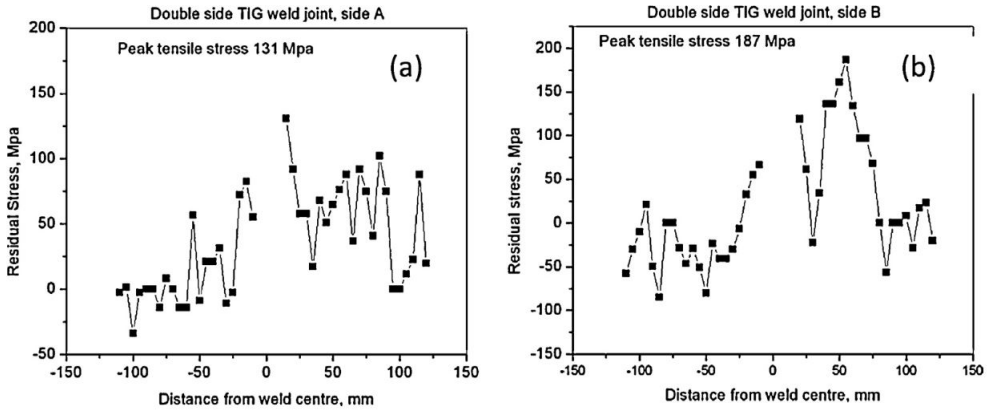

Figure 2.10: Residual stresses of a double V-groove TIG welded joint. Top (a) and bottom (b) [51]

Ye et al. [57] studied the residual stresses for a SUS304 austenitic stainless steel specimen. The final dimensions of each joint are 300mm x 300mm x10mm. Three configurations have been studied (V-groove, K-groove, and X-groove), linking the plates with four welding passes. The residual stresses are extrapolated from a line perpendicular to the weld. The results are shown below in Figure 2.9.

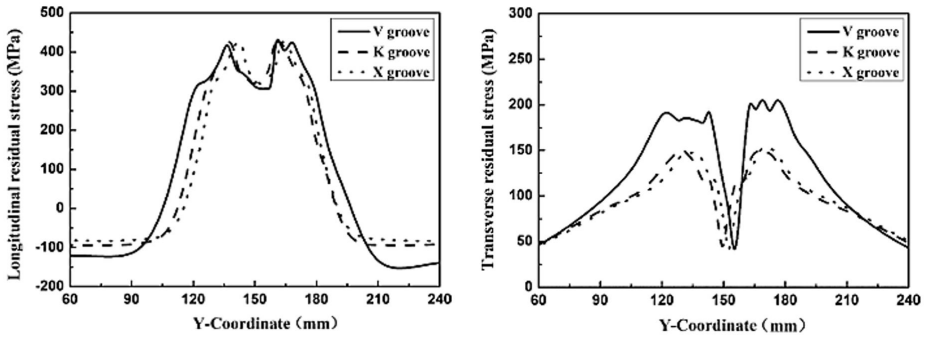

Figure 2.11: Longitudinal and transverse residual stresses of multiple welding configurations perpendicular to the weld [57]

Chen et al. [12] investigated the residual stresses while MAG welding two different steel types (S355JR and 316L). Four different configurations (K_L, K_Q, X, V) joined by welding passes have been considered in the research. The specimen dimension after being welded is 202mm x200mm x 8mm. The results are given in Figure 2.12.

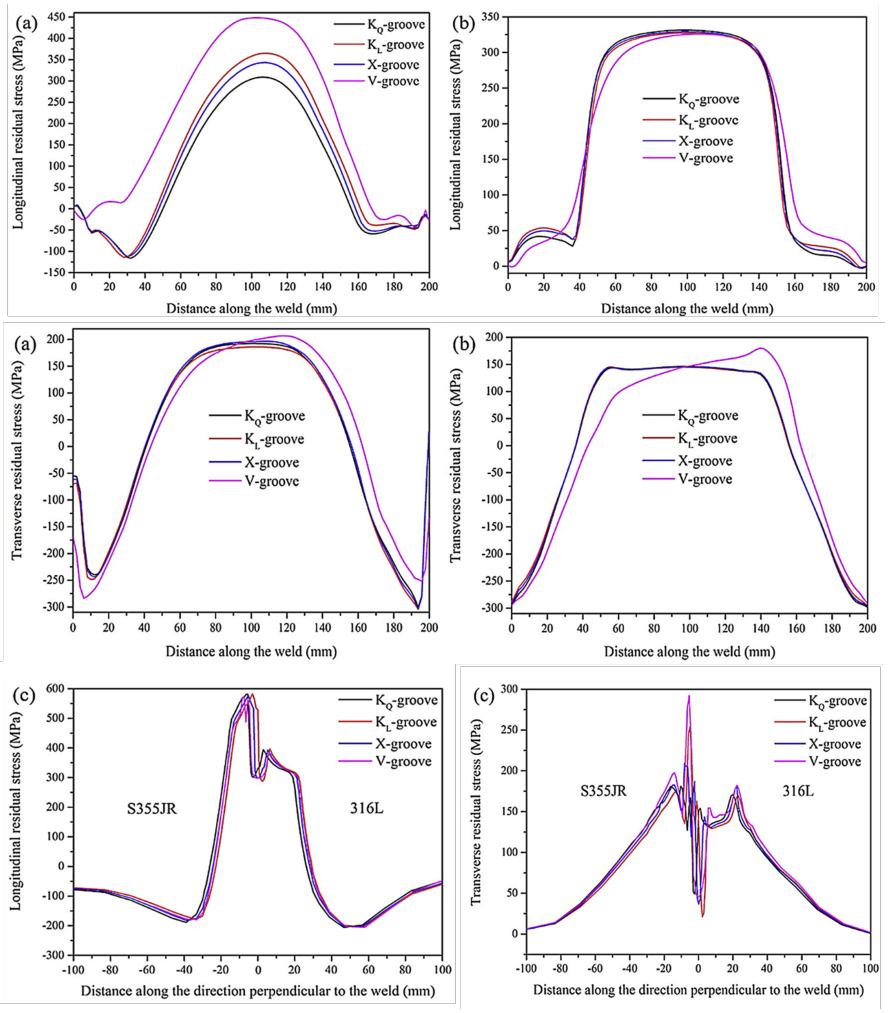

Figure 2.12: Residual stresses of multiple welding configurations parallel to the weld line (top four) and perpendicular to it (bottom two)[12]

Kiran et al. [26] researched the residual stresses for similar and dissimilar double V groove-angled butt welds. GWAM is the used technique in a 9 welding passes configuration for a 50mm × 100mm × 6mm S295 specimen.

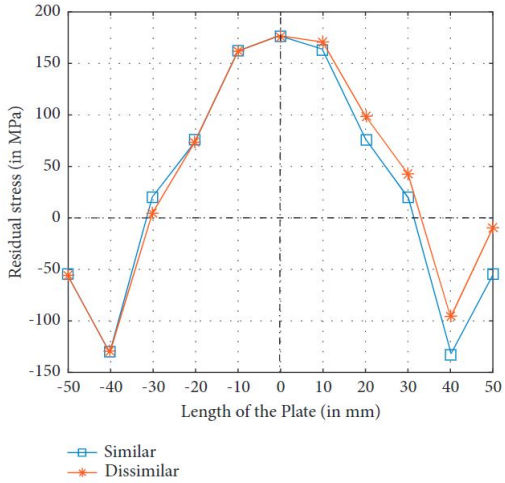

Figure 2.13: Residual stresses vs. length of the plate in double V groove weld specimen [26]

He [27] also discusses the use of simulation and mathematical modeling to analyze gas tungsten arc welding (GTAW) for different parameters of single and double V-groove butt joint welds. The study focuses on two types of materials, namely EN 10025 steel (grade S295) and D36 shipbuilding steel, which are known for their wide range of industrial applications and corrosion-resistant properties. The simulation modeling was conducted using ABAQUS software package and involved various groove angles (90°, 60°, 45°, and 30°) for both similar and dissimilar base metals. The objective of the study was to predict residual stresses in a two passes weld.

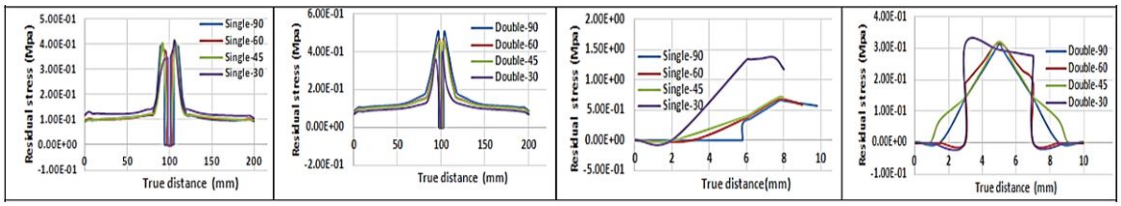

Figure 2.14: Plotted graphs for similar materials welding (S295). Transverse stresses (first two from the right) and Longitudinal stresses (last two). Single V groove (first and third from the right) and Double v groove (second and fourth)[27]

Taraphdar et al. [48] study aimed to examine the impact of different weld groove shapes on residual stresses in 40 mm thick multipass high strength low alloy (HSLA) steel butt-welds. Two welded joints were created with double-V type groove geometry, one with an equal double-V groove and the other with an unequal double-V groove. The residual stresses locked in the weld zone and heat-affected zone (HAZ) were measured using computational and experimental methods. Additionally, the effect of restricted conditions on the residual stresses of the equal double-V groove weld was investigated using computational modeling with varying weld pass sequences.

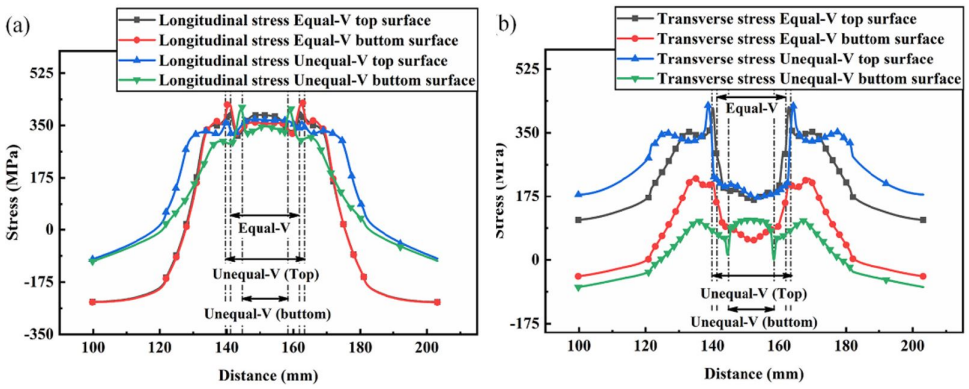

Figure 2.15: Surface residual stress distribution of equal and unequal-V groove joints (a) longitudinal stress, (b) transverse stress[48]

In [33] two butt-welded joints were produced between P92 steel (left) and SUS304 stainless steel (right) using gas tungsten arc welding. The welds had dissimilar metals and were made with different groove shapes, specifically a single V-groove and an X-groove. The first one was made with four passes while the second with five welding passes.

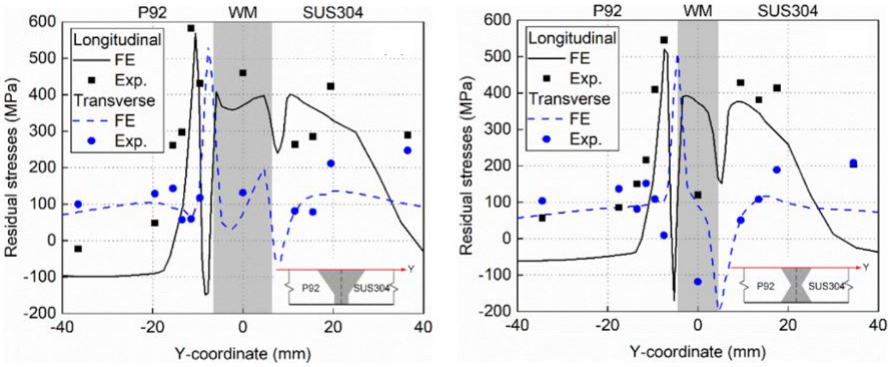

Figure 2.16: Longitudinal and transverse residual stresses perpendicular to the weld on top of the specimen [33]

In [47] Nasir et al. analyzed more different types of specimens giving an overview of the residual stress curves in Table 2.3.

Table 2.3: Residual stress distribution on types of welding sequence

Welding sequence	Residual stress	Tensile residual stress	Compressive residual stress
Single pass butt weld	Longitudinal	Close to the weld	Outer areas of the plate, far from the weld
	Transverse	Welded area	Sides of the plate
Multi-pass butt weld	Longitudinal	Close to the weld bead along the weld	Outer part
	Transverse	Top of the plate	Bottom of the plate

2.3.1.5 Post-Welding operations

Various techniques can be utilized after welding to decrease residual stresses in welded joints. One of these methods is stress relief **heat treatment**, where the welded structure is heated to a particular temperature and kept at that temperature for a specific duration to redistribute residual stresses and reduce their magnitude. Another approach is **shot peening**, which involves striking the welded structure's surface with small, high-velocity steel or ceramic particles, causing compressive stresses in the material's surface layer, thereby counteracting tensile residual stresses in the weld. **Grinding** and **machining** are other ways to relieve residual stresses by removing material from the welded structure. **Cold working** is another method that creates compressive stresses in the surface

layer of the material by applying plastic deformation to the welded structure using processes such as rolling, forging, or bending. **Vibratory stress relief** generates a uniform distribution of compressive stresses in the material by subjecting the welded structure to high-frequency vibrations for several hours to several days, depending on the material and thickness of the welded structure [13]. The choice of post-welding treatment depends on various factors, such as the material, thickness, and welding process used, as well as the magnitude and distribution of the residual stresses. Proper application of these treatments can substantially enhance the quality and durability of welded structures.

2.3.2 Distortions

The inconsistent heating and cooling during welding also produces possible distortions in the metal as it first expands and then contracts. If the nearby parts cannot tolerate the shrinkage, deformation will occur, generally in conjunction with residual strains [40]. There are several kinds of distortion in butt welds:

- Transverse deformation (shrinkage parallel to the weld line);
- Longitudinal misalignment (shrinkage perpendicular to the weld line);
- The specimen volume is reduced by longitudinal and/or transverse rotations depending on the weld;
- Angular change;
- Buckling distortions;
- Longitudinal bending.

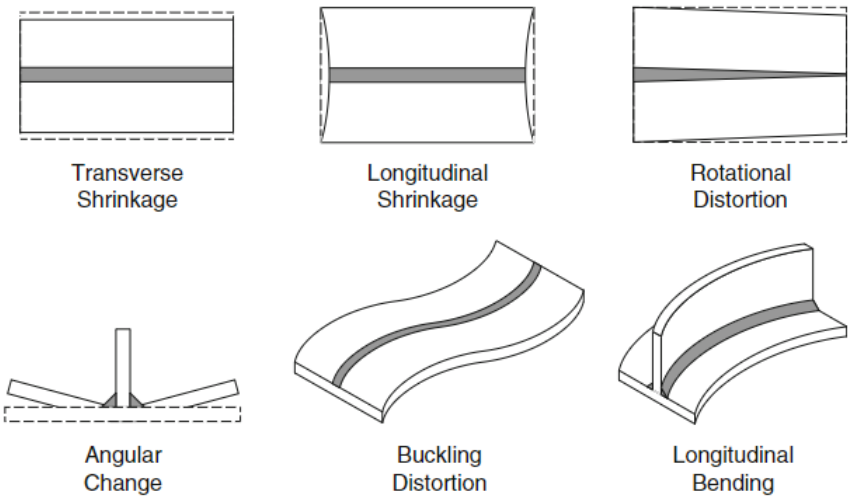

Figure 2.17: Types of welding distortion [38]

Components comprised of thin section panels, relative to their size, tend to be particularly susceptible to buckling distortion. The magnitude of such distortion resulting from welding can be substantial, thereby necessitating the implementation of distortion control techniques to eliminate the cause of buckling. Conversely, structures with substantial cross-sectional dimensions are more resilient to buckling, and typically exhibit bowing or angular out-of-plane modes of distortion [38].

The distortion problem is clearly influenced by the weld metal's properties. Because of the high thermal conductivity, welding will heat up a broader region, creating distortions. If the material has a large thermal capacity, more heat may be stored in it, which increases distortions. The larger the material's coefficient of heat expansion, the bigger the distortions [39].

The quantity of distortion is controlled by elements such as weld preparation (e.g. bevel angles), material thickness, and the amount of weld metal required, in addition to the material being welded. Because of the high amount of weld metal shrinkage, a single V butt weld will suffer considerable deformation. A square-edged closed butt weld, on the other hand, will exhibit negligible deformation [6].

There are several methods for dealing with residual stress and distortion. These are some examples [53]:

- **Mechanical restraints** like clamps and jigs can decrease distortion by keeping components in place [14]. Precambering, for example, keeps the component in a preset position during welding. The precamber is released after welding, and the component bounces back to a slightly deformed shape. These strategies, however, raise the degree of residual stress [18].
- **Presetting/offsetting**. Pieces are offset to a predetermined angle in presetting/offsetting. As the weld hardens and shrinks, it pushes the components into place. Because the parts are not constrained, residual stress is decreased as well. This easy procedure may also be used on fillet welded T-joints, for example.
- **Preheating** the pieces to be welded can help to decrease residual tensions. However, if the pieces are clamped, residual tensions will rise if they are preheated.
- **Limiting heat input and controlling other weld parameters**. Higher heat input causes a greater zone of high residual weld strains. Furthermore, compressive stresses will rise a short distance away from the weld. Limiting heat input might also help to decrease distortion. A more powerful heat source enables faster speeds, lower heat input, and less distortion. Fusion welding techniques frequently provide the most distortions, but laser, electron beam, and friction stir welding can produce smaller distortions. Other weld characteristics, such as travel speed and single-pass vs multiple-pass welds, can also impact stresses and distortions.
- **Thermal tensioning and heat sink welding**. Thermal tensioning entails shifting a heat source ahead of, beside, or behind the welding torch. By adjusting the heating and cooling speeds of the weld, this approach may regulate distortions and residual stresses. Heat sink welding is similar to thermal tensioning, except it uses a cooling source. Pipe welding is an example of this approach, which creates compressive weld residual stresses in the weld heat-affected zone along the inner surface of the pipe to reduce stress corrosion cracking.
- **Sequential welding** is the process of welding in which sections of the workpiece move throughout the welding process. Balanced welding, back step welding, and back skip welding are examples of sequential procedures [58].
- **Flame straightening/heat treatment** employs the use of a heated torch to generate highly localized heat that straightens out deformities. Post-weld heat treatment (using heated jackets put around components, for example) can also offer stress relief, reducing a large proportion of residual tensions.
- **Mechanical stress alleviation** methods such as ultrasonography or peening are used to disperse residual tensions. Laser shock peening deforms the surface and subsurface of a component with a high-density short-pulse laser, causing compressive residual stresses that can increase the component's damage tolerance.

3

Numerical simulation of a X-welded butt joint

In this chapter, multiple welding simulations are presented for two butt-welded joints that are described in the first two subchapters. The simulations are aimed at predicting the welding-induced residual stresses field through the use of ABAQUS 2019, which is a Finite Element Analysis software. The welding simulation process is carried out using a thermo-mechanical analysis, which is divided into two main phases. The first phase involves the analysis of the thermal model, which determines the heat transfer of the welding arc to the specimen. The second phase involves the mechanical model, which utilizes the results obtained from the thermal model to model the residual stresses that are caused by temperature changes and the restriction of material movement due to shrinkage and expansion of the elements in the mechanical modeling phase. The welding residual stress field obtained will be discussed to see how the effect of welding passes influences the residual stresses on multiple locations of the plates.

3.1 Reference model 1- Qiang et al. [41]

This study investigates the distribution of residual stress (RS) in a 30-mm-thick butt-welded joint of Q345qD steel. Table 3.1 provides the nominal chemical composition and mechanical properties of the material.

Table 3.1: Chemical composition of Q345qD steel (mass fraction, %) [41]

C	Si	Mn	P	S
0.14	0.31	1.46	0.016	0.006

Meanwhile, the temperature-dependent material parameters, such as specific heat, thermal conductivity, and density, as well as mechanical properties like yield strength, Young's modulus, Poisson's ratio, and strain-hardening properties are presented in Figure 3.1.

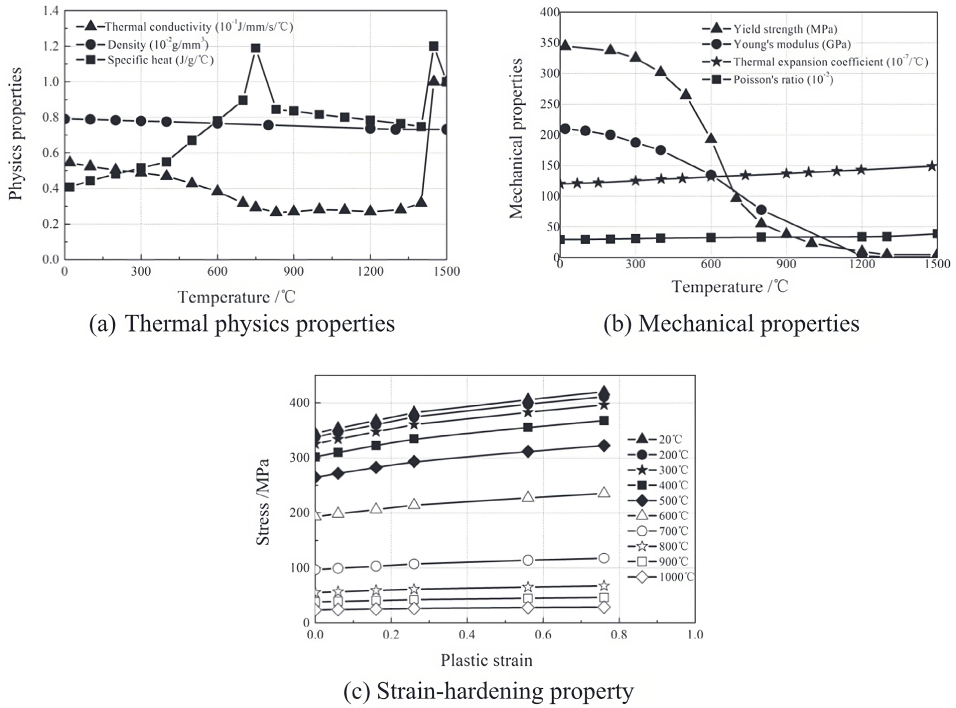

(a) Thermal physics properties

(b) Mechanical properties

(c) Strain-hardening property

Figure 3.1: (a) Thermo-physical properties, (b) Mechanical properties, (c) Strain hardening properties [41]

Both experimental measurements and finite-element simulations were used to obtain the RS distribution on the top and bottom of the plate along the path given in Figure 3.2a.

To conduct the experiments, two Q345qD steel plates with dimensions of $700 \cdot 200 \cdot 30\ mm^3$ were welded along x using submerged arc welding (SAW). Prior to welding, the plates were annealed to eliminate any pre-existing stress. As boundary conditions, weld tabs were arranged at both ends of the weld joint, which were later removed after welding. The test plate had an X-groove joint, as shown in Figure 3.2b, which required double-sided welding to achieve full penetration.

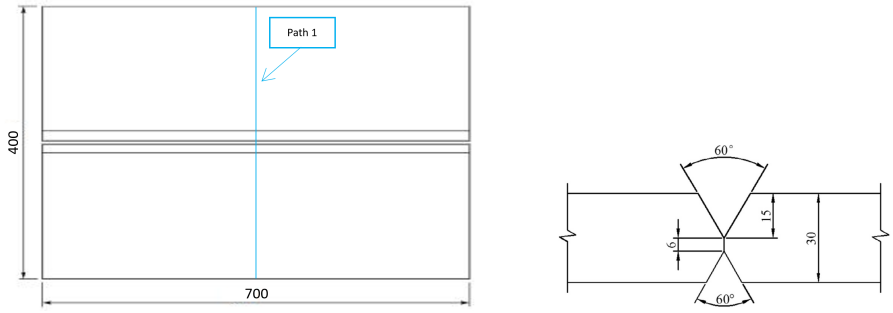

(a) Top view of the plate

(b) Front view of the plate (units in mm)

Figure 3.2: Plate dimensions

Seven weld passes were performed on the X-groove joint, for each welding pass a current (I) of $600 \pm 60A$, a voltage (U) of $29 \pm 4V$, and a speed of $400 \pm 30mm/min$. The welding parameters used in the experiment were within the same ranges as those commonly used in bridge plants in China for the same type of steel.

Due to limitations for the weight and size of the specimen, a water-jet cutter was used to cut and reduce the size of the welded specimen to $200 \cdot 400 \cdot 30\ mm^3$ from the center of the test plate. This size was chosen based on a previous conclusion that the length of the specimen should be two to three times the plate thickness to maintain the original residual stress field [41]. Hole drilling was used to measure the residual stresses on the specimen surface, with measurements taken on only one side

since the distribution of welding residual stress on both sides of the weld was nearly symmetrical. The measurement path was perpendicular to the weld line, with 10 mm between measurement points.

ABAQUS was used to create a three-dimensional finite-element model, as depicted in Figure 3.3. The model was designed to match the size of the test plate, thus $700 \cdot 400 \cdot 30\ mm^3$. The welding procedure for each pass, as well as the number of passes, are detailed in Figure 3.2b. The model consisted of 68,000 elements and 72,926 nodes, with a refined mesh implemented in the weld region. During the welding experiment, starting and runoff weld tabs were positioned at both ends of the weld joint. The model's boundary conditions were displacement constraints at both ends of the weld, as indicated by the red arrows in Figure 3.3, replicating the experimental conditions.

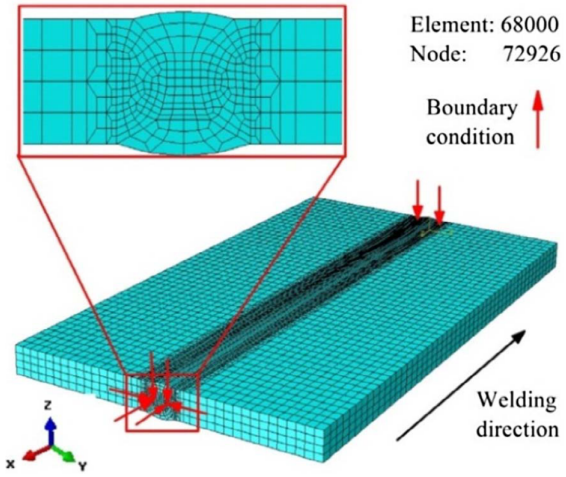

Figure 3.3: Mesh details and boundary conditions for the FEM [41]

For the thermal boundary conditions, heat losses via thermal radiation and convection were taken into account on all surfaces using a convective coefficient of $15W/(m^2 \cdot$℃) and a surface emissivity of 0.85, with an ambient temperature of 20 ℃. The analysis set the latent heat of fusion to 300 kJ/kg between a liquid temperature of 1535 ℃ and a solid temperature of 1500 ℃. The physical properties of Q345qD steel were dependent on temperature, as depicted in Figure 3.1, but the phase transformation in metal was not considered. The welding filler metal was assumed to have the same temperature-dependent material properties as the parent metal.

In the heat-transfer stage, the welding temperature field was calculated using the eight-node element DC3D8. The process of adding and removing elements was employed to simulate the sequential deposition of weld filler. When each weld pass was completed, the elements involved in that process were added to the finite element model by tracking the movement of the heat source. The DFLUX subroutine was used to apply the double-ellipsoidal Goldak model as a heat source moving along the welding path at a speed of 7 mm/s. The double-ellipsoidal heat source model consists of two different expressions that reflect the actual temperature gradients in the front and rear of the molten pool. The source model is described in detail in equation (3.2) and equation (3.3), where q is the heat flux, $Q = \eta UI$ is the total energy input (for submerged arc welding, $\eta = 0.9$ is the heat-energy transfer efficiency), α, b, c_f, c_r are geometrical factors for the ellipsoidal shape, x, y, and z are the geometry coordinates, and $f_f = 1.2$ and $f_r = 0.8$ are the heat-input fractions for the front and rear ellipsoidal quadrants, respectively. The shape parameters for the double-ellipsoidal heat source are listed in Table 3.2.

Table 3.2: Shape parameters of double-ellipsoidal heat source (units: mm) [41]

Weld Pass	c_r	c_f	a	b
1	10	15	4.5	4
2	10	15	5,5	4
3	10	15	7,3	4
4	10	15	9	8,7
5	10	15	9	8,7
6	10	15	6,2	4
7	10	15	13,5	10

The simulation of welding employed one-way coupling between the thermal and mechanical analyses. The temperature profile obtained from the heat transfer analysis for each node was imported as the initial state to compute the stress field in the static analysis step. The mechanical property assumed in this step was isotropic elastic-plastic. The temperature-dependent strain-hardening and mechanical properties of Q345qD steel were incorporated, as shown in Figure 3.1. The element geometries used for the thermal and stress analyses were the same, but the element type was changed from DC3D8 to C3D8R. Both the longitudinal and transverse residual stresses were calculated.

The results were proven through the dimension of the molten pool and the retrieved residual stresses from the experiments.

3.2 Reference model 2- Zhang et al. [58]

This research paper employs the thermoelastic-plastic finite element analysis (FEA) to investigate the residual stress and deformation of welded butt joints made of Q345qD steel (see table Table 3.3) using gas metal arc welding (GMAW) with an ER50-6 welding wire of 1.2 mm diameter and CO_2 as the shielding gas, that will be neglected in the FE model (all the material will be Q345qD steel). The model results have been verified by comparing the size of the molten pool, temperature data from multiple thermocouples, and vertical deformation found in the experiments.

Table 3.3: Chemical composition of Q345qD steel (mass fraction, %) [58]

C	Si	Mn	P	S	Cr	Ni	Cu
0.20	0.55	1.60	0.025	0.025	0.30	0.30	0.40

Three welded butt joint specimens were analyzed experimentally. The dimensions and groove parameters of the specimens are depicted in Figure 3.4.

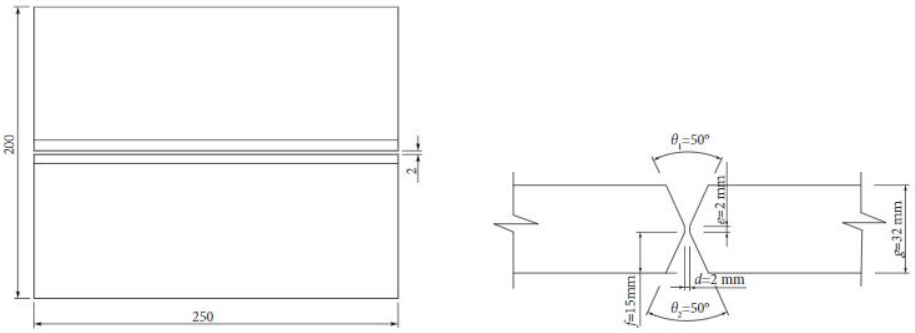

(a) Top view of the plate **(b)** Front view of the plate

Figure 3.4: Plate dimensions [58]

Welding parameters, including the current used, are shown in Table 3.4. The cooling time between different weld beads was maintained at 120s. Tack weldings were used to assist in welding the specimens.

Table 3.4: Heat source parameters [58]

Pass	Current I (A)	Voltage V (V)	Welding speed v (mm/s)	Heat input Q (kJ/mm)
1–12	140	23	4	0.805

In order to oversee the temperature changes that occur while welding, nine K-type thermocouples (Figure 3.5 were fixed to the upper surface of every welded sample, and connected to the R7100 paperless recorder, which has 16 channels and can accurately measure temperatures with a maximum error of 0.1 ℃. Additionally, the deformation of each welded joint was evaluated using a portable 3D scanner that employs a laser (FreeScan UE), which can achieve a high level of accuracy at 0.02 mm. After scanning, the data was processed using Geomagic Control 2014 and Geomagic Control X 2018 software.

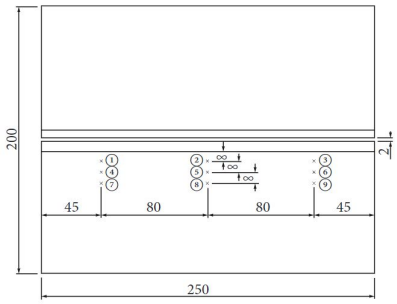

Figure 3.5: Location of the thermocouples [58]

The finite element model is verified against experimental results, and the effects of five welding sequences and two types of boundary constraint conditions on residual stress and deformation are examined. Of these, only the unidirectional welding depicted in Figure 3.6a has been analyzed with the corner boundaries given in Figure 3.6b.

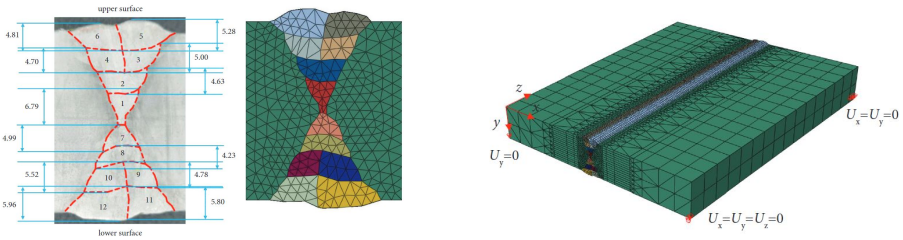

(a) Welding passes **(b)** Boundaries used in the model

Figure 3.6: Welding partition and boundaries [58]

The energy absorbed during the process of fusion, known as the latent heat of fusion, has a value of 270000 J/kg. In this case, the steel undergoes fusion between the temperatures of 1460 ℃ and 1530 ℃, which represent the solid and liquid phases, respectively. The welding efficiency, η, in the study is taken as 70%. In this research, the symbols T_0, ϵ, σ_s, and h_c denote the initial temperature, surface emissivity, Stefan-Boltzmann constant, and convective heat transfer coefficient, respectively. The value of T_0 used in this study is 20 ℃. In the numerical simulation, three of these parameters are generally kept constant due to limited experimental data. Specifically, h_c is assumed to be 10 W/m^2K^1, ϵ is assumed to be 0.8, and σ_s is assumed to be $5.67 \cdot 10^{-8}$ W/m^2K^4.

The welding torch is emulated in the FE model by the double-ellipsoidal heat source model [20]. The heat source values used for the ellipsoid are given in Table 3.5, where a is the width of half of the ellipsoid, b the depth, a_f and a_r the length of the front and rear portion.

Table 3.5: Heat source dimensions [58]

a (mm)	b (mm)	a_f(mm)	a_r(mm)
5.25	5.9	2	5

To retrieve the residual stresses and distortions a mechanical analysis, linked to the thermal one, is needed. This means that the thermal load for the mechanical model is derived from temperature data obtained through thermal analysis. The longitudinal and transverse residual stresses are retrieved from two different paths given in Figure 3.7. For lines A-B and C-D the transverse shrinkage while for A-C and B-D the longitudinal shrinkage was analyzed.

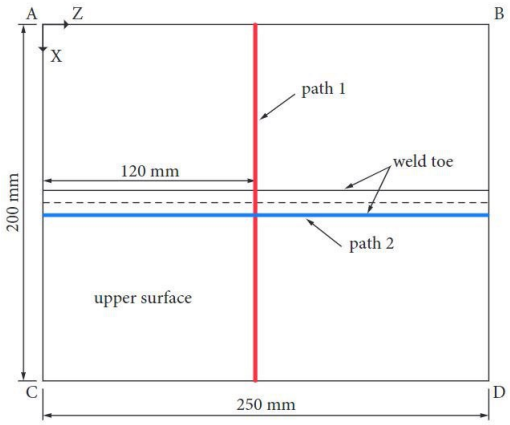

Figure 3.7: Measuring paths for residual stresses [58]

The analysis of the welding thermal stress field is considered a nonlinear transient problem, and therefore, an elastoplastic mechanical model is used, based on incremental theory. Assumptions made in the study include the von Mises yielding criterion for the material, plastic flow and isotropic hardening behavior in the plastic zone of the welded specimen, inseparable elastic-plastic strain and thermal strain, and linear changes in temperature-dependent thermal properties and stress-strain within small time increments. Additionally, the mechanical analysis does not consider the strain caused by phase transformation, as it only has a minor contribution to the total strain of low-carbon steel.

The overall strain, therefore, can be broken down into three subsequent constituents:

$$\epsilon_{total} = \epsilon_{thermal} + \epsilon_{elastic} + \epsilon_{plastic} \tag{3.1}$$

In order to get better results, the element birth and death technique is used to simulate the introduction of deposited metal to the base metal during welding. To achieve this, relevant elements are activated using this technique. Before welding, all elements of the weld are initially disabled. As the welding progresses, appropriate loading steps are used to activate the elements for each welding pass.

The material properties of Q345qD steel as a function of temperature used in the thermal and mechanical simulation are given in Table 3.6.

Table 3.6: Material properties of Q345qD

Temperature (℃)	Thermal conductivity $(\cdot 10^{-3} W/mm \cdot K)$	Density $(\cdot 10{-}9 kg/mm^3)$	Coefficient of expansion $(\cdot 10^{-5}$/℃)	Elastic modulus (N/mm^2)	Yield strength (N/mm^2)	Specific heat capacity $(J/kg \cdot K)$	Poisson's ratio -
20	50	7850	1.1	$2.05 \cdot 10^5$	$3.45 \cdot 10^2$	460	0.28
100	49	7850	1.05	$1.97 \cdot 10^5$	$3.10 \cdot 10^2$	465	0.28
250	47	7850	1.22	$1.87 \cdot 10^5$	$2.75 \cdot 10^2$	480	0.29
500	40	7850	1.39	$1.50 \cdot 10^5$	$2.4 \cdot 10^2$	575	0.31
750	27	7850	1.48	$7.00 \cdot 10^4$	40	625	0.35
1000	30	7850	1.35	$2.00 \cdot 10^4$	20	675	0.4
1500	35	7850	1.33	$1.00 \cdot 10^2$	1	650	0.45
2000	145	7850	1.31	1	1	820	0.49

To achieve both computational accuracy and efficiency, a fine mesh was implemented specifically in the area of the weld bead, while a coarse mesh was utilized elsewhere Figure 3.6. For the thermal

and mechanical analysis, DC3D6 and C3D6 element types were chosen, respectively. The number of elements and nodes used in the analysis were 92067 and 49010, respectively.

3.3 Thermal model

In this chapter, 5 thermal analyses were done to reproduce Qiang et al. [41] experimental and numerical results. the first model was a simple v-groove joint, to see how the specimen behaved if welded on a single side. Afterward, a two passes model was created and used as a first comparison with the full 7 passes model done by Qiang [41]. Then this model was modified with the aim of modeling 3, 5, and 7 welding passes. For the comparison with Zhang et al. [58] data, 7 models were created. As done for the first model, a single v-groove welding simulation was created. Then the complete groove joint was modeled with 2, 4, 6, 8, 10, and 12 passes.

3.3.1 Units

Abaqus software lacks the capability to consider units, therefore, it is crucial to maintain consistency in the units of geometry, material properties, and loading. Reporting the results for stresses and displacements in $\frac{N}{m^2}$ and m, respectively, is recommended to ensure compatibility with the SI. The quantities in Table 3.7, such as temperature, length, force, mass, time, stress, energy, temperature, voltage, amperage, density, conductivity, specific heat, latent heat, convection, heat input, and Stefan-Boltzmann constant, are represented in both SI and the units used in the reference models [41, 58], along with their corresponding multipliers and conversions.

Table 3.7: Units conversion

Quantity	SI	Qiang/Zhang	Conversion
Length	m	mm	$\cdot 10^3$
Force	N	N	1
Mass (1)	kg	kg	1
Mass (2)	kg	g	$\cdot 10^3$
Time (1)	s	min	$\div 60$
Time (2)	s	s	1
Stress	N/m^2	N/mm^2	$\cdot 10^6$
Energy	J	kJ	$\cdot 10^{-3}$
Temperature	K	℃	-273.15
Voltage	V	V	1
Amperage	A	A	1
Speed	m/s	mm/s	$\cdot 10^3$
Density	kg/m^3	kg/mm^3	$\cdot 10^{-9}$
Conductivity	$W/(m \cdot K)$	$W/(mm \cdot K)$	
Specific heat	$J/(kg \cdot K)$	$J/(kg \cdot K)$	1
Latent heat	J/kg	kJ/kg	$\cdot 10^{-3}$
Convection	$W/(m^2 \cdot K)$	$W/(m^2 \cdot K)$	1
Heat input	J/m	kJ/mm	$\cdot 10^{-6}$
Stefan-Boltzmann constant	$W/(m^2 \cdot K^4)$	$W/(mm^2 \cdot K^4)$	$\cdot 10^6$

3.3.2 Geometry and Mesh

The geometry with the respective dimensions used in Abaqus is given in Figure 3.17. The various regions of different element sizes are indicated with different colors. These regions are connected using tie constraints. With "Model 1" is meant the modified version of Qiang's model [41] whether with "Model 2" is defined the modified version of Zhang's model [58].

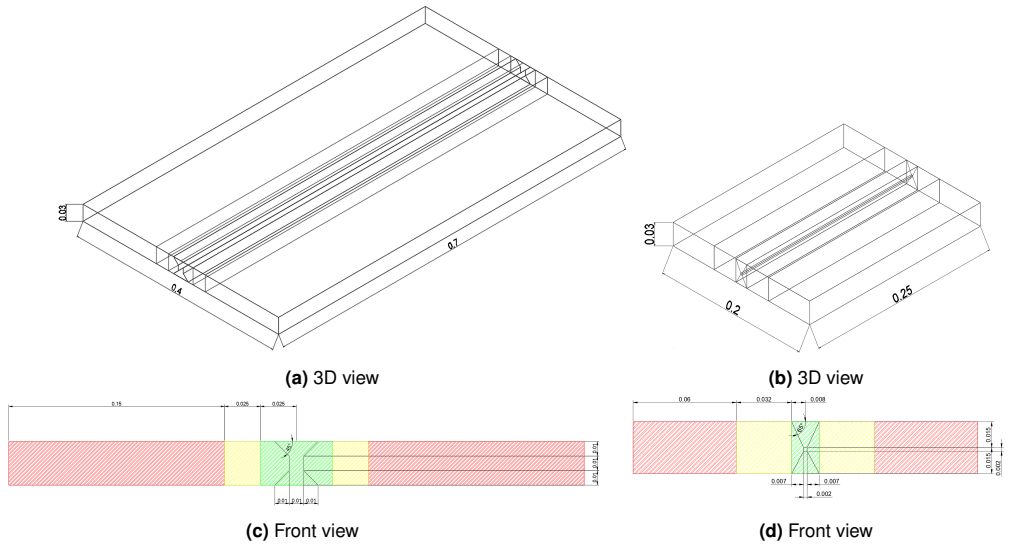

(a) 3D view **(b)** 3D view

(c) Front view **(d)** Front view

Figure 3.8: Model dimensions - (a) and (c) Model 1, (b) and (d) Model 2

To ensure the functionality of the model and the creation of a specific type of mesh throughout the thickness of all 12 models, divisions were established and illustrated in Figure 3.9 and Figure 3.10. The numbers and colors are also given the order of the welding passes, which is discussed further in Section 3.3.6.

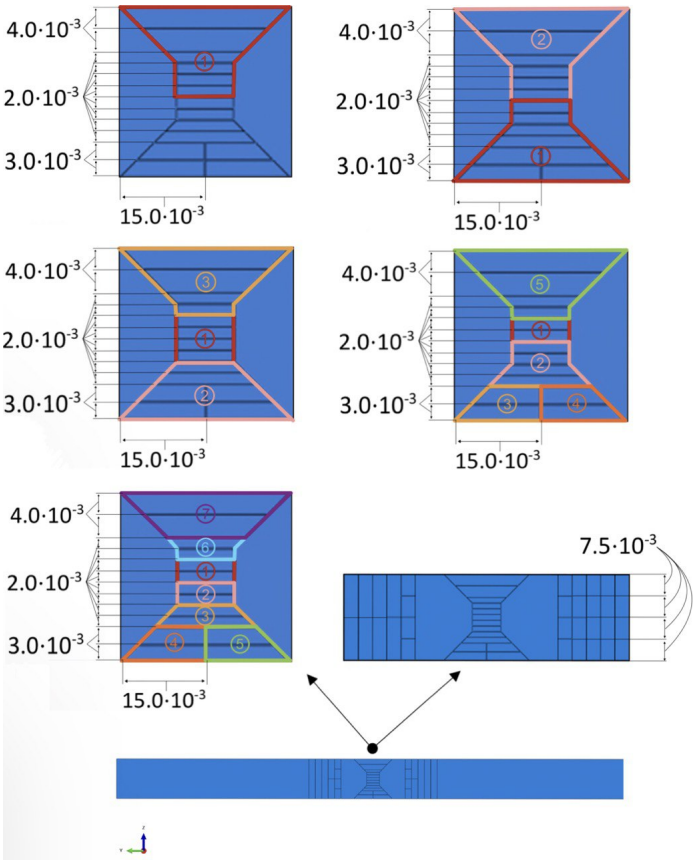

Figure 3.9: Model partitions and welding passes - Model 1 (dimensions in m) [58]

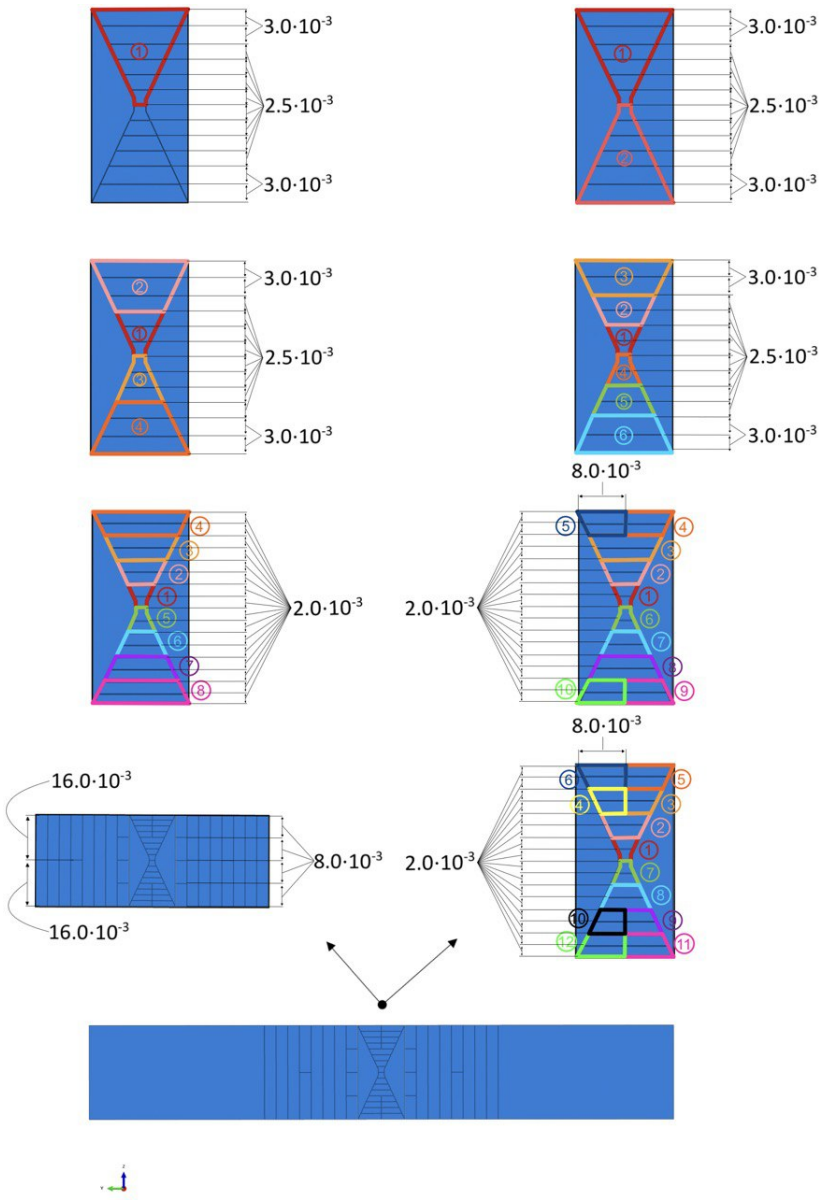

Figure 3.10: Model partitions and welding passes - Model 2 (dimensions in m) [41]

For each of the zone of the models, different types of meshes were created. These are clearly displayed in Figure 3.12, and Figure 3.11.

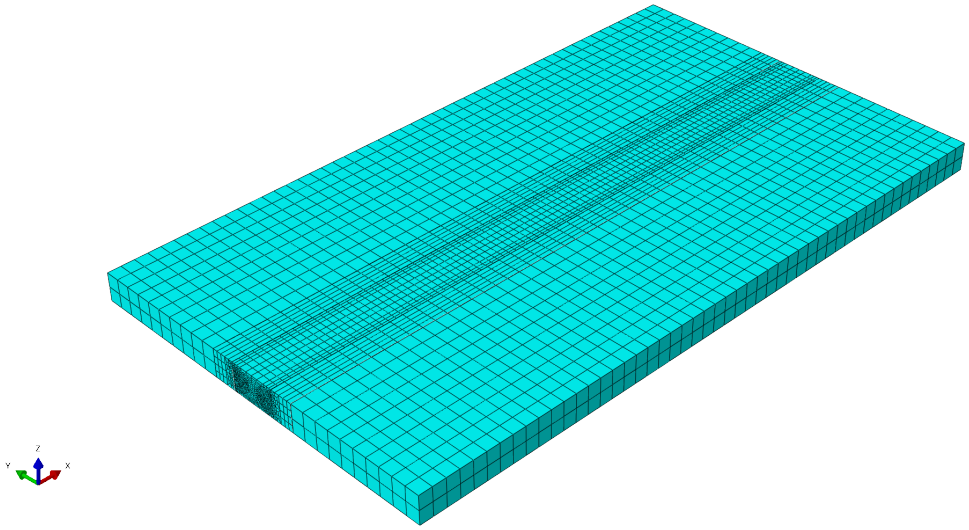

(a) 3D view of the mesh - Model 1 [41]

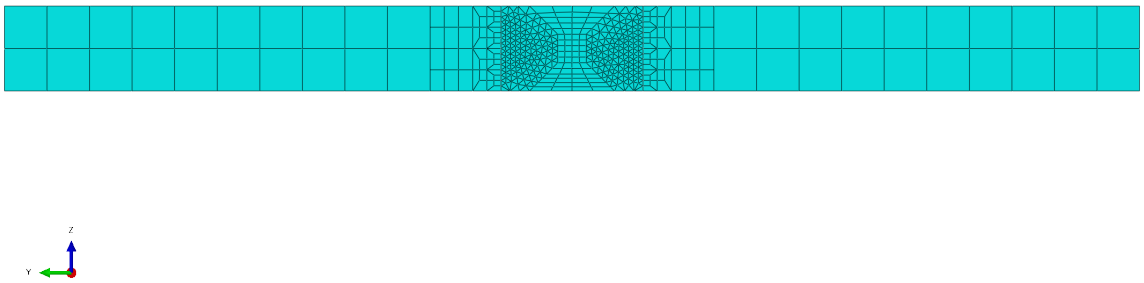

(b) Front view of the mesh - Model 1 [41]

Figure 3.11: Mesh - Model 1

In the first model, one mesh was created for the five simulations (1,2,3,5, and 7 welding passes). For the welding area, 4 DC3D8 elements are used along the width and 16 along the height. In the transition zone, between the inner and the middle partition, DC3D6 elements were chosen because of their versatility. Consequently, in the middle partition, a double subsequential 2:1 transition ratio was used in order to have a smooth transition from 1.875 mm and 7.5 mm elements. For the outer layer, 15 mm 8-node solid elements were used.

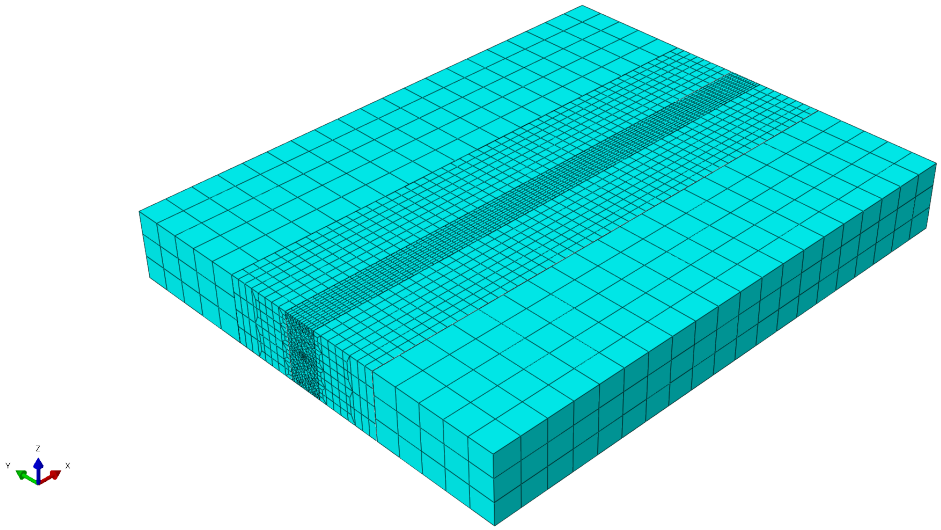

(a) 3D view - 12 Welding passes

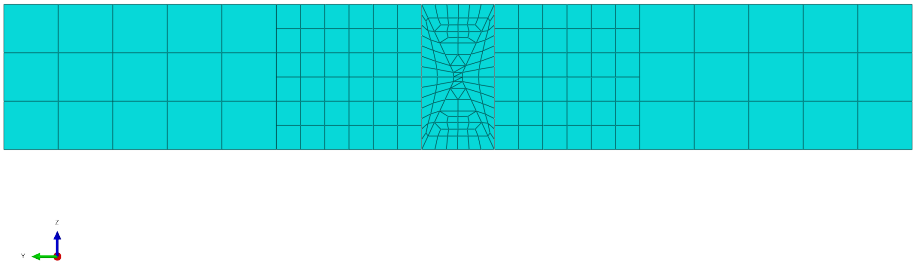

(b) Front view - 1 to 6 Welding passes

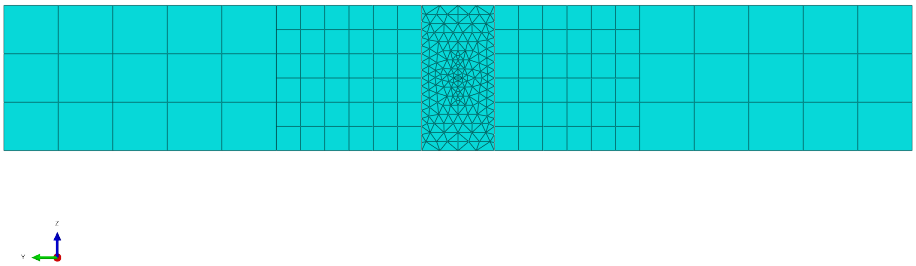

(c) Front view - 8 Welding passes

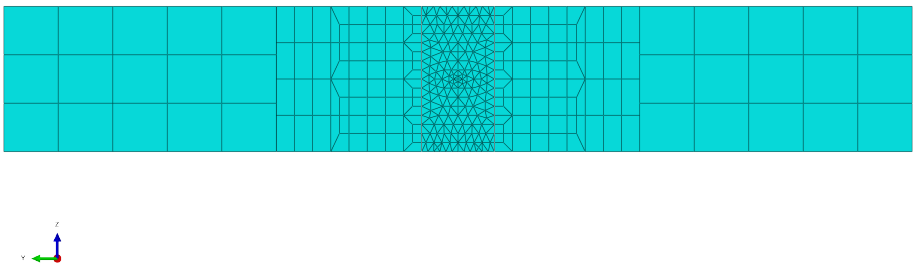

(d) Front view - 10 and 12 Welding passes

Figure 3.12: Mesh - Model 2

For the second model, the used mesh for one to six welding passes is the same. In the double V groove, for the inner welding areas, DC3D6 elements are used, with a 2:1 transition layer. From the top and bottom, in the last three layers, there is a double transition using DC3D8 elements, first a ratio between the elements of 2:1 and then a 3:2. For the middle and outer layers, the welding process results in fewer temperature fluctuations because of the distance from the torch, which suggests that a coarser mesh can be used in this area. Thus, for the first one, a 6mm mesh was used, and for the outermost a 12mm one, both with DC3D8 elements.

For the model with 8 welding passes the previous mesh had to be modified due to an overlap of the elements during the simulation. Therefore, in the welding area, only DC3D8 elements were utilized. In the inner zone, 4 elements are used along the width and 20 along the thickness. Again, for the middle and outer partitions a mesh with a size of 6 mm and 12 mm was applied, respectively.

Due to the complexity, a third mesh was created for the 10 and 12-welding passes model. In this case, for the inner partition, DC3D6 elements were chosen, 12 for each pass along the width. Subsequently, for the middle layer (DC3D8 elements), two 2:1 transition layers can be seen, that bring an element from 2 mm to 4 mm and consequently from 4 mm to 8 mm. For the outer zone, DC3D8 elements are used with a dimension of 10.67 mm.

The number of elements, divided per type, and nodes is given in Table 3.8. The original model made by Qiang et al. [41] consisted of 68,000 elements and 72,926 nodes while the one modeled by Zhang et al. [58] is composed of 92067 elements and 49010 nodes. To clarify, "Model 1" refers to the model originally developed by Qiang and then emulated using multiple welding pass configurations, while "Model 2" refers to the modified model that compares with Zhang's results.

Table 3.8: Amount of elements and nodes in each model

Model	Number of passes	Element type DC3D8	Element type DC3D6	Total Nodes	Total Elements
1	1	13200	47200	42921	60400
1	2	13200	47200	42921	60400
1	3	13200	47200	42921	60400
1	5	13200	47200	42921	60400
1	7	13200	47200	42921	60400
2	1	14200	1400	18934	15600
2	2	14200	1400	18934	15600
2	4	14200	1400	18934	15600
2	6	14200	1400	18934	15600
2	8	4200	31800	24388	36000
2	10	7800	32000	28975	39000
2	12	7800	32000	28975	39000

As it can be seen from Table 3.8, 4 types of mesh were created to complete all the analyses without occurring in aborted jobs in the modeling program.

3.3.3 Thermal properties

The heat transfer and temperature distribution during welding are governed by the thermal properties of the materials involved. In Abaqus, the thermal properties of the materials are defined using material models. These models define the thermal conductivity, specific heat, and density of the materials. The thermal conductivity represents the material's ability to conduct heat, while the specific heat represents the amount of energy required to raise the material's temperature by a given amount. The density of the material is also important in determining the amount of heat that is stored in the material. In welding simulations, the thermal properties are used to model the heat transfer and temperature distribution during the welding process. This information is critical in predicting the final properties of the welded joint, including its strength, toughness, and fatigue resistance. Some important factors to consider when selecting thermal properties for welding simulations include the type of material being welded, the welding process used, and the geometry of the weld joint. The thermal properties should be chosen to accurately represent the behavior of the materials during the welding process and to ensure that the simulation results are reliable. In addition to the thermal properties, other factors that influence the

welding process include the welding parameters, such as the welding speed, heat input, and welding sequence. These parameters should be optimized to ensure that the welded joint has the desired properties. In summary, thermal properties are a critical component of welding simulations in Abaqus and welding in general. Understanding the behavior of materials during the welding process and selecting appropriate thermal properties is essential for predicting the final properties of the welded joint.

The ones used in the simulations made in Abaqus are given below, indicating "Model 1" the one used to replicate the experiments done by Qiang et al. [41] and "Model 2" the experiments done by Zhang et al. [58]. These are used to describe Q345qD steel, which refers to a type of steel grade in the Chinese standard GB/T 714-2015, which is commonly used in the construction of bridges and other structures.

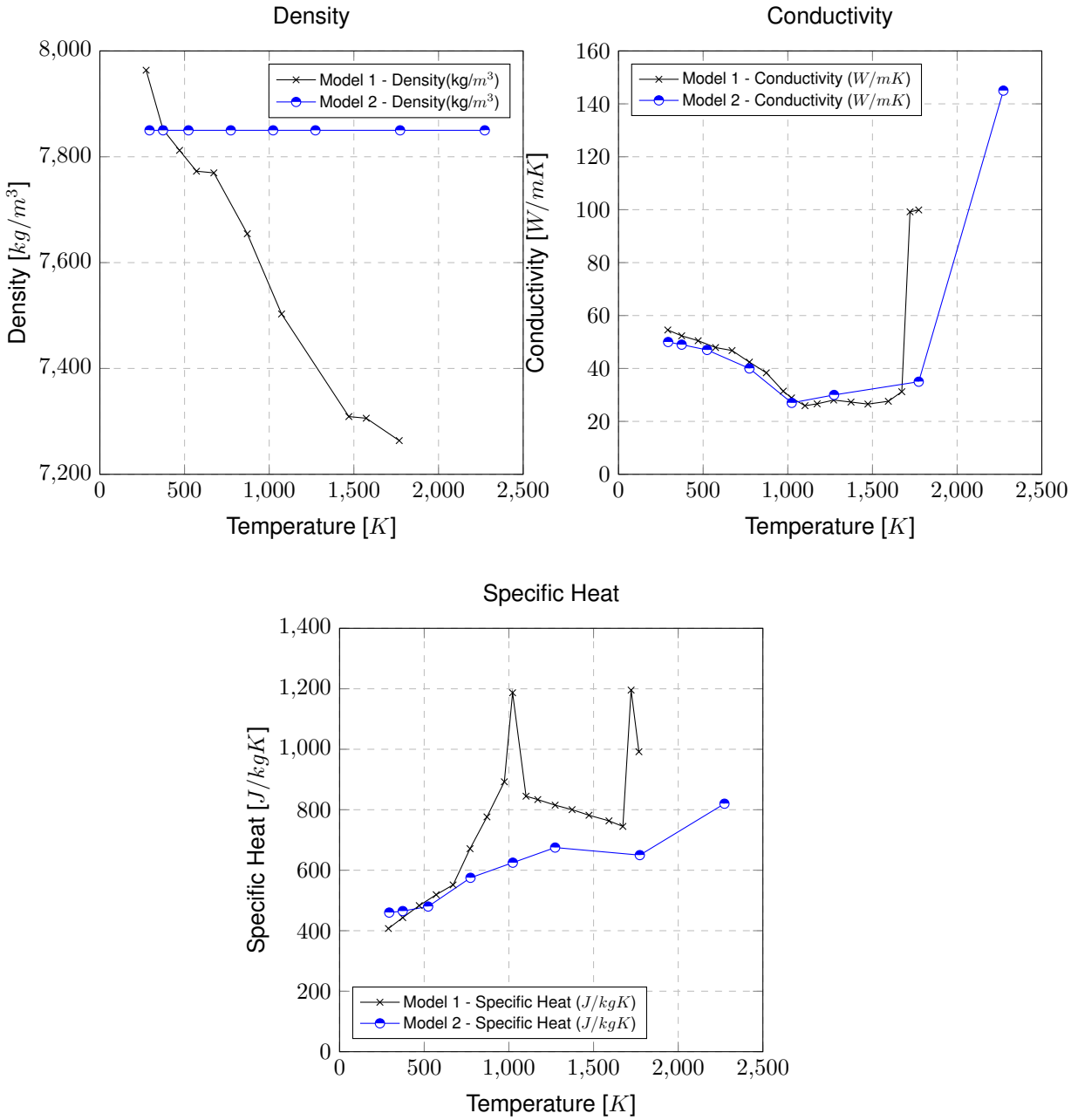

Figure 3.13: Thermal Properties

The density of steel is not significantly affected by a change of temperature, whereas the remaining

material properties are influenced by temperature gradients [46].

During the analysis, the latent heat of fusion was also incorporated, which was set at 300000 J/kg when the liquid temperature was 1808.15 °K and the solid temperature was 1773.15 °K. The absolute zero temperature was set to 0 °K and the Stefan Boltzmann constant to 5.67E-08 $W/(m^2K^4)$.

3.3.4 Thermal boundary conditions

The thermal model applied in this research study accounted for two crucial physical processes: surface radiation and convection. To define the thermal boundary conditions, the study considered heat losses on all surfaces through both convection and radiation. The heat transfer coefficient was set to $15W/(m^2K)$, while the emissivity was assigned a value of 0.85. The ambient temperature was maintained at 293.15 °K. It's important to note that these values determine how heat is dissipated to the surrounding cooler areas.

3.3.5 Thermal load

The heat input used can be described with Goldak's double ellipsoid heat source model [20], which is a mathematical model used in welding simulations to predict the temperature distribution and thermal history of a welded joint.

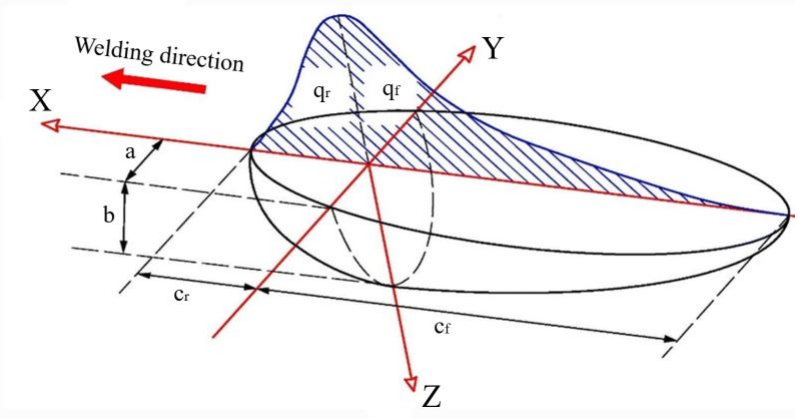

Figure 3.14: Goldak double ellipsoid model [20]

The model was developed by J. Goldak in 1984 and is based on the assumption that the heat source in welding can be approximated by two ellipsoids. The front and rear shapes are described respectively by:

$$q_f(x,y,z) = \frac{6\sqrt{3}f_fQ}{abc_f\pi\sqrt{\pi}}e^{-3[(\frac{x}{a})^2+(\frac{y}{b})^2)+(\frac{z}{c_f})^2)]} \tag{3.2}$$

$$q_r(x,y,z) = \frac{6\sqrt{3}f_rQ}{abc_r\pi\sqrt{\pi}}e^{-3[(\frac{x}{a})^2+(\frac{y}{b})^2)+(\frac{z}{c_r})^2)]} \tag{3.3}$$

The two equations above define the power input $Q = \eta UI$, defined in Watts [W], where η is the thermal efficiency, while the welding process employs an electric current, denoted as I [A], and the arc voltage, represented as U [V]. The parameters α, b, c_f, c_r represent the radial dimensions of the molten zone (Figure 3.14). The first two (α and b) correspond to the width and depth of the heat source. $f_f = 2c_f/(c_f + c_r)$ and $f_r = 2c_r/(c_f + c_r)$ [58] represent the heat deposited in the front and rear parts of the ellipsoids. These should satisfy the condition f_r + f_f = 2. The relationship between parameters c_f and c_r can be estimated by considering that the heat fluxes q_f and q_r must be equal at the origin of the coordinate system. This requirement implies that $c_r = 2.33c_f$, while c_f can be approximated to half of the weld width [46, 50].

The parameters used to describe the heat source in both the models are given in Table 3.9 and Table 3.10. The torch height and offset in each pass along the thickness of the plate is given in Appendix

D and shown graphically in Figure 3.9 and Figure 3.10. The thermal efficiency η is defined as 0.9 in the first model and 0.7 in the second one.

Table 3.9: Heat Flux parameters, Model 1

Welding pass	a [m]	b [m]	c_r [m]	c_f [m]	f_f [m]	f_r [m]
Pass 1	0,0045	0,004	0,015	0,01	0,8	1,2
Pass 2	0,0055	0,004	0,015	0,01	0,8	1,2
Pass 3	0,0073	0,004	0,015	0,01	0,8	1,2
Pass 4	0,009	0,0087	0,015	0,01	0,8	1,2
Pass 5	0,009	0,0087	0,015	0,01	0,8	1,2
Pass 6	0,0062	0,004	0,015	0,01	0,8	1,2
Pass 7	0,0135	0,01	0,015	0,01	0,8	1,2

In the first model, different values are used depending on the welding pass. In case fewer passes are simulated, the corresponding values are not included in the simulation. The torch efficieny

Table 3.10: Heat Flux parameters, Model 2

a [m]	b [m]	c_r [m]	c_f [m]	f_f [m]	f_r [m]
0,0045	0,004	0,00466	0,002	0,6	1,4

Differently from the other model, these values are used for all 7 simulations, independently from the welding pass.

In this work, Goldak's model is used to simulate the moving heat source, and the parameters related to the size of the welding arc were calibrated based on experimental results and implemented in the DFLUX subroutine.

The temperature distribution is used to predict the fluid flow during welding, which is important for understanding how the molten metal behaves as it cools and solidifies.

The Goldak double ellipsoid method has been widely used in the automotive, aerospace, and manufacturing industries to optimize welding parameters and improve the quality of welded joints. It is known for its accuracy and has been validated through experimental measurements of temperature and fluid flow during welding.

3.3.6 Steps

Here below, in Table 3.11 and Table 3.12, is presented a detailed description of the simulation process for both models, including the duration of each step, current and voltage values, welding speed, and heat input.

Table 3.11: Welding steps, Model 1

Action	Duration t [s]	Current I [A]	Voltage U [V]	Welding speed v [m/s]	Heat input Q [J/m]
Pre-step	1,00E-06	-	-	-	-
Tack welds	1,00E-06	-	-	-	-
Pass 1	100	600	30	0,007	16200
Cooling 1	5	600	30	0,007	16200
Pass 2	100	600	30	0,007	16200
Cooling 2	5	600	30	0,007	16200
Pass 3	100	600	30	0,007	16200
Cooling 3	5	600	30	0,007	16200
Pass 4	100	600	30	0,007	16200
Cooling 4	5	600	30	0,007	16200
Pass 5	100	600	30	0,007	16200
Cooling 5	5	600	30	0,007	16200
Pass 6	100	600	30	0,007	16200
Cooling 6	5	600	30	0,007	16200
Pass 7	100	600	30	0,007	16200
Cooling 7	15000	600	30	0,007	16200
	Total [s]				
	15730				

The simulation process involved several steps, including the deactivation of welds in the pre-step using the model change command. A static heating step was introduced, named Tack welds, to emulate the application of the tack weld at the beginning and end of the plate. The weld was initially absent in the inner areas of the plate, highlighted in Figure 3.9. The area was divided into 10 element sets along the length in Abaqus, with a length of 70 mm each in Model 1. This resulted in the deactivation of all elements along the weld length and initiated the thermal analysis. With each time step, weld elements were subsequently reactivated, leading to the "birth" of weld elements. Due to the fine mesh and the high number of elements in the weld region, a Python code was created to automatically select and place a specific number of elements into an element set. The code is given in Appendix A.

Table 3.12: Welding steps, Model 2

Action	Duration t [s]	Current I [A]	Voltage U [V]	Welding speed v [m/s]	Heat input Q [J/m]
Pre-step	1,00E-06	-	-	-	-
Tack welds	1,00E-06	-	-	-	-
Pass 1	62,5	140	23	0,004	2254
Cooling 1	120	140	23	0,004	2254
Pass 2	62,5	140	23	0,004	2254
Cooling 2	120	140	23	0,004	2254
Pass 3	62,5	140	23	0,004	2254
Cooling 3	120	140	23	0,004	2254
Pass 4	62,5	140	23	0,004	2254
Cooling 4	120	140	23	0,004	2254
Pass 5	62,5	140	23	0,004	2254
Cooling 5	120	140	23	0,004	2254
Pass 6	62,5	140	23	0,004	2254
Cooling 6	120	140	23	0,004	2254
Pass 7	62,5	140	23	0,004	2254
Cooling 7	120	140	23	0,004	2254
Pass 8	62,5	140	23	0,004	2254
Cooling 8	120	140	23	0,004	2254
Pass 9	62,5	140	23	0,004	2254
Cooling 9	120	140	23	0,004	2254
Pass 10	62,5	140	23	0,004	2254
Cooling 10	120	140	23	0,004	2254
Pass 11	62,5	140	23	0,004	2254
Cooling 11	120	140	23	0,004	2254
Pass 12	62,5	140	23	0,004	2254
Cooling 12	15000	140	23	0,004	2254
	Total [s] 17070				

For the second model, again, the simulation procedure involved multiple steps, one of which was the deactivation of welds during the pre-step using the model change command. A static heating step called Tack welds was introduced to model the application of the tack weld at the beginning and end of the plate. The inner areas of the plate, as shown in Figure 3.10, did not have the weld initially and were divided into ten element sets along their length in Abaqus, with each set having a length of 25 mm each in Model 2. This process deactivated all the elements along the weld length and initiated the thermal analysis. As the simulation progressed, weld elements were reactivated with each time step, resulting in the "birth" of weld elements. Due to the fine mesh and a high number of elements in the weld region, a Python code was developed to automatically choose and place a specific number of elements into an element set. The code is provided in Appendix A. An instance of this methodology is illustrated in Figure 3.15, showing that the model includes the first six increments, with the sixth one highlighted, and the remaining four will be incorporated as the torch approaches the corresponding increment.

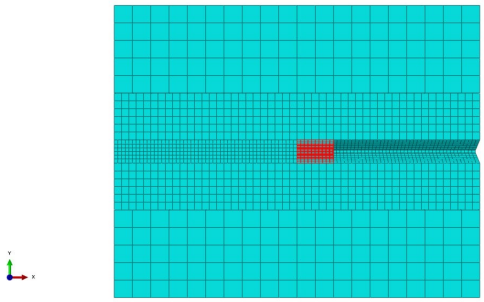

Figure 3.15: Birth-Death principle example - Model 2

3.4 Results

In this chapter, the thermal results for Model 2 are displayed in Figure 3.16. No data is given for the first model because the reference model [41] proved the results experimentally directly with residual stresses, whether Zhang et al. [58] proved the results experimentally through temperature and distortions. Afterward, in both the reference models, the residual stresses were modeled with multiple Abaqus simulations.

3.4.1 Temperature

Figure 3.16 displays the temperature distribution caused by the heat source along path 1 and 2 (see figure Figure 3.22) for multiple passes in four precise locations for the whole duration of each simulation. In each of the analyses the positive x-direction is the welding direction. The origin of the system is located at the top of the plate, at the location of the start of the weld defined as the begging of the plate from now on, in the exact middle of the weld. In Figure 3.16 for thermocouple 1 is meant the location (0.045mm, -0.018mm,0mm), for thermocouple 2 is (0.125mm, -0.018mm,0mm), for thermocouple 3 (0.125mm, -0.028mm,0mm), and for thermocouple 4 is (0.125mm, -0.038mm,0mm). These position are assumed, as in Zhang's et al. paper [58] the exact location of the thermocouples is not given explicitly.

The data of the temperature is given in Kelvin's [°K]. For the first five passes, excluding the peaks, the temperatures have a difference below 30 °K. After that amount of passes, an different growth can be observed in the results obtained by Zhang. The peak temperature reached after 12 passes is around 450 °K, 100 °K lower than the experimental data.

Moreover, a different cooling rate can be observed in the 8 passes simulation.

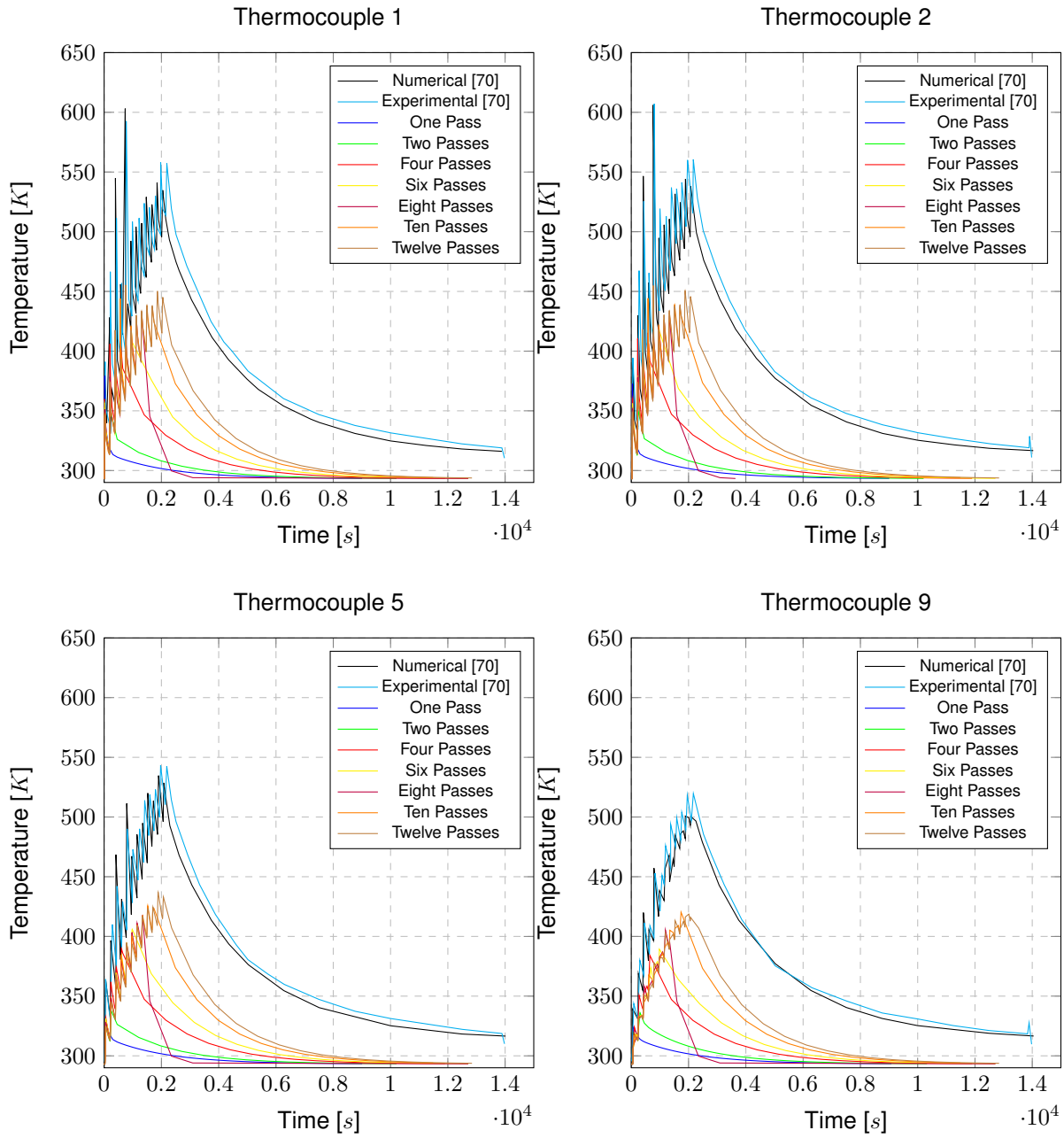

Figure 3.16: Comparable thermal data with the experiments done by Zhang [58]

3.4.1.1 Discussion

For Model 2, the comparison of thermal data between the numerical simulations and the reference paper [58] revealed a discrepancy of 100℃, corresponding to a maximum difference of 25% in results. This discrepancy can be attributed to the lack of precise information regarding the exact location of the thermocouples in the reference paper. Although attempts were made to place the thermocouples at various locations, including the weld toe, a scatter in results of 10% was observed. Moreover, these alternative locations yielded significantly different temperature profiles, indicating the complexity and sensitivity of temperature measurements in the system. Consequently, the original location of the thermocouples used in the numerical simulations was retained.

In addition, the size of thermocouples has a significant impact on the results of thermal evaluations within a butt welding experiment. The influence of thermocouple size on the outcomes of residual stress

assessments in butt welding experiments can be detailed as follows:

- **Spatial Resolution**: Thermocouple dimensions directly affect the spatial resolution of temperature measurements. Smaller thermocouples provide localized temperature data, enabling a more accurate representation of temperature gradients across the weld and heat-affected areas. This accuracy is crucial, as the temperature distribution during welding directly impacts the distribution and magnitude of residual stresses.
- **Thermal Gradient Measurement**: Welding processes involve rapid heating and cooling of the material. Smaller thermocouples are better equipped to capture rapid temperature gradient changes, leading to a more nuanced understanding of the thermal history. Accurately assessing temperature gradients is essential for predicting how the material will experience phase transformations, microstructural changes, and resulting residual stresses.
- **Interference with Welding Process**: The placement of thermocouples can sometimes disrupt the welding process itself. Smaller thermocouples may cause fewer disruptions to heat flow and material movement during welding, minimizing their impact on the process.
- **Averaging Effects**: Larger thermocouples tend to provide more averaged temperature measurements due to their size. This could mask localized temperature variations critical for accurately predicting residual stress patterns. Smaller thermocouples are better at capturing fine temperature details.
- **Material Influence**: The size of thermocouples can affect the local thermal conductivity of the material around them. Smaller thermocouples lead to less disruption in heat flow, providing a more accurate representation of the material's natural behavior during welding. This is crucial for precise modeling of the thermal history and subsequent distribution of residual stresses.
- **Statistical Significance**: Statistical significance is crucial when studying residual stresses. The use of smaller thermocouples can allow for more measurement points within a given area, resulting in a more robust dataset for analyzing residual stress patterns.

In summary, the choice of thermocouple size in a welding experiment significantly influences the accuracy and precision of residual stress results. Smaller thermocouples generally offer advantages in terms of spatial resolution, capturing rapid temperature changes, minimizing interference with the welding process, and providing more detailed data for modeling and analysis. However, practical considerations such as installation ease and the potential introduction of artifacts (unintended distortions or errors) should be balanced when selecting thermocouple size. In this instance, should the discrepancy stem from experimental variables, the utilization of smaller thermocouples may serve to enhance the accuracy of the acquired data.

Should the error originate from computational considerations, a meticulous examination of two key parameters becomes imperative: radiation and conductivity. Conductivity refers to a material's ability to conduct heat. In a welding process, the thermal conductivity of the materials being joined can affect the rate at which heat propagates through the components. This, in turn, affects how temperature changes are distributed across the welded region. Here's how thermal conductivity comes into play:

- **Heat Distribution**: Materials with varying thermal conductivities will exhibit non-uniform heat distribution during welding. A material with high thermal conductivity will rapidly dissipate heat, leading to less heat accumulation and lower temperatures in that region. Conversely, a material with low thermal conductivity will retain heat, resulting in elevated temperatures.
- **Interfacial Effects**: In a butt welding setup, the interface between the two components might have different thermal conductivities. This can lead to temperature gradients across the joint, influencing the distribution of residual stresses and distortions.
- **Heat Sink Effect**: High-conductivity materials can act as heat sinks, drawing heat away from the weld zone and affecting its temperature evolution. This can lead to a significant impact on the overall thermal history and subsequent residual stress development.

Radiation encompasses the transfer of thermal energy between surfaces via electromagnetic waves. This phenomenon is particularly relevant in high-temperature processes like welding, where intense heat sources can emit thermal radiation. The influence of radiation on temperature data is as follows:

- **Non-contact Temperature Measurement**: Welding processes often generate high-intensity heat sources that emit thermal radiation. When measuring temperature using non-contact methods such as infrared thermometry, the emitted radiation can be captured by the measuring instrument. This might lead to overestimation or underestimation of the actual surface temperature if not properly compensated.
- **Absorption and Reflection**: The materials involved in welding can absorb or reflect thermal radiation differently due to their surface properties. This can lead to variations in temperature measurement depending on the type of material being welded.
- **Ambient Conditions**: Radiation heat transfer is influenced by the surroundings and ambient conditions. The presence of shielding gases or the welding environment can alter the radiative heat exchange, influencing the temperature distribution during welding.

Hence, slightly reducing thermal conductivity or a minor increase in radiation can contribute to attaining elevated temperatures within a given context. Alternatively, an effective strategy involves optimizing the material properties of the wire utilized in the weld zone. This strategic manipulation of wire properties can induce variations in heat distribution and dissipation across the plate, ultimately influencing temperature profiles. This approach capitalizes on the intricate interplay between material characteristics and heat transfer dynamics, offering a means to strategically tailor temperature outcomes in pursuit of specific welding objectives.

3.5 Mechanical Model

The predetermined temperature field obtained from the thermal model is utilized to derive the distortions and residual stress field resulting from the welding process. The mechanical analysis involves the adoption of comparable time steps as the thermal analysis, utilizing the "birth and death" principle with the same sequence. The stresses developed during this process arise from the restrained deformations that occur during the expansion and shrinkage of the material. The mechanical model employs elastic-plastic analysis and defines temperature-dependent elastic and plastic material properties.

In the mechanical analysis instead of DC3D8 that are used in the thermal analysis, 8-node linear 3D stress bricks (C3D8R) are defined, and instead of DC3D6 elements 6-node linear triangular 3D stress prisms (C3D6) are defined for welds, both of which consist of translational and rotational degrees of freedom. The number of elements and nodes are the same as the one defined in Table 3.8.

The steps are the same as the ones described in section 3.3.6.

3.5.1 Mechanical properties

When performing a welding simulation in any simulation program, such as Abaqus, as part of a mechanical analysis, it is often necessary to import thermal data from another model. This is because, during the welding process, the material experiences high-temperature changes that can significantly affect its mechanical behavior. By importing thermal data from a separate model, the mechanical analysis can take into account the temperature-dependent material properties, such as Young's modulus, Poisson's ratio, thermal expansion coefficient, and density. This allows for an accurate prediction of the residual stresses and deformation that occur during the welding process, which is crucial in designing and optimizing welded structures. In steel welding simulations, the Young's modulus, which is a measure of the material's stiffness, can change with temperature. As the temperature increases, the Young's modulus of steel can decrease, resulting in less stiffness and greater susceptibility to deformation. Similarly, the Poisson's ratio of steel, which is a measure of the material's lateral contraction under stress, can also change with temperature. This can affect the material's deformation behavior and is important to consider when designing structures that are subject to high temperatures. The thermal expansion coefficient of steel is another important factor to consider in welding simulations. Steel will expand or contract with temperature changes, and the thermal expansion coefficient determines the degree of this expansion or contraction. This can be significant in applications where temperature changes are frequent, such as in pipelines or bridges. Finally, the density of steel can also change with temperature. This can be due to thermal expansion or changes in the material's molecular structure.

Understanding how the density of steel changes with temperature is crucial for accurately predicting the behavior of welded structures subjected to high temperatures.

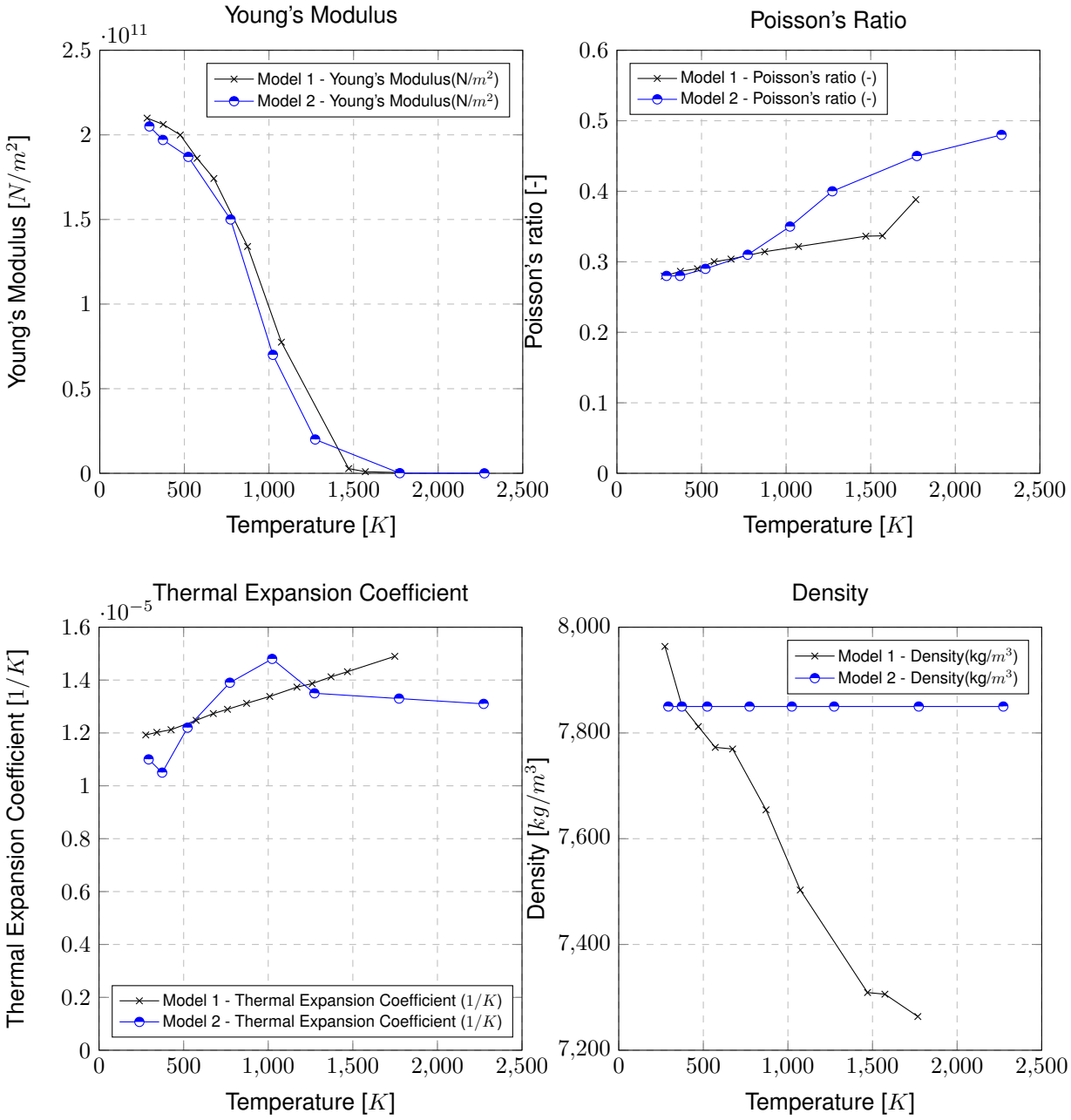

Figure 3.17: Mechanical Properties

In a steel welding mechanical simulation, the yield stress vs. plastic strain graph can provide valuable insights into the behavior of the material at different temperatures. The yield stress represents the stress at which the material starts to deform plastically, while the plastic strain is a measure of the permanent deformation that occurs beyond the material's elastic limit. At lower temperatures, the yield stress of steel is higher, indicating that it can withstand greater amounts of stress before plastic deformation occurs. This means that the material is stiffer and more resistant to deformation at lower temperatures. As the temperature increases, the yield stress of the steel decreases. This is due to the fact that at higher temperatures, the material's microstructure changes, causing it to become softer and more prone to plastic deformation. This can be seen in the graph as a shift to the right, indicating that more stress is

needed to induce plastic deformation. The plastic strain at higher temperatures is also generally higher than at lower temperatures, indicating that the material is more susceptible to permanent deformation. This is due to the fact that at higher temperatures, the material is softer and more ductile, allowing it to deform more easily. Overall, understanding the relationship between yield stress and plastic strain at different temperatures is crucial for accurately predicting the behavior of steel in welding simulations. This information can be used to optimize welding parameters and design welded structures that can withstand the heat, stresses, and strains imposed on them during operation.

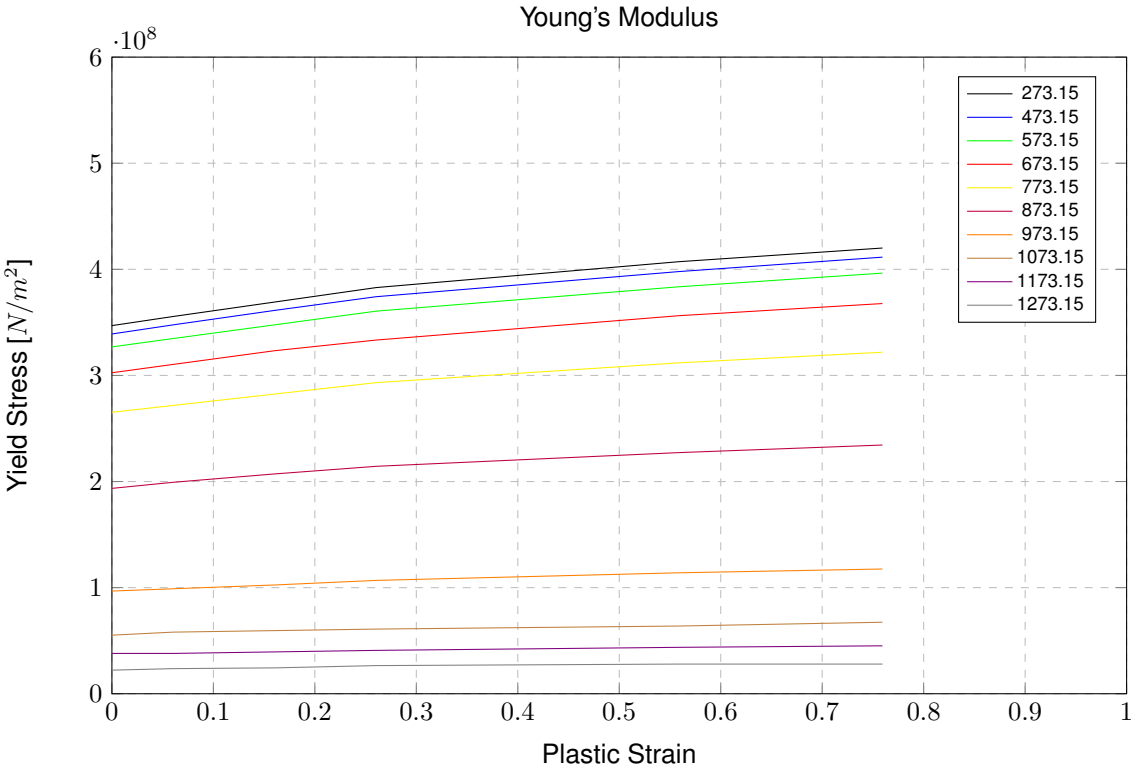

Figure 3.18: Yield stress vs Plastic strain defined for each temperature [K]

3.5.2 Mechanical boundary conditions

The mechanical boundary conditions are shown in Figure 3.20 for the first model and in Figure 3.21 for the second one.

In the welding experiment, for Model 1 weld tabs were placed at both ends of the weld joint, specifically at the starting and runoff points. According to Okano et al. [37], these have minor effects and can be modeled as a local boundary (point or area). The boundary conditions used are clearly shown in Figure 3.20a and Figure 3.20b. It is expected that the points defined in the figures will have zero displacement in the z-direction. This means that the points will not move vertically and will remain fixed at their initial z-coordinates. This condition is commonly known as a "no displacement boundary condition" or "fixed boundary condition" and is often used in engineering and physics to model the behavior of structures or systems under different loads and constraints. In the case of the points in the figure, the no displacement boundary condition may be necessary to ensure that the structural integrity and stability of the system are maintained. Moreover, in order to get a converging solution, one or more points need to be restrained in x and y directions, and these can be seen in Figure 3.20a.

In addition, tack welds are implemented, at the beginning of the simulation in the homonym step. These are placed at the start and end of the plate, in the middle of the weld, with a thickness of 4mm and a length of 5mm (see Figure 3.19).

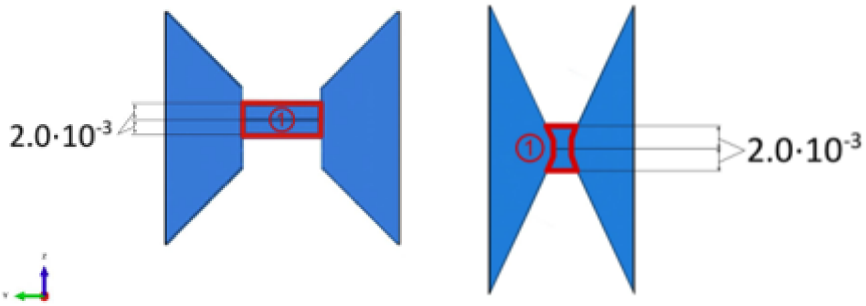

(a) Tack welds Model 1 **(b)** Tack welds Model 2

Figure 3.19: Tack welds dimensions

Tack welds are commonly used in welding for a variety of reasons. Firstly, they help to ensure that the workpieces are properly aligned during the welding process, which is particularly important when welding large or complex structures. Additionally, tack welds provide stability to the workpieces and prevent them from shifting or moving during welding, which can lead to poor-quality welds or defects. Furthermore, tack welds can help to distribute heat evenly across the workpiece, reducing the risk of warping or distortion. Finally, the use of tack welds can improve welding efficiency by allowing the welder to focus on making quality welds rather than spending time aligning the workpieces. In summary, the importance of tack welds in welding cannot be overstated, as they play a crucial role in ensuring that the final weld is of high quality and meets the desired specifications.

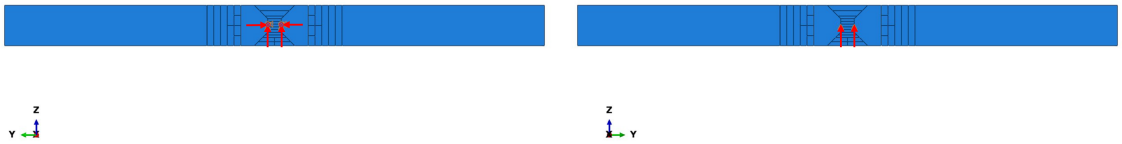

(a) Boundary conditions, Model 1, front **(b)** Boundary conditions, Model 1, back

Figure 3.20: Model 1, Boundary conditions

In Model 2, at least three points are necessary to prevent global translations and rotations. These boundary conditions (see Figure 3.21) include restraining the bottom side of the plate in the front left corner in the z-direction ($u_z = 0$), the front right corner in x, y, and z-directions ($u_x = u_y = u_z = 0$), and the back right corner in the y-direction and z-direction ($u_y = u_z = 0$). These boundary conditions were selected to achieve convergence and prevent excessive deformation during the welding simulation. It is important to note that the specific boundary conditions were selected based on the geometry and material properties of the model, and may not be applicable to other models or simulation setups. The implementation of these boundary conditions is crucial to accurately simulate the welding process and obtain reliable results.

Here again, tack welds are implemented, with the same size and location as Model 1 (at the center of the weld, 4mm thick and 5mm long).

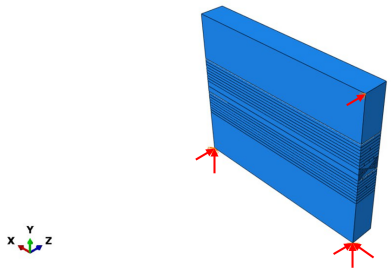

Figure 3.21: Boundary conditions, Model 2, bottom

3.6 Results

In Figure 3.22 and Figure 3.23 the location of where the results are extrapolated in the two models are given. In model one, residual stresses are taken perpendicular to the weld in the middle of the plate, while in model two, residual stresses are studied both longitudinally and perpendicularly to the weld, and vertical distortions are studied along the line perpendicular to the weld (i.e., "path 1"). Furthermore, an examination of transverse shrinkage is conducted for the left edge of the plate, while the longitudinal deformation is analyzed at the edge where x=0. The contour plots for all the results can be found inAppendix E. For convenience, the results were converted back to mm, in order to be able to display also the residual stresses in MPa. All the results are taken at the last step of the analysis, precisely at the end of the last cooling step.

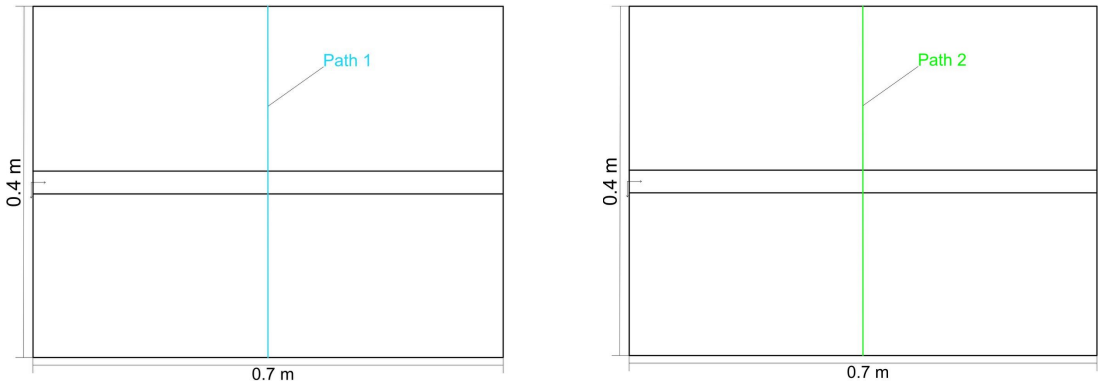

(a) Path 1 Top **(b)** Path 2 Bottom

Figure 3.22: Model 1, Paths for results

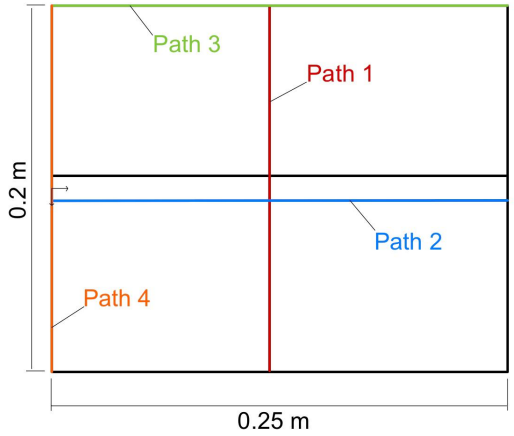

Figure 3.23: Model 2, Paths for results

3.6.1 Distortions

In this chapter the distortions only for model 2 will be given as these are used to prove the experimental results by Zhang et al. [58]. The contour plots for the distortions for both the models can be found in Appendix E.

In Figure 3.24 the longitudinal shrinkage along path 4 for model 2 is displayed. As for the one pass model, only one side is welded the results are slightly different compared to the other simulations, in fact some compression can be seen at the edges of the plate. The models with six and eight have more deformation along y than the ten and twelve passes ones. A narrower tensile zone can be seen here because of the finer mesh. The results for the 12 passes model has slightly higher deformations, around double than what the original model has found.

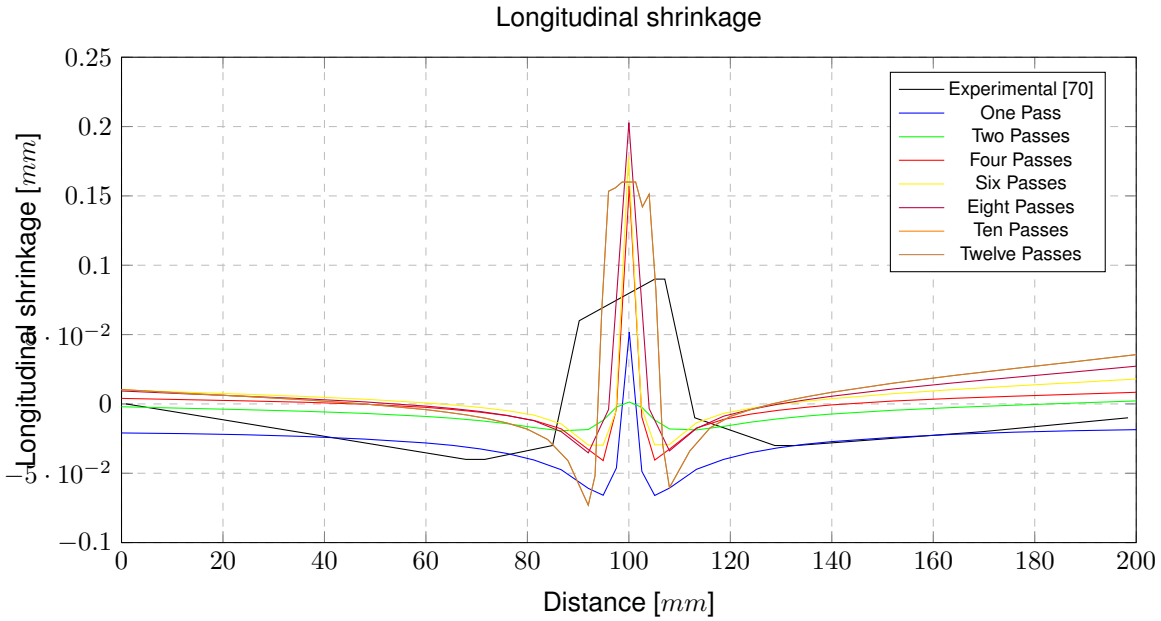

Figure 3.24: Longitudinal shrinkage comparison - Path 4

The visual representation of the transverse shrinkage along path 3 for model 2 is presented in Figure 3.25. In all the modeled simulations the results for this path will not go above 3mm. It can be clearly seen how this was not the case for the original model, with a deformation along x between 1.1mm and 1.5mm.

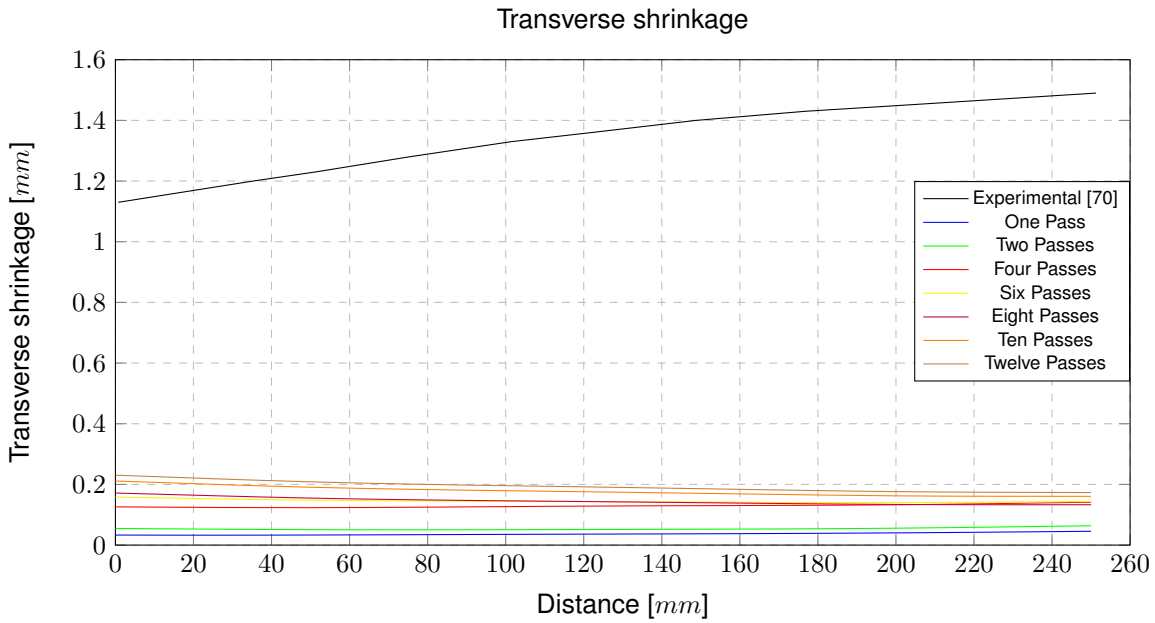

Figure 3.25: Transverse shrinkage comparison - Path 3

In Figure 3.26, a graphical depiction of the vertical deformation along path 1 for model 2 is displayed. The one-pass model shows an uplift in the outer region, which is logical given that only a single welding pass is applied to the top surface. Differently, the other models have a negative displacement as the original model. Again, the maximum value retrieved in the simulations is lower than the one found in the original model.

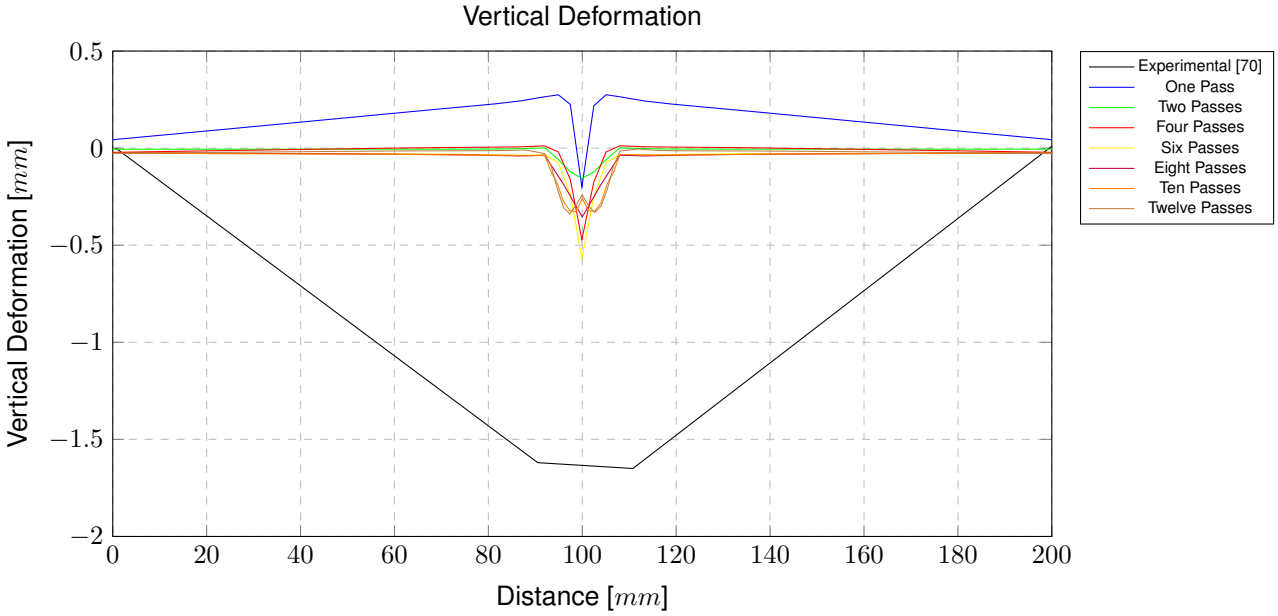

Figure 3.26: Vertical deformation comparison - Path 1

An overview of all the distortion for both the models is given in Table 3.13.

Table 3.13: Overview deformations

	Number of passes	Maximum u_x [mm]	Minimum u_x [mm]	Maximum u_y [mm]	Minimum u_y [mm]	Maximum u_z [mm]	Minimum u_z [mm]
Model 1	1	0,1245	1,867	0,4607	0,4961	3,493	0,2135
Model 1	2	7,553	1,469	0,365	0,5649	0,7143	1,348
Model 1	3	1,322	1,352	0,3995	0,4873	0,7635	1,269
Model 1	5	2,123	1,087	4,861	0,3045	0,8221	2,527
Model 1	7	2,607	1,509	4,496	0,3543	0,7546	2,445
Model 2	1	1,772	0,4024	0,1364	0,1072	0,4335	0,2759
Model 2	2	0,47	0,9875	0,03716	0,1081	0,1855	0,1564
Model 2	4	0,4285	0,5665	0,06796	0,1902	0,625	0,6974
Model 2	6	0,6339	1,285	0,5373	0,1998	0,5773	0,5151
Model 2	8	0,8323	0,8078	0,03483	0,1986	0,3568	0,3097
Model 2	10	0,6821	0,6945	0,05126	0,2664	0,3476	0,3009
Model 2	12	0,7392	0,7069	0,06595	0,2799	0,3615	0,3099

3.6.1.1 Discussion

The observed shrinkage and distortions in Model 2 deviate from the expected results observed in the experimental studies. This discrepancy suggests that there may be factors or variables not fully captured or accurately represented in the numerical model. These disparities between the simulated and experimental results highlight the complexity and intricacies of the real-world phenomena being investigated. However, it is crucial to note that despite the observed differences in shrinkage and distortions, the residual stresses obtained from Model 2 exhibit a consistent alignment with each other. This consistency implies that the numerical model successfully captures the underlying stress distribution within the system. The agreement in residual stress patterns demonstrates the capability of the model to accurately simulate and predict the residual stresses in the analyzed structure.

3.6.2 Residual stresses

In this section the residual stresses results for both models will be discussed. In the context of this discussion, the terms "longitudinal" and "transverse" refer to the directions of the residual stresses along the x-axis (s11) and y-axis (s22), respectively.

The longitudinal residual stresses (s11) represent the stresses acting parallel to the welding direction or the primary axis of the plate. These stresses are observed along the perpendicular path to the weld on the top and bottom surfaces of the specimen. They provide insights into the magnitude and distribution of stresses in the direction of the weld, which is crucial for assessing the structural integrity and performance of welded components.

On the other hand, the transverse residual stresses (s22) represent the stresses acting perpendicular to the welding direction or the secondary axis of the plate. These stresses are observed along paths that are perpendicular to the weld on the top and bottom surfaces of the specimen. They provide information about the stresses exerted in the transverse direction, which is orthogonal to the weld. Understanding these stresses is essential for evaluating the potential for distortion, warping, and dimensional changes in the welded structure.

By investigating both the longitudinal (s11) and transverse (s22) residual stresses, a comprehensive analysis of the stress distribution in the welded structure can be obtained. This information is critical for evaluating the mechanical behavior, structural performance, and potential failure mechanisms of thick plate components subjected to welding processes. In Figure 3.27 the longitudinal residual stresses for model 1 along the perpendicular path to the weld on the top of the specimen are given. It can be seen how the peaks are close to the results found in the simulations by Qiang et al.[41] but higher than the experiments. In addition, it can be seen how the compressive residual stresses increase proportionally with the number of passes at the edges of the plate.

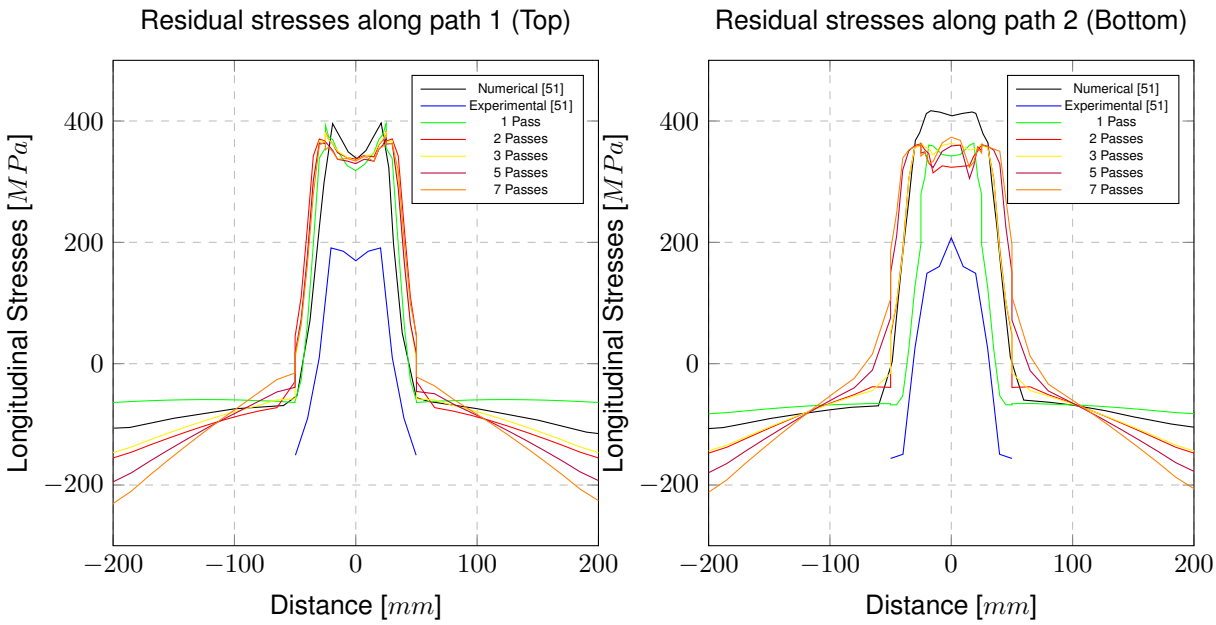

(a) Residual stresses along Path 1 (Top)

(b) Residual stresses along Path 2 (Bottom)

Figure 3.27: Model 1, Longitudinal residual stresses

The transverse residual stresses for model 1 along the path parallel and perpendicular to the weld on the top of the specimen are illustrated in Figure 3.28. In this instance, unlike the longitudinal stresses, the experimental outcomes for path 1 are greater than the numerical outcomes. Nonetheless, the achieved results remain in proximity to the numerical ones. Along path 2, the compressive zone in the middle of the model aligns with the experimental results; however, the peaks of the tensile stresses are lower than those obtained in the experiments.

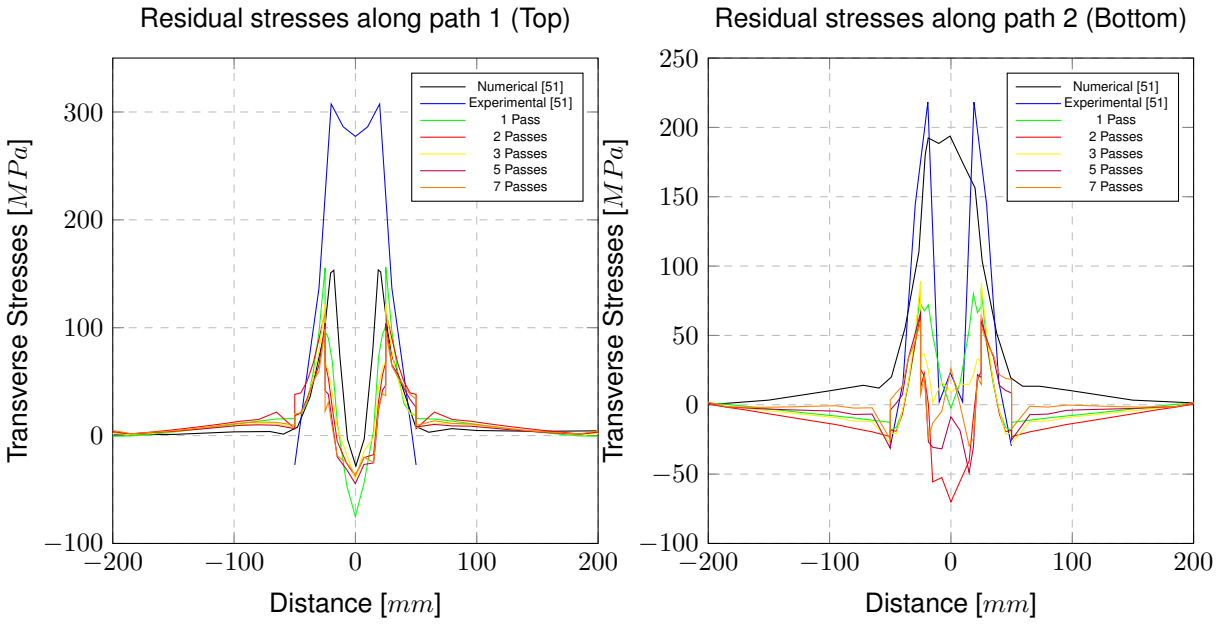

(a) Residual stresses along Path 1 (Top)

(b) Residual stresses along Path 2 (Bottom)

Figure 3.28: Model 1, Transverse residual stresses

Figure 3.29 presents a visualization of the longitudinal residual stresses in Model 2 along the paths parallel and perpendicular to the weld on top of the specimen. On both paths, except for the two-pass

model, the outcomes obtained are similar to those obtained by Zhang [58].

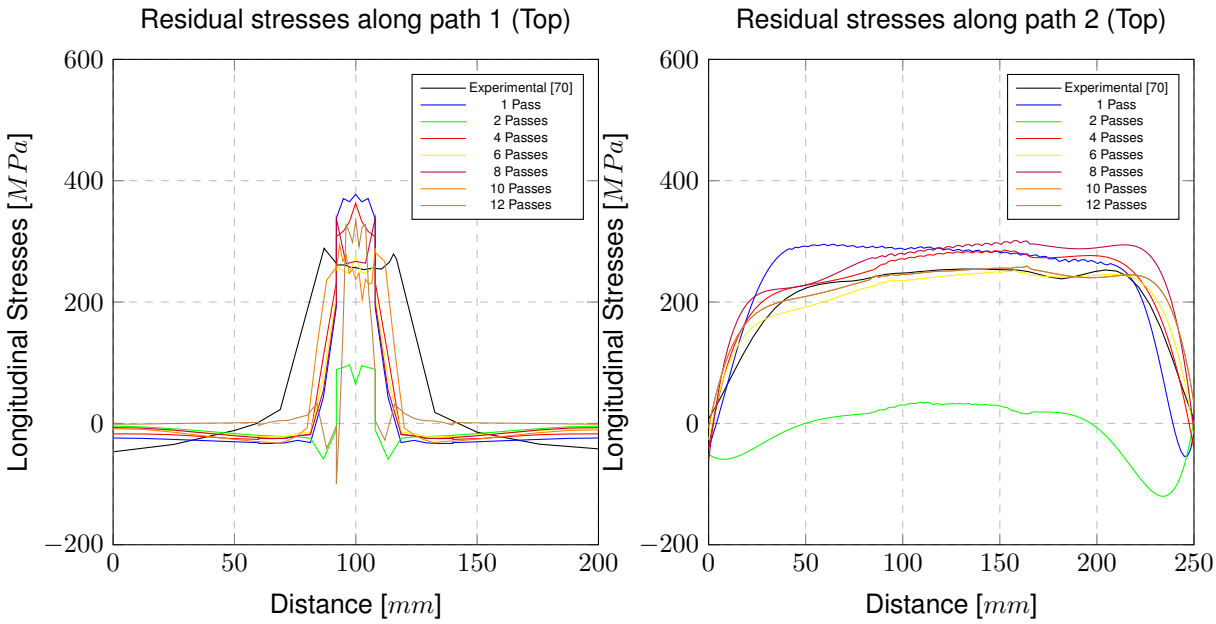

(a) Residual stresses along Path 1 (Top)

(b) Residual stresses along Path 2 (Top)

Figure 3.29: Model 2, Longitudinal residual stresses

The transverse residual stresses in model 2, along both the paths parallel and perpendicular to the weld, on the top surface of the specimen are illustrated in Figure 3.30. Just as in Figure 3.29, the results obtained along both paths, except for the two-pass model, are comparable to those achieved experimentally. Moreover, the model with one pass demonstrates a slightly compressive zone that is absent in the model with 12 passes.

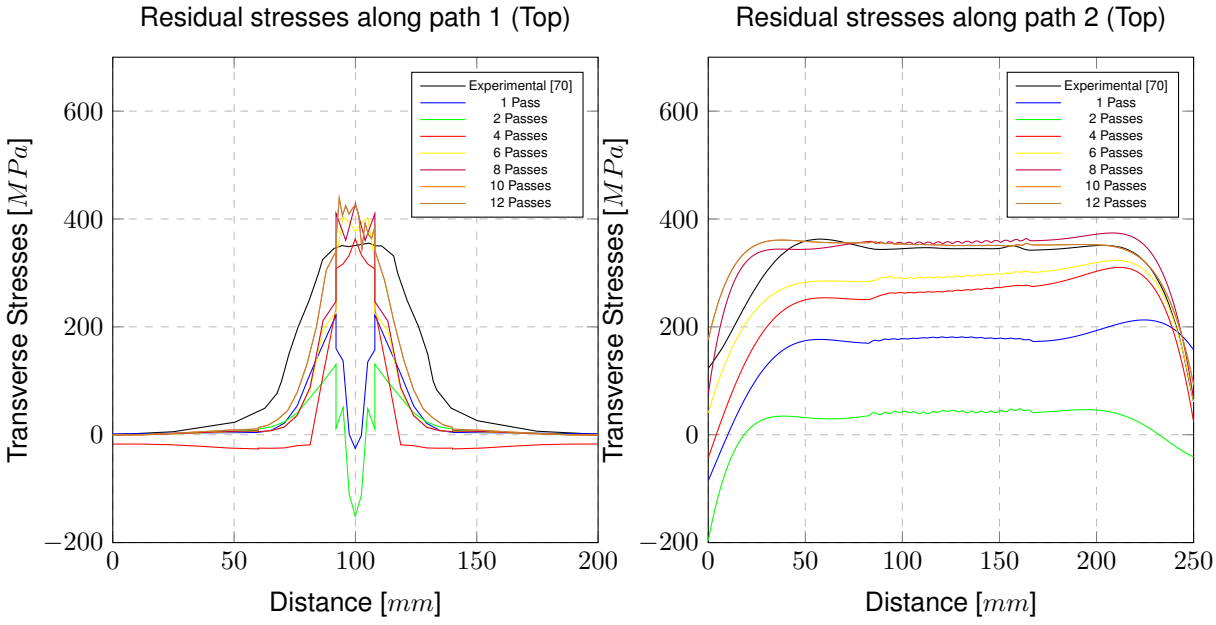

(a) Residual stresses along Path 1 (Top)

(b) Residual stresses along Path 2 (Top)

Figure 3.30: Model 2, Transverse residual stresses

To sum up, Table 3.14 presents the maximum and minimum values for both models across the entire

plate.

Table 3.14: Overview residual stresses

	Number of passes	Maximum longitudinal stress [N/mm^2]	Minimum longitudinal stress [N/mm^2]	Maximum transverse stress [N/mm^2]	Minimum transverse stress [N/mm^2]
Model 1	1	506,99	-1442,23	311,68	-1701,22
Model 1	2	508,83	-1355,63	288,13	-1626,99
Model 1	3	658,77	-602,05	364,34	-815,40
Model 1	5	694,53	-639,97	394,21	-815,32
Model 1	7	1929,82	-1041,38	1594,53	-1391,39
Model 2	1	561,69	-217,95	528,98	-471,17
Model 2	2	714,45	-217,66	636,37	-524,18
Model 2	4	887,34	-916,10	529,16	-1268,95
Model 2	6	1473,91	-1460,90	1188,35	-1837,42
Model 2	8	2112,57	-1313,01	2152,51	-1758,01
Model 2	10	1484,31	-1543,19	850,36	-1959,11
Model 2	12	1117,08	-1616,29	487,92	-641,59

3.6.2.1 Discussion

A comprehensive exposition of the outcomes pertaining to residual stresses will be presented herein. The residual stresses observed in Model 1 are consistent with the numerical results reported in the reference paper [41]. Specifically, the transverse residual stresses along Path 1 for the 7-pass model deviated from the reference simulation by only 20%. However, a notable discrepancy arises when comparing the numerical values, which peak at around 150 MPa, with the experimental values that exceed double that magnitude (305 MPa). This indicates that the numerical model underestimates the actual transverse residual stresses in the system. Similar deviations are observed in the longitudinal residual stresses along the same path. The 7-pass model shows a 15 MPa deviation from the reference simulation, but again, it significantly surpasses the experimental values (200 MPa vs. 400 MPa). Moreover, an interesting trend is observed, where the compression at the plate's edges increases with an increase in the number of passes. These findings highlight the limitations of the numerical model in accurately capturing the exact magnitude of residual stresses compared to experimental data. The numerical results align reasonably well with the reference simulations but fail to fully replicate the higher values observed in experiments. Further improvements to the numerical model and potential refinements in the modeling approach are recommended to better reconcile the disparities and enhance the accuracy of residual stress predictions.

At the bottom surface of the plate, specifically along path 2 of Model 1, a good agreement between the numerical simulations and experimental data is observed for the longitudinal residual stresses. The one-pass simulation shows a thinner region experiencing higher stresses, which aligns well with the experimental observations. The maximum discrepancy between the different models created in Abaqus is 35 MPa. Moreover, similar to the previous cases, an increasing compression is observed at the sides of the plate due to multiple cooling processes. It is worth noting that the numerical simulations consistently yield double the reference experimental values (200 MPa vs. 400 MPa). In contrast, for the transverse stresses along the same path, some differences are observed. Firstly, all five simulations exhibit values half of those reported by Qiang et al. [41]. The experiments show no compression, while the simulations indicate tension values of around 200 MPa. In the simulations conducted in this thesis to investigate the influence of welding passes on the results, it is observed that all the models display tension values around 100 MPa, but with an increased compression at the middle of the plate as the number of passes increases. These findings highlight the complex nature of residual stresses and the challenges in accurately capturing their behavior through numerical simulations. While there is generally good agreement between the numerical results and experimental data for the longitudinal stresses, discrepancies arise in the transverse stresses. Further investigation and refinement of the modeling approach are recommended to improve the accuracy of the transverse stress predictions and better understand the underlying factors influencing their distribution.

In Model 2, a high level of agreement is observed in the results. Specifically, for the longitudinal residual stresses along Path 1, except for the simulation with two passes, all the other seven simulations show similar results to the experimental data, with a maximum scatter of 26%. The peaks in the stress distribution are slightly narrower compared to the reference model, with varying trends in stresses. The one-pass simulation exhibits the highest stress value at around 380 MPa, while the ten-pass simulation shows the closest results with a peak difference of only 2%. Regarding the transverse residual stresses along Path 1, excluding the first two models with one and two welding passes, the results align closely with the experimental data, with a maximum error of 19.5%. The specimen exhibits compression in the

middle region, but the stress distribution undergoes a change from the four-pass simulation onwards. Notably, the four-pass simulation produces the closest match to the experimental data obtained by Zhang et al. [41]. The peaks observed in the simulations are narrower compared to the experimental data, indicating more localized stress concentration in the middle region of the plate. Overall, these findings demonstrate the effectiveness of Model 2 in capturing the behavior of residual stresses in thick plates. The simulations show a high degree of agreement with experimental data, albeit with some localized differences in stress distribution. These results provide valuable insights into the influence of welding passes on the residual stress patterns and offer a basis for further analysis and optimization of welding processes in thick plate structures.

Along path 2 in Model 2, which corresponds to the right weld line, the longitudinal residual stresses of the various analyses exhibit a good agreement with the results, except for the two-pass simulation. The six-pass and eight-pass simulations yield the closest results, with a maximum scatter of only 3%. These findings indicate the robustness of the numerical model in capturing the longitudinal residual stresses along this path, with a high level of consistency among the simulations. Regarding the transverse stresses, it is observed that the two-pass simulation produces the lowest results, suggesting that further modifications to the mesh configuration may be necessary to improve the accuracy of the simulation in this area. However, from the one-pass simulation onwards, the stresses increase with the number of passes. Notably, a good agreement with the experimental data is achieved at approximately 370 MPa with the eight-pass, ten-pass, and twelve-pass models. It is interesting to observe that the last two models exhibit the same stress values, mirroring the trend observed in the longitudinal stresses along path 2. These results indicate that the numerical model in Model 2 can effectively capture the longitudinal and transverse residual stresses along the right weld line. The simulations demonstrate a consistent pattern of stress distribution with increasing numbers of welding passes, and the agreement with the experimental data provides confidence in the accuracy and reliability of the model. These findings offer valuable insights for the optimization of welding processes and the design of thick plate structures in practical applications.

4

Numerical Simulations - Pores

This chapter examines a modified iteration of Model 2. Specifically, 19 welding simulations were conducted in Abaqus FEA to investigate the impact of various pore sizes and configurations on the residual stresses and distortions observed in a thick plate.

4.1 Dimensions and Partitions

The models examined in this chapter are based on the framework established by Model 2. However, certain distinctions exist between them. While the material, plate dimensions, heat source parameters and size, boundary conditions (both thermal and mechanical), welding procedure, and construction methodology (steps) of the model remain consistent with the depiction outlined in Chapter 3 for the second model, there are some notable variations. In fact, many pores configurations were analyzed; These are displayed in Figure 4.5 and Figure 4.7.

The study encompassed the comparison of five different pore sizes, ranging from 0.5mm to 4mm. Each pore was positioned at the center, denoted by coordinates (x=0.125m, y=0m, z=-0.006m). Furthermore, three arrangements were examined: two pores of 1mm each, and one configuration with three linear pores, all 1mm in size. Two distinct meshes were used for each simulation, and their impact on the results was evaluated.

In the first mesh, the pores were located at three specific positions: (x=0.0625m/0.125m/0.1875m, y=0m, z=-0.006m), depending on the configuration. The symbols X and O in Figure 4.5 and Figure 4.7 represented locations with and without a pore, respectively. For instance, configuration XXX implied the presence of three sequential 1mm pores positioned at (x=0.0625m, y=0m, z=-0.006m), (x=0.125m, y=0m, z=-0.006m), and (x=0.1875m, y=0m, z=-0.006m). On the other hand, configuration XOX indicated the absence of a pore in the middle but with pores at the first and last positions.

In the second mesh, since the pores were too distant to impact residual stresses, three new pore locations were investigated: (x=0.122m/0.125m/0.128m, y=0m, z=-0.006m), depending on the configuration. Here, each pore was 1mm away from the next one.

Finally, a simulation with five linear pores was conducted to observe the effects of increased pore quantity on the outcomes. The coordinates of the center of each 1mm pore, in this case, were (x=0.119m/0.122m/0.125m/0.128m, y=0m, z=-0.006m).

In the welding simulation, a total of 19 models were analyzed, considering only a single welding pass. This approach aimed to create a simplified model that primarily focused on the pores rather than the welding passes. The analysis of multiple welding passes was previously addressed in Chapter 3 of the study.

The plate dimensions are given in Figure 4.1. In these models two different meshes were studied: the first one was divided into three main parts (see Figure 4.1b) and the second one is divided into four parts (see Figure 4.1d), all constrained to each other using tie constraints.

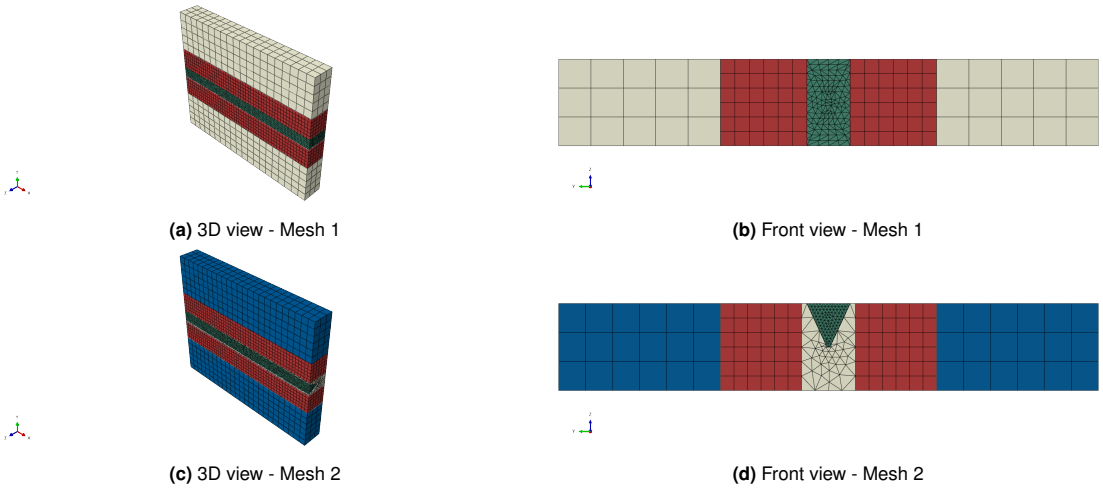

(a) 3D view - Mesh 1

(b) Front view - Mesh 1

(c) 3D view - Mesh 2

(d) Front view - Mesh 2

Figure 4.1: Model Partitions

4.2 Thermal properties and Boundary conditions

The thermal properties used for all the models are given in Figure 3.13. During the simulation, the calculation took into account the inclusion of the latent heat of fusion, which was designated as 300000 J/kg when the liquid temperature was 1808.15 Kelvin and the solid temperature was 1773.15 Kelvin. The reference point for absolute zero temperature was established as 0 Kelvin, and the Stefan-Boltzmann constant was assigned a value of 5.67E-08 $W/(m^2K^4)$.

The thermal framework utilized in this scholarly investigation encompassed two fundamental physical mechanisms, namely surface radiation and convection. In order to establish the thermal boundary conditions, the study took into account the dissipation of heat from all surfaces through both convection and radiation. The heat transfer coefficient was determined as $15W/(m^2K)$, and the emissivity was assigned a value of 0.85. Additionally, the ambient temperature was maintained at 293.15 Kelvin. It is crucial to acknowledge that these specified values govern the dissipation of heat to the cooler surrounding regions. For the thermal load, the heat flux parameters are the same as Model 2, given in Table 3.10. Goldak's model is utilized for the purpose of replicating the motion of a heat source, while the parameters associated with the dimensions of the welding arc were adjusted according to empirical findings and incorporated into the DFLUX subroutine. Below, in Table 4.1 the location of the heat through the thickness of the specimen is given. The torch then stays at the same position on Z and Y and moves along X at a welding speed of 0.007 m/s.

Table 4.1: Torch location through thickness [m], 1 Pass, Model 1

	Torch height Z	Torch offset Y
Pass 1	-0,004	0

4.3 Steps

Each simulation procedure comprised multiple steps, summarized in Table 4.2, one of which involved deactivating welds during the pre-step using the "model change" command. To accurately represent the application of tack welds at the beginning and end of the plate, a static heating step called "Tack welds" was introduced (as in Model 2, see Figure 3.19). The inner areas of the plate, depicted in green in Figure 4.1d and Figure 4.1c are divided into ten element sets along their length in the Abaqus software. Each set consisted of elements with a length of 25 mm. This division enabled the deactivation of all elements along the weld length and initiated the thermal analysis.

As the simulation progressed, weld elements were gradually reactivated with each time step, simulating the formation of welds. The weld region had a fine mesh and a significant number of elements, necessitating the development of a Python code. This code automatically selected and placed a specific number of elements into an element set. For further reference, the code can be found in Appendix A.

Table 4.2: Welding steps

Action	Duration t [s]	Current I [A]	Voltage U [V]	Welding speed v [m/s]	Heat input Q [J/m]
Pre-step	1.00E-06	-	-	-	-
Tack welds	1.00E-06	-	-	-	-
Pass 1	62.5	140	23	0,004	2254
Cooling 1	15000	-	-	-	-
	Total [s]				
	15062.5				

4.4 Mechanical properties and Boundary conditions

By incorporating thermal data from a distinct model, the mechanical analysis is capable of considering material properties that vary with temperature, including Young's modulus, Poisson's ratio, thermal expansion coefficient, and density. This integration enables precise forecasting of the residual stresses and deformations that transpire throughout the welding procedure. The mechanical properties of the model can be found in Figure 3.17 and Figure 3.18.

To prevent global translations and rotations, a minimum of three boundary conditions are required. In this case, the specified boundary conditions (given in Figure 3.21 involve constraining specific regions of the plate. These conditions consist of: restraining the bottom side of the plate in the front left corner along the z-direction, denoted as $u_z = 0$; restraining the front right corner of the plate in all three directions, namely x, y, and z, indicated as $u_x = u_y = u_z = 0$; restraining the back right corner of the plate in the y-direction and z-direction, given as $u_y = u_z = 0$. These particular boundary conditions were deliberately chosen to ensure convergence and prevent excessive deformation during the welding simulation.

4.5 Mesh

In order to ensure the integrity of the model and achieve a specific type of mesh throughout the thickness of all the models, divisions were implemented as depicted in Figure 3.10, where the single weld pass is the only one considered (top left).

Distinct types of meshes were generated for each zone of the models. These variations in mesh types are clearly illustrated in Figure 4.2 and Figure 4.3.

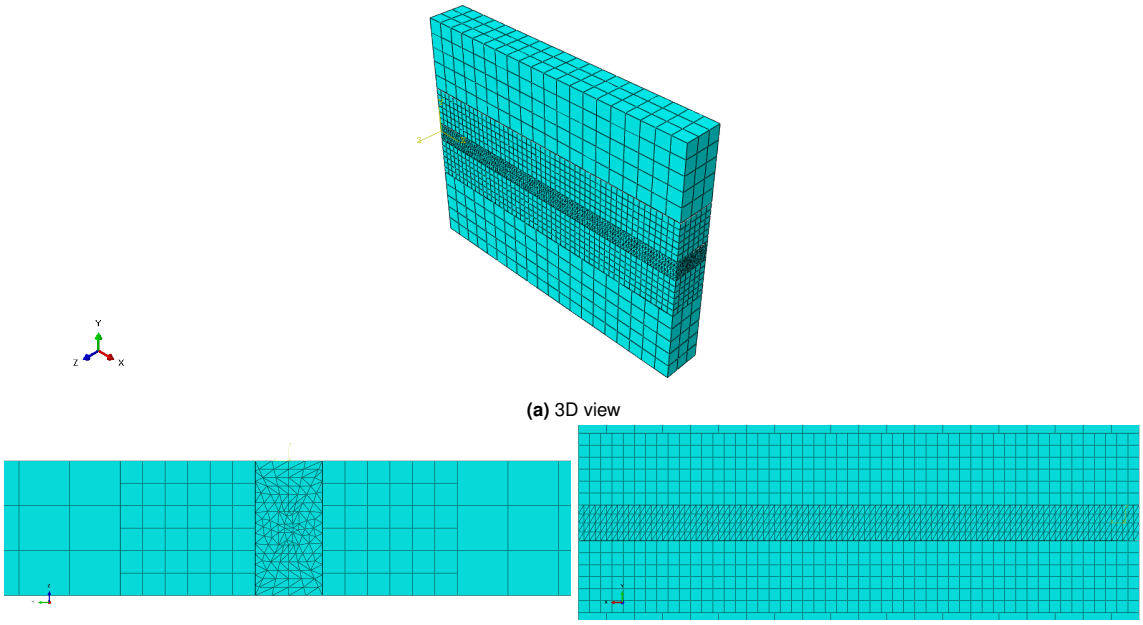

(a) 3D view

(b) Front view

(c) Top view

Figure 4.2: General model - Mesh 1

As it can be clearly seen in Figure 4.3, noticeable alterations have been made to the mesh configuration within the internal partition. Specifically, the second mesh iteration exhibits deliberate modifications intended to optimize model performance in terms of execution time, while simultaneously ensuring minimal output file dimensions. This optimization strategy involves reducing the element size around the pore by half, thereby achieving finer resolution in that specific region. Conversely, in areas where a high level of mesh refinement is unnecessary, the element size has been doubled in comparison to the initial Mesh 1 configuration.

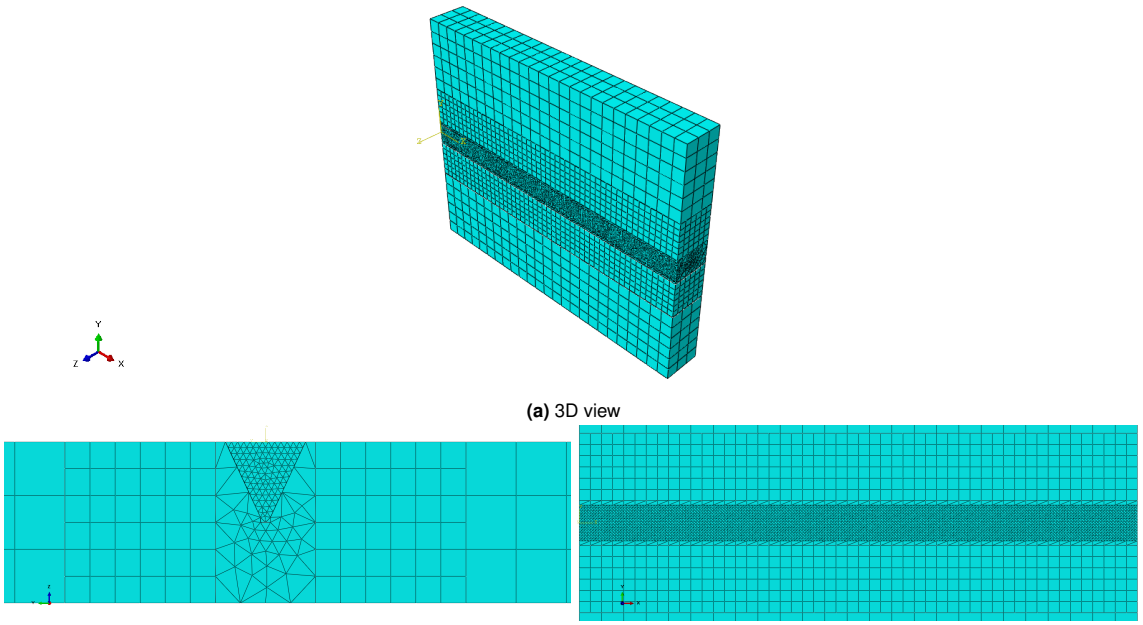

(a) 3D view

(b) Front view

(c) Top view

Figure 4.3: General model - Mesh 2

The mesh subdivision, categorized by element type, is visually represented in Figure 4.4. In the

case of Mesh 1, the inner region (depicted in light grey) incorporates DC3D10 elements, specifically 10-node quadratic tetrahedral elements, for thermal analysis, while C3D10 elements are utilized for mechanical analysis. These elements possess an element size of 2.5mm. The outer zone (depicted in green) comprises DC3D8 elements, namely 3D 8-node linear isoparametric elements, for thermal analysis, and C3D8 elements for mechanical analysis. Within the middle partition, the element size measures 5mm, while in the outermost area, it increases to 10mm. The precise count of elements can be found in Table 4.3.

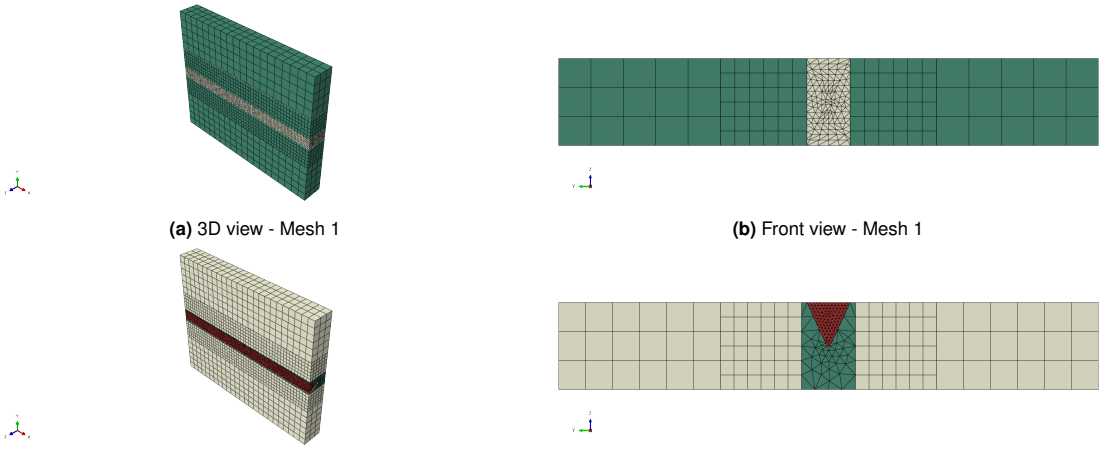

(a) 3D view - Mesh 1

(b) Front view - Mesh 1

(c) 3D view - Mesh 2

(d) Front view - Mesh 2

Figure 4.4: Element types

Table 4.3: Mesh 1 - Overview

Number of pores	Configuration	Size	Element type (D)C3D8	Element type (D)C3D10	Total Nodes	Total Elements
1	0X0	0.5mm	4200	68188	104306	72388
1	0X0	1mm	4200	63581	98124	67781
1	0X0	2mm	4200	70125	107682	74325
1	0X0	3mm	4200	70293	110370	74493
1	0X0	4mm	4200	65234	100335	69434
2	XX0	1mm	4200	68148	104217	72348
2	X0X	1mm	4200	68183	104266	72383
2	0XX	1mm	4200	68000	104027	72200
3	XXX	1mm	4200	67889	103886	72089

In the case of Mesh 2, an additional type of element, C3D4 (4-node linear tetrahedral element), is introduced. This choice aims to expedite the simulation process while increasing the mesh size in an area deemed less critical. For the welding area (depicted in red), 1.25mm DC3D10 and C3D10 elements are selected for thermal and mechanical analysis, respectively. In the lower part of this zone (depicted in green), 5mm DC3D4 and C3D4 elements are employed for thermal and mechanical analysis. Lastly, in the white area, DC3D8 and C3D8 elements are utilized for thermal and mechanical analysis, respectively, with the inner elements measuring 5mm and the outer elements measuring 10mm. The precise number of elements can be found in Table 4.4.

Table 4.4: Mesh 2 - Overview

Number of pores	Configuration	Size	Element type (D)C3D4	Element type (D)C3D8	Element type (D)C3D10	Total Nodes	Total Elements
1	0X0	0.5mm	9376	4500	107995	170597	121871
1	0X0	1mm	9376	4500	107861	170439	121737
1	0X0	2mm	9376	4500	108840	171849	122716
1	0X0	3mm	9376	4500	108332	171223	122208
1	0X0	4mm	9376	4500	108037	170804	121913
2	XX0	1mm	9376	4500	109266	172328	123142
2	X0X	1mm	9376	4500	110698	174256	124574
2	0XX	1mm	9376	4500	109519	172677	123395
3	XXX	1mm	9376	4500	110493	174015	124369
5	XXXXX	1mm	9376	4500	114270	179098	128146

To have an insight of how the pores look along the length, some cut of the model along x (in the middle of the plate, y=0) are shown in Figure 4.5 for the first mesh.

(a) 0.5mm pore, CUT

(b) 1mm pore, CUT

(c) 2mm pore, CUT

(d) 3mm pore, CUT

(e) 4mm pore, CUT

(f) 1mm pores - XXO configuration, CUT

(g) 1mm pores - OXX configuration, CUT

(h) 1mm pores - XOX configuration, CUT

(i) 1mm pores - XXX configuration, CUT

Figure 4.5: Sections displaying the pores configuration - Mesh 1

In Figure 4.6, a detailed view of the mesh around the pores is presented for each configuration in the first model. The pores are identified with a crescent "x" symbol. It is important to note that the naming convention assigns "Pore 1" to the pore with the lowest x value, while "Pore 3" refers to the pore closest to the end of the plate. This labeling scheme allows for clear identification and differentiation of the individual pores within the model.

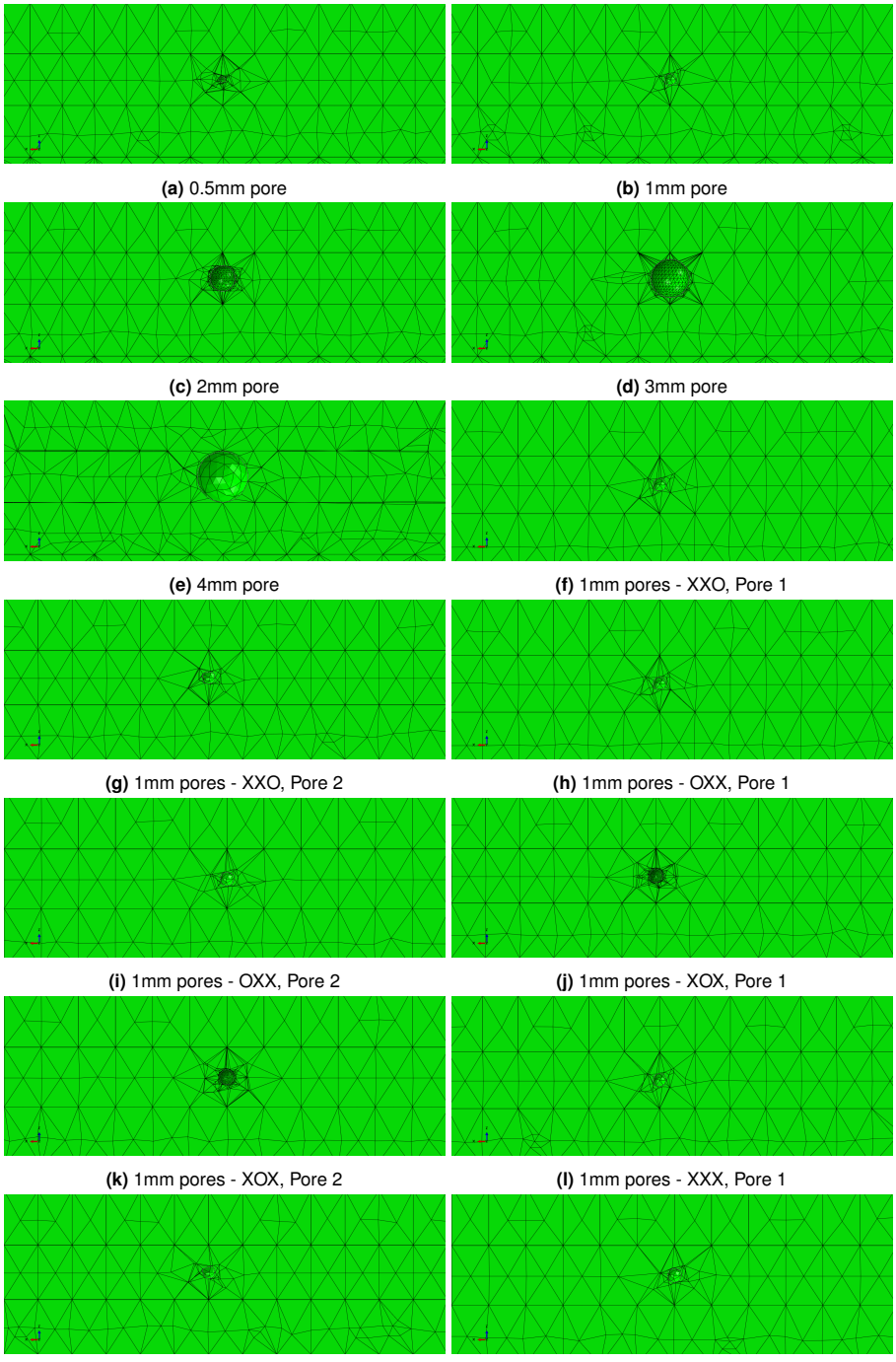

(a) 0.5mm pore **(b)** 1mm pore **(c)** 2mm pore **(d)** 3mm pore **(e)** 4mm pore **(f)** 1mm pores - XXO, Pore 1 **(g)** 1mm pores - XXO, Pore 2 **(h)** 1mm pores - OXX, Pore 1 **(i)** 1mm pores - OXX, Pore 2 **(j)** 1mm pores - XOX, Pore 1 **(k)** 1mm pores - XOX, Pore 2 **(l)** 1mm pores - XXX, Pore 1 **(m)** 1mm pores - XXX, Pore 2 **(n)** 1mm pores - XXX, Pore 2

Figure 4.6: Sections displaying the pores - Mesh 1

For the second mesh, to gain a visual understanding of the pore distribution along the length of the model, cross-sectional cuts along the x-axis (specifically in the middle of the plate, y=0) are presented in Figure 4.7. These cut sections provide insight into the spatial arrangement of the pores within the model.

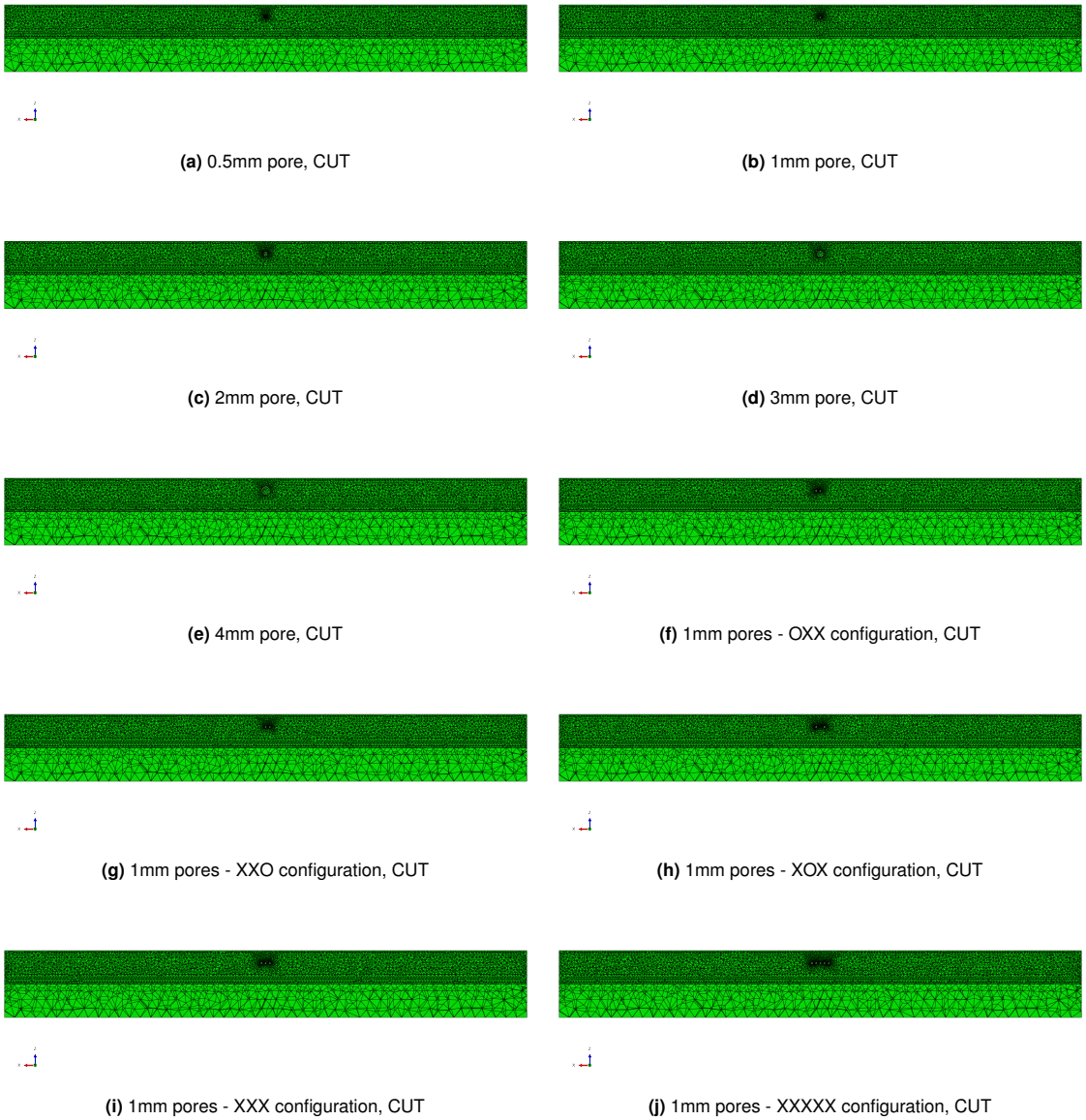

(a) 0.5mm pore, CUT

(b) 1mm pore, CUT

(c) 2mm pore, CUT

(d) 3mm pore, CUT

(e) 4mm pore, CUT

(f) 1mm pores - OXX configuration, CUT

(g) 1mm pores - XXO configuration, CUT

(h) 1mm pores - XOX configuration, CUT

(i) 1mm pores - XXX configuration, CUT

(j) 1mm pores - XXXXX configuration, CUT

Figure 4.7: Sections displaying the pores configuration - Mesh 2

Displayed in Figure 4.8 is a close-up view of the mesh surrounding the pores for each configuration in the second model. Similar to the previous model, the pores are marked with a crescent "x" symbol for identification purposes. This visualization allows for a detailed examination of the mesh refinement and arrangement around each pore in the second model configuration.

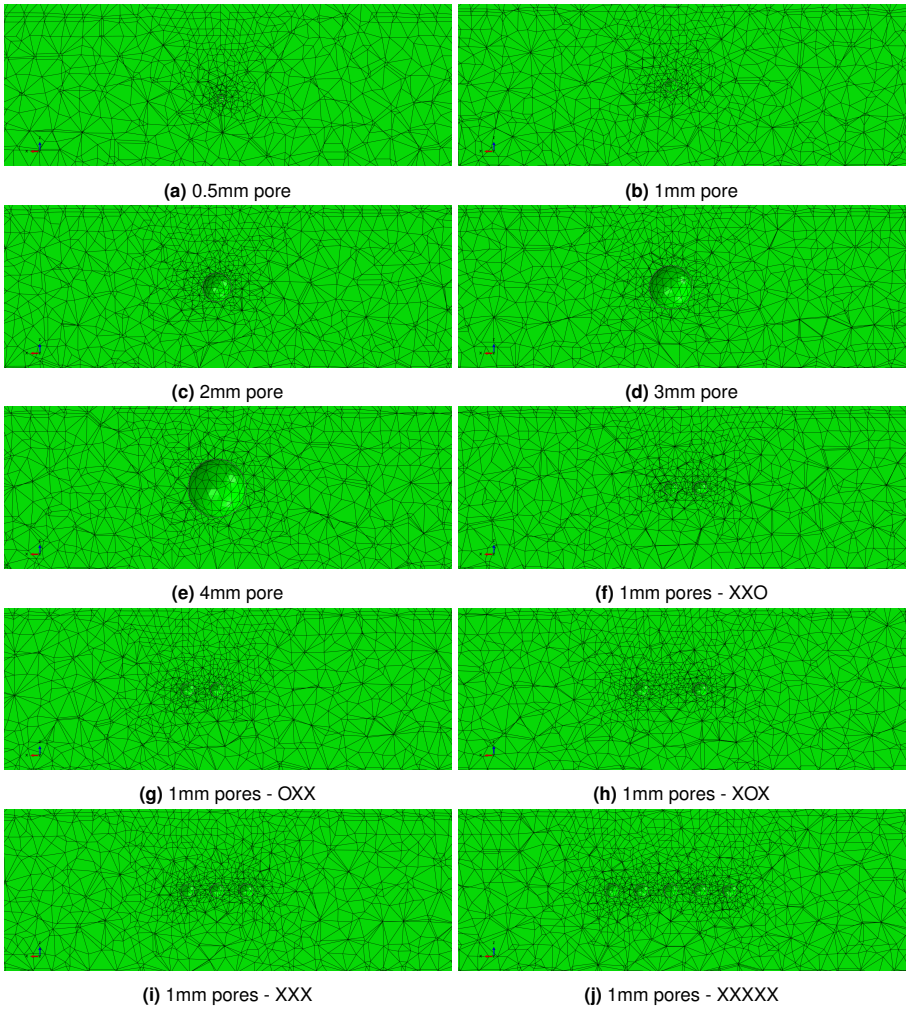

(a) 0.5mm pore **(b)** 1mm pore

(c) 2mm pore **(d)** 3mm pore

(e) 4mm pore **(f)** 1mm pores - XXO

(g) 1mm pores - OXX **(h)** 1mm pores - XOX

(i) 1mm pores - XXX **(j)** 1mm pores - XXXXX

Figure 4.8: Sections displaying the pores - Mesh 2

4.6 Results

In Figure 4.9, the location of where the results are extrapolated in the models with two different meshes is provided. The analysis focuses on studying residual stresses both longitudinally (referred to as Path 1) and perpendicularly to the weld (referred to as Path 2). In addition to Model 2, through-thickness residual stresses have been analyzed to understand the behavior of areas close to the pores. These analyzed stresses are defined as longitudinal along the x-axis and transverse along the y-axis in the current chapter.

Vertical distortions in the z-direction are studied along the line perpendicular to the weld (Path 1). Furthermore, an examination of transverse shrinkage, which refers to the horizontal movement of the top edge line of the plate, is conducted for both the left and right edges of the plate. The longitudinal deformation, representing the displacement of the starting and ending top lines of the plate along its length, is analyzed at the edges where x=0 and x=0.25m.

The contour plots illustrating all the results can be found in Appendix F. To ensure consistency, the results have been converted to millimeters (mm) to display the residual stresses in MegaPascals (MPa). It is important to note that all the results are obtained at the final step of the analysis, precisely at the end of the last cooling phase.

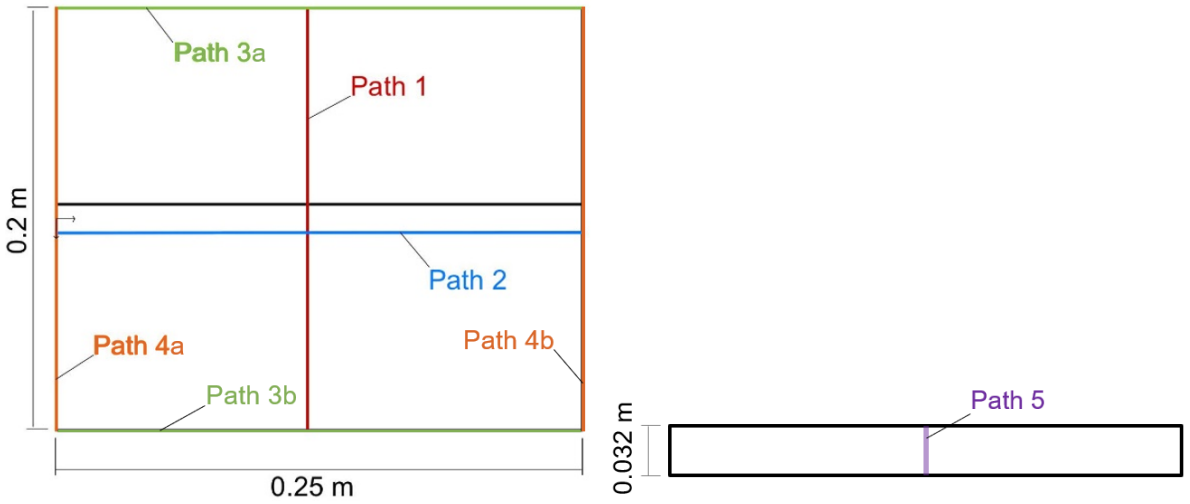

(a) Paths - Top view

(b) Paths - Through thickness view (CUT)

Figure 4.9: Paths for results

4.6.1 Distortions

In Figure 4.10, the longitudinal shrinkage along path 4a (top starting line of the plate) is shown for both meshes. The model without any pores exhibits a tendency to shrink more in the middle of the plate.

For the first mesh, the curves display closely aligned values, with a maximum discrepancy of 0.01mm at the peak. However, when using a finer mesh (Figure 4.10b), slight differences in the values become apparent. The model with five pores demonstrates a higher negative value (indicating expansion), but at the peak, the simulation without any pores exhibits shrinkage that is double the magnitude of the five-pore model.

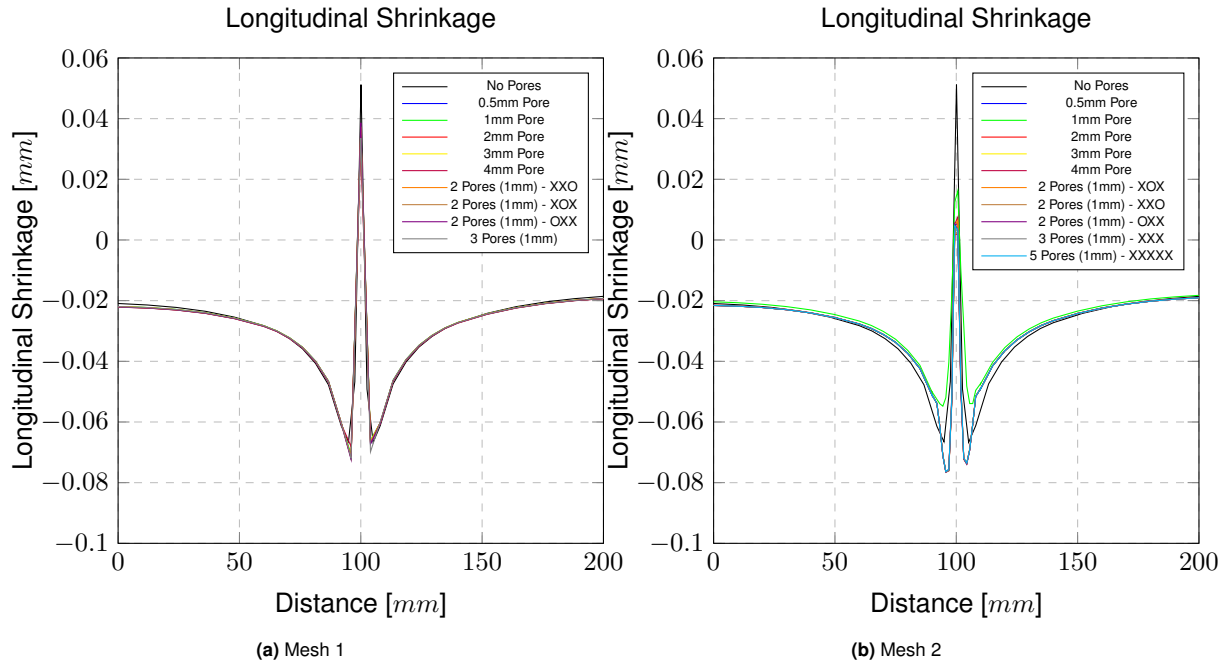

(a) Mesh 1

(b) Mesh 2

Figure 4.10: Longitudinal shrinkage comparison - Path 4a

In Figure 4.11, the longitudinal shrinkage along path 4b (top end line of the plate) is shown for both meshes. It can be observed that, unlike in Figure 4.10, there is a reversal of behavior where the model was originally shrinking, it now exhibits elongation, and vice versa.

Similarly to the previous figure, in the first mesh, there are no significant differences in the results, with the simulation without any pores having the highest values. However, in the second mesh, more noticeable variations can be observed. In this case, the simulation without any pores demonstrates the most significant shrinkage and elongation, while the simulation with five pores exhibits the least amount of shrinkage. Additionally, all the specimens with pores do not show elongation.

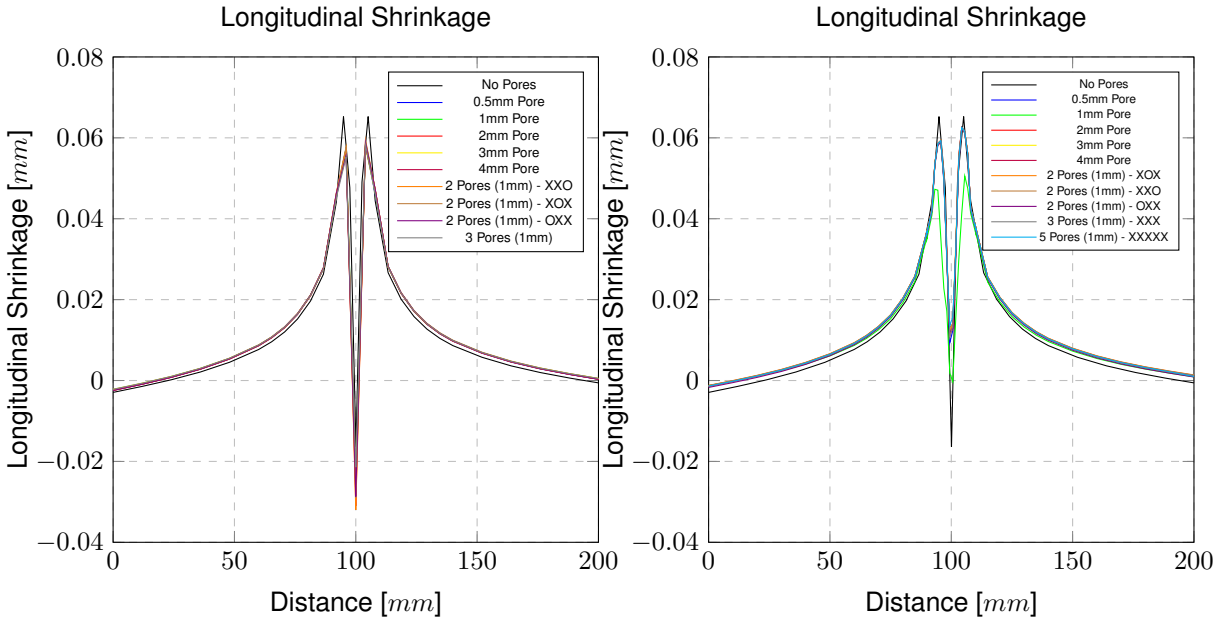

(a) Mesh 1 **(b)** Mesh 2

Figure 4.11: Longitudinal shrinkage comparison - Path 4b

In Figure 4.12, the transverse shrinkage along path 3a (top left side of the plate) is displayed for both meshes. It is evident that there are minimal differences in the results between the two meshes, with a maximum scatter of less than 0.005mm. Shrinkage can be observed consistently throughout the analyzed path, indicating a consistent behavior across both mesh configurations.

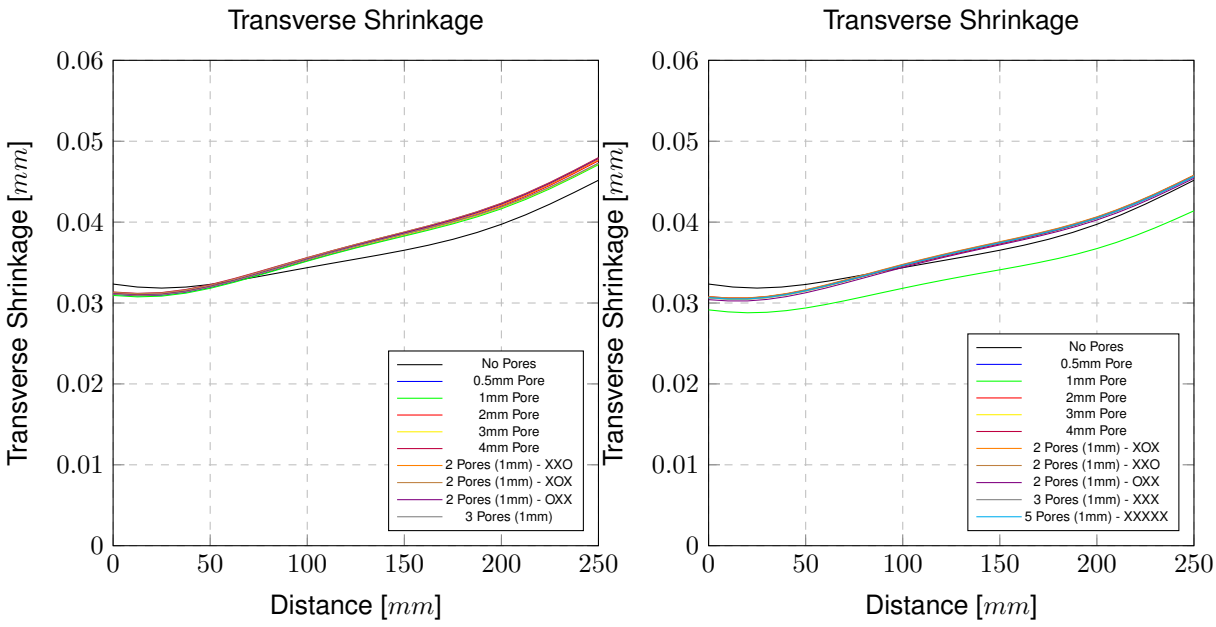

(a) Mesh 1 **(b)** Mesh 2

Figure 4.12: Transverse shrinkage comparison - Path 3a

In Figure 4.13, the transverse shrinkage along path 3b (top right side of the plate) is displayed for both meshes. It can be observed that a slight expansion is present along the analyzed path. Similarly to previous figures, a small scatter in results can be noticed in all the models, with a maximum difference of 0.01mm.

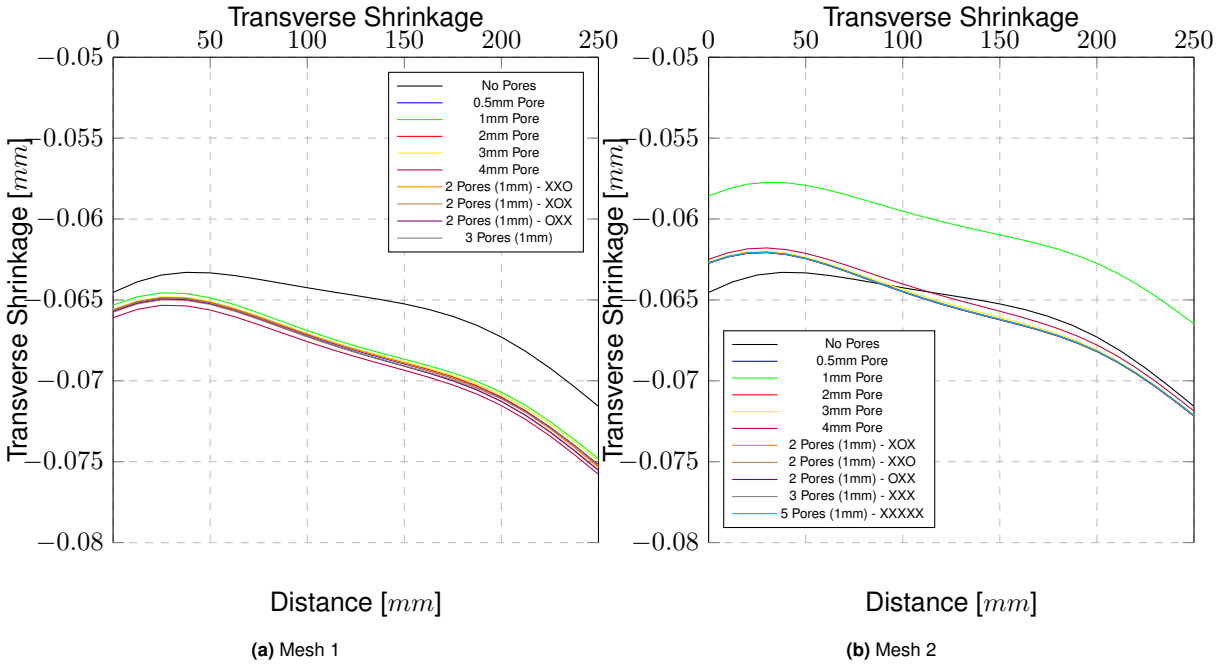

(a) Mesh 1 **(b)** Mesh 2

Figure 4.13: Transverse shrinkage comparison - Path 3b

Lastly, in Figure 4.14, the vertical deformation along path 1 (top middle of the plate, perpendicular to the weld) is displayed for both meshes. The one-pass model exhibits an uplift in the outer region, which is expected since only a single welding pass is applied to the top surface. This uplift can be attributed to the localized heating and subsequent cooling during the welding process, resulting in a distortion

that causes the outer region to rise or uplift. Once again, there is not much difference observed in the results between the models.

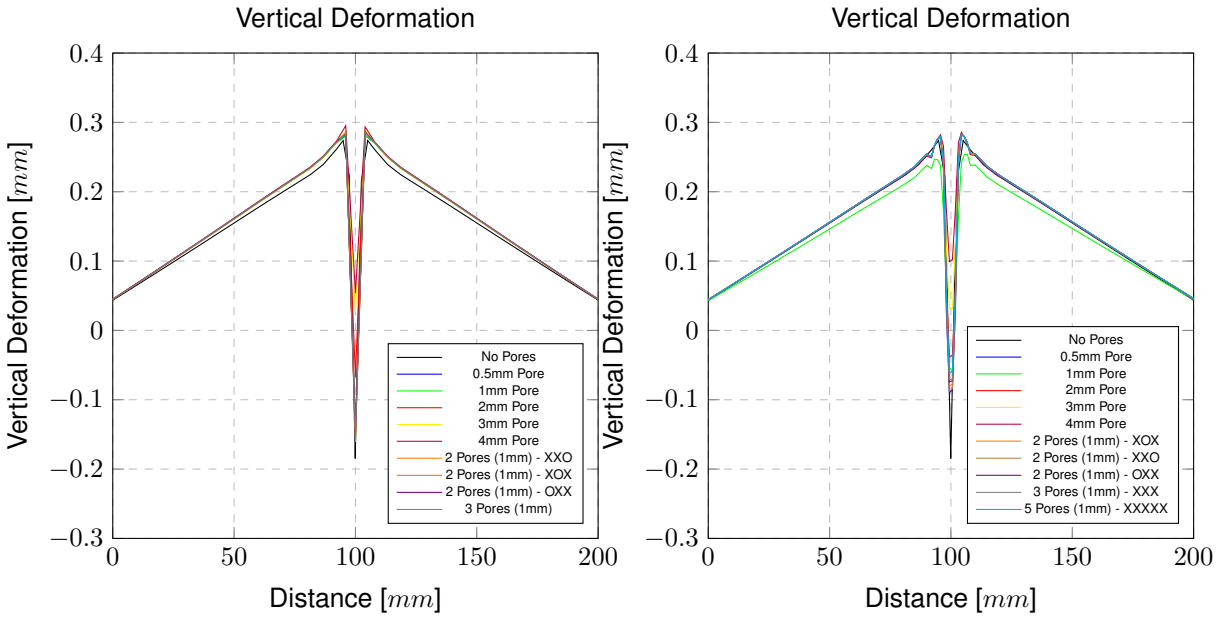

(a) Mesh 1 **(b)** Mesh 2

Figure 4.14: Vertical deformation comparison - Path 1

An overview of all the distortion for the first mesh is given in Table 4.5.

Table 4.5: Mesh 1 - Overview Distortions

Number of pores	Configuration	Size	Maximum u_x [mm]	Minimum u_x [mm]	Maximum u_y [mm]	Minimum u_y [mm]	Maximum u_z [mm]	Minimum u_z [mm]	Maximum u [mm]	Minimum u [mm]
1	0X0	0.5mm	0.166393	-0.363434	0.223388	-0.172321	0.247631	-0.387085	0.474813	0
1	0X0	1mm	0.154991	-0.466801	0.318373	-0.1851	0.250907	-0.446396	0.514657	0
1	0X0	2mm	0.331361	-0.548001	0.375703	-0.332493	0.257684	-0.745977	0.767425	0
1	0X0	3mm	0.334532	-0.590116	0.224567	-0.225224	0.253207	-0.596734	0.756997	0
1	0X0	4mm	0.268765	-0.483624	0.161255	-0.192949	0.261303	-0.487287	0.621127	0
2	XX0	1mm	0.267156	-0.582445	0.338741	-0.243463	0.248105	-0.534681	0.790951	0
2	X0X	1mm	0.17103	-0.576811	0.446555	-0.229031	0.247394	-0.49138	0.673771	0
2	0XX	1mm	0.207124	-0.649907	0.39976	-0.190366	0.245565	-0.485348	0.811139	0
3	XXX	1mm	0.213703	-0.576547	0.382146	-0.30051	0.251712	-0.552514	0.703261	0

An overview of all the distortions for the second mesh is provided in Table Table 4.6.

Table 4.6: Mesh 2 - Overview Distortions

Number of pores	Configuration	Size	Maximum u_x [mm]	Minimum u_x [mm]	Maximum u_y [mm]	Minimum u_y [mm]	Maximum u_z [mm]	Minimum u_z [mm]	Maximum u [mm]	Minimum u [mm]
1	0X0	0.5mm	0.135361	-0.297922	0.18132	-0.0956738	0.243239	-0.289923	0.40739	0
1	0X0	1mm	0.0587153	-0.216255	0.104147	-0.0836699	0.0693296	-0.25713	0.26642	0
1	0X0	2mm	0.274013	-0.481545	0.307672	-0.29893	0.245077	-0.635591	0.67686	0
1	0X0	3mm	0.255694	-0.494168	0.212526	-0.215968	0.242759	-0.705565	0.73531	0
1	0X0	4mm	0.239221	-0.491796	0.151267	-0.148503	0.246822	-0.628487	0.654948	0
2	XX0	1mm	0.140078	-0.366095	0.270628	-0.206607	0.238721	-0.457376	0.488122	0
2	X0X	1mm	0.167291	-0.393161	0.227506	-0.254238	0.238627	-0.479576	0.544819	0
2	0XX	1mm	0.140232	-0.415388	0.211629	-0.20668	0.242477	-0.517323	0.575381	0
3	XXX	1mm	0.131768	-0.360155	0.276447	-0.241164	0.248885	-0.475035	0.536254	0
5	XXXXX	1mm	0.151962	-0.435497	0.260961	-0.246917	0.241386	-0.432942	0.565561	0

4.6.1.1 Discussion

In the models with pores, a minor change in distortions was observed for the longitudinal shrinkage at the end and beginning of the top of the plate in the first mesh. By halving the size of the mesh in the area of interest, more noticeable differences started to emerge. Regarding the presence of pores, the model with five pores exhibited a higher negative value for shrinkage, indicating expansion in that specific region. However, at the peak point, the simulation without any pores demonstrated shrinkage that was twice as large as the shrinkage observed in the five-pore model. It is important to note that the simulation without any pores showed the most significant overall shrinkage and elongation, indicating a higher level of deformation in the material. Conversely, the simulation with five pores exhibited the

least amount of shrinkage, suggesting that the presence of pores has a mitigating effect on the overall shrinkage behavior. Furthermore, all the specimens with pores, including the five-pore model, did not exhibit any elongation. This suggests that the presence of pores restricts the expansion of the material, leading to a more constrained deformation response. These observations emphasize the influence of pore characteristics on the shrinkage behavior of the material. The results indicate that the presence, size, and distribution of pores can affect the overall dimensional changes and deformation patterns in the material during the welding process but not significantly in the case of single pores or small linear patterns. For the transverse shrinkage at the left and right top sides of the plates in the models with pores, there were no significant differences observed in the results for both meshes. In both cases, the presence of pores did not have a substantial impact on the deformations. When examining path 3a, the mesh used did not influence the results, indicating that the choice of mesh size did not significantly affect the transverse shrinkage in the pores models. Similarly, for path 3b, although the mesh size was reduced, the deformations in all the pores models were only slightly reduced by a negligible value of less than 0.05mm. This suggests that the mesh refinement had minimal effect on the transverse shrinkage in the presence of pores. Overall, these findings indicate that the deformations in the transverse direction near the top sides of the plates were not significantly influenced by the presence or size of the pores, as well as the choice of the mesh size. In the case of the vertical deformation in the pores models along path 1, the results demonstrate variations depending on the location of the pores. Particularly, with the smallest pore sizes of 0.5mm and 1mm, the entire plate exhibits no negative deformation, which is in contrast to the other graphs where negative deformations are observed. Among the different pore configurations, the graph with five sequential pores at 0.02mm shows the highest negative deformation value. This indicates a greater degree of shrinkage or contraction in that particular region compared to the other simulations. Interestingly, all the simulations display a similar tension value of 0.3mm, suggesting a consistent response to the applied loads. These findings highlight the influence of pore size and arrangement on the vertical deformation behavior of the material. The presence of smaller pores appears to minimize the occurrence of negative deformation, while larger or sequential pore configurations contribute to a more pronounced contraction effect.

4.6.2 Residual stresses

In this section, the results of residual stresses for both meshes will be discussed. In Figure 4.15, the longitudinal residual stresses along the perpendicular path to the weld on the top of the specimen are presented.

For the first mesh, the "No pores" model reaches a peak at approximately 380 MPa. The other models exhibit slightly higher peaks, with the 4mm pore model reaching around 550 MPa and the middle of the plate experiencing stresses around 250 MPa. It can be observed that as the size of the pore increases, the stresses also increase.

In the second mesh, the configuration with 5 pores reaches the same peak value as the 4mm pore model, while the 1mm pore model reaches a peak of around 600 MPa.

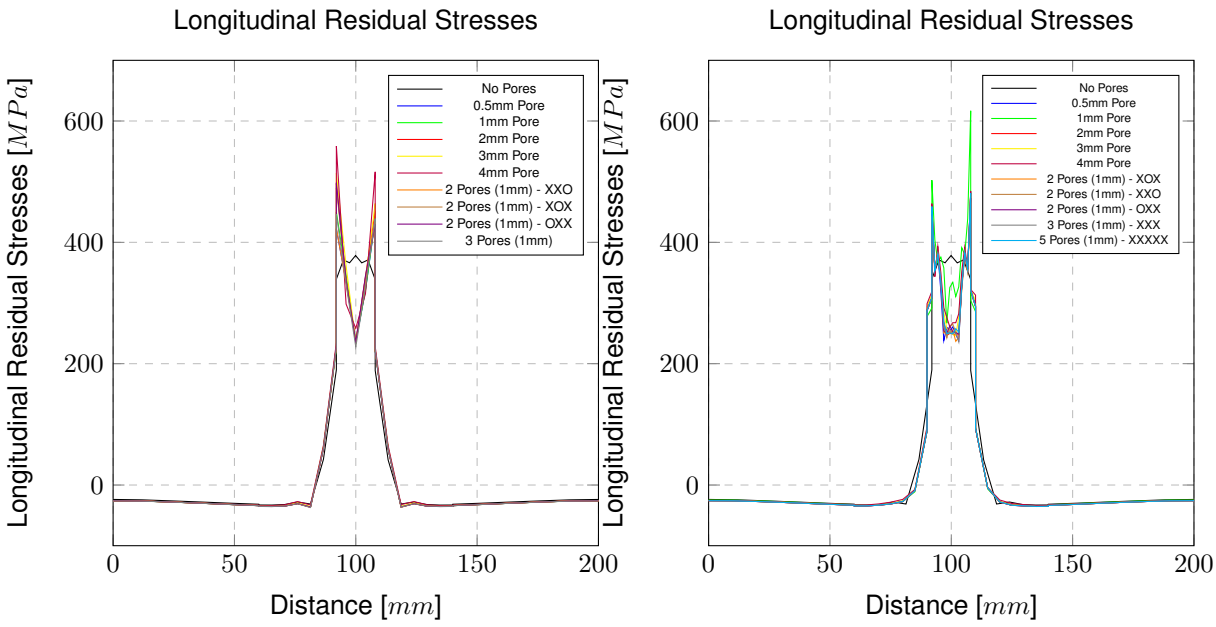

(a) Mesh 1 **(b)** Mesh 2

Figure 4.15: Longitudinal residual stresses - Path 1

In Figure 4.16, the transverse residual stresses along the perpendicular path to the weld on the top of the specimen are shown. In the first mesh, the model without any pores exhibits minimal compression in the middle of the path, while the other models reach compression values of up to approximately 250 MPa at the same location. The "XOX" configuration reaches the peak tension value of 480 MPa.

In the second mesh, there is compression observed in the middle of the path, but with a lower magnitude compared to the first mesh, reaching around 180 MPa. The 1mm pore configuration once again exhibits the highest tension value but the lowest compression value (after the "No pores" configuration).

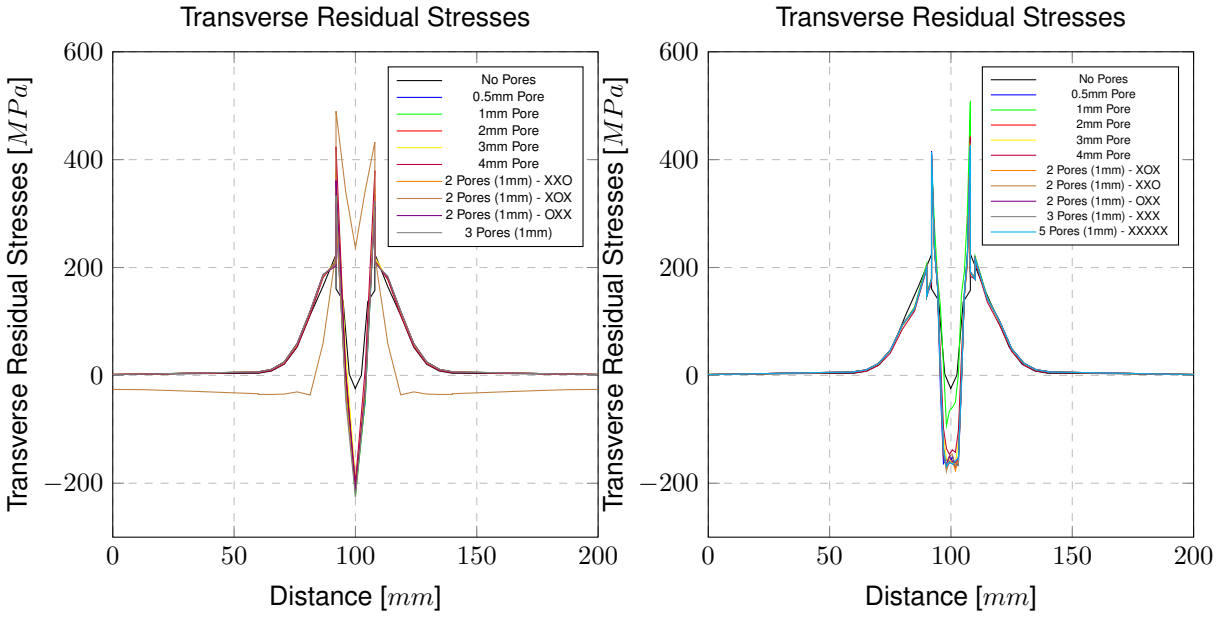

(a) Mesh 1 **(b)** Mesh 2

Figure 4.16: Transverse residual stresses - Path 1

In Figure 4.17, the longitudinal residual stresses along the top right weld toe are displayed. It can be observed that the "No pores" model exhibits a lower value compared to the average of the other models, with a difference of approximately 100 MPa. In the first mesh, the 4mm pore simulation demonstrates a marginally higher value compared to the other models. Similarly, in the second mesh, the 1mm pore model shows a slightly elevated value.

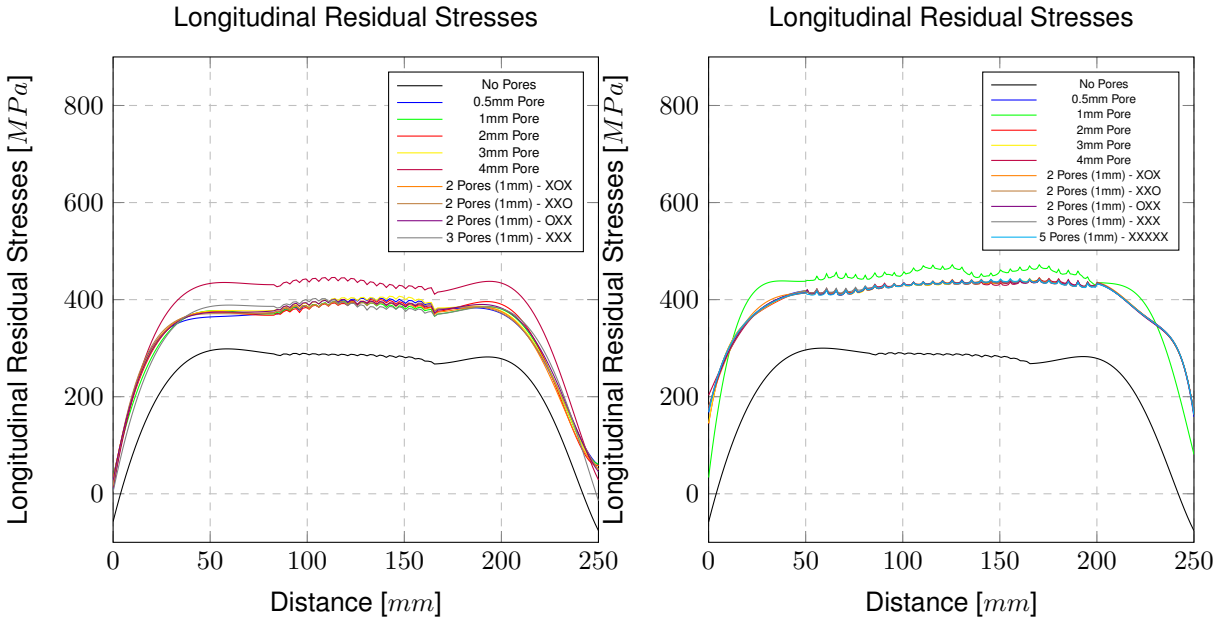

(a) Mesh 1 **(b)** Mesh 2

Figure 4.17: Longitudinal residual stresses - Path 2

In Figure 4.18, the transverse residual stresses along path 2 are depicted. In both meshes, the model without pores exhibits a maximum residual stress of 215 MPa. In the first mesh, all the curves display similar trends, with the 4mm pore simulation standing out at approximately 50 MPa higher than the other curves. In the second mesh, the analysis with a single 1mm pore shows a lower maximum value, around 30 MPa. Furthermore, in the second mesh, the simulation with a 2mm pore exhibits a different shape compared to the other results but peaks at around the same value.

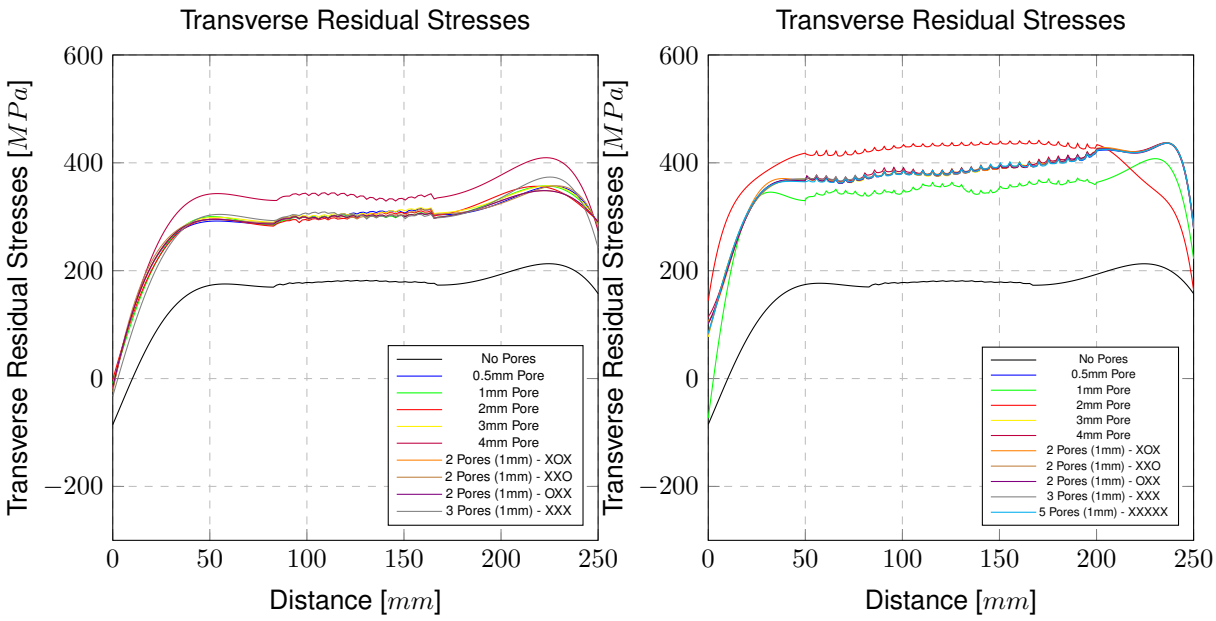

(a) Mesh 1 **(b)** Mesh 2

Figure 4.18: Transverse residual stresses - Path 2

In Figure 4.19, the through-thickness longitudinal residual stresses at the middle of the plate are presented. It is evident that there is a significant scatter in values around the pores, attributed to the presence of singularities. This highlights the motivation behind creating the second mesh, as it can be observed that the peak values around the pores are significantly reduced by halving the size of the mesh. This refinement in mesh size helps to mitigate the effects of singularities and provides more accurate and reliable results.

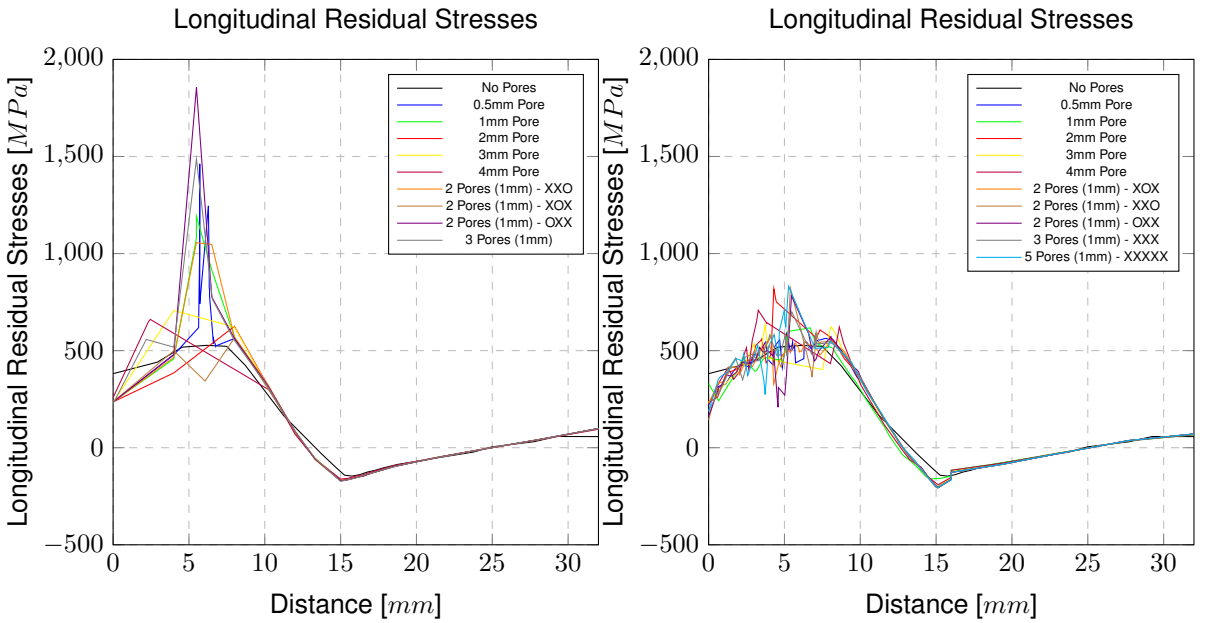

(a) Mesh 1 **(b)** Mesh 2

Figure 4.19: Longitudinal residual stresses - Path 5

To conclude, in Figure 4.19, the through-thickness transverse residual stresses at the middle of the plate (path 5) are displayed. Once again, it is evident that improving the quality of the mesh is highly

beneficial when there are cavities present in the model.

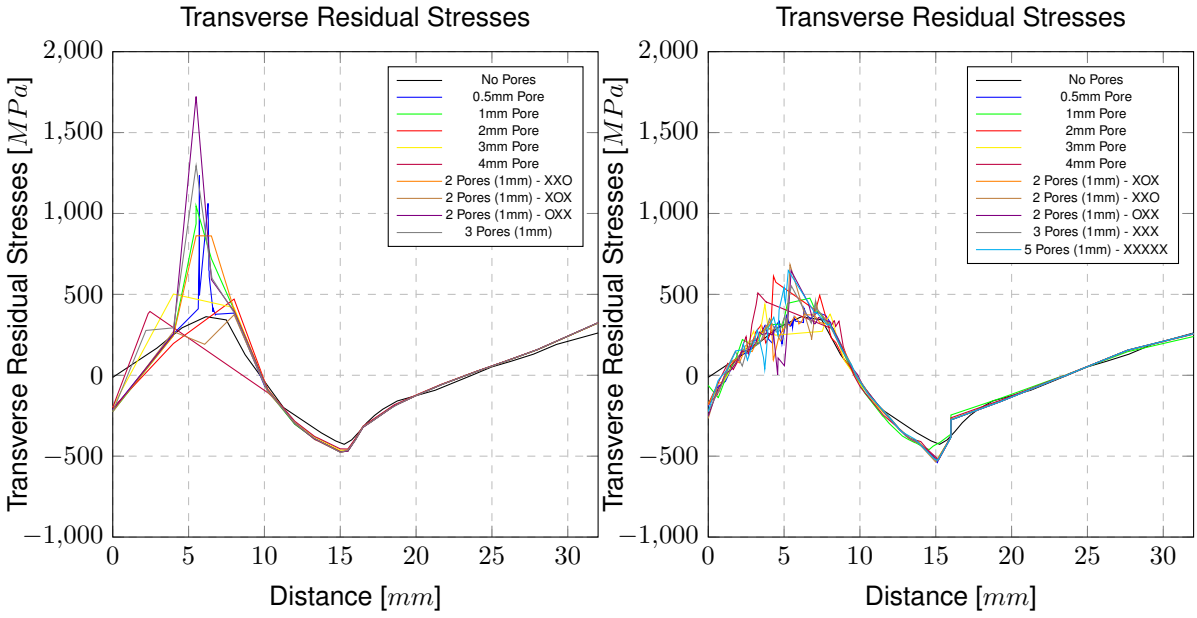

(a) Mesh 1 **(b)** Mesh 2

Figure 4.20: Transverse residual stresses - Path 5

The omission of an overview of the stresses in this context is attributed to the presence of singularities. This decision was made deliberately to prevent the reporting of inflated results that do not align with the realistic behavior of the system.

A sensitivity analysis was performed on the location of the pore within the finite element, and two possible approaches were considered. The first approach involved moving the pore within the element from its original position, while the second approach involves creating multiple increments where the pore is located at different positions within the element at a linear distance, varying only the location on the x-axis of 0.25mm. For the first approach, the pore can be systematically moved within the element to evaluate its effect on the resulting behavior. This can be achieved by adjusting the coordinates of the pore within the element and re-running the simulation for each new position. By comparing the outcomes of these simulations, the sensitivity of the model to the pore location can be assessed, allowing for a better understanding of its influence on the overall response. This approach led to a difference in results of less than 1% so was not inserted in the results. In the second approach, multiple increments can be created where the pore is positioned at different locations within the element. This involves dividing the element into sections and introducing the pore at the beginning, middle, and end of each section. Subsequently, simulations can be performed for each increment, and the resulting behaviors can be compared to evaluate the sensitivity of the model to the pore position. The pore in this situation was located at the middle of the increment and at the end of the increment, to be precise in between two birth-death elements. This technique was used and led to no difference in results. Both approaches provide valuable insights into the influence of pore location on the system's response. By systematically varying the pore position, the sensitivity analysis helps to identify critical locations within the element and provides information on the most influential regions with respect to the presence of pores. This information can be used to optimize design and manufacturing processes, enhance the understanding of structural behavior, and guide future research efforts in the field.

4.6.3 Discussion

For the residual stresses along Path 1 in Mesh 1, the results indicate that there is no significant difference among the various models. The variations observed primarily occur at the peak locations, which can be attributed to the mesh size utilized. However, overall, the differences are relatively small.

Comparing the models with and without pores, a difference of approximately 20% in the results can be observed. This suggests that the presence of pores has a noticeable impact on the residual stresses. Interestingly, it is the increase in the number of pores rather than the addition of individual pores that appear to have a more significant influence on the results. In terms of transverse residual stresses in Mesh 1, the addition of pores leads to higher compression values in the middle of the plate. This indicates that the presence of pores contributes to increased compressive stresses in that region. Moving on to Mesh 2, more pronounced differences in results are observed. The simulation with five sequential pores exhibits the highest value among all the simulations, reaching a peak of 620MPa. In contrast, the simulation without any pores demonstrates a peak value close to 400MPa. In both Mesh 1 and Mesh 2, distinct trends can be observed in the transverse and longitudinal residual stresses. In Mesh 1, the simulation without any pores exhibits peak values of approximately 300 MPa for longitudinal stresses and 220 MPa for transverse stresses. Excluding the simulation with 4 mm pores, the remaining pore simulations demonstrate similar values, averaging between 305 MPa and 380 MPa for longitudinal stresses, and between 305 MPa and 380 MPa for transverse stresses. Notably, the simulation with 4 mm pores shows slightly higher values, approximately 10-15% higher than the other pore simulations. Moving to Mesh 2, a similar pattern is observed. The simulation without any pores still exhibits peak values of around 30 MPa for longitudinal stresses and 220 MPa for transverse stresses. However, the simulation with 5 pores shows slightly higher longitudinal residual stresses, approximately 5% higher compared to the other models. Conversely, the transverse residual stresses in the 5 pores simulation are approximately 7% lower compared to the other models. Additionally, the simulation with 3 pores in Mesh 2 displays transverse residual stresses that are approximately 10% higher compared to the other models. For Path 5, the influence of mesh size on the results is evident. Halving the mesh size leads to a significant reduction in the values of singularities, resulting in improved agreement with the simulation without any pores (No pores). The reduction in mesh size effectively mitigates the impact of singularities and helps to achieve results that align closely with the reference simulation. Furthermore, in the vicinity of the pores, some fluctuations in values can be observed, but overall, the presence of pores does not cause drastic deviations from the results obtained in the simulation without any pores. The values remain relatively close to the original value observed in the absence of pores, indicating that the presence of pores has a limited influence on the stress distribution along Path 5.

5

Conclusion and recommendation

The concluding chapter of this thesis is dedicated to summarizing the key findings and insights derived from the conducted research. Initially, the conclusions drawn from the study are presented, highlighting the main outcomes and implications. Subsequently, a comprehensive discussion is provided, allowing for a deeper analysis and interpretation of the results obtained throughout the research process.

Furthermore, this chapter also encompasses recommendations for future research, offering suggestions and directions for further investigations in the field. These recommendations serve to address any potential limitations or gaps identified during the study and encourage the exploration of new avenues for advancing knowledge and understanding in the respective domain. By providing a well-rounded conclusion, discussion, and recommendations, this final chapter aims to encapsulate the significance of the research and its potential impact on the broader scientific community.

5.1 Conclusion

The main findings of this thesis are as follows:

- In the context of the pores, for the case studied, the scrutinized configurations demonstrate marginal influence on both distortions and residual stresses manifested at the surface of the plate. Notably, within the vicinity of the pores, distinctive singularities become evident.
- A significant influence on the outcomes is observed in relation to the mesh size surrounding the pore. Employing a mesh size that closely aligns with the one utilized within the pore yields substantial enhancements in the results.
- In the specific situation analyzed, the findings indicate that if the number of simulated passes is decreased to two-thirds of the actual number of passes, the results remain relatively stable and show minimal alteration. This adjustment additionally confers the advantage of considerably curtailing the duration of each simulation.

5.2 Discussion

The ensuing section will offer a comprehensive culmination of the preceding discourse. This summative deliberation serves as an avenue to synthesize the multifaceted aspects explored and expound upon their implications, thereby furnishing a more elaborate understanding of the subject matter. In doing so, it aims to encapsulate the essence of the exchanged insights, fostering a bridge between theoretical underpinnings and practical applications. Through a methodical analysis and reflection, this final discussion endeavors to underscore the significance of the topics discussed, elucidate any emergent patterns or interrelationships, and potentially pave the way for future investigations or considerations within the domain. Consequently, the subsequent discourse constitutes a vital juncture where scholarly exploration converges with pragmatic applications, culminating in a holistic perspective that enhances the depth and breadth of comprehension.

In Model 1, the assumption that cutting the specimen to three times the thickness size would result in negligible differences in residual stresses requires further investigation. It is essential to delve deeper into this assumption, as variations in plate dimensions can indeed lead to disparities in residual stress levels, albeit potentially small. Moreover, the absence of a defined cooling time in the reference paper [41] introduces an additional element of uncertainty. Despite numerous attempts to determine the most probable value, the assumed cooling time might still be incorrect.

Furthermore, the reference study [41] lacks detailed information regarding the position and support of the plate during welding. While it mentions the presence of starting and runoff tabs, crucial details about the precise plate orientation and clamping mechanisms are absent. The positioning and support of the plate during welding significantly influence the outcomes of residual stress analysis. The interplay between the plate's orientation and clamping mechanisms can yield diverse stress distributions within the welded structure. These outcomes encompass variations in thermal gradients, potential distortions, and alterations in cooling rates that subsequently impact microstructural changes. Collectively, these factors contribute to the emergence of non-uniform residual stress patterns.

For accurate and reliable results, meticulous attention must be directed towards fixture design, alignment procedures, and the establishment of appropriate boundary conditions. Thoughtful and careful positioning and support strategies serve to mitigate deformations and uneven temperature distributions, thereby elevating the credibility and significance of the experimental findings.

The analysis of thermal information in Model 2 unveiled a variation amounting to 100℃. Enhancing the radiation and/or reducing the conductivity value incorporated into the simulation holds the potential to align the results more closely with the experimental data. Nonetheless, it's essential to acknowledge that these adjustments do not rule out the potential for errors within the experiment itself. In situations where uncertainties in the experimental setup persist, the utilization of smaller thermocouples offers a promising avenue to achieve outcomes with reduced averaging effects and greater precision in capturing exact temperature locations.

Incorporating the thermal and mechanical properties specific to the ER50-6 wire in the weld area, rather than those of the plate, holds the potential to elevate the realism of the model, thereby enhancing the quality of the simulation's output. This adjustment could align the simulation more closely with the actual conditions present during welding, leading to more accurate predictions and insights.

Furthermore, a modification of the thermocouple placement can offer significant improvements. For example, relocating the thermocouples to different positions can enhance the comprehensiveness and accuracy of temperature data collection. The new positions can be, as an example to improve the experiments, near the groove toe, which is the point where the groove intersects the base material, and at the groove root, representing the deepest point of the groove. This positioning strategy provides valuable insights into temperature variations at crucial junctures, thereby influencing the analysis of heat distribution patterns. Additionally, the placement of thermocouples at intermediate positions between the groove and plate edges on both sides serves to gather data on temperature fluctuations across the width of the plate. This arrangement takes into account the complex dynamics of heat transfer in the vicinity of the groove joint. Moreover, by positioning thermocouples at the edges of the groove itself, the monitoring of temperature fluctuations within the groove structure becomes more focused and informative. To ensure comprehensive coverage, a symmetrical distribution of the remaining thermocouples around the groove joint and its neighboring areas is recommended. This symmetrical arrangement contributes to capturing temperature variations in a balanced manner, aiding in achieving a comprehensive dataset. As an established practice, the inclusion of control thermocouples in regions unaffected by welding remains essential. These control points serve as references for baseline temperatures, facilitating comparative analysis and enhancing the accuracy of temperature measurements in relation to the welding process.

In the context of the Pores Model, a potential approach for enhancing the accuracy of results involves further reduction of the mesh size within the weld area. This adjustment holds the promise of minimizing fluctuations observed in through-thickness residual stresses. A suggested mesh size of approximately 0.5mm is proposed, which represents a reduction of more than half the original mesh size while concurrently increasing precision. However, it's important to note that this refinement comes with a trade-off in terms of computational demands. To accommodate this computational load, employing a CPU with a minimum of 16 cores or utilizing a robust server configuration is recommended. Such enhancements in processing capacity can facilitate faster calculations and data analysis.

Alternatively, the step size can be reduced. A smaller step size allows for a more accurate repre-

sentation of transient phenomena and dynamic changes during the welding process. Using a smaller time step can help in capturing rapid variations in temperature, stress, and other parameters. However, again, reducing the step size can also increase the computational time, as more time steps are required to cover the entire welding process.

While both mesh refinement and step size modifications can impact the accuracy of welding simulations, the largest effect on the simulation results is often expected to come from mesh refinement. This is because a refined mesh allows for better spatial resolution, capturing fine details and gradients accurately. Welding processes involve localized temperature variations, phase changes, and stress concentrations that can be better captured with a finer mesh. In contrast, while adjusting the step size is important for capturing transient effects, its effect might be slightly overshadowed by the benefits of a more refined mesh, especially when dealing with complex welding scenarios.

Lastly, expanding the investigation to encompass various pore configurations is advisable. Given that the studied pore configuration did not exhibit a significant influence on the residual stresses, exploring additional configurations can provide a more comprehensive understanding of their effects. To approach an ideal scenario, a combination of experimental and numerical methods could be employed. This entails conducting an experiment, capturing the three-dimensional profile of the plate, and subsequently replicating this real-world data within a finite element model. This integrated approach aligns experimental observations with computational simulations, enabling a more accurate representation of pore effects on residual stresses and advancing the overall accuracy of the analysis.

5.3 Recommendations and Future Research

The following recommendations are proposed to further advance and enhance the current research on welded plates under thermal loading:

- **Laboratory Experiments**: Conduct comprehensive laboratory experiments to validate and verify the obtained results, considering the influence of residual stresses, welding defects, and relevant parameters on the fatigue performance of welded joints. These experiments will provide empirical evidence for the findings of numerical simulations.
- **Sensitivity Analysis**: Perform a sensitivity analysis to evaluate the impact of varying factors such as plate dimensions, boundary conditions, and pore configurations on residual stresses, distortions, and fatigue behavior. The width, length, and height of welded joints can be changed to identify critical parameters and provide insights for optimizing the design of welded connections for different plate dimensions. Diverse boundary conditions in numerical simulations, including constraint levels, cooling speeds, and thermal conditions, can be explored. Investigating different pore configurations in welded joints, considering varying sizes, shapes, and distributions, can provide insight into how these configurations affect residual stresses, deformations, and fatigue performance, aiding in understanding the importance of pore characteristics and developing strategies to control and minimize porosity during welding processes.
- **Increase number of increments per step**: Adopting an approach that involves a higher number of increments per step, reducing the amount of time used per increment and thus increasing the number of cycles, carries the promise of yielding substantial improvements in the quality and reliability of analysis outcomes.
- **Mesh refinement**: It is recommended to conduct a detailed study on the refinement of the mesh around the pores to obtain more reliable results. By improving the mesh resolution in the vicinity of the pores, a more accurate representation of stress concentration and deformation patterns can be achieved. This will enable a better understanding of the local effects of pores on the overall behavior of the welded joints, including stress redistribution and crack initiation. Such a study will enhance the accuracy and credibility of numerical simulations, improving the reliability of predictions and assessments related to pore characteristics in the welding process.
- **Reduce the dimension of birth-death elements**: Lowering the size of each birth-death element enhances the congruence between material deposition in simulations and actual experimental conditions, given that the wire deposition, in reality, tends to be lower than the presumed values in the simulations. However, it's important to note that the adoption of a smaller size of elements leads to a higher number of steps, therefore could necessitate greater computational resources

and time. Thus, a judicious balance needs to be struck between achieving a higher resolution analysis and practical considerations related to computational efficiency.

- **Consider Thermally Independent Properties**: This will reduce the accuracy of predictions regarding residual stresses and distortions. However, if the variance in outcomes is negligible, it has the potential to slightly curtail computational resources and time.

References

[1] M. Adak and C. Guedes Soares. “Effects of different restraints on the weld-induced residual deformations and stresses in a steel plate”. In: *International Journal of Advanced Manufacturing Technology* 71.1-4 (Mar. 2014), pp. 699–710. ISSN: 02683768. DOI: 10.1007/s00170-013-5521-9.

[2] Shamail Ahmad. “Presence of golden ratio relationships in Fe-Fe3C, Cu-Zn and Cu-Sn alloy systems”. In: *International Journal of Design and Nature and Ecodynamics* 10.2 (2015), pp. 174–181. ISSN: 17557445. DOI: 10.2495/DNE-V10-N2-174-181.

[3] Alain Nussbaumer, Luis Borges, and Laurence Davaine. *Fatigue design of steel and composite structures*. Tech. rep. ECCS – European Convention for Constructional Steelwork, 2011.

[4] American Welding Society. “D 1.1 - Porosity”. In: ().

[5] American Welding Society. Structural Welding Committee, American Welding Society. Technical Activities Committee, and American National Standards Institute. *Structural welding code–steel*. 2020, p. 634. ISBN: 9781643220871.

[6] Bill Lucas. *Distortions - Types and causes*. 2014. URL: https://welding.org.au/welding/distortion/.

[7] British Standard Committee. “EN 10025-2”. In: (2019).

[8] British Standards Institution. “EN 60974-1”. In: ().

[9] British Standards Institution. “EN-1011-1”. In: ().

[10] British Standards Institution. “Welding: recommendations for welding of metallic materials, Part 1”. In: (2009).

[11] British Standards Institution. *Welding : recommendations for welding of metallic materials, Part 2: Arc welding of ferritic steels*. British Standards Institution, 2001, p. 56. ISBN: 0580362248.

[12] Quan Chen et al. “Effect of the groove type when considering a thermometallurgical-mechanical model of the welding residual stress and deformation in an S355JR-316L dissimilar welded joint”. In: *Journal of Manufacturing Processes* 45 (Sept. 2019), pp. 290–303. ISSN: 15266125. DOI: 10.1016/j.jmapro.2019.07.011.

[13] H. E. Coules. *Contemporary approaches to reducing weld induced residual stress*. Jan. 2013. DOI: 10.1179/1743284712Y.0000000106.

[14] Dean Deng et al. “Investigating the influence of external restraint on welding distortion in thin-plate bead-on joint by means of numerical simulation and experiment”. In: *International Journal of Advanced Manufacturing Technology* 82.5-8 (Feb. 2016), pp. 1049–1062. ISSN: 14333015. DOI: 10.1007/s00170-015-7413-7.

[15] John Michael. Dowden. *The mathematics of thermal modeling : an introduction to the theory of laser material processing*. Chapman & Hall/CRC, 2001, p. 291. ISBN: 1584882301.

[16] ECCS. *Fatigue Design of Steel and Composite Structures*. John Wiley & Sons, Ltd, 2018. ISBN: 9783433608791. URL: https://onlinelibrary.wiley.com/doi/abs/10.1002/9783433608791.ch1.

[17] European committee for standardization. *Eurocode 3-Design of steel structures-Part 2: Steel Bridges*. Tech. rep. 2006.

[18] F.W.BRUST and D.S.KIM. “Mitigating welding residual stress and distortion”. In: (2005).

[19] G. E. Totten. “Steel Heat Treatment Handbook, Second Edition”. In: (2006).

[20] John Goldak, Aditya Chakravarti, and Malcolm Bibby. *A New Finite Element Model for Welding Heat Sources*. Tech. rep.

[21] Nanasaheb Gurule and K K Wagh. “STUDY & DEVELOPMENT OF A COMPUTER ASSISTANCE IN THE SELECTION OF FATIGUE DESIGN RECOMMENDATIONS FOR WELDED JOINTS”. PhD thesis. 2014. DOI: 10.13140/2.1.3044.7045. URL: https://www.researchgate.net/publication/261985343.

[22] Howard B. Cary. “Welding And The World Of Metals”. In: *Modern Welding Technology* (1998). URL: www.MillerWelds.com.

[23] International Organization for Standardization. “EN-ISO 6520-1:2007”. In: (2007).

[24] International Organization for Standardization. “NEN-EN-ISO 5817 - Pores and Slag inclusion limits”. In: (2014).

[25] Cynthia L. Jenney et al. *Welding handbook*. American Welding Society, 2001. ISBN: 0871716577.

[26] Bandaru Kiran et al. “Experimental and Mathematical Studies for Optimality of GTAW Parameters on Similar and Dissimilar Steel Substrates”. In: *Advances in Materials Science and Engineering* 2022 (2022). ISSN: 16878442. DOI: 10.1155/2022/5118566.

[27] Bandaru Kiran et al. “Structural and thermal analysis of butt joint GTAW of similar and dissimilar materials with distinct groove angles through simulation and mathematical modelling”. In: *FME Transactions* 48.3 (2020), pp. 667–680. ISSN: 2406128X. DOI: 10.5937/fme2003667B.

[28] Klas Weman. *Welding processes handbook*. Tech. rep. 2012.

[29] D. J. Kotecki. *Welding metallurgy and weldability of stainless steels*. Wiley-Interscience, 2003.

[30] Kou Sindo. *WELDING METALLURGY SECOND EDITION*. John Wiley & Sons, 2003.

[31] Larry Jeffus. *Welding Principles and Applications*. Tech. rep. 2017. URL: www.cengage.com/highered.

[32] R. H. Leggatt. “Residual stresses in welded structures”. In: *International Journal of Pressure Vessels and Piping* 85.3 (Mar. 2008), pp. 144–151. ISSN: 03080161. DOI: 10.1016/j.ijpvp.2007.10.004.

[33] Suo Li et al. “Influence of the groove shape on welding residual stresses in P92/SUS304 dissimilar metal butt-welded joints”. In: *Journal of Manufacturing Processes* 66 (June 2021), pp. 376–386. ISSN: 15266125. DOI: 10.1016/j.jmapro.2021.04.030.

[34] Ruben Lostado Lorza et al. “Residual stresses with time-independent cyclic plasticity in finite element analysis of welded joints”. In: *Metals* 7.4 (Apr. 2017). ISSN: 20754701. DOI: 10.3390/met7040136.

[35] Arvid Maarleveld. *Welding induced residual stresses in a segment of an orthotropic steel deck*. Tech. rep. 2022. URL: http://repository.tudelft.nl/..

[36] Mthobisi Zondi. *ANALYSIS OF RESIDUAL STRESSES AND DISTORTIONS RESULTING FROM MULTI-PASS WELDING OF NOZZLES TO CYLINDRICAL PRESSURE VESSELS Supervisor: Professor Sarp Adali*. Tech. rep. 2012.

[37] Shigetaka OKANO et al. “Assembling a database of inherent strain for simplified distortion analysis in multi-layer and multi-pass welding of heavy section plate (Development of accuracy management system for high quality construction in welded structures on the basis of advanced theory of inherent strain)”. In: *Transactions of the JSME (in Japanese)* 82.837 (2016), pp. 16–00005. DOI: 10.1299/transjsme.16-00005.

[38] Panagiotis Michaleris. *Encyclopedia of Thermal Stresses*. Springer Netherlands, 2014. DOI: 10.1007/978-94-007-2739-7.

[39] Sang Cheol Park, Hee Seon Bang, and Woo Jae Seong. “Effects of material properties on angular distortion in wire arc additive manufacturing: Experimental and computational analyses”. In: *Materials* 13.6 (Mar. 2020). ISSN: 19961944. DOI: 10.3390/ma13061399.

[40] Artem Pilipenko. *Computer simulation of residual stress and distortion of thick plates in multi-electrode submerged arc welding. Their mitigation techniques ACKNOWLEDGEMENTS*. Tech. rep. 2001.

[41] Bin Qiang et al. “Through-thickness welding residual stress and its effect on stress intensity factors for semi-elliptical surface cracks in a butt-welded steel plate”. In: *Engineering Fracture Mechanics* 193 (Apr. 2018), pp. 17–31. ISSN: 00137944. DOI: 10.1016/j.engfracmech.2018.02.016.

[42] A. Venugopal. Reddy. *Investigation of aeronautical and engineering component failures*. CRC Press, 2004, p. 348. ISBN: 0849323142.

[43] N. S. Rossini et al. *Methods of measuring residual stresses in components*. Mar. 2012. DOI: 10.1016/j.matdes.2011.08.022.

[44] César Rezende Silva, Valtair Antonio Ferraresi, and Américo Scotti. “A quality and cost approach for welding process selection”. In: *Journal of the Brazilian Society of Mechanical Sciences* 22.3 (2000), pp. 389–398. ISSN: 0100-7386. DOI: 10.1590/S0100-73862000000300002. URL: http://www.scielo.br/scielo.php?script=sci_arttext&pid=S0100-73862000000300002&lng=en&tlng=en.

[45] Edward H. (Mechanical engineer) Smith. *Mechanical engineer’s reference book*. Butterworth Heinemann, 1994. ISBN: 0750611952.

[46] K Spyridoni. *Prediction of residual stress of an orthotropic plate due to welding*. Tech. rep. URL: http://repository.tudelft.nl/..

[47] Nurul Syahida Mohd Nasir et al. *REVIEW ON WELDING RESIDUAL STRESS*. Tech. rep. 9. 2016, pp. 1819–6608. URL: www.arpnjournals.com.

[48] P. K. Taraphdar et al. “Residual stress distribution in thick double-V butt welds with varying groove configuration, restraints and mechanical tensioning”. In: *Journal of Manufacturing Processes* 68 (Aug. 2021), pp. 1405–1417. ISSN: 15266125. DOI: 10.1016/j.jmapro.2021.06.046.

[49] Tso Liang Teng, Peng Hsiang Chang, and Wen Cheng Tseng. “Effect of welding sequences on residual stresses”. In: *Computers and Structures* 81.5 (Mar. 2003), pp. 273–286. ISSN: 00457949. DOI: 10.1016/S0045-7949(02)00447-9.

[50] N J H Van Den Berg. *Effects of residual stresses on the fatigue crack propagation of an orthotropic steel bridge deck*. Tech. rep. 2020. URL: http://repository.tudelft.nl/..

[51] P. Vasantharaja, M. Vasudevan, and P. Palanichamy. “Effect of welding processes on the residual stress and distortion in type 316LN stainless steel weld joints”. In: *Journal of Manufacturing Processes* 19 (Aug. 2015), pp. 187–193. ISSN: 15266125. DOI: 10.1016/j.jmapro.2014.09.004.

[52] Xiaojia Wang, Qingchun Meng, and Weiping Hu. “Fatigue life prediction for butt-welded joints considering weld-induced residual stresses and initial damage, relaxation of residual stress, and elasto-plastic fatigue damage”. In: *Fatigue and Fracture of Engineering Materials and Structures* 42.6 (June 2019), pp. 1373–1386. ISSN: 14602695. DOI: 10.1111/ffe.12993.

[53] Klas Weman. “Welding residual stress and distortion”. In: *Welding Processes Handbook*. Elsevier, 2012, pp. 185–189. DOI: 10.1533/9780857095183.185.

[54] P. J. Withers and H. K.D.H. Bhadeshia. *Residual stress part 1 - Measurement techniques*. 2001. DOI: 10.1179/026708301101509980.

[55] P. J. Withers and H. K.D.H. Bhadeshia. *Residual stress part 2 - Nature and origins*. 2001. DOI: 10.1179/026708301101510087.

[56] P. J. Withers et al. “Recent advances in residual stress measurement”. In: *International Journal of Pressure Vessels and Piping* 85.3 (Mar. 2008), pp. 118–127. ISSN: 03080161. DOI: 10.1016/j.ijpvp.2007.10.007.

[57] Yanhong Ye et al. “Influence of groove type on welding-induced residual stress, deformation and width of sensitization region in a SUS304 steel butt welded joint”. In: *Advances in Engineering Software* 86 (Aug. 2015), pp. 39–48. ISSN: 18735339. DOI: 10.1016/j.advengsoft.2015.04.001.

[58] Yi Zhang et al. “Effect of Welding Sequence and Constraint on the Residual Stress and Deformation of Thick Welded Butt Joint Made of Q345qD Steel”. In: *Advances in Civil Engineering* 2022 (2022). ISSN: 16878094. DOI: 10.1155/2022/5966274.

A

Python scripts-Thermal

This appendix contains the scripts to create the steps and activation of the elements in the thermal and mechanical analyses.

A.0.1 1 Pass-Thermal

```
from interaction import *
from load import *
from mesh import *
from optimization import *
from job import *
from sketch import *
from visualization import *
from connectorBehavior import *



Tol=0.0000001
Speed=0.004
Nsteps = 10
NPass = 1
Nincrement=10
Weld_length = 0.25
Step_time = Weld_length/Speed/Nsteps
WeldIncrement = Weld_length/Nsteps
Model_name = '1Pass_TH'

a = mdb.models[Model_name].rootAssembly

# Creating steps Pass 1
mdb.models[Model_name].HeatTransferStep(deltmx=5000, initialInc=0.05,maxInc=0.2
    , maxNumInc=1000000, minInc=1e-11, timePeriod=Step_time, name='Welding1-1', previous='TackWelds')

for i in range (2,Nsteps+1):
    mdb.models[Model_name].HeatTransferStep(deltmx=5000, initialInc=0.05,maxInc=0.2
    , maxNumInc=1000000, minInc=1e-11, timePeriod=Step_time, name='Welding1-'+str(i), previous='Welding1-'+str(i-1))

# Creating sets for weld increments pass 1
for ii in range(1,Nsteps+1):
    e1 = a.sets['CUT-2.Weld1'].elements
    elements1 = e1.getByBoundingBox((ii-1)*WeldIncrement-Tol, -1, -1, Tol+ii*WeldIncrement, 1, 1)
    a.Set(elements=elements1, name='Weld_incr_1_'+str(ii))

# Activation of elements in weld pass 1
for ii in range(1,Nsteps+1):
    region =a.sets['Weld_incr_1_'+str(ii)]
    mdb.models[Model_name].ModelChange(name='Weld_incr_1_'+str(ii), createStepName='Welding1-'+str(ii),
    region=region, activeInStep=True, includeStrain=False)

# Cooling Step 1
```

```
mdb.models[Model_name].HeatTransferStep(name='Cooling_after_pass_1', previous='Welding1-'+str(Nsteps),
    timePeriod=15000, deltmx=5000, initialInc=0.2, maxInc=15, maxNumInc=1000000, minInc=1e-11)

for i in range (1,NPass+1):
    if i==1:
        mdb.models[Model_name].interactions['Weld_incr_'+str(i)+'_'+str(i)].move('Welding'+str(i)+'-'+str(i),'TackWelds')
    for j in range (1,Nincrement+1):
        if j==1 and i!=1:
            mdb.models[Model_name].interactions['Weld_incr_'+str(i)+'_'+str(j)].move('Welding'+str(i)+'-'+str(j),
            'Cooling_after_pass_'+str(i-1))
        if j!=1:
            mdb.models[Model_name].interactions['Weld_incr_'+str(i)+'_'+str(j)].move('Welding'+str(i)+'-'+str(j),
            'Welding'+str(i)+'-'+str(j-1))

mdb.models[Model_name].interactions['Weld_incr_1_10'].move('Welding1-9','TackWelds')
```

A.0.2 7 Passes-Thermal

```
from interaction import *
from load import *
from mesh import *
from optimization import *
from job import *
from sketch import *
from visualization import *
from connectorBehavior import *



Tol=0.0000001
Speed=0.007
Nsteps = 10
Weld_length = 0.7
Step_time = Weld_length/Speed/Nsteps
WeldIncrement = Weld_length/Nsteps
Model_name = '1_Thermal_model'

a = mdb.models[Model_name].rootAssembly

# Creating steps Pass 1
mdb.models[Model_name].HeatTransferStep(deltmx=5000, initialInc=0.1,maxInc=0.2
    , maxNumInc=1000000, minInc=1e-11, timePeriod=Step_time, name='Welding1-1', previous='TackWelds')

for i in range (2,Nsteps+1):
    mdb.models[Model_name].HeatTransferStep(deltmx=5000, initialInc=0.1,maxInc=0.2
    , maxNumInc=1000000, minInc=1e-11, timePeriod=Step_time, name='Welding1-'+str(i), previous='Welding1-'+str(i-1))

# Creating sets for weld increments pass 1
for ii in range(1,Nsteps+1):
    e1 = a.sets['New-IN-1.Weld1'].elements
    elements1 = e1.getByBoundingBox((ii-1)*WeldIncrement-Tol, -1, -1, Tol+ii*WeldIncrement, 1, 1)
    a.Set(elements=elements1, name='Weld_incr_1_'+str(ii))

# Activation of elements in weld pass 1
for ii in range(1,Nsteps+1):
    region =a.sets['Weld_incr_1_'+str(ii)]
    mdb.models[Model_name].ModelChange(name='Weld_incr_1_'+str(ii), createStepName='Welding1-'+str(ii),
    region=region, activeInStep=True, includeStrain=False)

# Cooling Step 1
mdb.models[Model_name].HeatTransferStep(name='Cooling_after_pass_1', previous='Welding1-'+str(Nsteps),
    timePeriod=5, deltmx=5000, initialInc=0.5, maxInc=1, maxNumInc=1000000, minInc=1e-11)



# Creating steps Pass 2
mdb.models[Model_name].HeatTransferStep(deltmx=5000, initialInc=0.1,maxInc=0.2
    , maxNumInc=1000000, minInc=1e-11, timePeriod=Step_time, name='Welding2-1', previous='Cooling_after_pass_1')
```

```
# Creating steps Pass 2
for i in range (2,Nsteps+1):
    mdb.models[Model_name].HeatTransferStep(deltmx=5000, initialInc=0.1,maxInc=0.2
    , maxNumInc=1000000, minInc=1e-11, timePeriod=Step_time, name='Welding2-'+str(i), previous='Welding2-'+str(i-1))

# Creating sets for weld increments pass 2
for ii in range(1,Nsteps+1):
    e1 = a.sets['New-IN-1.Weld2'].elements
    elements1 = e1.getByBoundingBox((ii-1)*WeldIncrement-Tol, -1, -1, Tol+ii*WeldIncrement, 1, 1)
    a.Set(elements=elements1, name='Weld_incr_2_'+str(ii))

# Activation of elements in weld pass 2
for ii in range(1,Nsteps+1):
    region =a.sets['Weld_incr_2_'+str(ii)]
    mdb.models[Model_name].ModelChange(name='Weld_incr_2_'+str(ii), createStepName='Welding2-'+str(ii),
    region=region, activeInStep=True, includeStrain=False)

# Cooling Step 2
mdb.models[Model_name].HeatTransferStep(name='Cooling_after_pass_2', previous='Welding2-'+str(Nsteps),
    timePeriod=5, deltmx=5000, initialInc=0.5, maxInc=1, maxNumInc=1000000, minInc=1e-11)



# Creating steps Pass 3
mdb.models[Model_name].HeatTransferStep(deltmx=5000, initialInc=0.1,maxInc=0.2
    , maxNumInc=1000000, minInc=1e-11, timePeriod=Step_time, name='Welding3-1', previous='Cooling_after_pass_2')

# Creating steps Pass 3
for i in range (2,Nsteps+1):
    mdb.models[Model_name].HeatTransferStep(deltmx=5000, initialInc=0.1,maxInc=0.2
    , maxNumInc=1000000, minInc=1e-11, timePeriod=Step_time, name='Welding3-'+str(i), previous='Welding3-'+str(i-1))

# Creating sets for weld increments pass 3
for ii in range(1,Nsteps+1):
    e1 = a.sets['New-IN-1.Weld3'].elements
    elements1 = e1.getByBoundingBox((ii-1)*WeldIncrement-Tol, -1, -1, Tol+ii*WeldIncrement, 1, 1)
    a.Set(elements=elements1, name='Weld_incr_3_'+str(ii))

# Activation of elements in weld pass 3
for ii in range(1,Nsteps+1):
    region =a.sets['Weld_incr_3_'+str(ii)]
    mdb.models[Model_name].ModelChange(name='Weld_incr_3_'+str(ii), createStepName='Welding3-'+str(ii),
    region=region, activeInStep=True, includeStrain=False)

# Cooling Step 3
mdb.models[Model_name].HeatTransferStep(name='Cooling_after_pass_3', previous='Welding3-'+str(Nsteps),
    timePeriod=5, deltmx=5000, initialInc=0.5, maxInc=1, maxNumInc=1000000, minInc=1e-11)



# Creating steps Pass 4
mdb.models[Model_name].HeatTransferStep(deltmx=5000, initialInc=0.1,maxInc=0.2
    , maxNumInc=1000000, minInc=1e-11, timePeriod=Step_time, name='Welding4-1', previous='Cooling_after_pass_3')

# Creating steps Pass 4
for i in range (2,Nsteps+1):
    mdb.models[Model_name].HeatTransferStep(deltmx=5000, initialInc=0.1,maxInc=0.2
    , maxNumInc=1000000, minInc=1e-11, timePeriod=Step_time, name='Welding4-'+str(i), previous='Welding4-'+str(i-1))

# Creating sets for weld increments pass 4
for ii in range(1,Nsteps+1):
    e1 = a.sets['New-IN-1.Weld4'].elements
    elements1 = e1.getByBoundingBox((ii-1)*WeldIncrement-Tol, -1, -1, Tol+ii*WeldIncrement, 1, 1)
    a.Set(elements=elements1, name='Weld_incr_4_'+str(ii))

# Activation of elements in weld pass 4
for ii in range(1,Nsteps+1):
    region =a.sets['Weld_incr_4_'+str(ii)]
    mdb.models[Model_name].ModelChange(name='Weld_incr_4_'+str(ii), createStepName='Welding4-'+str(ii),
```

```
    region=region, activeInStep=True, includeStrain=False)

# Cooling Step 4
mdb.models[Model_name].HeatTransferStep(name='Cooling_after_pass_4', previous='Welding4-'+str(Nsteps),
    timePeriod=5, deltmx=5000, initialInc=0.5, maxInc=1, maxNumInc=1000000, minInc=1e-11)



# Creating steps Pass 5
mdb.models[Model_name].HeatTransferStep(deltmx=5000, initialInc=0.1,maxInc=0.2
    , maxNumInc=1000000, minInc=1e-11, timePeriod=Step_time, name='Welding5-1', previous='Cooling_after_pass_4')

# Creating steps Pass 5
for i in range (2,Nsteps+1):
    mdb.models[Model_name].HeatTransferStep(deltmx=5000, initialInc=0.1,maxInc=0.2
    , maxNumInc=1000000, minInc=1e-11, timePeriod=Step_time, name='Welding5-'+str(i), previous='Welding5-'+str(i-1))

# Creating sets for weld increments pass 5
for ii in range(1,Nsteps+1):
    e1 = a.sets['New-IN-1.Weld5'].elements
    elements1 = e1.getByBoundingBox((ii-1)*WeldIncrement-Tol, -1, -1, Tol+ii*WeldIncrement, 1, 1)
    a.Set(elements=elements1, name='Weld_incr_5_'+str(ii))

# Activation of elements in weld pass 5
for ii in range(1,Nsteps+1):
    region =a.sets['Weld_incr_5_'+str(ii)]
    mdb.models[Model_name].ModelChange(name='Weld_incr_5_'+str(ii), createStepName='Welding5-'+str(ii),
    region=region, activeInStep=True, includeStrain=False)

# Cooling Step 5
mdb.models[Model_name].HeatTransferStep(name='Cooling_after_pass_5', previous='Welding5-'+str(Nsteps),
    timePeriod=5, deltmx=5000, initialInc=0.5, maxInc=1, maxNumInc=1000000, minInc=1e-11)



# Creating steps Pass 6
mdb.models[Model_name].HeatTransferStep(deltmx=5000, initialInc=0.1,maxInc=0.2
    , maxNumInc=1000000, minInc=1e-11, timePeriod=Step_time, name='Welding6-1', previous='Cooling_after_pass_5')

# Creating steps Pass 6
for i in range (2,Nsteps+1):
    mdb.models[Model_name].HeatTransferStep(deltmx=5000, initialInc=0.1,maxInc=0.2
    , maxNumInc=1000000, minInc=1e-11, timePeriod=Step_time, name='Welding6-'+str(i), previous='Welding6-'+str(i-1))

# Creating sets for weld increments pass 6
for ii in range(1,Nsteps+1):
    e1 = a.sets['New-IN-1.Weld6'].elements
    elements1 = e1.getByBoundingBox((ii-1)*WeldIncrement-Tol, -1, -1, Tol+ii*WeldIncrement, 1, 1)
    a.Set(elements=elements1, name='Weld_incr_6_'+str(ii))

# Activation of elements in weld pass 6
for ii in range(1,Nsteps+1):
    region =a.sets['Weld_incr_6_'+str(ii)]
    mdb.models[Model_name].ModelChange(name='Weld_incr_6_'+str(ii), createStepName='Welding6-'+str(ii),
    region=region, activeInStep=True, includeStrain=False)

# Cooling Step 6
mdb.models[Model_name].HeatTransferStep(name='Cooling_after_pass_6', previous='Welding6-'+str(Nsteps),
    timePeriod=5, deltmx=5000, initialInc=0.5, maxInc=1, maxNumInc=1000000, minInc=1e-11)



# Creating steps Pass 7
mdb.models[Model_name].HeatTransferStep(deltmx=5000, initialInc=0.1,maxInc=0.2
    , maxNumInc=1000000, minInc=1e-11, timePeriod=Step_time, name='Welding7-1', previous='Cooling_after_pass_6')

# Creating steps Pass 7
for i in range (2,Nsteps+1):
```

```
    mdb.models[Model_name].HeatTransferStep(deltmx=5000, initialInc=0.1,maxInc=0.2
    , maxNumInc=1000000, minInc=1e-11, timePeriod=Step_time, name='Welding7-'+str(i), previous='Welding7-'+str(i-1))

# Creating sets for weld increments pass 7
for ii in range(1,Nsteps+1):
    e1 = a.sets['New-IN-1.Weld7'].elements
    elements1 = e1.getByBoundingBox((ii-1)*WeldIncrement-Tol, -1, -1, Tol+ii*WeldIncrement, 1, 1)
    a.Set(elements=elements1, name='Weld_incr_7_'+str(ii))

# Activation of elements in weld pass 7
for ii in range(1,Nsteps+1):
    region =a.sets['Weld_incr_7_'+str(ii)]
    mdb.models[Model_name].ModelChange(name='Weld_incr_7_'+str(ii), createStepName='Welding7-'+str(ii),
    region=region, activeInStep=True, includeStrain=False)

# Cooling Step 7
mdb.models[Model_name].HeatTransferStep(name='Cooling_after_pass_7', previous='Welding7-'+str(Nsteps),
    timePeriod=15000, deltmx=5000, initialInc=2, maxInc=10, maxNumInc=1000000, minInc=1e-11)
```

A.0.3 12 Passes-Thermal

```
from interaction import *
from load import *
from mesh import *
from optimization import *
from job import *
from sketch import *
from visualization import *
from connectorBehavior import *



Tol=0.0000001
Speed=0.004
Nsteps = 10
Weld_length = 0.25
Step_time = Weld_length/Speed/Nsteps
WeldIncrement = Weld_length/Nsteps
Model_name = '10v2_TH'

a = mdb.models[Model_name].rootAssembly

# Creating steps Pass 1
mdb.models[Model_name].HeatTransferStep(deltmx=5000, initialInc=0.05,maxInc=0.2
    , maxNumInc=1000000, minInc=1e-11, timePeriod=Step_time, name='Welding1-1', previous='TackWelds')

for i in range (2,Nsteps+1):
    mdb.models[Model_name].HeatTransferStep(deltmx=5000, initialInc=0.05,maxInc=0.2
    , maxNumInc=1000000, minInc=1e-11, timePeriod=Step_time, name='Welding1-'+str(i), previous='Welding1-'+str(i-1))

# Creating sets for weld increments pass 1
for ii in range(1,Nsteps+1):
    e1 = a.sets['New-IN-1.Weld1'].elements
    elements1 = e1.getByBoundingBox((ii-1)*WeldIncrement-Tol, -1, -1, Tol+ii*WeldIncrement, 1, 1)
    a.Set(elements=elements1, name='Weld_incr_1_'+str(ii))

# Activation of elements in weld pass 1
for ii in range(1,Nsteps+1):
    region =a.sets['Weld_incr_1_'+str(ii)]
    mdb.models[Model_name].ModelChange(name='Weld_incr_1_'+str(ii), createStepName='Welding1-'+str(ii),
    region=region, activeInStep=True, includeStrain=False)

# Cooling Step 1
mdb.models[Model_name].HeatTransferStep(name='Cooling_after_pass_1', previous='Welding1-'+str(Nsteps),
    timePeriod=120, deltmx=5000, initialInc=0.5, maxInc=15, maxNumInc=1000000, minInc=1e-11)
```

```
# Creating steps Pass 2
mdb.models[Model_name].HeatTransferStep(deltmx=5000, initialInc=0.05,maxInc=0.2
    , maxNumInc=1000000, minInc=1e-11, timePeriod=Step_time, name='Welding2-1', previous='Cooling_after_pass_1')

# Creating steps Pass 2
for i in range (2,Nsteps+1):
    mdb.models[Model_name].HeatTransferStep(deltmx=5000, initialInc=0.05,maxInc=0.2
    , maxNumInc=1000000, minInc=1e-11, timePeriod=Step_time, name='Welding2-'+str(i), previous='Welding2-'+str(i-1))

# Creating sets for weld increments pass 2
for ii in range(1,Nsteps+1):
    e1 = a.sets['New-IN-1.Weld2'].elements
    elements1 = e1.getByBoundingBox((ii-1)*WeldIncrement-Tol, -1, -1, Tol+ii*WeldIncrement, 1, 1)
    a.Set(elements=elements1, name='Weld_incr_2_'+str(ii))

# Activation of elements in weld pass 2
for ii in range(1,Nsteps+1):
    region =a.sets['Weld_incr_2_'+str(ii)]
    mdb.models[Model_name].ModelChange(name='Weld_incr_2_'+str(ii), createStepName='Welding2-'+str(ii),
    region=region, activeInStep=True, includeStrain=False)

# Cooling Step 2
mdb.models[Model_name].HeatTransferStep(name='Cooling_after_pass_2', previous='Welding2-'+str(Nsteps),
    timePeriod=120, deltmx=5000, initialInc=0.5, maxInc=15, maxNumInc=1000000, minInc=1e-11)



# Creating steps Pass 3
mdb.models[Model_name].HeatTransferStep(deltmx=5000, initialInc=0.05,maxInc=0.2
    , maxNumInc=1000000, minInc=1e-11, timePeriod=Step_time, name='Welding3-1', previous='Cooling_after_pass_2')

# Creating steps Pass 3
for i in range (2,Nsteps+1):
    mdb.models[Model_name].HeatTransferStep(deltmx=5000, initialInc=0.05,maxInc=0.2
    , maxNumInc=1000000, minInc=1e-11, timePeriod=Step_time, name='Welding3-'+str(i), previous='Welding3-'+str(i-1))

# Creating sets for weld increments pass 3
for ii in range(1,Nsteps+1):
    e1 = a.sets['New-IN-1.Weld3'].elements
    elements1 = e1.getByBoundingBox((ii-1)*WeldIncrement-Tol, -1, -1, Tol+ii*WeldIncrement, 1, 1)
    a.Set(elements=elements1, name='Weld_incr_3_'+str(ii))

# Activation of elements in weld pass 3
for ii in range(1,Nsteps+1):
    region =a.sets['Weld_incr_3_'+str(ii)]
    mdb.models[Model_name].ModelChange(name='Weld_incr_3_'+str(ii), createStepName='Welding3-'+str(ii),
    region=region, activeInStep=True, includeStrain=False)

# Cooling Step 3
mdb.models[Model_name].HeatTransferStep(name='Cooling_after_pass_3', previous='Welding3-'+str(Nsteps),
    timePeriod=120, deltmx=5000, initialInc=0.5, maxInc=15, maxNumInc=1000000, minInc=1e-11)



# Creating steps Pass 4
mdb.models[Model_name].HeatTransferStep(deltmx=5000, initialInc=0.05,maxInc=0.2
    , maxNumInc=1000000, minInc=1e-11, timePeriod=Step_time, name='Welding4-1', previous='Cooling_after_pass_3')

# Creating steps Pass 4
for i in range (2,Nsteps+1):
    mdb.models[Model_name].HeatTransferStep(deltmx=5000, initialInc=0.05,maxInc=0.2
    , maxNumInc=1000000, minInc=1e-11, timePeriod=Step_time, name='Welding4-'+str(i), previous='Welding4-'+str(i-1))

# Creating sets for weld increments pass 4
for ii in range(1,Nsteps+1):
    e1 = a.sets['New-IN-1.Weld4'].elements
    elements1 = e1.getByBoundingBox((ii-1)*WeldIncrement-Tol, -1, -1, Tol+ii*WeldIncrement, 1, 1)
    a.Set(elements=elements1, name='Weld_incr_4_'+str(ii))
```

```
# Activation of elements in weld pass 4
for ii in range(1,Nsteps+1):
    region =a.sets['Weld_incr_4_'+str(ii)]
    mdb.models[Model_name].ModelChange(name='Weld_incr_4_'+str(ii), createStepName='Welding4-'+str(ii),
    region=region, activeInStep=True, includeStrain=False)

# Cooling Step 4
mdb.models[Model_name].HeatTransferStep(name='Cooling_after_pass_4', previous='Welding4-'+str(Nsteps),
    timePeriod=120, deltmx=5000, initialInc=0.5, maxInc=15, maxNumInc=1000000, minInc=1e-11)



# Creating steps Pass 5
mdb.models[Model_name].HeatTransferStep(deltmx=5000, initialInc=0.05,maxInc=0.2
    , maxNumInc=1000000, minInc=1e-11, timePeriod=Step_time, name='Welding5-1', previous='Cooling_after_pass_4')

# Creating steps Pass 5
for i in range (2,Nsteps+1):
    mdb.models[Model_name].HeatTransferStep(deltmx=5000, initialInc=0.05,maxInc=0.2
    , maxNumInc=1000000, minInc=1e-11, timePeriod=Step_time, name='Welding5-'+str(i), previous='Welding5-'+str(i-1))

# Creating sets for weld increments pass 5
for ii in range(1,Nsteps+1):
    e1 = a.sets['New-IN-1.Weld5'].elements
    elements1 = e1.getByBoundingBox((ii-1)*WeldIncrement-Tol, -1, -1, Tol+ii*WeldIncrement, 1, 1)
    a.Set(elements=elements1, name='Weld_incr_5_'+str(ii))

# Activation of elements in weld pass 5
for ii in range(1,Nsteps+1):
    region =a.sets['Weld_incr_5_'+str(ii)]
    mdb.models[Model_name].ModelChange(name='Weld_incr_5_'+str(ii), createStepName='Welding5-'+str(ii),
    region=region, activeInStep=True, includeStrain=False)

# Cooling Step 5
mdb.models[Model_name].HeatTransferStep(name='Cooling_after_pass_5', previous='Welding5-'+str(Nsteps),
    timePeriod=120, deltmx=5000, initialInc=0.5, maxInc=15, maxNumInc=1000000, minInc=1e-11)



# Creating steps Pass 6
mdb.models[Model_name].HeatTransferStep(deltmx=5000, initialInc=0.05,maxInc=0.2
    , maxNumInc=1000000, minInc=1e-11, timePeriod=Step_time, name='Welding6-1', previous='Cooling_after_pass_5')

# Creating steps Pass 6
for i in range (2,Nsteps+1):
    mdb.models[Model_name].HeatTransferStep(deltmx=5000, initialInc=0.05,maxInc=0.2
    , maxNumInc=1000000, minInc=1e-11, timePeriod=Step_time, name='Welding6-'+str(i), previous='Welding6-'+str(i-1))

# Creating sets for weld increments pass 6
for ii in range(1,Nsteps+1):
    e1 = a.sets['New-IN-1.Weld6'].elements
    elements1 = e1.getByBoundingBox((ii-1)*WeldIncrement-Tol, -1, -1, Tol+ii*WeldIncrement, 1, 1)
    a.Set(elements=elements1, name='Weld_incr_6_'+str(ii))

# Activation of elements in weld pass 6
for ii in range(1,Nsteps+1):
    region =a.sets['Weld_incr_6_'+str(ii)]
    mdb.models[Model_name].ModelChange(name='Weld_incr_6_'+str(ii), createStepName='Welding6-'+str(ii),
    region=region, activeInStep=True, includeStrain=False)

# Cooling Step 6
mdb.models[Model_name].HeatTransferStep(name='Cooling_after_pass_6', previous='Welding6-'+str(Nsteps),
    timePeriod=120, deltmx=5000, initialInc=0.5, maxInc=15, maxNumInc=1000000, minInc=1e-11)



# Creating steps Pass 7
mdb.models[Model_name].HeatTransferStep(deltmx=5000, initialInc=0.05,maxInc=0.2
```

```
    , maxNumInc=1000000, minInc=1e-11, timePeriod=Step_time, name='Welding7-1', previous='Cooling_after_pass_6')

# Creating steps Pass 7
for i in range (2,Nsteps+1):
    mdb.models[Model_name].HeatTransferStep(deltmx=5000, initialInc=0.05,maxInc=0.2
    , maxNumInc=1000000, minInc=1e-11, timePeriod=Step_time, name='Welding7-'+str(i), previous='Welding7-'+str(i-1))

# Creating sets for weld increments pass 7
for ii in range(1,Nsteps+1):
    e1 = a.sets['New-IN-1.Weld7'].elements
    elements1 = e1.getByBoundingBox((ii-1)*WeldIncrement-Tol, -1, -1, Tol+ii*WeldIncrement, 1, 1)
    a.Set(elements=elements1, name='Weld_incr_7_'+str(ii))

# Activation of elements in weld pass 7
for ii in range(1,Nsteps+1):
    region =a.sets['Weld_incr_7_'+str(ii)]
    mdb.models[Model_name].ModelChange(name='Weld_incr_7_'+str(ii), createStepName='Welding7-'+str(ii),
    region=region, activeInStep=True, includeStrain=False)

# Cooling Step 7
mdb.models[Model_name].HeatTransferStep(name='Cooling_after_pass_7', previous='Welding7-'+str(Nsteps),
    timePeriod=120, deltmx=5000, initialInc=0.5, maxInc=15, maxNumInc=1000000, minInc=1e-11)


# Creating steps Pass 8
mdb.models[Model_name].HeatTransferStep(deltmx=5000, initialInc=0.05,maxInc=0.2
    , maxNumInc=1000000, minInc=1e-11, timePeriod=Step_time, name='Welding8-1', previous='Cooling_after_pass_7')

# Creating steps Pass 8
for i in range (2,Nsteps+1):
    mdb.models[Model_name].HeatTransferStep(deltmx=5000, initialInc=0.05,maxInc=0.2
    , maxNumInc=1000000, minInc=1e-11, timePeriod=Step_time, name='Welding8-'+str(i), previous='Welding8-'+str(i-1))

# Creating sets for weld increments pass 8
for ii in range(1,Nsteps+1):
    e1 = a.sets['New-IN-1.Weld8'].elements
    elements1 = e1.getByBoundingBox((ii-1)*WeldIncrement-Tol, -1, -1, Tol+ii*WeldIncrement, 1, 1)
    a.Set(elements=elements1, name='Weld_incr_8_'+str(ii))

# Activation of elements in weld pass 8
for ii in range(1,Nsteps+1):
    region =a.sets['Weld_incr_8_'+str(ii)]
    mdb.models[Model_name].ModelChange(name='Weld_incr_8_'+str(ii), createStepName='Welding8-'+str(ii),
    region=region, activeInStep=True, includeStrain=False)

# Cooling Step 8
mdb.models[Model_name].HeatTransferStep(name='Cooling_after_pass_8', previous='Welding8-'+str(Nsteps),
    timePeriod=120, deltmx=5000, initialInc=0.5, maxInc=15, maxNumInc=1000000, minInc=1e-11)


    # Creating steps Pass 9
mdb.models[Model_name].HeatTransferStep(deltmx=5000, initialInc=0.05,maxInc=0.2
    , maxNumInc=1000000, minInc=1e-11, timePeriod=Step_time, name='Welding9-1', previous='Cooling_after_pass_8')

# Creating steps Pass 9
for i in range (2,Nsteps+1):
    mdb.models[Model_name].HeatTransferStep(deltmx=5000, initialInc=0.05,maxInc=0.2
    , maxNumInc=1000000, minInc=1e-11, timePeriod=Step_time, name='Welding9-'+str(i), previous='Welding9-'+str(i-1))

# Creating sets for weld increments pass 9
for ii in range(1,Nsteps+1):
    e1 = a.sets['New-IN-1.Weld9'].elements
    elements1 = e1.getByBoundingBox((ii-1)*WeldIncrement-Tol, -1, -1, Tol+ii*WeldIncrement, 1, 1)
    a.Set(elements=elements1, name='Weld_incr_9_'+str(ii))

# Activation of elements in weld pass 9
for ii in range(1,Nsteps+1):
    region =a.sets['Weld_incr_9_'+str(ii)]
    mdb.models[Model_name].ModelChange(name='Weld_incr_9_'+str(ii), createStepName='Welding9-'+str(ii),
    region=region, activeInStep=True, includeStrain=False)
```

```
# Cooling Step 9
mdb.models[Model_name].HeatTransferStep(name='Cooling_after_pass_9', previous='Welding9-'+str(Nsteps),
    timePeriod=120, deltmx=5000, initialInc=0.5, maxInc=15, maxNumInc=1000000, minInc=1e-11)

# Creating steps Pass 10
mdb.models[Model_name].HeatTransferStep(deltmx=5000, initialInc=0.05,maxInc=0.2
    , maxNumInc=1000000, minInc=1e-11, timePeriod=Step_time, name='Welding10-1', previous='Cooling_after_pass_9')

# Creating steps Pass 10
for i in range (2,Nsteps+1):
    mdb.models[Model_name].HeatTransferStep(deltmx=5000, initialInc=0.05,maxInc=0.2
    , maxNumInc=1000000, minInc=1e-11, timePeriod=Step_time, name='Welding10-'+str(i), previous='Welding10-'+str(i-1))

# Creating sets for weld increments pass 10
for ii in range(1,Nsteps+1):
    e1 = a.sets['New-IN-1.Weld10'].elements
    elements1 = e1.getByBoundingBox((ii-1)*WeldIncrement-Tol, -1, -1, Tol+ii*WeldIncrement, 1, 1)
    a.Set(elements=elements1, name='Weld_incr_10_'+str(ii))

# Activation of elements in weld pass 10
for ii in range(1,Nsteps+1):
    region =a.sets['Weld_incr_10_'+str(ii)]
    mdb.models[Model_name].ModelChange(name='Weld_incr_10_'+str(ii), createStepName='Welding10-'+str(ii),
    region=region, activeInStep=True, includeStrain=False)

# Cooling Step 10
mdb.models[Model_name].HeatTransferStep(name='Cooling_after_pass_10', previous='Welding10-'+str(Nsteps),
    timePeriod=120, deltmx=5000, initialInc=0.5, maxInc=15, maxNumInc=1000000, minInc=1e-11)

# Creating steps Pass 11
mdb.models[Model_name].HeatTransferStep(deltmx=5000, initialInc=0.05,maxInc=0.2
    , maxNumInc=1000000, minInc=1e-11, timePeriod=Step_time, name='Welding11-1', previous='Cooling_after_pass_10')

# Creating steps Pass 11
for i in range (2,Nsteps+1):
    mdb.models[Model_name].HeatTransferStep(deltmx=5000, initialInc=0.05,maxInc=0.2
    , maxNumInc=1000000, minInc=1e-11, timePeriod=Step_time, name='Welding11-'+str(i), previous='Welding11-'+str(i-1))

# Creating sets for weld increments pass 11
for ii in range(1,Nsteps+1):
    e1 = a.sets['New-IN-1.Weld11'].elements
    elements1 = e1.getByBoundingBox((ii-1)*WeldIncrement-Tol, -1, -1, Tol+ii*WeldIncrement, 1, 1)
    a.Set(elements=elements1, name='Weld_incr_11_'+str(ii))

# Activation of elements in weld pass 11
for ii in range(1,Nsteps+1):
    region =a.sets['Weld_incr_11_'+str(ii)]
    mdb.models[Model_name].ModelChange(name='Weld_incr_11_'+str(ii), createStepName='Welding11-'+str(ii),
    region=region, activeInStep=True, includeStrain=False)

# Cooling Step 11
mdb.models[Model_name].HeatTransferStep(name='Cooling_after_pass_11', previous='Welding11-'+str(Nsteps),
    timePeriod=120, deltmx=5000, initialInc=0.5, maxInc=15, maxNumInc=1000000, minInc=1e-11)

# Creating steps Pass 12
mdb.models[Model_name].HeatTransferStep(deltmx=5000, initialInc=0.05,maxInc=0.2
    , maxNumInc=1000000, minInc=1e-11, timePeriod=Step_time, name='Welding12-1', previous='Cooling_after_pass_11')

# Creating steps Pass 12
for i in range (2,Nsteps+1):
    mdb.models[Model_name].HeatTransferStep(deltmx=5000, initialInc=0.05,maxInc=0.2
    , maxNumInc=1000000, minInc=1e-11, timePeriod=Step_time, name='Welding12-'+str(i), previous='Welding12-'+str(i-1))

# Creating sets for weld increments pass 12
for ii in range(1,Nsteps+1):
    e1 = a.sets['New-IN-1.Weld12'].elements
    elements1 = e1.getByBoundingBox((ii-1)*WeldIncrement-Tol, -1, -1, Tol+ii*WeldIncrement, 1, 1)
    a.Set(elements=elements1, name='Weld_incr_12_'+str(ii))

# Activation of elements in weld pass 12
for ii in range(1,Nsteps+1):
```

```
    region =a.sets['Weld_incr_12_'+str(ii)]
    mdb.models[Model_name].ModelChange(name='Weld_incr_12_'+str(ii), createStepName='Welding12-'+str(ii),
    region=region, activeInStep=True, includeStrain=False)

# Cooling Step 12
mdb.models[Model_name].HeatTransferStep(name='Cooling_after_pass_12', previous='Welding12-'+str(Nsteps),
    timePeriod=15000, deltmx=5000, initialInc=0.5, maxInc=15, maxNumInc=1000000, minInc=1e-11)
```

B

Python scripts-Mechanical

B.0.1 1 Pass-Mechanical

```
from interaction import *
from load import *
from mesh import *
from optimization import *
from job import *
from sketch import *
from visualization import *
from connectorBehavior import *



Tol=0.0000001
Speed=0.004
Nsteps = 10
Nincrement=Nsteps
NPass = 1
Weld_length = 0.25
Step_time = Weld_length/Speed/Nsteps
WeldIncrement = Weld_length/Nsteps
Model_name = 'PoreM4mm_MECH'

a = mdb.models[Model_name].rootAssembly

#Deactivate steps
mdb.models[Model_name].steps['TackWelds'].suppress()

for i in range (1,Nsteps):
    mdb.models[Model_name].steps['Welding1-'+str(i)].suppress()

mdb.models[Model_name].steps['Cooling_after_pass_1'].suppress()

#Replace initial steps
mdb.models[Model_name].StaticStep(initialInc=1e-06, maintainAttributes=
    True, maxInc=1e-06, maxNumInc=1000000, minInc=1e-11, name='Pre-Step',
    nlgeom=ON, previous='Initial', timePeriod=1e-06)

mdb.models[Model_name].StaticStep(initialInc=1e-06,
    maintainAttributes=True, maxInc=1e-06, maxNumInc=1000000, minInc=1e-11,
    name='TackWelds', nlgeom=ON, previous='Pre-Step', timePeriod=1e-06)

# Replacing steps Pass 1
mdb.models[Model_name].StaticStep(initialInc=0.05, maintainAttributes=True,
    maxInc=0.2, maxNumInc=1000000, minInc=1e-11, name='Welding1-1', nlgeom=ON,
    previous='TackWelds', timePeriod=Step_time)

for i in range (2,Nsteps+1):
    mdb.models[Model_name].StaticStep(initialInc=0.05, maintainAttributes=True,
        maxInc=0.2, maxNumInc=1000000, minInc=1e-11, name='Welding1-'+str(i), nlgeom=ON,
```

```
        previous='Welding1-'+str(i-1), timePeriod=Step_time)

# Cooling Step 1
mdb.models[Model_name].StaticStep(name='Cooling_after_pass_1', previous='Welding1-'+str(Nsteps), nlgeom=ON,
        timePeriod=15000, initialInc=0.2, maxInc=15, maxNumInc=1000000, minInc=1e-11)

# Replacing sets for weld increments pass 1
for ii in range(1,Nsteps+1):
    e1 = a.sets['CUT-2.Weld1'].elements
    elements1 = e1.getByBoundingBox((ii-1)*WeldIncrement-Tol, -1, -1, Tol+ii*WeldIncrement, 1, 1)
    a.Set(elements=elements1, name='Weld_incr_1_'+str(ii))

# Activation of elements in weld pass 1
for ii in range(1,Nsteps+1):
    region =a.sets['Weld_incr_1_'+str(ii)]
    mdb.models[Model_name].ModelChange(name='Weld_incr_1_'+str(ii), createStepName='Welding1-'+str(ii),
    region=region, activeInStep=True, includeStrain=False)

for i in range (1,NPass+1):
    if i==1:
        mdb.models[Model_name].interactions['Weld_incr_'+str(i)+'_'+str(i)].move('Welding'+str(i)+'-'+str(i),'TackWelds')
    for j in range (1,Nincrement+1):
        if j==1 and i!=1:
            mdb.models[Model_name].interactions['Weld_incr_'+str(i)+'_'+str(j)].move('Welding'+str(i)+'-'+str(j),
            'Cooling_after_pass_'+str(i-1))
        if j!=1:
            mdb.models[Model_name].interactions['Weld_incr_'+str(i)+'_'+str(j)].move('Welding'+str(i)+'-'+str(j),
            'Welding'+str(i)+'-'+str(j-1))

mdb.models[Model_name].interactions['Weld_incr_1_10'].move('Welding1-9','TackWelds')
```

B.0.2 7 Passes-Mechanical

```
from interaction import *
from load import *
from mesh import *
from optimization import *
from job import *
from sketch import *
from visualization import *
from connectorBehavior import *



Tol=0.0000001
Speed=0.007
Nsteps = 10
Weld_length = 0.7
Step_time = Weld_length/Speed/Nsteps
WeldIncrement = Weld_length/Nsteps
Model_name = '1_Mechanical_model'

a = mdb.models[Model_name].rootAssembly

mdb.models[Model_name].StaticStep(initialInc=1e-06,
    maintainAttributes=True, maxInc=1e-06, maxNumInc=1000000, minInc=1e-11,
    name='TackWelds', nlgeom=ON, previous='Pre-step', timePeriod=1e-06)

# Creating steps Pass 1
mdb.models[Model_name].StaticStep(initialInc=0.05, maintainAttributes=True,
    maxInc=0.2, maxNumInc=1000000, minInc=1e-11, name='Welding1-1', nlgeom=ON,
    previous='TackWelds', timePeriod=Step_time)

for i in range (2,Nsteps+1):
    mdb.models[Model_name].StaticStep(initialInc=0.05, maintainAttributes=True,
        maxInc=0.2, maxNumInc=1000000, minInc=1e-11, name='Welding1-'+str(i), nlgeom=ON,
        previous='Welding1-'+str(i-1), timePeriod=Step_time)

# Replacing sets for weld increments pass 1
for ii in range(1,Nsteps+1):
```

```
    e1 = a.sets[Model_name].elements
    elements1 = e1.getByBoundingBox((ii-1)*WeldIncrement-Tol, -1, -1, Tol+ii*WeldIncrement, 1, 1)
    a.Set(elements=elements1, name='Weld_incr_1_'+str(ii))

# Activation of elements in weld pass 1
for ii in range(1,Nsteps+1):
    region =a.sets['Weld_incr_1_'+str(ii)]
    mdb.models[Model_name].ModelChange(name='Weld_incr_1_'+str(ii), createStepName='Welding1-'+str(ii),
    region=region, activeInStep=True, includeStrain=False)

# Cooling Step 1
mdb.models[Model_name].StaticStep(name='Cooling_after_pass_1', previous='Welding1-'+str(Nsteps), nlgeom=ON,
        timePeriod=5, initialInc=0.5, maxInc=1, maxNumInc=1000000, minInc=1e-11)



# Creating steps Pass 2
mdb.models[Model_name].StaticStep(initialInc=0.05, maintainAttributes=True,
    maxInc=0.2, maxNumInc=1000000, minInc=1e-11, name='Welding2-1', nlgeom=ON,
    previous='Cooling_after_pass_1', timePeriod=Step_time)

# Creating steps Pass 2
for i in range (2,Nsteps+1):
    mdb.models[Model_name].StaticStep(initialInc=0.05, maintainAttributes=True,
        maxInc=0.2, maxNumInc=1000000, minInc=1e-11, name='Welding2-'+str(i), nlgeom=ON,
        previous='Welding2-'+str(i-1), timePeriod=Step_time)

# Replacing sets for weld increments pass 2
for ii in range(1,Nsteps+1):
    e1 = a.sets[Model_name].elements
    elements1 = e1.getByBoundingBox((ii-1)*WeldIncrement-Tol, -1, -1, Tol+ii*WeldIncrement, 1, 1)
    a.Set(elements=elements1, name='Weld_incr_2_'+str(ii))

# Activation of elements in weld pass 2
for ii in range(1,Nsteps+1):
    region =a.sets['Weld_incr_2_'+str(ii)]
    mdb.models[Model_name].ModelChange(name='Weld_incr_2_'+str(ii), createStepName='Welding2'+str(ii),
    region=region, activeInStep=True, includeStrain=False)

# Cooling Step 2
mdb.models[Model_name].StaticStep(name='Cooling_after_pass_2', previous='Welding2-'+str(Nsteps), nlgeom=ON,
            timePeriod=5, initialInc=0.5, maxInc=1, maxNumInc=1000000, minInc=1e-11)



# Creating steps Pass 3
mdb.models[Model_name].StaticStep(initialInc=0.05, maintainAttributes=True,
    maxInc=0.2, maxNumInc=1000000, minInc=1e-11, name='Welding3-1', nlgeom=ON,
    previous='Cooling_after_pass_2', timePeriod=Step_time)

# Creating steps Pass 3
for i in range (2,Nsteps+1):
    mdb.models[Model_name].StaticStep(initialInc=0.05, maintainAttributes=True,
        maxInc=0.2, maxNumInc=1000000, minInc=1e-11, name='Welding3-'+str(i), nlgeom=ON,
        previous='Welding3-'+str(i-1), timePeriod=Step_time)

# Replacing sets for weld increments pass 3
for ii in range(1,Nsteps+1):
    e1 = a.sets[Model_name].elements
    elements1 = e1.getByBoundingBox((ii-1)*WeldIncrement-Tol, -1, -1, Tol+ii*WeldIncrement, 1, 1)
    a.Set(elements=elements1, name='Weld_incr_3_'+str(ii))

# Activation of elements in weld pass 3
for ii in range(1,Nsteps+1):
    region =a.sets['Weld_incr_3_'+str(ii)]
    mdb.models[Model_name].ModelChange(name='Weld_incr_3_'+str(ii), createStepName='Welding3-'+str(ii),
    region=region, activeInStep=True, includeStrain=False)
```

```
# Cooling Step 3
mdb.models[Model_name].StaticStep(name='Cooling_after_pass_3', previous='Welding3-'+str(Nsteps), nlgeom=ON,
            timePeriod=5, initialInc=0.5, maxInc=1, maxNumInc=1000000, minInc=1e-11)



# Creating steps Pass 4
mdb.models[Model_name].StaticStep(initialInc=0.05, maintainAttributes=True,
    maxInc=0.2, maxNumInc=1000000, minInc=1e-11, name='Welding4-1', nlgeom=ON,
    previous='Cooling_after_pass_3', timePeriod=Step_time)

# Creating steps Pass 4
for i in range (2,Nsteps+1):
    mdb.models[Model_name].StaticStep(initialInc=0.05, maintainAttributes=True,
        maxInc=0.2, maxNumInc=1000000, minInc=1e-11, name='Welding4-'+str(i), nlgeom=ON,
        previous='Welding4-'+str(i-1), timePeriod=Step_time)

# Replacing sets for weld increments pass 4
for ii in range(1,Nsteps+1):
    e1 = a.sets[Model_name].elements
    elements1 = e1.getByBoundingBox((ii-1)*WeldIncrement-Tol, -1, -1, Tol+ii*WeldIncrement, 1, 1)
    a.Set(elements=elements1, name='Weld_incr_4_'+str(ii))

# Activation of elements in weld pass 4
for ii in range(1,Nsteps+1):
    region =a.sets['Weld_incr_4_'+str(ii)]
    mdb.models[Model_name].ModelChange(name='Weld_incr_4_'+str(ii), createStepName='Welding4-'+str(ii),
    region=region, activeInStep=True, includeStrain=False)

# Cooling Step 4
mdb.models[Model_name].StaticStep(name='Cooling_after_pass_4', previous='Welding4-'+str(Nsteps), nlgeom=ON,
            timePeriod=5, initialInc=0.5, maxInc=1, maxNumInc=1000000, minInc=1e-11)



# Creating steps Pass 5
mdb.models[Model_name].StaticStep(initialInc=0.05, maintainAttributes=True,
    maxInc=0.2, maxNumInc=1000000, minInc=1e-11, name='Welding5-1', nlgeom=ON,
    previous='Cooling_after_pass_4', timePeriod=Step_time)

# Creating steps Pass 5
for i in range (2,Nsteps+1):
    mdb.models[Model_name].StaticStep(initialInc=0.05, maintainAttributes=True,
        maxInc=0.2, maxNumInc=1000000, minInc=1e-11, name='Welding5-'+str(i), nlgeom=ON,
        previous='Welding5-'+str(i-1), timePeriod=Step_time)

# Replacing sets for weld increments pass 5
for ii in range(1,Nsteps+1):
    e1 = a.sets[Model_name].elements
    elements1 = e1.getByBoundingBox((ii-1)*WeldIncrement-Tol, -1, -1, Tol+ii*WeldIncrement, 1, 1)
    a.Set(elements=elements1, name='Weld_incr_5_'+str(ii))

# Activation of elements in weld pass 5
for ii in range(1,Nsteps+1):
    region =a.sets['Weld_incr_5_'+str(ii)]
    mdb.models[Model_name].ModelChange(name='Weld_incr_5_'+str(ii), createStepName='Welding5-'+str(ii),
    region=region, activeInStep=True, includeStrain=False)

# Cooling Step 5
mdb.models[Model_name].StaticStep(name='Cooling_after_pass_5', previous='Welding5-'+str(Nsteps), nlgeom=ON,
            timePeriod=5, initialInc=0.5, maxInc=1, maxNumInc=1000000, minInc=1e-11)



# Creating steps Pass 6
mdb.models[Model_name].StaticStep(initialInc=0.05, maintainAttributes=True,
```

```
    maxInc=0.2, maxNumInc=1000000, minInc=1e-11, name='Welding6-1', nlgeom=ON,
    previous='Cooling_after_pass_5', timePeriod=Step_time)

# Creating steps Pass 6
for i in range (2,Nsteps+1):
    mdb.models[Model_name].StaticStep(initialInc=0.05, maintainAttributes=True,
        maxInc=0.2, maxNumInc=1000000, minInc=1e-11, name='Welding6-'+str(i), nlgeom=ON,
        previous='Welding6-'+str(i-1), timePeriod=Step_time)

# Replacing sets for weld increments pass 6
for ii in range(1,Nsteps+1):
    e1 = a.sets[Model_name].elements
    elements1 = e1.getByBoundingBox((ii-1)*WeldIncrement-Tol, -1, -1, Tol+ii*WeldIncrement, 1, 1)
    a.Set(elements=elements1, name='Weld_incr_6_'+str(ii))

# Activation of elements in weld pass 6
for ii in range(1,Nsteps+1):
    region =a.sets['Weld_incr_6_'+str(ii)]
    mdb.models[Model_name].ModelChange(name='Weld_incr_6_'+str(ii), createStepName='Welding6-'+str(ii),
    region=region, activeInStep=True, includeStrain=False)

# Cooling Step 6
mdb.models[Model_name].StaticStep(name='Cooling_after_pass_6', previous='Welding6-'+str(Nsteps), nlgeom=ON,
            timePeriod=5, initialInc=0.5, maxInc=1, maxNumInc=1000000, minInc=1e-11)




# Creating steps Pass 7
mdb.models[Model_name].StaticStep(initialInc=0.05, maintainAttributes=True,
    maxInc=0.2, maxNumInc=1000000, minInc=1e-11, name='Welding7-1', nlgeom=ON,
    previous='Cooling_after_pass_6', timePeriod=Step_time)

# Creating steps Pass 7
for i in range (2,Nsteps+1):
    mdb.models[Model_name].StaticStep(initialInc=0.05, maintainAttributes=True,
        maxInc=0.2, maxNumInc=1000000, minInc=1e-11, name='Welding7-'+str(i), nlgeom=ON,
        previous='Welding7-'+str(i-1), timePeriod=Step_time)

# Replacing sets for weld increments pass 7
for ii in range(1,Nsteps+1):
    e1 = a.sets[Model_name].elements
    elements1 = e1.getByBoundingBox((ii-1)*WeldIncrement-Tol, -1, -1, Tol+ii*WeldIncrement, 1, 1)
    a.Set(elements=elements1, name='Weld_incr_7_'+str(ii))

# Activation of elements in weld pass 7
for ii in range(1,Nsteps+1):
    region =a.sets['Weld_incr_7_'+str(ii)]
    mdb.models[Model_name].ModelChange(name='Weld_incr_7_'+str(ii), createStepName='Welding7-'+str(ii),
    region=region, activeInStep=True, includeStrain=False)

# Cooling Step 7
mdb.models[Model_name].StaticStep(name='Cooling_after_pass_7', previous='Welding7-'+str(Nsteps), nlgeom=ON,
            timePeriod=15000, initialInc=0.5, maxInc=15, maxNumInc=1000000, minInc=1e-11)
```

B.0.3 12 Passes-Mechanical

```
from interaction import *
from load import *
from mesh import *
from optimization import *
from job import *
from sketch import *
from visualization import *
from connectorBehavior import *
```

```
Tol=0.0000001
Speed=0.004
Nsteps = 10
Weld_length = 0.25
Step_time = Weld_length/Speed/Nsteps
WeldIncrement = Weld_length/Nsteps
Model_name = '12_MECH'

a = mdb.models[Model_name].rootAssembly

mdb.models[Model_name].StaticStep(initialInc=1e-06,
    maintainAttributes=True, maxInc=1e-06, maxNumInc=1000000, minInc=1e-11,
    name='TackWelds', nlgeom=ON, previous='Pre-Step', timePeriod=1e-06)

# Creating steps Pass 1
mdb.models[Model_name].StaticStep(initialInc=0.05, maintainAttributes=True,
    maxInc=0.2, maxNumInc=1000000, minInc=1e-11, name='Welding1-1', nlgeom=ON,
    previous='TackWelds', timePeriod=Step_time)

for i in range (2,Nsteps+1):
    mdb.models[Model_name].StaticStep(initialInc=0.05, maintainAttributes=True,
        maxInc=0.2, maxNumInc=1000000, minInc=1e-11, name='Welding1-'+str(i), nlgeom=ON,
        previous='Welding1-'+str(i-1), timePeriod=Step_time)

# Replacing sets for weld increments pass 1
for ii in range(1,Nsteps+1):
    e1 = a.sets[Model_name].elements
    elements1 = e1.getByBoundingBox((ii-1)*WeldIncrement-Tol, -1, -1, Tol+ii*WeldIncrement, 1, 1)
    a.Set(elements=elements1, name='Weld_incr_1_'+str(ii))

# Activation of elements in weld pass 1
for ii in range(1,Nsteps+1):
    region =a.sets['Weld_incr_1_'+str(ii)]
    mdb.models[Model_name].ModelChange(name='Weld_incr_1_'+str(ii), createStepName='Welding1-'+str(ii),
    region=region, activeInStep=True, includeStrain=False)

# Cooling Step 1
mdb.models[Model_name].StaticStep(name='Cooling_after_pass_1', previous='Welding1-'+str(Nsteps), nlgeom=ON,
        timePeriod=120, initialInc=0.5, maxInc=15, maxNumInc=1000000, minInc=1e-11)

# Creating steps Pass 2
mdb.models[Model_name].StaticStep(initialInc=0.01, maintainAttributes=True,
    maxInc=0.05, maxNumInc=1000000, minInc=1e-11, name='Welding2-1', nlgeom=ON,
    previous='Cooling_after_pass_1', timePeriod=Step_time)

# Creating steps Pass 2
for i in range (2,Nsteps+1):
    mdb.models[Model_name].StaticStep(initialInc=0.01, maintainAttributes=True,
        maxInc=0.05, maxNumInc=1000000, minInc=1e-11, name='Welding2-'+str(i), nlgeom=ON,
        previous='Welding2-'+str(i-1), timePeriod=Step_time)

# Replacing sets for weld increments pass 2
for ii in range(1,Nsteps+1):
    e1 = a.sets[Model_name].elements
    elements1 = e1.getByBoundingBox((ii-1)*WeldIncrement-Tol, -1, -1, Tol+ii*WeldIncrement, 1, 1)
    a.Set(elements=elements1, name='Weld_incr_2_'+str(ii))

# Activation of elements in weld pass 2
for ii in range(1,Nsteps+1):
    region =a.sets['Weld_incr_2_'+str(ii)]
    mdb.models[Model_name].ModelChange(name='Weld_incr_2_'+str(ii), createStepName='Welding2-'+str(ii),
    region=region, activeInStep=True, includeStrain=False)

# Cooling Step 2
mdb.models[Model_name].StaticStep(name='Cooling_after_pass_2', previous='Welding2-'+str(Nsteps), nlgeom=ON,
            timePeriod=120, initialInc=0.5, maxInc=15, maxNumInc=1000000, minInc=1e-11)

# Creating steps Pass 3
mdb.models[Model_name].StaticStep(initialInc=0.01, maintainAttributes=True,
```

```
    maxInc=0.05, maxNumInc=1000000, minInc=1e-11, name='Welding3-1', nlgeom=ON,
    previous='Cooling_after_pass_2', timePeriod=Step_time)

# Creating steps Pass 3
for i in range (2,Nsteps+1):
    mdb.models[Model_name].StaticStep(initialInc=0.01, maintainAttributes=True,
        maxInc=0.05, maxNumInc=1000000, minInc=1e-11, name='Welding3-'+str(i), nlgeom=ON,
        previous='Welding3-'+str(i-1), timePeriod=Step_time)

# Replacing sets for weld increments pass 3
for ii in range(1,Nsteps+1):
    e1 = a.sets[Model_name].elements
    elements1 = e1.getByBoundingBox((ii-1)*WeldIncrement-Tol, -1, -1, Tol+ii*WeldIncrement, 1, 1)
    a.Set(elements=elements1, name='Weld_incr_3_'+str(ii))

# Activation of elements in weld pass 3
for ii in range(1,Nsteps+1):
    region =a.sets['Weld_incr_3_'+str(ii)]
    mdb.models[Model_name].ModelChange(name='Weld_incr_3_'+str(ii), createStepName='Welding3-'+str(ii),
    region=region, activeInStep=True, includeStrain=False)

# Cooling Step 3
mdb.models[Model_name].StaticStep(name='Cooling_after_pass_3', previous='Welding3-'+str(Nsteps), nlgeom=ON,
            timePeriod=120, initialInc=0.5, maxInc=15, maxNumInc=1000000, minInc=1e-11)

# Creating steps Pass 4
mdb.models[Model_name].StaticStep(initialInc=0.01, maintainAttributes=True,
    maxInc=0.05, maxNumInc=1000000, minInc=1e-11, name='Welding4-1', nlgeom=ON,
    previous='Cooling_after_pass_3', timePeriod=Step_time)

# Creating steps Pass 4
for i in range (2,Nsteps+1):
    mdb.models[Model_name].StaticStep(initialInc=0.01, maintainAttributes=True,
        maxInc=0.05, maxNumInc=1000000, minInc=1e-11, name='Welding4-'+str(i), nlgeom=ON,
        previous='Welding4-'+str(i-1), timePeriod=Step_time)

# Replacing sets for weld increments pass 4
for ii in range(1,Nsteps+1):
    e1 = a.sets[Model_name].elements
    elements1 = e1.getByBoundingBox((ii-1)*WeldIncrement-Tol, -1, -1, Tol+ii*WeldIncrement, 1, 1)
    a.Set(elements=elements1, name='Weld_incr_4_'+str(ii))

# Activation of elements in weld pass 4
for ii in range(1,Nsteps+1):
    region =a.sets['Weld_incr_4_'+str(ii)]
    mdb.models[Model_name].ModelChange(name='Weld_incr_4_'+str(ii), createStepName='Welding4-'+str(ii),
    region=region, activeInStep=True, includeStrain=False)

# Cooling Step 4
mdb.models[Model_name].StaticStep(name='Cooling_after_pass_4', previous='Welding4-'+str(Nsteps), nlgeom=ON,
            timePeriod=120, initialInc=0.5, maxInc=15, maxNumInc=1000000, minInc=1e-11)

# Creating steps Pass 5
mdb.models[Model_name].StaticStep(initialInc=0.01, maintainAttributes=True,
    maxInc=0.05, maxNumInc=1000000, minInc=1e-11, name='Welding5-1', nlgeom=ON,
    previous='Cooling_after_pass_4', timePeriod=Step_time)

# Creating steps Pass 5
for i in range (2,Nsteps+1):
    mdb.models[Model_name].StaticStep(initialInc=0.01, maintainAttributes=True,
        maxInc=0.05, maxNumInc=1000000, minInc=1e-11, name='Welding5-'+str(i), nlgeom=ON,
        previous='Welding5-'+str(i-1), timePeriod=Step_time)

# Replacing sets for weld increments pass 5
for ii in range(1,Nsteps+1):
    e1 = a.sets[Model_name].elements
    elements1 = e1.getByBoundingBox((ii-1)*WeldIncrement-Tol, -1, -1, Tol+ii*WeldIncrement, 1, 1)
    a.Set(elements=elements1, name='Weld_incr_5_'+str(ii))

# Activation of elements in weld pass 5
for ii in range(1,Nsteps+1):
```

```
    region =a.sets['Weld_incr_5_'+str(ii)]
    mdb.models[Model_name].ModelChange(name='Weld_incr_5_'+str(ii), createStepName='Welding5-'+str(ii),
    region=region, activeInStep=True, includeStrain=False)

# Cooling Step 5
mdb.models[Model_name].StaticStep(name='Cooling_after_pass_5', previous='Welding5-'+str(Nsteps), nlgeom=ON,
            timePeriod=120, initialInc=0.5, maxInc=15, maxNumInc=1000000, minInc=1e-11)

# Creating steps Pass 6
mdb.models[Model_name].StaticStep(initialInc=0.01, maintainAttributes=True,
    maxInc=0.05, maxNumInc=1000000, minInc=1e-11, name='Welding6-1', nlgeom=ON,
    previous='Cooling_after_pass_5', timePeriod=Step_time)

# Creating steps Pass 6
for i in range (2,Nsteps+1):
    mdb.models[Model_name].StaticStep(initialInc=0.01, maintainAttributes=True,
        maxInc=0.05, maxNumInc=1000000, minInc=1e-11, name='Welding6-'+str(i), nlgeom=ON,
        previous='Welding6-'+str(i-1), timePeriod=Step_time)

# Replacing sets for weld increments pass 6
for ii in range(1,Nsteps+1):
    e1 = a.sets[Model_name].elements
    elements1 = e1.getByBoundingBox((ii-1)*WeldIncrement-Tol, -1, -1, Tol+ii*WeldIncrement, 1, 1)
    a.Set(elements=elements1, name='Weld_incr_6_'+str(ii))

# Activation of elements in weld pass 6
for ii in range(1,Nsteps+1):
    region =a.sets['Weld_incr_6_'+str(ii)]
    mdb.models[Model_name].ModelChange(name='Weld_incr_6_'+str(ii), createStepName='Welding6-'+str(ii),
    region=region, activeInStep=True, includeStrain=False)

# Cooling Step 6
mdb.models[Model_name].StaticStep(name='Cooling_after_pass_6', previous='Welding6-'+str(Nsteps), nlgeom=ON,
            timePeriod=120, initialInc=0.5, maxInc=15, maxNumInc=1000000, minInc=1e-11)

# Creating steps Pass 7
mdb.models[Model_name].StaticStep(initialInc=0.01, maintainAttributes=True,
    maxInc=0.05, maxNumInc=1000000, minInc=1e-11, name='Welding7-1', nlgeom=ON,
    previous='Cooling_after_pass_6', timePeriod=Step_time)

# Creating steps Pass 7
for i in range (2,Nsteps+1):
    mdb.models[Model_name].StaticStep(initialInc=0.01, maintainAttributes=True,
        maxInc=0.05, maxNumInc=1000000, minInc=1e-11, name='Welding7-'+str(i), nlgeom=ON,
        previous='Welding7-'+str(i-1), timePeriod=Step_time)

# Replacing sets for weld increments pass 7
for ii in range(1,Nsteps+1):
    e1 = a.sets[Model_name].elements
    elements1 = e1.getByBoundingBox((ii-1)*WeldIncrement-Tol, -1, -1, Tol+ii*WeldIncrement, 1, 1)
    a.Set(elements=elements1, name='Weld_incr_7_'+str(ii))

# Activation of elements in weld pass 7
for ii in range(1,Nsteps+1):
    region =a.sets['Weld_incr_7_'+str(ii)]
    mdb.models[Model_name].ModelChange(name='Weld_incr_7_'+str(ii), createStepName='Welding7-'+str(ii),
    region=region, activeInStep=True, includeStrain=False)

# Cooling Step 7
mdb.models[Model_name].StaticStep(name='Cooling_after_pass_7', previous='Welding7-'+str(Nsteps), nlgeom=ON,
            timePeriod=120, initialInc=0.5, maxInc=15, maxNumInc=1000000, minInc=1e-11)

# Creating steps Pass 8
mdb.models[Model_name].StaticStep(initialInc=0.01, maintainAttributes=True,
    maxInc=0.05, maxNumInc=1000000, minInc=1e-11, name='Welding8-1', nlgeom=ON,
    previous='Cooling_after_pass_7', timePeriod=Step_time)

# Creating steps Pass 8
for i in range (2,Nsteps+1):
    mdb.models[Model_name].StaticStep(initialInc=0.01, maintainAttributes=True,
        maxInc=0.05, maxNumInc=1000000, minInc=1e-11, name='Welding8-'+str(i), nlgeom=ON,
```

```
        previous='Welding8-'+str(i-1), timePeriod=Step_time)

# Replacing sets for weld increments pass 8
for ii in range(1,Nsteps+1):
    e1 = a.sets[Model_name].elements
    elements1 = e1.getByBoundingBox((ii-1)*WeldIncrement-Tol, -1, -1, Tol+ii*WeldIncrement, 1, 1)
    a.Set(elements=elements1, name='Weld_incr_8_'+str(ii))

# Activation of elements in weld pass 8
for ii in range(1,Nsteps+1):
    region =a.sets['Weld_incr_8_'+str(ii)]
    mdb.models[Model_name].ModelChange(name='Weld_incr_8_'+str(ii), createStepName='Welding8-'+str(ii),
    region=region, activeInStep=True, includeStrain=False)

# Cooling Step 8
mdb.models[Model_name].StaticStep(name='Cooling_after_pass_8', previous='Welding8-'+str(Nsteps), nlgeom=ON,
            timePeriod=120, initialInc=0.5, maxInc=15, maxNumInc=1000000, minInc=1e-11)

# Creating steps Pass 9
mdb.models[Model_name].StaticStep(initialInc=0.01, maintainAttributes=True,
    maxInc=0.05, maxNumInc=1000000, minInc=1e-11, name='Welding9-1', nlgeom=ON,
    previous='Cooling_after_pass_8', timePeriod=Step_time)

# Creating steps Pass 9
for i in range (2,Nsteps+1):
    mdb.models[Model_name].StaticStep(initialInc=0.01, maintainAttributes=True,
        maxInc=0.05, maxNumInc=1000000, minInc=1e-11, name='Welding9-'+str(i), nlgeom=ON,
        previous='Welding9-'+str(i-1), timePeriod=Step_time)

# Replacing sets for weld increments pass 9
for ii in range(1,Nsteps+1):
    e1 = a.sets[Model_name].elements
    elements1 = e1.getByBoundingBox((ii-1)*WeldIncrement-Tol, -1, -1, Tol+ii*WeldIncrement, 1, 1)
    a.Set(elements=elements1, name='Weld_incr_9_'+str(ii))

# Activation of elements in weld pass 9
for ii in range(1,Nsteps+1):
    region =a.sets['Weld_incr_9_'+str(ii)]
    mdb.models[Model_name].ModelChange(name='Weld_incr_9_'+str(ii), createStepName='Welding9-'+str(ii),
    region=region, activeInStep=True, includeStrain=False)

# Cooling Step 9
mdb.models[Model_name].StaticStep(name='Cooling_after_pass_9', previous='Welding9-'+str(Nsteps), nlgeom=ON,
            timePeriod=120, initialInc=0.5, maxInc=15, maxNumInc=1000000, minInc=1e-11)

# Creating steps Pass 10
mdb.models[Model_name].StaticStep(initialInc=0.01, maintainAttributes=True,
    maxInc=0.05, maxNumInc=1000000, minInc=1e-11, name='Welding10-1', nlgeom=ON,
    previous='Cooling_after_pass_9', timePeriod=Step_time)

# Creating steps Pass 10
for i in range (2,Nsteps+1):
    mdb.models[Model_name].StaticStep(initialInc=0.01, maintainAttributes=True,
        maxInc=0.05, maxNumInc=1000000, minInc=1e-11, name='Welding10-'+str(i), nlgeom=ON,
        previous='Welding10-'+str(i-1), timePeriod=Step_time)

# Replacing sets for weld increments pass 10
for ii in range(1,Nsteps+1):
    e1 = a.sets[Model_name].elements
    elements1 = e1.getByBoundingBox((ii-1)*WeldIncrement-Tol, -1, -1, Tol+ii*WeldIncrement, 1, 1)
    a.Set(elements=elements1, name='Weld_incr_10_'+str(ii))

# Activation of elements in weld pass 10
for ii in range(1,Nsteps+1):
    region =a.sets['Weld_incr_10_'+str(ii)]
    mdb.models[Model_name].ModelChange(name='Weld_incr_10_'+str(ii), createStepName='Welding10-'+str(ii),
    region=region, activeInStep=True, includeStrain=False)

# Cooling Step 10
mdb.models[Model_name].StaticStep(name='Cooling_after_pass_10', previous='Welding10-'+str(Nsteps), nlgeom=ON,
            timePeriod=120, initialInc=0.5, maxInc=15, maxNumInc=1000000, minInc=1e-11)
```

```
# Creating steps Pass 11
mdb.models[Model_name].StaticStep(initialInc=0.01, maintainAttributes=True,
    maxInc=0.05, maxNumInc=1000000, minInc=1e-11, name='Welding11-1', nlgeom=ON,
    previous='Cooling_after_pass_10', timePeriod=Step_time)

# Creating steps Pass 11
for i in range (2,Nsteps+1):
    mdb.models[Model_name].StaticStep(initialInc=0.01, maintainAttributes=True,
        maxInc=0.05, maxNumInc=1000000, minInc=1e-11, name='Welding11-'+str(i), nlgeom=ON,
        previous='Welding11-'+str(i-1), timePeriod=Step_time)

# Replacing sets for weld increments pass 11
for ii in range(1,Nsteps+1):
    e1 = a.sets[Model_name].elements
    elements1 = e1.getByBoundingBox((ii-1)*WeldIncrement-Tol, -1, -1, Tol+ii*WeldIncrement, 1, 1)
    a.Set(elements=elements1, name='Weld_incr_11_'+str(ii))

# Activation of elements in weld pass 11
for ii in range(1,Nsteps+1):
    region =a.sets['Weld_incr_11_'+str(ii)]
    mdb.models[Model_name].ModelChange(name='Weld_incr_11_'+str(ii), createStepName='Welding11-'+str(ii),
    region=region, activeInStep=True, includeStrain=False)

# Cooling Step 11
mdb.models[Model_name].StaticStep(name='Cooling_after_pass_11', previous='Welding11-'+str(Nsteps), nlgeom=ON,
            timePeriod=120, initialInc=0.5, maxInc=15, maxNumInc=1000000, minInc=1e-11)

# Creating steps Pass 12
mdb.models[Model_name].StaticStep(initialInc=0.01, maintainAttributes=True,
    maxInc=0.05, maxNumInc=1000000, minInc=1e-11, name='Welding12-1', nlgeom=ON,
    previous='Cooling_after_pass_11', timePeriod=Step_time)

# Creating steps Pass 12
for i in range (2,Nsteps+1):
    mdb.models[Model_name].StaticStep(initialInc=0.01, maintainAttributes=True,
        maxInc=0.05, maxNumInc=1000000, minInc=1e-11, name='Welding12-'+str(i), nlgeom=ON,
        previous='Welding12-'+str(i-1), timePeriod=Step_time)

# Replacing sets for weld increments pass 12
for ii in range(1,Nsteps+1):
    e1 = a.sets[Model_name].elements
    elements1 = e1.getByBoundingBox((ii-1)*WeldIncrement-Tol, -1, -1, Tol+ii*WeldIncrement, 1, 1)
    a.Set(elements=elements1, name='Weld_incr_12_'+str(ii))

# Activation of elements in weld pass 12
for ii in range(1,Nsteps+1):
    region =a.sets['Weld_incr_12_'+str(ii)]
    mdb.models[Model_name].ModelChange(name='Weld_incr_12_'+str(ii), createStepName='Welding12-'+str(ii),
    region=region, activeInStep=True, includeStrain=False)

# Cooling Step 12
mdb.models[Model_name].StaticStep(name='Cooling_after_pass_12', previous='Welding12-'+str(Nsteps), nlgeom=ON,
            timePeriod=15000, initialInc=0.5, maxInc=15, maxNumInc=1000000, minInc=1e-11)
```

C

Fortran scripts

This appendix contains the script for the Dflux subroutine, in which the moving Goldak double ellipsoid heat source model is defined. The script includes a loop that sets the welding parameters for each pass, with each pass having its own unique set of Goldak parameters.

C.0.1 1 Pass

```
      SUBROUTINE DFLUX(FLUX,SOL,KSTEP,KINC,TIME,NOEL,NPT,COORDS,
     1 JLTYP,TEMP,PRESS,SNAME)
C
      INCLUDE 'ABA_PARAM.INC'
C
      DIMENSION FLUX(2), TIME(2), COORDS(3)
      CHARACTER*80 SNAME
          INTEGER I

          X=COORDS(1)
          Y=COORDS(2)
          Z=COORDS(3)
          T=TIME(2)

          XO=0.0
          YO=0.0
          ZO=0.0

          Am = 140
          Vo = 23
          Q1= Am*Vo

          PI=3.141593
          V=0.004
          WeldLength=0.25

          Prestep=1E-06
          TackWeld=1E-06


          a=0.00525
          b=0.00590


          cr=0.005
          cf=0.002
          ff=0.833333
          fr=0.333333
          ETTA=0.7
```

```
          XC=X0+V*T
          YC=Y0
          ZC=Z0-(4.E-03)



          Q=(ETTA*Q1*6*(3**0.5))/((a*b)*(PI**1.5))
C     Rear
      IF (X<=XC) THEN
          IF(((((X-XC)**2)/(cr**2)+((Y-YC)**2)/(a**2)+((Z-ZC)**2)/(b**2))<1)) THEN
          FLUX(1)=Q*(fr/cr)*EXP(-3*(((X-XC)**2)/(cr**2)+((Y-YC)**2)/(a**2)+((Z-ZC)**2)/(b**2)))
          END IF
C     Front
      ELSEIF (X>XC) THEN
          IF(((((X-XC)**2)/(cf**2)+((Y-YC)**2)/(a**2)+((Z-ZC)**2)/(b**2))<1)) THEN
          FLUX(1)=Q*(ff/cf)*EXP(-3*(((X-XC)**2)/(cf**2)+((Y-YC)**2)/(a**2)+((Z-ZC)**2)/(b**2)))
          END IF
          END IF


          FLUX(2)=0.0

      RETURN
      END
```

C.0.2 7 Passes

```
      SUBROUTINE DFLUX(FLUX,SOL,KSTEP,KINC,TIME,NOEL,NPT,COORDS,
     1 JLTYP,TEMP,PRESS,SNAME)
C
      INCLUDE 'ABA_PARAM.INC'
C
      DIMENSION FLUX(2), TIME(2), COORDS(3)
      CHARACTER*80 SNAME
          INTEGER I

          X=COORDS(1)
          Y=COORDS(2)
          Z=COORDS(3)
          T=TIME(2)

          X0=0.0
          Y0=0.0
          Z0=0.0

          Am = 600 !Amperes
          Vo = 30 !Voltage
          Q= Am*Vo !Power

          PI=3.141593
          V=0.007 !Speed of the torch
          WeldLength=0.7
          Coolingtime1=5
          Coolingtime2=5
          Coolingtime3=5
          Coolingtime4=5
          Coolingtime5=5
          Coolingtime6=5
          Prestep=1E-06
          TackWelds=1E-06

C          !Goldak heat source model
          a=0.0045
          b=0.004
          a1=0.0055
          b1=0.004
          a2=0.0073
          b2=0.004
          a3=0.009
          b3=0.0087
```

```
      a4=0.009
      b4=0.0087
      a5=0.0062
      b5=0.004
      a6=0.0135
      b6=0.01
      cr=0.015
      cf=0.010
      ff=0.8
      fr=1.2
      ETTA=0.9


C      !Set local coordinates of weldpasses, translations
      XC=X0+V*T
      XC1=X0+V*(T-WeldLength/V-Coolingtime1-Prestep-TackWelds)
      XC2=X0+V*(T-2*WeldLength/V-Coolingtime1-Coolingtime2-Prestep-TackWelds)
      XC3=X0+V*(T-3*WeldLength/V-Coolingtime1-Coolingtime2-Coolingtime3-Prestep-TackWelds)
      XC4=X0+V*(T-4*WeldLength/V-Coolingtime1-Coolingtime2-Coolingtime3-Coolingtime4-Prestep-TackWelds)
      XC5=X0+V*(T-5*WeldLength/V-Coolingtime1-Coolingtime2-Coolingtime3-Coolingtime4-Coolingtime5-Prestep-TackWelds)
      XC6=X0+V*(T-6*WeldLength/V-Coolingtime1-Coolingtime2-Coolingtime3-Coolingtime4-Coolingtime5-Coolingtime6-Prestep
      -TackWelds)

      YC=Y0
      YC0=Y0
      YC1=Y0+(6.E-03)
      YC2=Y0-(6.E-03)

      ZC=Z0-(14.E-03)
      ZC1=Z0-(18.E-03)
      ZC2=Z0-(22.E-03)
      ZC3=Z0-(27.5E-03)
      ZC4=Z0-(27.5E-03)
      ZC5=Z0-(10.E-03)
      ZC6=Z0-(4.E-03)


      FLUX(1) = 0
      DO I = 1,7
            IF (T.LT.WeldLength/V+Prestep+TackWelds) THEN
                  Q1=(ETTA*Q*6*(3**0.5))/((a*b)*(PI**1.5))
C           Rear
                  IF (X.LE.XC) THEN
                        IF(((((X-XC)**2)/(cr**2)+((Y-YC)**2)/(a**2)+((Z-ZC)**2)/(b**2)).LT.1)) THEN
                              FLUX(1)=Q1*(fr/cr)*EXP(-3*(((X-XC)**2)/(cr**2)+((Y-YC)**2)/(a**2)+
                              ((Z-ZC)**2)/(b**2)))
                        END IF
C           Front
                  ELSEIF (X.GT.XC) THEN
                        IF(((((X-XC)**2)/(cf**2)+((Y-YC)**2)/(a**2)+((Z-ZC)**2)/(b**2)).LT.1)) THEN
                              FLUX(1)=Q1*(ff/cf)*EXP(-3*(((X-XC)**2)/(cf**2)+((Y-YC)**2)/(a**2)+
                              ((Z-ZC)**2)/(b**2)))
                        END IF
                  END IF
                  FLUX(2)=0.0


            ELSEIF (WeldLength/V+Coolingtime1+Prestep+TackWelds.LE.T .AND. T.LT.2*WeldLength/V+
            Coolingtime1+Prestep+TackWelds) THEN
                  Q2=(ETTA*Q*6*(3**0.5))/((a1*b1)*(PI**1.5))
C           Rear
                  IF (X.LE.XC1) THEN
                        IF(((((X-XC1)**2)/(cr**2)+((Y-YC)**2)/(a1**2)+((Z-ZC1)**2)/(b1**2)).LT.1)) THEN
                              FLUX(1)=Q2*(fr/cr)*EXP(-3*(((X-XC1)**2)/(cr**2)+((Y-YC)**2)/(a1**2)+
                              ((Z-ZC1)**2)/(b1**2)))
                        END IF
C           Front
                  ELSEIF (X.GT.XC1) THEN
                        IF(((((X-XC1)**2)/(cf**2)+((Y-YC)**2)/(a1**2)+((Z-ZC1)**2)/(b1**2)).LT.1)) THEN
                              FLUX(1)=Q2*(ff/cf)*EXP(-3*(((X-XC1)**2)/(cf**2)+((Y-YC)**2)/(a1**2)+
                              ((Z-ZC1)**2)/(b1**2)))
```

```
                        END IF
                    END IF
                    FLUX(2)=0.0

C       !PASS3
                ELSEIF (2*WeldLength/V+Coolingtime1+Coolingtime2+Prestep+TackWelds.LE.T .AND.
                T.LT.3*WeldLength/V+Coolingtime1+Coolingtime2+Prestep+TackWelds) THEN
                    Q3=(ETTA*Q*6*(3**0.5))/((a2*b2)*(PI**1.5))
C           Rear
                    IF (X.LE.XC2) THEN
                        IF(((((X-XC2)**2)/(cr**2)+((Y-YC0)**2)/(a2**2)+((Z-ZC2)**2)/(b2**2)).LT.1)) THEN
                            FLUX(1)=Q3*(fr/cr)*EXP(-3*(((X-XC2)**2)/(cr**2)+((Y-YC0)**2)/(a2**2)+
                            ((Z-ZC2)**2)/(b2**2)))
                        END IF
C           Front
                    ELSEIF (X.GT.XC2) THEN
                        IF(((((X-XC2)**2)/(cf**2)+((Y-YC0)**2)/(a2**2)+((Z-ZC2)**2)/(b2**2)).LT.1)) THEN
                        FLUX(1)=Q3*(ff/cf)*EXP(-3*(((X-XC2)**2)/(cf**2)+((Y-YC0)**2)/(a2**2)+
                        ((Z-ZC2)**2)/(b2**2)))
                        END IF
                    END IF
                    FLUX(2)=0.0

C       !PASS4
                ELSEIF (3*WeldLength/V+Coolingtime1+Coolingtime2+Coolingtime3+Prestep+TackWelds.LE.T .AND.
                T.LT.4*WeldLength/V+Coolingtime1+Coolingtime2+Coolingtime3+Prestep+TackWelds) THEN
                    Q4=(ETTA*Q*6*(3**0.5))/((a3*b3)*(PI**1.5))
C           Rear
                    IF (X.LE.XC3) THEN
                        IF(((((X-XC3)**2)/(cr**2)+((Y-YC1)**2)/(a3**2)+((Z-ZC3)**2)/(b3**2)).LT.1)) THEN
                            FLUX(1)=Q4*(fr/cr)*EXP(-3*(((X-XC3)**2)/(cr**2)+((Y-YC1)**2)/(a3**2)+
                            ((Z-ZC3)**2)/(b3**2)))
                        END IF
C           Front
                    ELSEIF (X.GT.XC3) THEN
                        IF(((((X-XC3)**2)/(cf**2)+((Y-YC1)**2)/(a3**2)+((Z-ZC3)**2)/(b3**2)).LT.1)) THEN
                        FLUX(1)=Q4*(ff/cf)*EXP(-3*(((X-XC3)**2)/(cf**2)+((Y-YC1)**2)/(a3**2)+
                        ((Z-ZC3)**2)/(b3**2)))
                        END IF
                    END IF
                    FLUX(2)=0.0

C       !PASS5
                ELSEIF (4*WeldLength/V+Coolingtime1+Coolingtime2+Coolingtime3+Coolingtime4+Prestep+TackWelds.LE.T .AND.
                T.LT.5*WeldLength/V+Coolingtime1+Coolingtime2+Coolingtime3+Coolingtime4+Prestep+TackWelds) THEN
                    Q5=(ETTA*Q*6*(3**0.5))/((a4*b4)*(PI**1.5))
C           Rear
                    IF (X.LE.XC4) THEN
                        IF(((((X-XC4)**2)/(cr**2)+((Y-YC2)**2)/(a4**2)+((Z-ZC4)**2)/(b4**2)).LT.1)) THEN
                            FLUX(1)=Q5*(fr/cr)*EXP(-3*(((X-XC4)**2)/(cr**2)+((Y-YC2)**2)/(a4**2)+
                            ((Z-ZC4)**2)/(b4**2)))
                        END IF
C           Front
                    ELSEIF (X.GT.XC4) THEN
                        IF(((((X-XC4)**2)/(cf**2)+((Y-YC2)**2)/(a4**2)+((Z-ZC4)**2)/(b4**2))<1)) THEN
                        FLUX(1)=Q5*(ff/cf)*EXP(-3*(((X-XC4)**2)/(cf**2)+((Y-YC2)**2)/(a4**2)+
                        ((Z-ZC4)**2)/(b4**2)))
                        END IF
                    END IF
                    FLUX(2)=0.0

C       !PASS6
                ELSEIF (5*WeldLength/V+Coolingtime1+Coolingtime2+Coolingtime3+Coolingtime4+
                Coolingtime5+Prestep+TackWelds.LE.T .AND.T.LT.6*WeldLength/V+Coolingtime1+
                Coolingtime2+Coolingtime3+Coolingtime4+Coolingtime5+Prestep+TackWelds) THEN
                    Q6=(ETTA*Q*6*(3**0.5))/((a5*b5)*(PI**1.5))
C           Rear
                    IF (X.LE.XC5) THEN
                        IF(((((X-XC5)**2)/(cr**2)+((Y-YC)**2)/(a5**2)+((Z-ZC5)**2)/(b5**2)).LT.1)) THEN
                            FLUX(1)=Q6*(fr/cr)*EXP(-3*(((X-XC5)**2)/(cr**2)+((Y-YC)**2)/(a5**2)+
                            ((Z-ZC5)**2)/(b5**2)))
```

```
                              END IF
C             Front
                      ELSEIF (X.GT.XC5) THEN
                              IF(((((X-XC5)**2)/(cf**2)+((Y-YC)**2)/(a5**2)+((Z-ZC5)**2)/(b5**2))<1)) THEN
                              FLUX(1)=Q6*(ff/cf)*EXP(-3*(((X-XC5)**2)/(cf**2)+((Y-YC)**2)/(a5**2)+
                              ((Z-ZC5)**2)/(b5**2)))
                              END IF
                      END IF
                      FLUX(2)=0.0

C         !PASS7
                  ELSEIF (6*WeldLength/V+Coolingtime1+Coolingtime2+Coolingtime3+Coolingtime4+
                  Coolingtime5+Coolingtime6+Prestep+TackWelds.LE.T .AND.T.LT.7*WeldLength/V+
                  Coolingtime1+Coolingtime2+Coolingtime3+Coolingtime4+Coolingtime5+
                  Coolingtime6+Prestep+TackWelds) THEN
                        Q7=(ETTA*Q*6*(3**0.5))/((a6*b6)*(PI**1.5))
C             Rear
                      IF (X.LE.XC6) THEN
                              IF(((((X-XC6)**2)/(cr**2)+((Y-YC)**2)/(a6**2)+((Z-ZC6)**2)/(b6**2)).LT.1)) THEN
                                      FLUX(1)=Q7*(fr/cr)*EXP(-3*(((X-XC6)**2)/(cr**2)+((Y-YC)**2)/(a6**2)+
                                      ((Z-ZC6)**2)/(b6**2)))
                              END IF
C             Front
                      ELSEIF (X.GT.XC6) THEN
                              IF(((((X-XC6)**2)/(cf**2)+((Y-YC)**2)/(a6**2)+((Z-ZC6)**2)/(b6**2)).LT.1)) THEN
                              FLUX(1)=Q7*(ff/cf)*EXP(-3*(((X-XC6)**2)/(cf**2)+((Y-YC)**2)/(a6**2)+
                              ((Z-ZC6)**2)/(b6**2)))
                              END IF
                      END IF
                      FLUX(2)=0.0

                  ELSE
                        FLUX(1) = 0
                  END IF

      RETURN
          END DO
      END
```

C.0.3 12 Passes

```
      SUBROUTINE DFLUX(FLUX,SOL,KSTEP,KINC,TIME,NOEL,NPT,COORDS,
     1 JLTYP,TEMP,PRESS,SNAME)
C
      INCLUDE 'ABA_PARAM.INC'
C
      DIMENSION FLUX(2), TIME(2), COORDS(3)
      CHARACTER*80 SNAME
          INTEGER I

          X=COORDS(1)
          Y=COORDS(2)
          Z=COORDS(3)
          T=TIME(2)

          XO=0.0
          YO=0.0
          ZO=0.0

          Am = 140
          Vo = 23
          Q= Am*Vo

          PI=3.141593
          V=0.004
          WeldLength=0.25
          Coolingtime=120

          Prestep=1E-06
          TackWeld=1E-06
```

```
      a=0.00525
      b=0.00590

      cr=0.00466
      cf=0.002
      ff=0.6
      fr=1.4
      ETTA=0.7

      XC=X0+V*T
      XC1=X0+V*(T-WeldLength/V-Coolingtime-Prestep-TackWeld)
      XC2=X0+V*(T-2*WeldLength/V-2*Coolingtime-Prestep-TackWeld)
      XC3=X0+V*(T-3*WeldLength/V-3*Coolingtime-Prestep-TackWeld)
      XC4=X0+V*(T-4*WeldLength/V-4*Coolingtime-Prestep-TackWeld)
      XC5=X0+V*(T-5*WeldLength/V-5*Coolingtime-Prestep-TackWeld)
      XC6=X0+V*(T-6*WeldLength/V-6*Coolingtime-Prestep-TackWeld)
      XC7=X0+V*(T-7*WeldLength/V-7*Coolingtime-Prestep-TackWeld)
      XC8=X0+V*(T-8*WeldLength/V-8*Coolingtime-Prestep-TackWeld)
      XC9=X0+V*(T-9*WeldLength/V-9*Coolingtime-Prestep-TackWeld)
      XC10=X0+V*(T-10*WeldLength/V-10*Coolingtime-Prestep-TackWeld)
      XC11=X0+V*(T-11*WeldLength/V-11*Coolingtime-Prestep-TackWeld)

      YC=Y0
      YC1=Y0-(2.6E-03)
      YC2=Y0+(2.6E-03)
      YC3=Y0-(3.533E-03)
      YC4=Y0+(3.533E-03)

      ZC=Z0-(14.E-03)
      ZC1=Z0-(10.E-03)
      ZC2=Z0-(6.E-03)
      ZC3=Z0-(6.E-03)
      ZC4=Z0-(2.E-03)
      ZC5=Z0-(2.E-03)
      ZC6=Z0-(18.E-03)
      ZC7=Z0-(22.E-03)
      ZC8=Z0-(26.13E-03)
      ZC9=Z0-(26.E-03)
      ZC10=Z0-(30.E-03)
      ZC11=Z0-(30.E-03)

      FLUX(1) = 0
      DO I = 1,12
            IF (T.LT.WeldLength/V) THEN
                  Q1=(ETTA*Q*6*(3**0.5))/((a*b)*(PI**1.5))
C           Rear
                  IF (X.LE.XC) THEN
                        IF(((((X-XC)**2)/(cr**2)+((Y-YC)**2)/(a**2)+((Z-ZC)**2)/(b**2)).LT.1)) THEN
                              FLUX(1)=Q1*(fr/cr)*EXP(-3*(((X-XC)**2)/(cr**2)+((Y-YC)**2)/(a**2)+
                              ((Z-ZC)**2)/(b**2)))
                        END IF
C           Front
                  ELSEIF (X.GT.XC) THEN
                        IF(((((X-XC)**2)/(cf**2)+((Y-YC)**2)/(a**2)+((Z-ZC)**2)/(b**2)).LT.1)) THEN
                              FLUX(1)=Q1*(ff/cf)*EXP(-3*(((X-XC)**2)/(cf**2)+((Y-YC)**2)/(a**2)+
                              ((Z-ZC)**2)/(b**2)))
                        END IF
                  END IF
                  FLUX(2)=0.0

               ELSEIF (WeldLength/V+Coolingtime+Prestep+TackWeld.LE.T .AND.
               T.LT.2*WeldLength/V+Coolingtime+Prestep+TackWeld) THEN
                  Q2=(ETTA*Q*6*(3**0.5))/((a*b)*(PI**1.5))
C           Rear
                  IF (X.LE.XC1) THEN
                        IF(((((X-XC1)**2)/(cr**2)+((Y-YC)**2)/(a**2)+((Z-ZC1)**2)/(b**2)).LT.1)) THEN
                              FLUX(1)=Q2*(fr/cr)*EXP(-3*(((X-XC1)**2)/(cr**2)+((Y-YC)**2)/(a**2)+
                              ((Z-ZC1)**2)/(b**2)))
                        END IF
C           Front
```

```
                        ELSEIF (X.GT.XC1) THEN
                                IF(((((X-XC1)**2)/(cf**2)+((Y-YC)**2)/(a**2)+((Z-ZC1)**2)/(b**2)).LT.1)) THEN
                                        FLUX(1)=Q2*(ff/cf)*EXP(-3*(((X-XC1)**2)/(cf**2)+((Y-YC)**2)/(a**2)+
                                        ((Z-ZC1)**2)/(b**2)))
                                END IF
                        END IF
                        FLUX(2)=0.0

                    ELSEIF (2*WeldLength/V+2*Coolingtime+Prestep+TackWeld.LE.T .AND.
                    T.LT.3*WeldLength/V+2*Coolingtime+Prestep+TackWeld) THEN
                        Q3=(ETTA*Q*6*(3**0.5))/((a*b)*(PI**1.5))
C               Rear
                        IF (X.LE.XC2) THEN
                                IF(((((X-XC2)**2)/(cr**2)+((Y-YC1)**2)/(a**2)+((Z-ZC2)**2)/(b**2)).LT.1)) THEN
                                        FLUX(1)=Q3*(fr/cr)*EXP(-3*(((X-XC2)**2)/(cr**2)+((Y-YC1)**2)/(a**2)+
                                        ((Z-ZC2)**2)/(b**2)))
                                END IF
C               Front
                        ELSEIF (X.GT.XC2) THEN
                                IF(((((X-XC2)**2)/(cf**2)+((Y-YC1)**2)/(a**2)+((Z-ZC2)**2)/(b**2)).LT.1)) THEN
                                        FLUX(1)=Q3*(ff/cf)*EXP(-3*(((X-XC2)**2)/(cf**2)+((Y-YC1)**2)/(a**2)+
                                        ((Z-ZC2)**2)/(b**2)))
                                END IF
                        END IF
                        FLUX(2)=0.0

                    ELSEIF (3*WeldLength/V+3*Coolingtime+Prestep+TackWeld.LE.T .AND.
                    T.LT.4*WeldLength/V+3*Coolingtime+Prestep+TackWeld) THEN
                        Q4=(ETTA*Q*6*(3**0.5))/((a*b)*(PI**1.5))
C               Rear
                        IF (X.LE.XC3) THEN
                                IF(((((X-XC3)**2)/(cr**2)+((Y-YC2)**2)/(a**2)+((Z-ZC3)**2)/(b**2)).LT.1)) THEN
                                        FLUX(1)=Q4*(fr/cr)*EXP(-3*(((X-XC3)**2)/(cr**2)+((Y-YC2)**2)/(a**2)+
                                        ((Z-ZC3)**2)/(b**2)))
                                END IF
C               Front
                        ELSEIF (X.GT.XC3) THEN
                                IF(((((X-XC3)**2)/(cf**2)+((Y-YC2)**2)/(a**2)+((Z-ZC3)**2)/(b**2)).LT.1)) THEN
                                        FLUX(1)=Q4*(ff/cf)*EXP(-3*(((X-XC3)**2)/(cf**2)+((Y-YC2)**2)/(a**2)+
                                        ((Z-ZC3)**2)/(b**2)))
                                END IF
                        END IF
                        FLUX(2)=0.0

                    ELSEIF (4*WeldLength/V+4*Coolingtime+Prestep+TackWeld.LE.T .AND.
                    T.LT.5*WeldLength/V+4*Coolingtime+Prestep+TackWeld) THEN
                        Q5=(ETTA*Q*6*(3**0.5))/((a*b)*(PI**1.5))
C               Rear
                        IF (X.LE.XC4) THEN
                                IF(((((X-XC4)**2)/(cr**2)+((Y-YC3)**2)/(a**2)+((Z-ZC4)**2)/(b**2)).LT.1)) THEN
                                        FLUX(1)=Q5*(fr/cr)*EXP(-3*(((X-XC4)**2)/(cr**2)+((Y-YC3)**2)/(a**2)+
                                        ((Z-ZC4)**2)/(b**2)))
                                END IF
C               Front
                        ELSEIF (X.GT.XC4) THEN
                                IF(((((X-XC4)**2)/(cf**2)+((Y-YC3)**2)/(a**2)+((Z-ZC4)**2)/(b**2)).LT.1)) THEN
                                        FLUX(1)=Q5*(ff/cf)*EXP(-3*(((X-XC4)**2)/(cf**2)+((Y-YC3)**2)/(a**2)+
                                        ((Z-ZC4)**2)/(b**2)))
                                END IF
                        END IF
                        FLUX(2)=0.0

                    ELSEIF (5*WeldLength/V+5*Coolingtime+Prestep+TackWeld.LE.T .AND.
                    T.LT.6*WeldLength/V+5*Coolingtime+Prestep+TackWeld) THEN
                        Q6=(ETTA*Q*6*(3**0.5))/((a*b)*(PI**1.5))
C               Rear
                        IF (X.LE.XC5) THEN
                                IF(((((X-XC5)**2)/(cr**2)+((Y-YC4)**2)/(a**2)+((Z-ZC5)**2)/(b**2)).LT.1)) THEN
                                        FLUX(1)=Q6*(fr/cr)*EXP(-3*(((X-XC5)**2)/(cr**2)+((Y-YC4)**2)/(a**2)+
                                        ((Z-ZC5)**2)/(b**2)))
                                END IF
```

```
C             Front
                      ELSEIF (X.GT.XC5) THEN
                              IF(((((X-XC5)**2)/(cf**2)+((Y-YC4)**2)/(a**2)+((Z-ZC5)**2)/(b**2)).LT.1)) THEN
                                      FLUX(1)=Q6*(ff/cf)*EXP(-3*(((X-XC5)**2)/(cf**2)+((Y-YC4)**2)/(a**2)+
                                      ((Z-ZC5)**2)/(b**2)))
                              END IF
                      END IF
                      FLUX(2)=0.0

                  ELSEIF (6*WeldLength/V+6*Coolingtime+Prestep+TackWeld.LE.T .AND.
                  T.LT.7*WeldLength/V+6*Coolingtime+Prestep+TackWeld) THEN
                        Q7=(ETTA*Q*6*(3**0.5))/((a*b)*(PI**1.5))
C             Rear
                      IF (X.LE.XC6) THEN
                              IF(((((X-XC6)**2)/(cr**2)+((Y-YC)**2)/(a**2)+((Z-ZC6)**2)/(b**2)).LT.1)) THEN
                                      FLUX(1)=Q7*(fr/cr)*EXP(-3*(((X-XC6)**2)/(cr**2)+((Y-YC)**2)/(a**2)+
                                      ((Z-ZC6)**2)/(b**2)))
                              END IF
C             Front
                      ELSEIF (X.GT.XC6) THEN
                              IF(((((X-XC6)**2)/(cf**2)+((Y-YC)**2)/(a**2)+((Z-ZC6)**2)/(b**2)).LT.1)) THEN
                                      FLUX(1)=Q7*(ff/cf)*EXP(-3*(((X-XC6)**2)/(cf**2)+((Y-YC)**2)/(a**2)+
                                      ((Z-ZC6)**2)/(b**2)))
                              END IF
                      END IF
                      FLUX(2)=0.0

                  ELSEIF (7*WeldLength/V+7*Coolingtime+Prestep+TackWeld.LE.T .AND.
                  T.LT.8*WeldLength/V+7*Coolingtime+Prestep+TackWeld) THEN
                        Q8=(ETTA*Q*6*(3**0.5))/((a*b)*(PI**1.5))
C             Rear
                      IF (X.LE.XC7) THEN
                              IF(((((X-XC7)**2)/(cr**2)+((Y-YC)**2)/(a**2)+((Z-ZC7)**2)/(b**2)).LT.1)) THEN
                                      FLUX(1)=Q8*(fr/cr)*EXP(-3*(((X-XC7)**2)/(cr**2)+((Y-YC)**2)/(a**2)+
                                      ((Z-ZC7)**2)/(b**2)))
                              END IF
C             Front
                      ELSEIF (X.GT.XC7) THEN
                              IF(((((X-XC7)**2)/(cf**2)+((Y-YC)**2)/(a**2)+((Z-ZC7)**2)/(b**2)).LT.1)) THEN
                                      FLUX(1)=Q8*(ff/cf)*EXP(-3*(((X-XC7)**2)/(cf**2)+((Y-YC)**2)/(a**2)+
                                      ((Z-ZC7)**2)/(b**2)))
                              END IF
                      END IF
                      FLUX(2)=0.0


                  ELSEIF (8*WeldLength/V+8*Coolingtime+Prestep+TackWeld.LE.T .AND.
                  T.LT.9*WeldLength/V+8*Coolingtime+Prestep+TackWeld) THEN
                        Q9=(ETTA*Q*6*(3**0.5))/((a*b)*(PI**1.5))
C             Rear
                      IF (X.LE.XC8) THEN
                              IF(((((X-XC8)**2)/(cr**2)+((Y-YC1)**2)/(a**2)+((Z-ZC8)**2)/(b**2)).LT.1)) THEN
                                      FLUX(1)=Q9*(fr/cr)*EXP(-3*(((X-XC8)**2)/(cr**2)+((Y-YC1)**2)/(a**2)+
                                      ((Z-ZC8)**2)/(b**2)))
                              END IF
C             Front
                      ELSEIF (X.GT.XC8) THEN
                              IF(((((X-XC8)**2)/(cf**2)+((Y-YC1)**2)/(a**2)+((Z-ZC8)**2)/(b**2)).LT.1)) THEN
                                      FLUX(1)=Q9*(ff/cf)*EXP(-3*(((X-XC8)**2)/(cf**2)+((Y-YC1)**2)/(a**2)+
                                      ((Z-ZC7)**2)/(b**2)))
                              END IF
                      END IF
                      FLUX(2)=0.0

                  ELSEIF (9*WeldLength/V+9*Coolingtime+Prestep+TackWeld.LE.T .AND.
                  T.LT.10*WeldLength/V+9*Coolingtime+Prestep+TackWeld) THEN
                        Q10=(ETTA*Q*6*(3**0.5))/((a*b)*(PI**1.5))
C             Rear
                      IF (X.LE.XC9) THEN
                              IF(((((X-XC9)**2)/(cr**2)+((Y-YC2)**2)/(a**2)+((Z-ZC9)**2)/(b**2)).LT.1)) THEN
                                      FLUX(1)=Q10*(fr/cr)*EXP(-3*(((X-XC9)**2)/(cr**2)+((Y-YC2)**2)/(a**2)+
```

```
                                        ((Z-ZC9)**2)/(b**2)))
                                END IF
C               Front
                        ELSEIF (X.GT.XC9) THEN
                                IF(((((X-XC9)**2)/(cf**2)+((Y-YC2)**2)/(a**2)+((Z-ZC9)**2)/(b**2)).LT.1)) THEN
                                        FLUX(1)=Q10*(ff/cf)*EXP(-3*(((X-XC9)**2)/(cf**2)+((Y-YC2)**2)/(a**2)+
                                        ((Z-ZC9)**2)/(b**2)))
                                END IF
                        END IF
                        FLUX(2)=0.0

                    ELSEIF (10*WeldLength/V+10*Coolingtime+Prestep+TackWeld.LE.T .AND.
                    T.LT.11*WeldLength/V+10*Coolingtime+Prestep+TackWeld) THEN
                          Q11=(ETTA*Q*6*(3**0.5))/((a*b)*(PI**1.5))
C               Rear
                        IF (X.LE.XC10) THEN
                                IF(((((X-XC10)**2)/(cr**2)+((Y-YC3)**2)/(a**2)+((Z-ZC10)**2)/(b**2)).LT.1)) THEN
                                        FLUX(1)=Q11*(fr/cr)*EXP(-3*(((X-XC10)**2)/(cr**2)+((Y-YC3)**2)/(a**2)+
                                        ((Z-ZC10)**2)/(b**2)))
                                END IF
C               Front
                        ELSEIF (X.GT.XC10) THEN
                                IF(((((X-XC10)**2)/(cf**2)+((Y-YC3)**2)/(a**2)+((Z-ZC10)**2)/(b**2)).LT.1)) THEN
                                        FLUX(1)=Q11*(ff/cf)*EXP(-3*(((X-XC10)**2)/(cf**2)+((Y-YC3)**2)/(a**2)+
                                        ((Z-ZC10)**2)/(b**2)))
                                END IF
                        END IF
                        FLUX(2)=0.0

                    ELSEIF (11*WeldLength/V+11*Coolingtime+Prestep+TackWeld.LE.T .AND.
                    T.LT.12*WeldLength/V+11*Coolingtime+Prestep+TackWeld) THEN
                          Q12=(ETTA*Q*6*(3**0.5))/((a*b)*(PI**1.5))
C               Rear
                        IF (X.LE.XC11) THEN
                                IF(((((X-XC11)**2)/(cr**2)+((Y-YC4)**2)/(a**2)+((Z-ZC11)**2)/(b**2)).LT.1)) THEN
                                        FLUX(1)=Q12*(fr/cr)*EXP(-3*(((X-XC11)**2)/(cr**2)+((Y-YC4)**2)/(a**2)+
                                        ((Z-ZC11)**2)/(b**2)))
                                END IF
C               Front
                        ELSEIF (X.GT.XC11) THEN
                                IF(((((X-XC11)**2)/(cf**2)+((Y-YC4)**2)/(a**2)+((Z-ZC11)**2)/(b**2)).LT.1)) THEN
                                        FLUX(1)=Q12*(ff/cf)*EXP(-3*(((X-XC11)**2)/(cf**2)+((Y-YC4)**2)/(a**2)+
                                        ((Z-ZC11)**2)/(b**2)))
                                END IF
                        END IF
                        FLUX(2)=0.0

                    ELSE
                          FLUX(1)= 0.0
                    END IF

      RETURN
          END DO
      END
```

D

Torch location along the thickness

Here the location of the heat through the thickness of the specimen is given. The torch then stays at the same position on Z and Y and moves along X at a precise welding speed.

Table D.1: Torch location through thickness [m], 1 Pass, Model 1

	Torch height Z	Torch offset Y
Pass 1	-0,008	0

Table D.2: Torch location through thickness [m], 2 Passes, Model 1

	Torch height Z	Torch offset Y
Pass 1	-0,008	0
Pass 2	0	0

Table D.3: Torch location through thickness [m], 3 Passes, Model 1

3Passes	Torch height Z	Torch offset Y
Pass 1	-0,016	0
Pass 2	-0,024	0

Table D.4: Torch location through thickness [m], 5 Passes, Model 1

	Torch height Z	Torch offset Y
Pass 1	-0,014	0
Pass 2	-0,02	0
Pass 3	-0,027	0,006
Pass 4	-0,027	-0,006
Pass 5	-0,008	0

Table D.5: Torch location through thickness [m], 7 Passes, Model 1

	Torch height	Torch offset
	Z	Y
Pass 1	-0,014	0
Pass 2	-0,018	0
Pass 3	-0,022	0
Pass 4	-0,0275	0,006
Pass 5	-0,0275	-0,006
Pass 6	-0,01	0
Pass 7	-0,004	0

Table D.6: Torch location through thickness [m], 1 Pass, Model 2

1Pass		
	Torch height	Torch offset
	Z	Y
Pass 1	-0,004	0

Table D.7: Torch location through thickness [m], 2 Passes, Model 2

2Passes		
	Torch height	Torch offset
	Z	Y
Pass 1	-0,004	0
Pass 2	-0,024	0

Table D.8: Torch location through thickness [m], 4 Passes, Model 2

	Torch height	Torch offset
	Z	Y
Pass 1	-0,012	0
Pass 2	-0,00425	0
Pass 3	-0,01975	0
Pass 4	-0,02775	0

Table D.9: Torch location through thickness [m], 6 Passes, Model 2

	Torch height	Torch offset
	Z	Y
Pass 1	-0,0135	0
Pass 2	-0,0085	0
Pass 3	-0,003	0
Pass 4	-0,0185	0
Pass 5	-0,0235	0
Pass 6	-0,029	0

Table D.10: Torch location through thickness [m], 8 Passes, Model 2

	Torch height	Torch offset
	Z	Y
Pass 1	-0,014	0
Pass 2	-0,01	0
Pass 3	-0,006	0
Pass 4	-0,002	0
Pass 5	-0,018	0
Pass 6	-0,022	0
Pass 7	-0,026	0
Pass 8	-0,03	0

Table D.11: Torch location through thickness [m], 10 Passes, Model 2

	Torch height Z	Torch offset Y
Pass 1	-0,014	0
Pass 2	-0,01	0
Pass 3	-0,006	0
Pass 4	-0,002	-0,003533
Pass 5	-0,002	0,003533
Pass 6	-0,018	0
Pass 7	-0,022	0
Pass 8	-0,026	0
Pass 9	-0,03	-0,003533
Pass 10	-0,03	0,003533

Table D.12: Torch location through thickness [m], 12 Passes, Model 2

	Torch height Z	Torch offset Y
Pass 1	-0,014	0
Pass 2	-0,01	0
Pass 3	-0,006	-0,0026
Pass 4	-0,006	0,0026
Pass 5	-0,002	-0,003533
Pass 6	-0,002	0,003533
Pass 7	-0,018	0
Pass 8	-0,022	0
Pass 9	-0,026	-0,0026
Pass 10	-0,026	-0,0026
Pass 11	-0,03	-0,003533
Pass 12	-0,03	0,003533

E

Contour plots - Distortions and Residual stresses from Chapter 3

This chapter gives the contour plots for the deformations and residual stresses.

E.0.1 Distortions

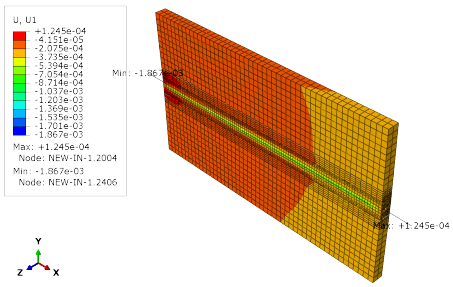

(a) 1 Pass

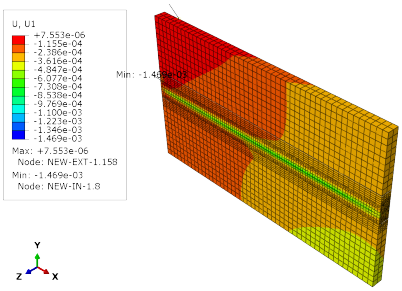

(b) 2 Passes

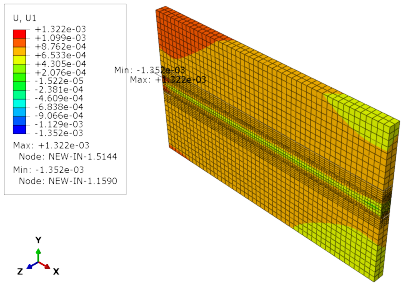

(c) 3 Passes

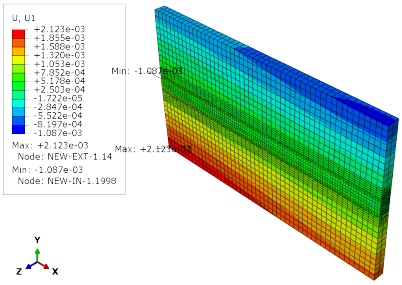

(d) 5 Passes

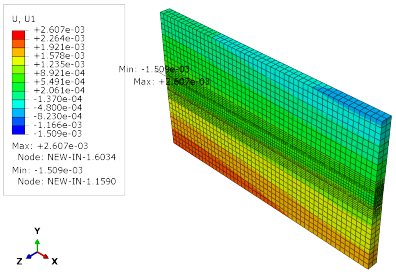

(e) 7 Passes

Figure E.1: Nodal displacement in x direction, Model 1

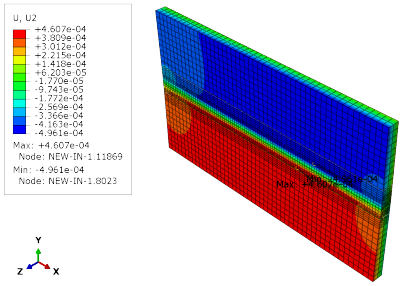

(a) 1 Pass

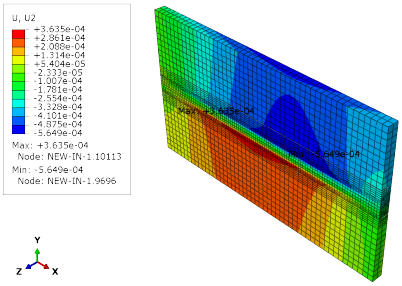

(b) 2 Passes

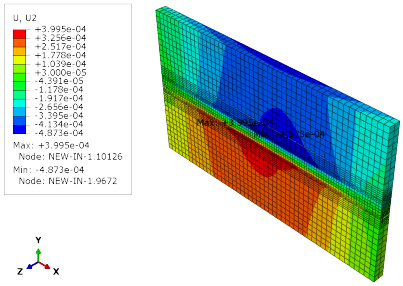

(c) 3 Passes

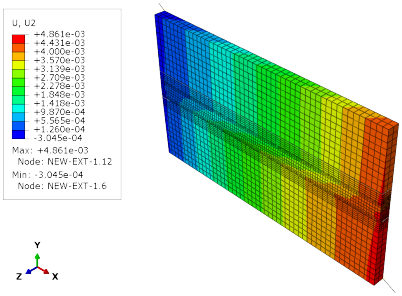

(d) 5 Passes

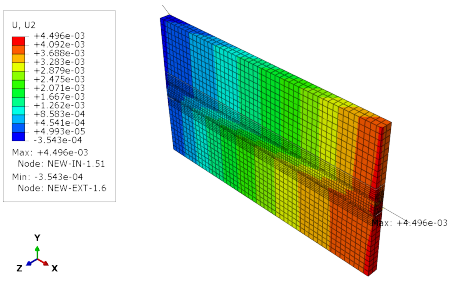

(e) 7 Passes

Figure E.2: Nodal displacement in y direction, Model 1

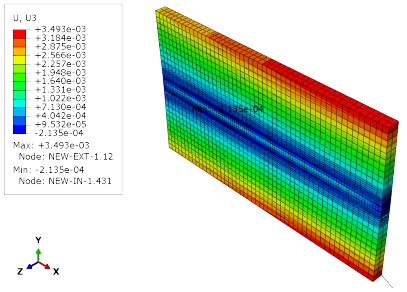

(a) 1 Pass

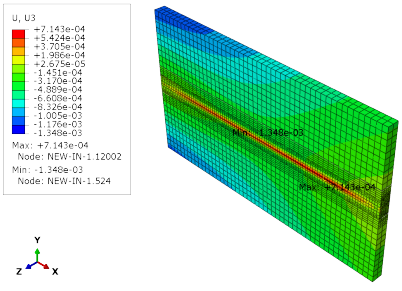

(b) 2 Passes

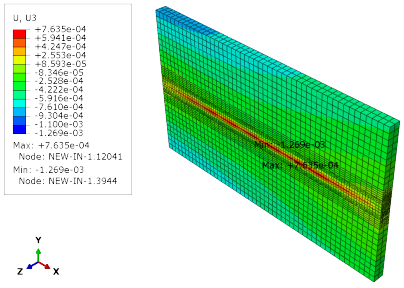

(c) 3 Passes

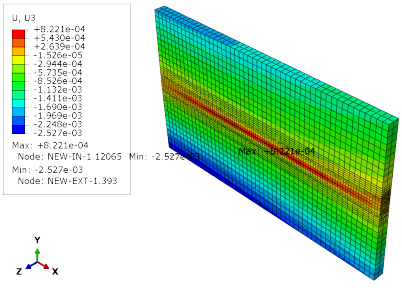

(d) 5 Passes

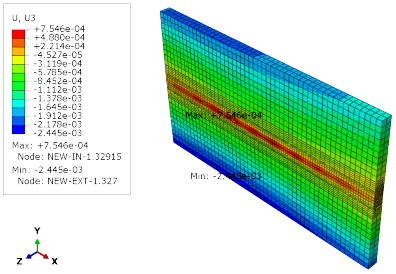

(e) 7 Passes

Figure E.3: Nodal displacement in z direction, Model 1

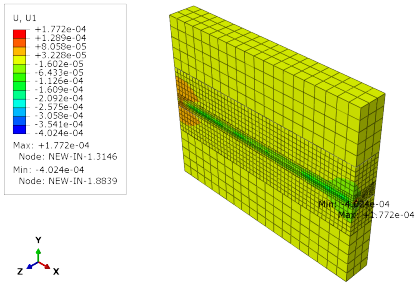

(a) 1 Pass

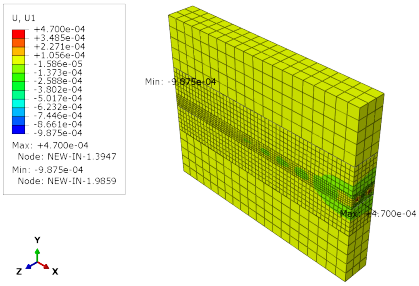

(b) 2 Passes

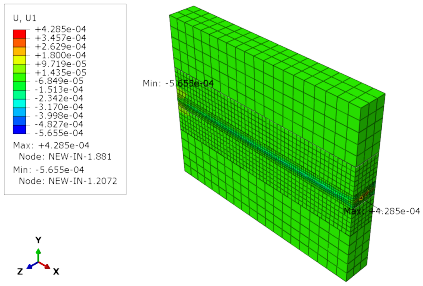

(c) 4 Passes

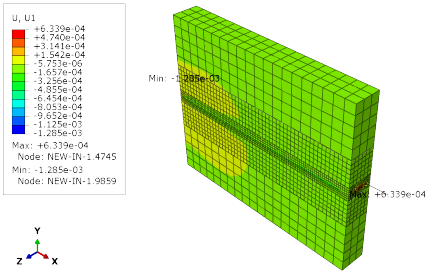

(d) 6 Passes

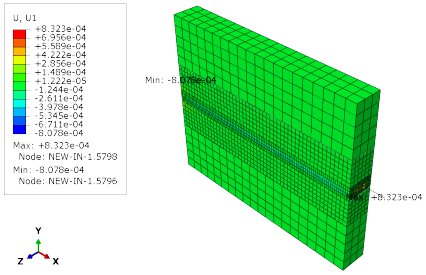

(e) 8 Passes

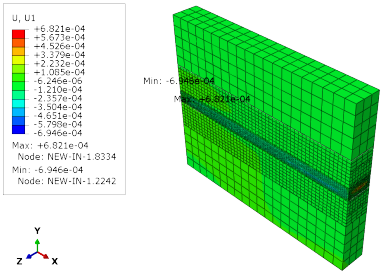

(f) 10 Passes

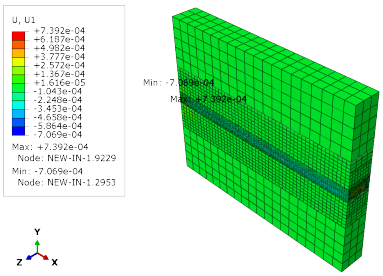

(g) 12 Passes

Figure E.4: Nodal displacement in x direction, Model 2

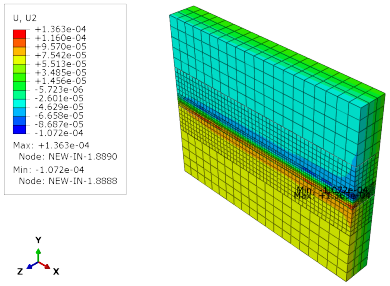

(a) 1 Pass

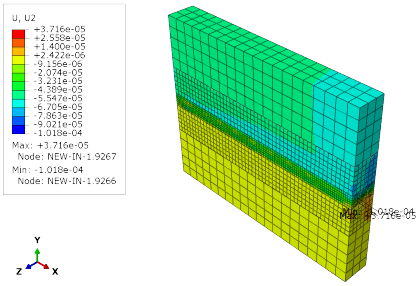

(b) 2 Passes

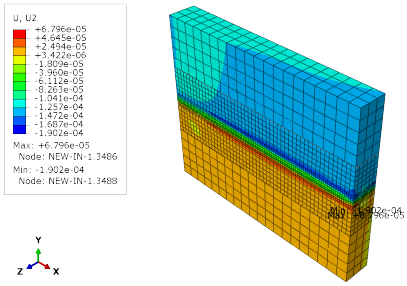

(c) 4 Passes

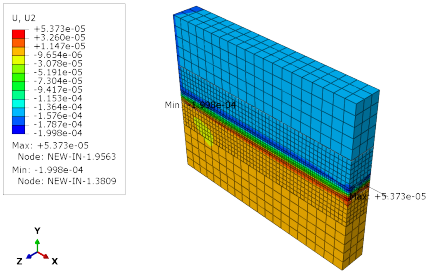

(d) 6 Passes

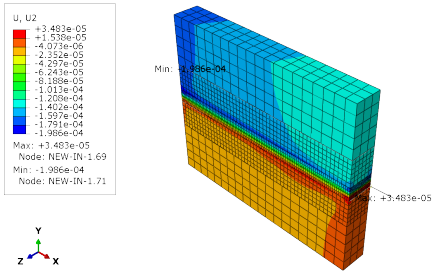

(e) 8 Passes

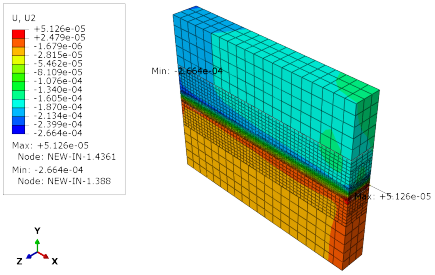

(f) 10 Passes

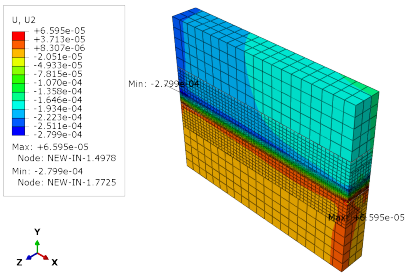

(g) 12 Passes

Figure E.5: Nodal displacement in y direction, Model 2

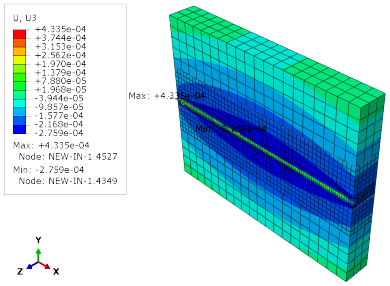

(a) 1 Pass

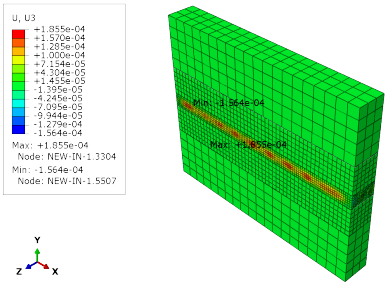

(b) 2 Passes

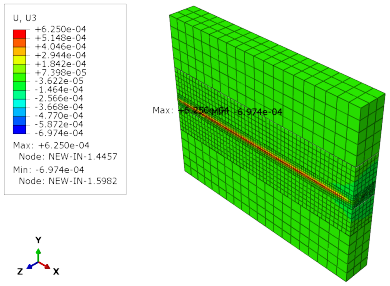

(c) 4 Passes

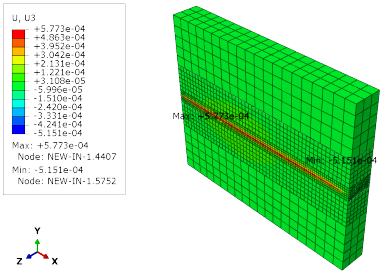

(d) 6 Passes

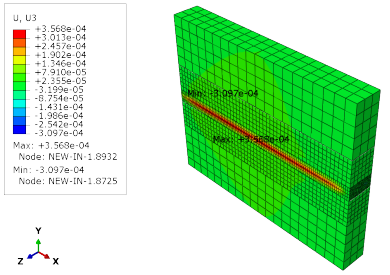

(e) 8 Passes

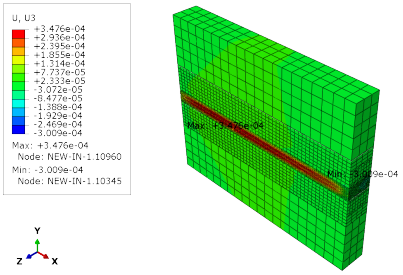

(f) 10 Passes

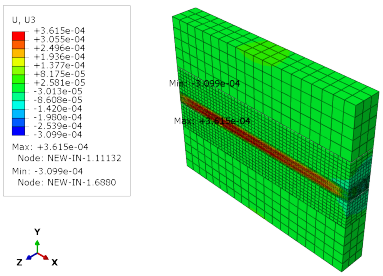

(g) 12 Passes

Figure E.6: Nodal displacement in z direction, Model 2

E.0.2 Residual stresses

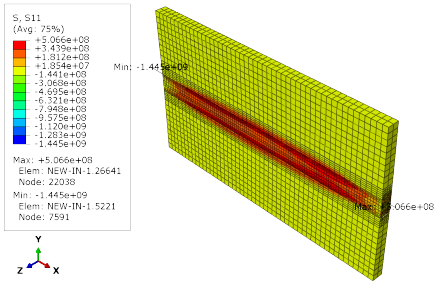

(a) 1 Pass

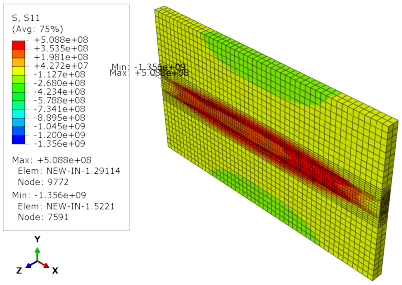

(b) 2 Passes

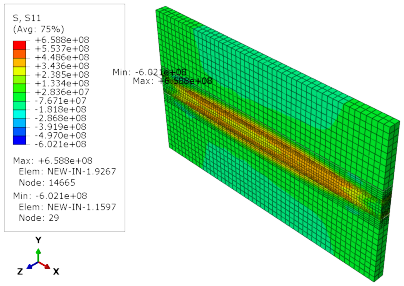

(c) 3 Passes

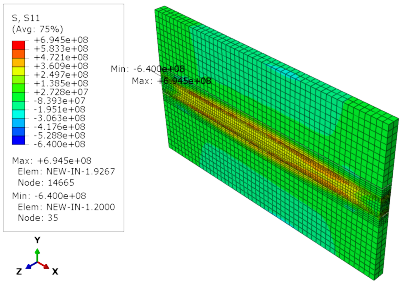

(d) 5 Passes

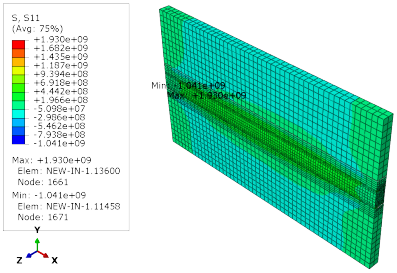

(e) 7 Passes

Figure E.7: Longitudinal stresses, Model 1

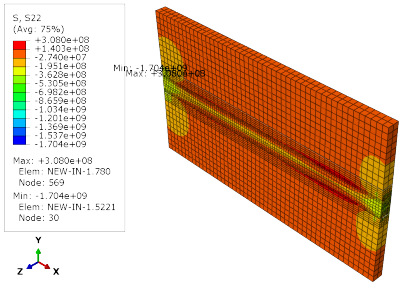

(a) 1 Pass

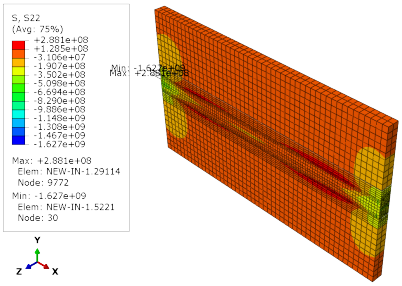

(b) 2 Passes

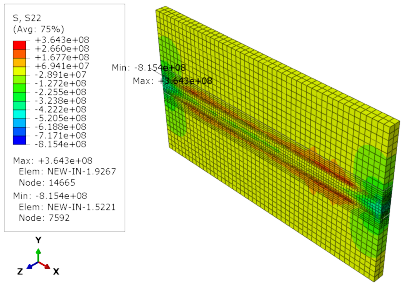

(c) 3 Passes

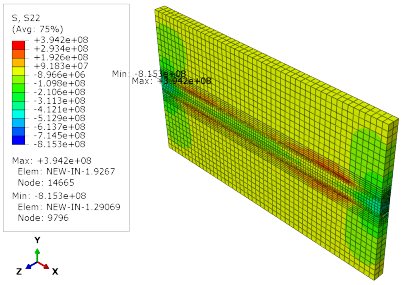

(d) 5 Passes

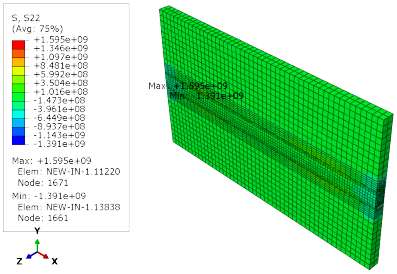

(e) 7 Passes

Figure E.8: Transverse stresses, Model 1

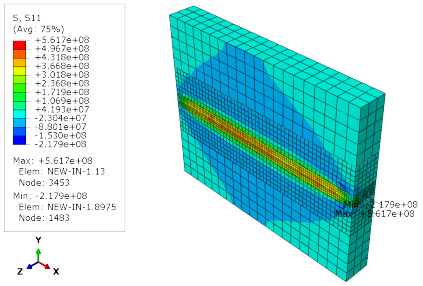

(a) 1 Pass

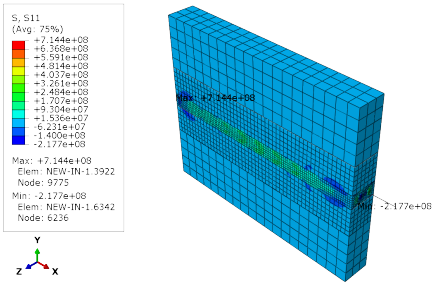

(b) 2 Passes

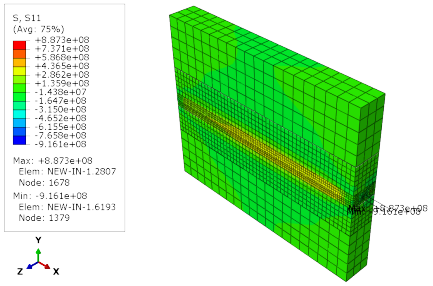

(c) 4 Passes

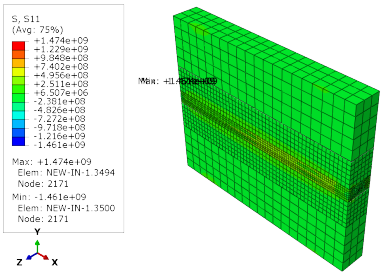

(d) 6 Passes

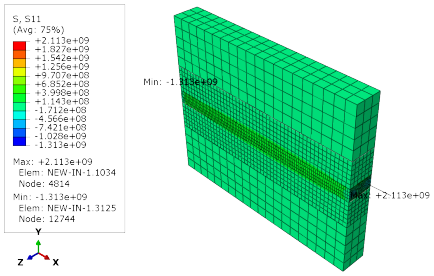

(e) 8 Passes

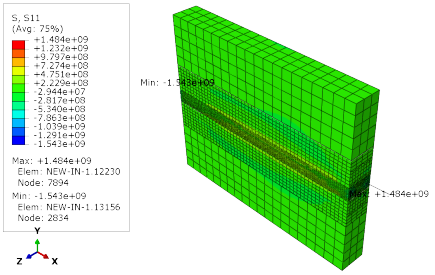

(f) 10 Passes

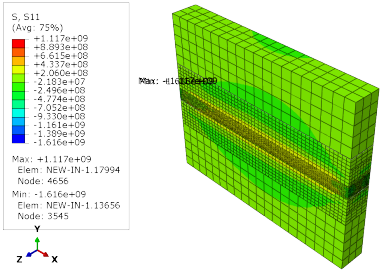

(g) 12 Passes

Figure E.9: Longitudinal stresses, Model 2

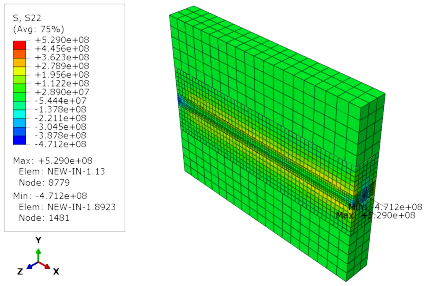

(a) 1 Pass

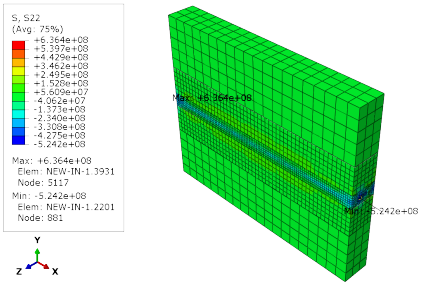

(b) 2 Passes

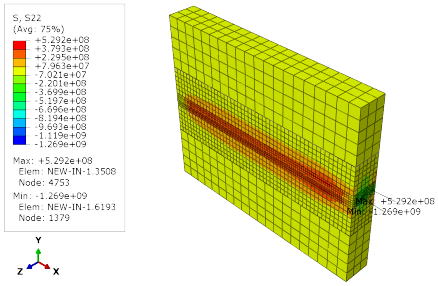

(c) 4 Passes

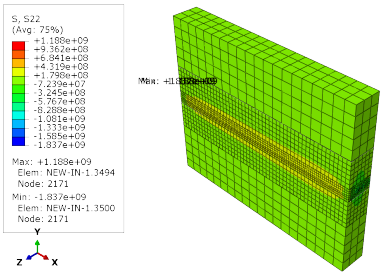

(d) 6 Passes

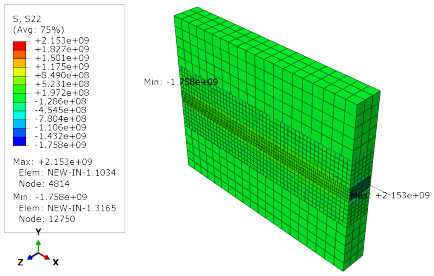

(e) 8 Passes

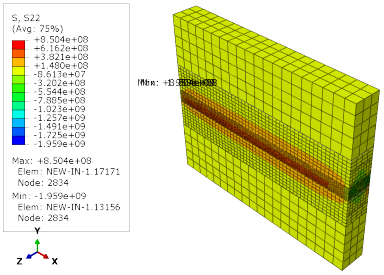

(f) 10 Passes

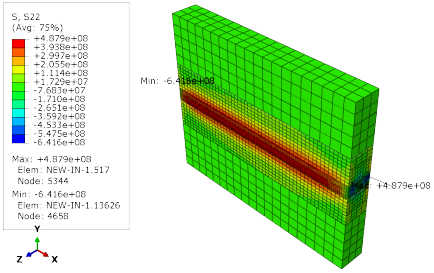

(g) 12 Passes

Figure E.10: Transverse stresses, Model 2

F

Contour plots - Distortions and Residual stresses from Chapter 4

This chapter gives the contour plots for the deformations and residual stresses of the pores models.

F.0.1 Distortions

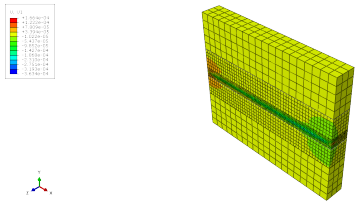

(a) 0.5mm Pore

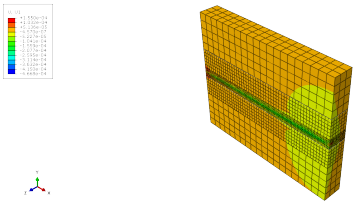

(b) 1mm Pore

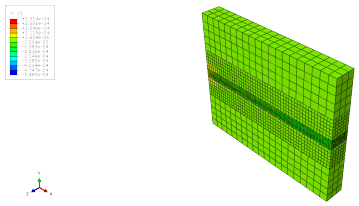

(c) 2mm Pore

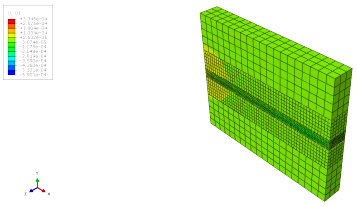

(d) 3mm Pore

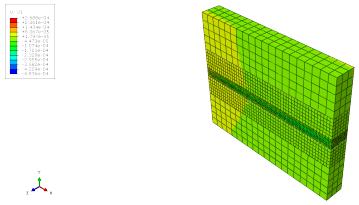

(e) 4mm Pore

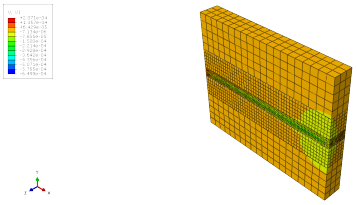

(f) 1mm pores - OXX configuration

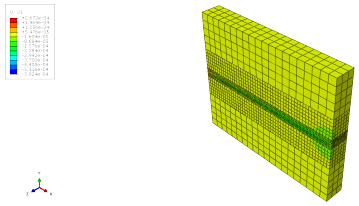

(g) 1mm pores - XXO configuration

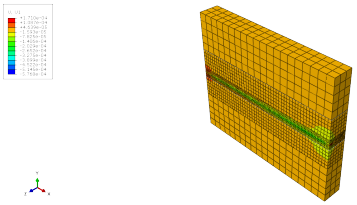

(h) 1mm pores - XOX configuration

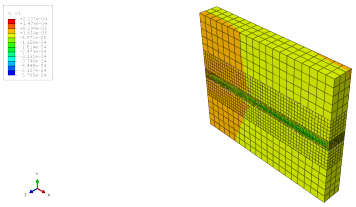

(i) 1mm pores - XXX configuration

Figure F.1: Nodal displacement in x direction, Mesh 1

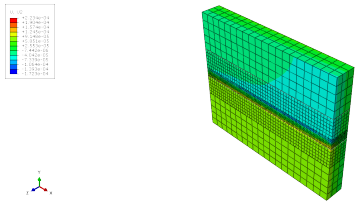

(a) 0.5mm Pore

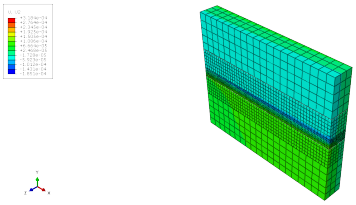

(b) 1mm Pore

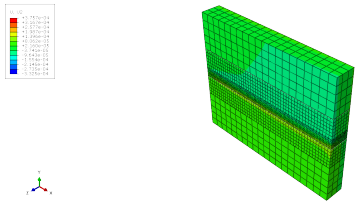

(c) 2mm Pore

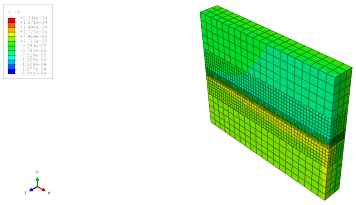

(d) 3mm Pore

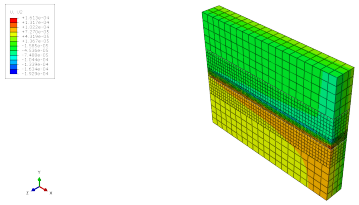

(e) 4mm Pore

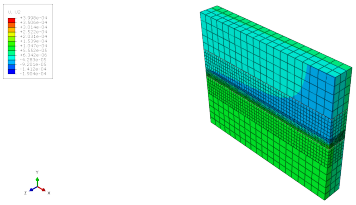

(f) 1mm pores - OXX configuration

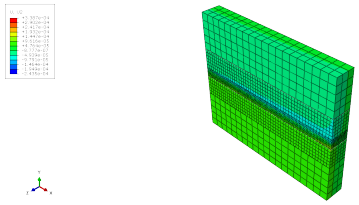

(g) 1mm pores - XXO configuration

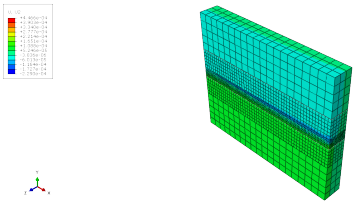

(h) 1mm pores - XOX configuration

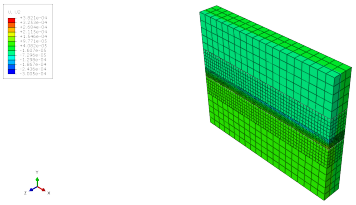

(i) 1mm pores - XXX configuration

Figure F.2: Nodal displacement in y direction, Mesh 1

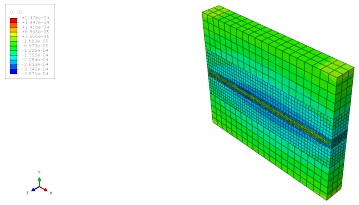

(a) 0.5mm Pore

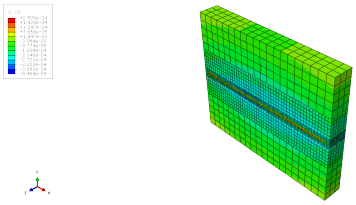

(b) 1mm Pore

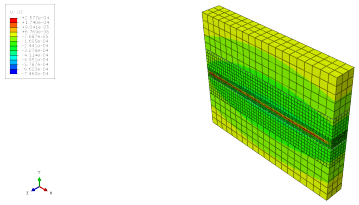

(c) 2mm Pore

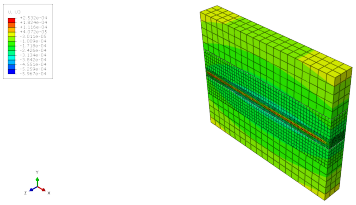

(d) 3mm Pore

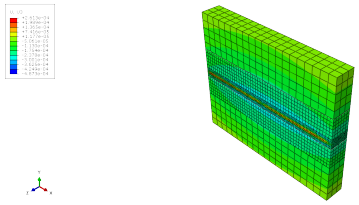

(e) 4mm Pore

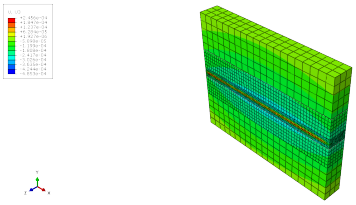

(f) 1mm pores - OXX configuration

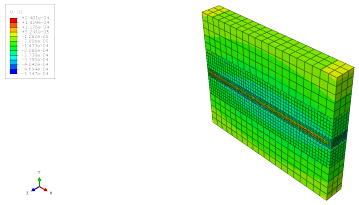

(g) 1mm pores - XXO configuration

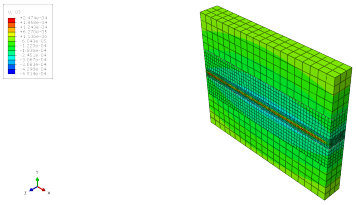

(h) 1mm pores - XOX configuration

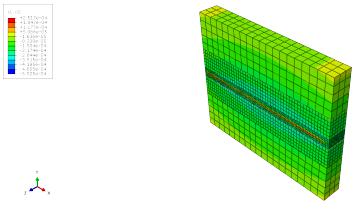

(i) 1mm pores - XXX configuration

Figure F.3: Nodal displacement in z direction, Mesh 1

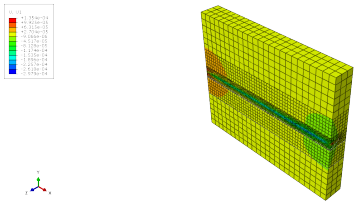

(a) 0.5mm Pore

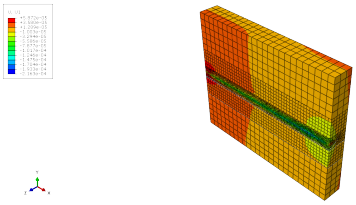

(b) 1mm Pore

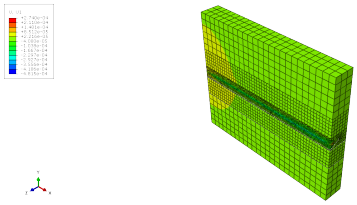

(c) 2mm Pore

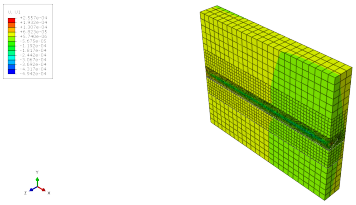

(d) 3mm Pore

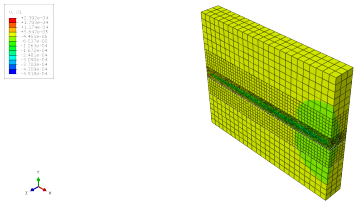

(e) 4mm Pore

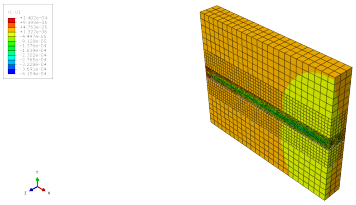

(f) 1mm pores - OXX configuration

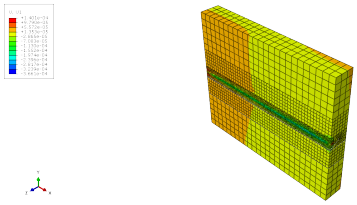

(g) 1mm pores - XXO configuration

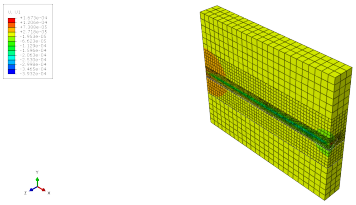

(h) 1mm pores - XOX configuration

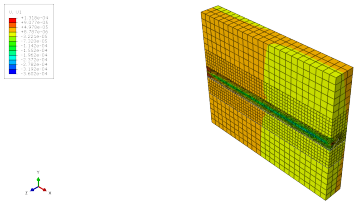

(i) 1mm pores - XXX configuration

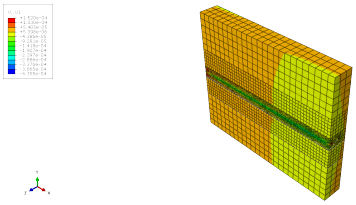

(j) 1mm pores - XXXXX configuration

Figure F.4: Nodal displacement in x direction, Mesh 2

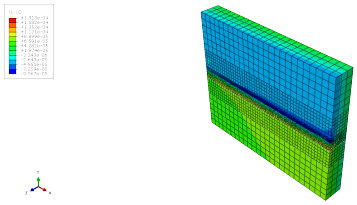

(a) 0.5mm Pore

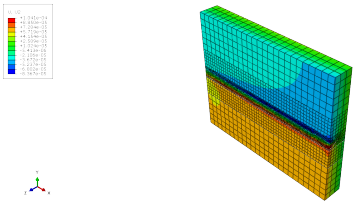

(b) 1mm Pore

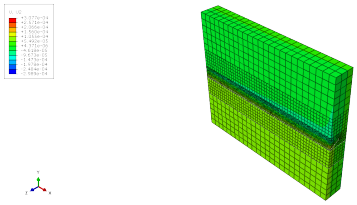

(c) 2mm Pore

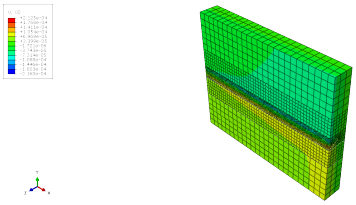

(d) 3mm Pore

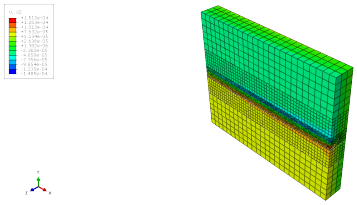

(e) 4mm Pore

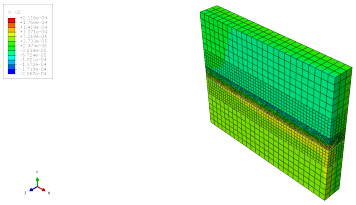

(f) 1mm pores - OXX configuration

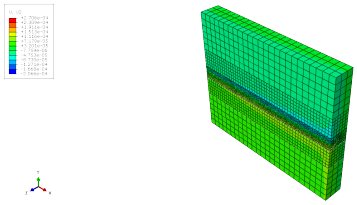

(g) 1mm pores - XXO configuration

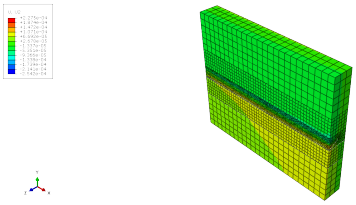

(h) 1mm pores - XOX configuration

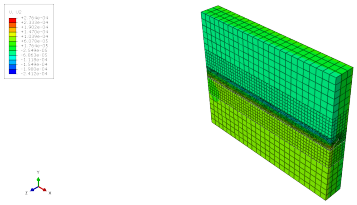

(i) 1mm pores - XXX configuration

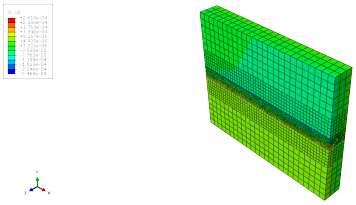

(j) 1mm pores - XXXXX configuration

Figure F.5: Nodal displacement in y direction, Mesh 2

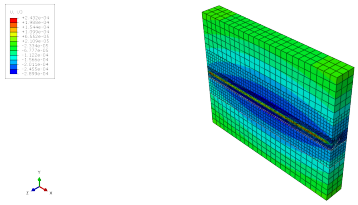

(a) 0.5mm Pore

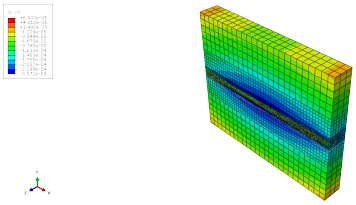

(b) 1mm Pore

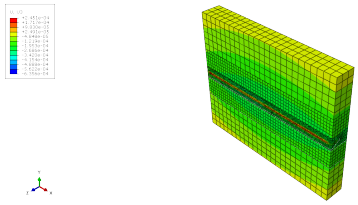

(c) 2mm Pore

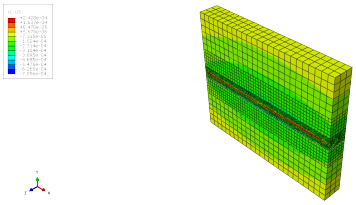

(d) 3mm Pore

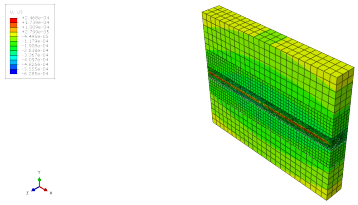

(e) 4mm Pore

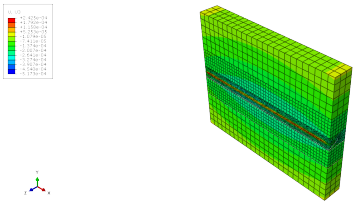

(f) 1mm pores - OXX configuration

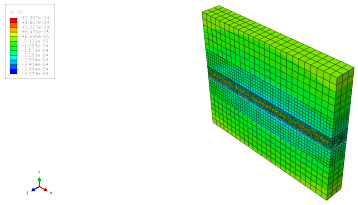

(g) 1mm pores - XXO configuration

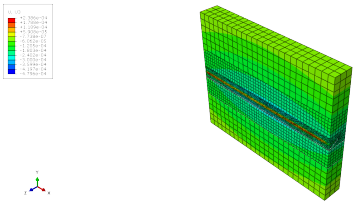

(h) 1mm pores - XOX configuration

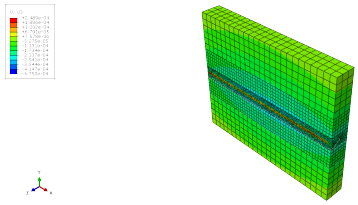

(i) 1mm pores - XXX configuration

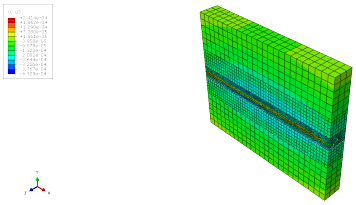

(j) 1mm pores - XXXXX configuration

Figure F.6: Nodal displacement in z direction, Mesh 2

F.0.2 Residual Stresses

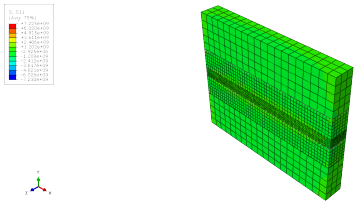

(a) 0.5mm Pore

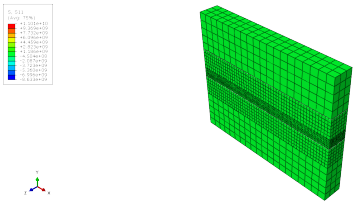

(b) 1mm Pore

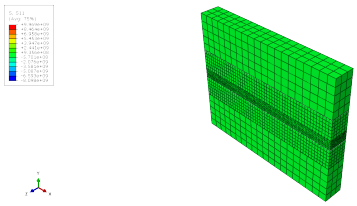

(c) 2mm Pore

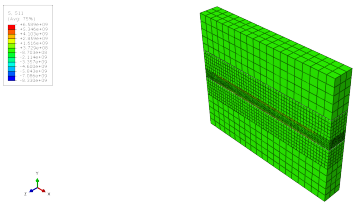

(d) 3mm Pore

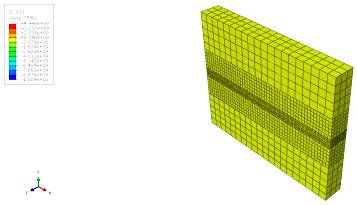

(e) 4mm Pore

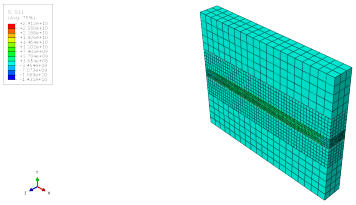

(f) 1mm pores - OXX configuration

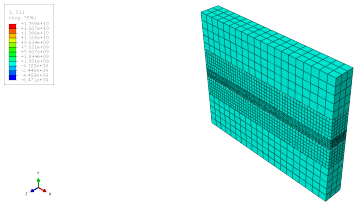

(g) 1mm pores - XXO configuration

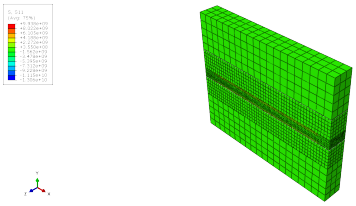

(h) 1mm pores - XOX configuration

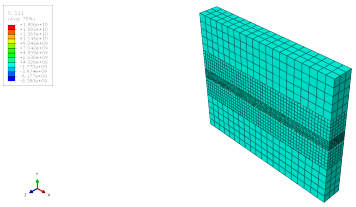

(i) 1mm pores - XXX configuration

Figure F.7: Longitudinal stresses, Mesh 1

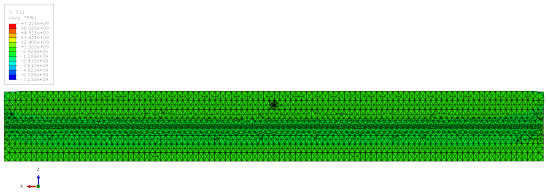

(a) 0.5mm Pore - CUT

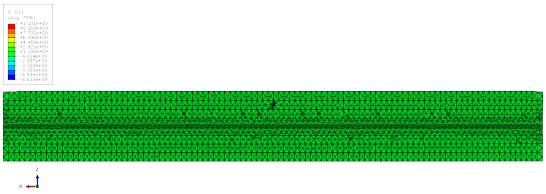

(b) 1mm Pore - CUT

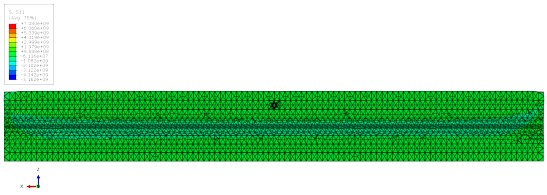

(c) 2mm Pore - CUT

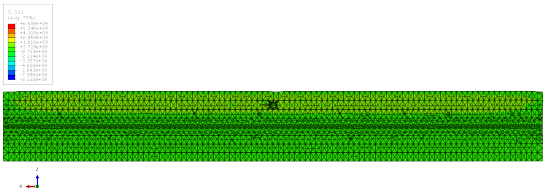

(d) 3mm Pore - CUT

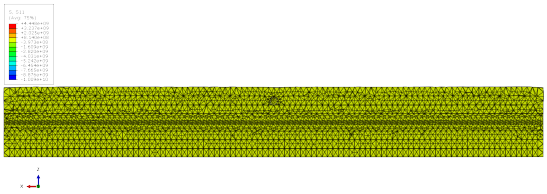

(e) 4mm Pore - CUT

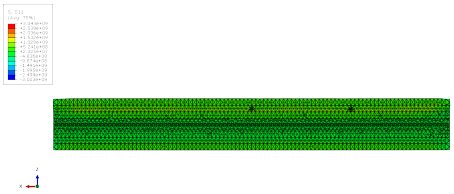

(f) 1mm pores - OXX configuration (CUT)

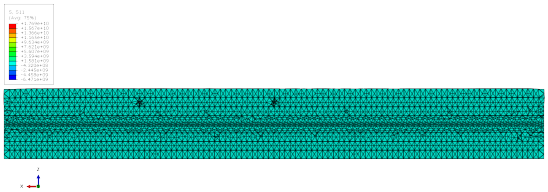

(g) 1mm pores - XXO configuration (CUT)

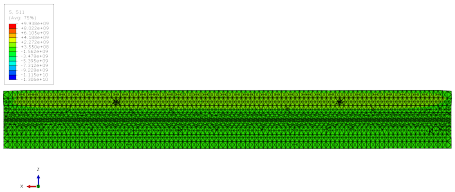

(h) 1mm pores - XOX configuration (CUT)

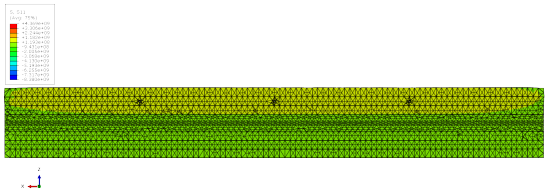

(i) 1mm pores - XXX configuration (CUT)

Figure F.8: Longitudinal stresses, Mesh 1 (CUT)

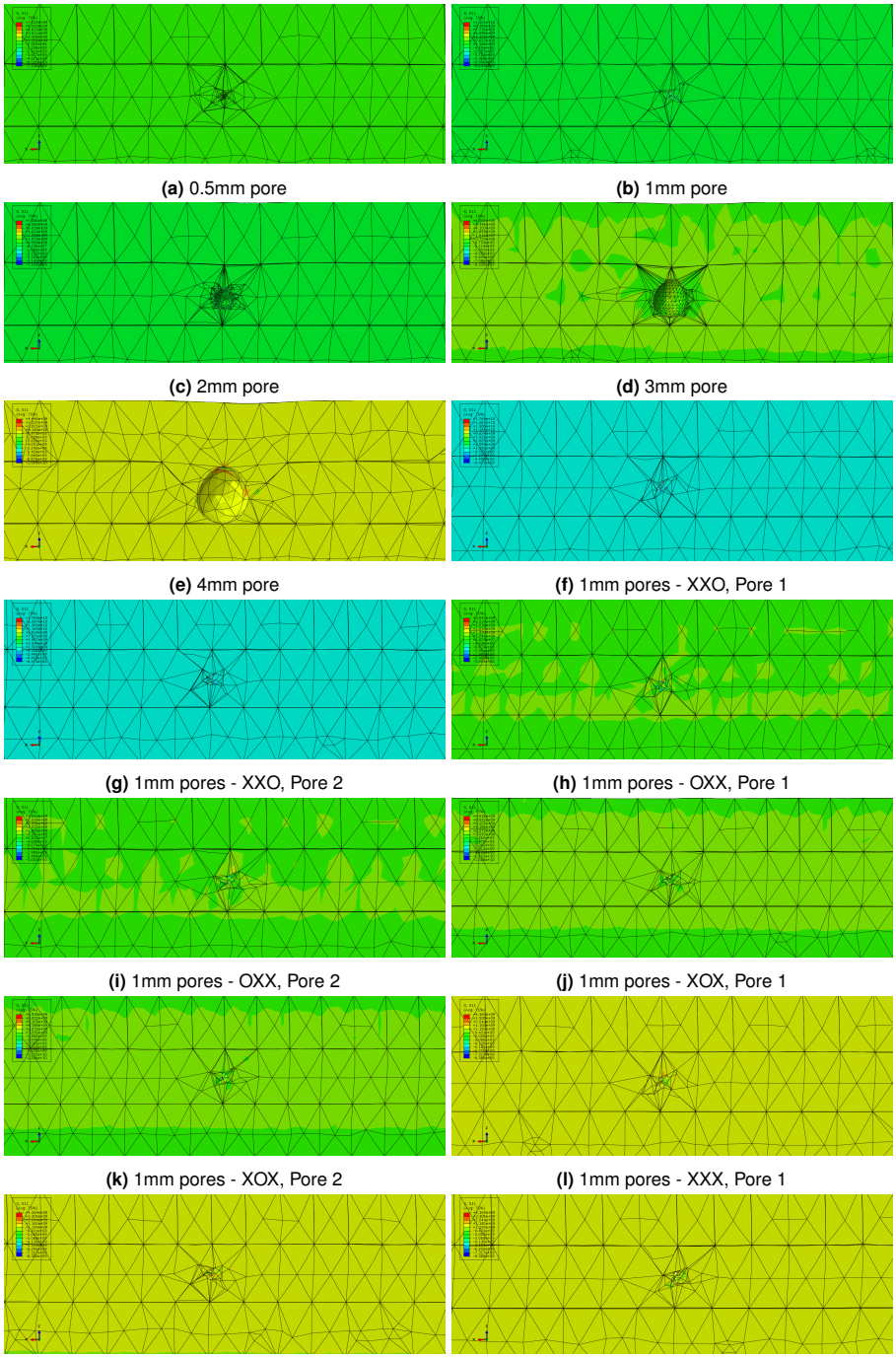

(a) 0.5mm pore **(b)** 1mm pore

(c) 2mm pore **(d)** 3mm pore

(e) 4mm pore **(f)** 1mm pores - XXO, Pore 1

(g) 1mm pores - XXO, Pore 2 **(h)** 1mm pores - OXX, Pore 1

(i) 1mm pores - OXX, Pore 2 **(j)** 1mm pores - XOX, Pore 1

(k) 1mm pores - XOX, Pore 2 **(l)** 1mm pores - XXX, Pore 1

(m) 1mm pores - XXX, Pore 2 **(n)** 1mm pores - XXX, Pore 3

Figure F.9: Longitudinal stresses, Mesh 1 (CUT - Zoom on the pores)

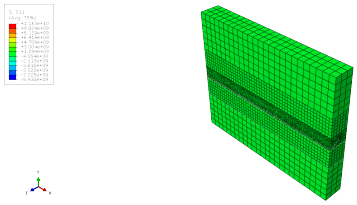

(a) 0.5mm Pore

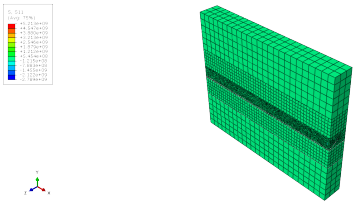

(b) 1mm Pore

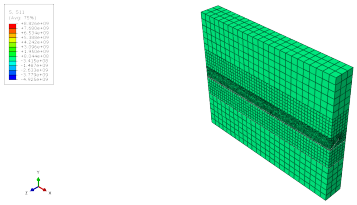

(c) 2mm Pore

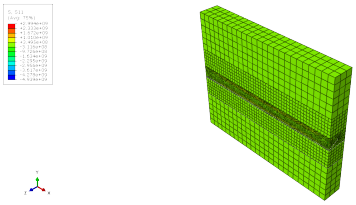

(d) 3mm Pore

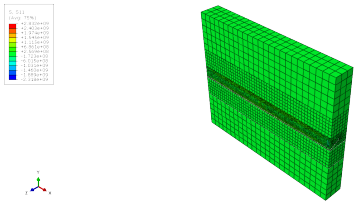

(e) 4mm Pore

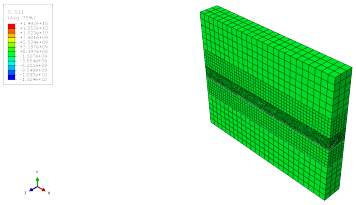

(f) 1mm pores - OXX configuration

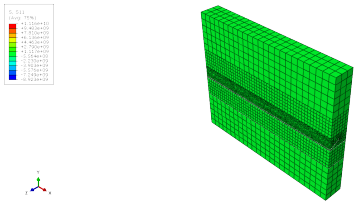

(g) 1mm pores - XXO configuration

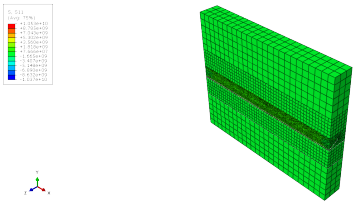

(h) 1mm pores - XOX configuration

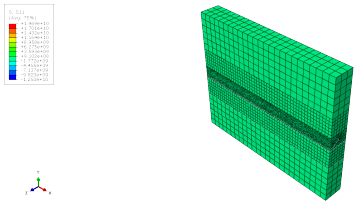

(i) 1mm pores - XXX configuration

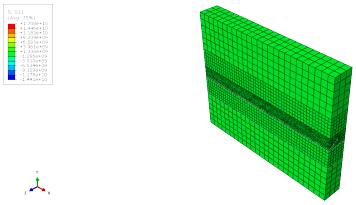

(j) 1mm pores - XXXXX configuration

Figure F.10: Longitudinal stresses, Mesh 2

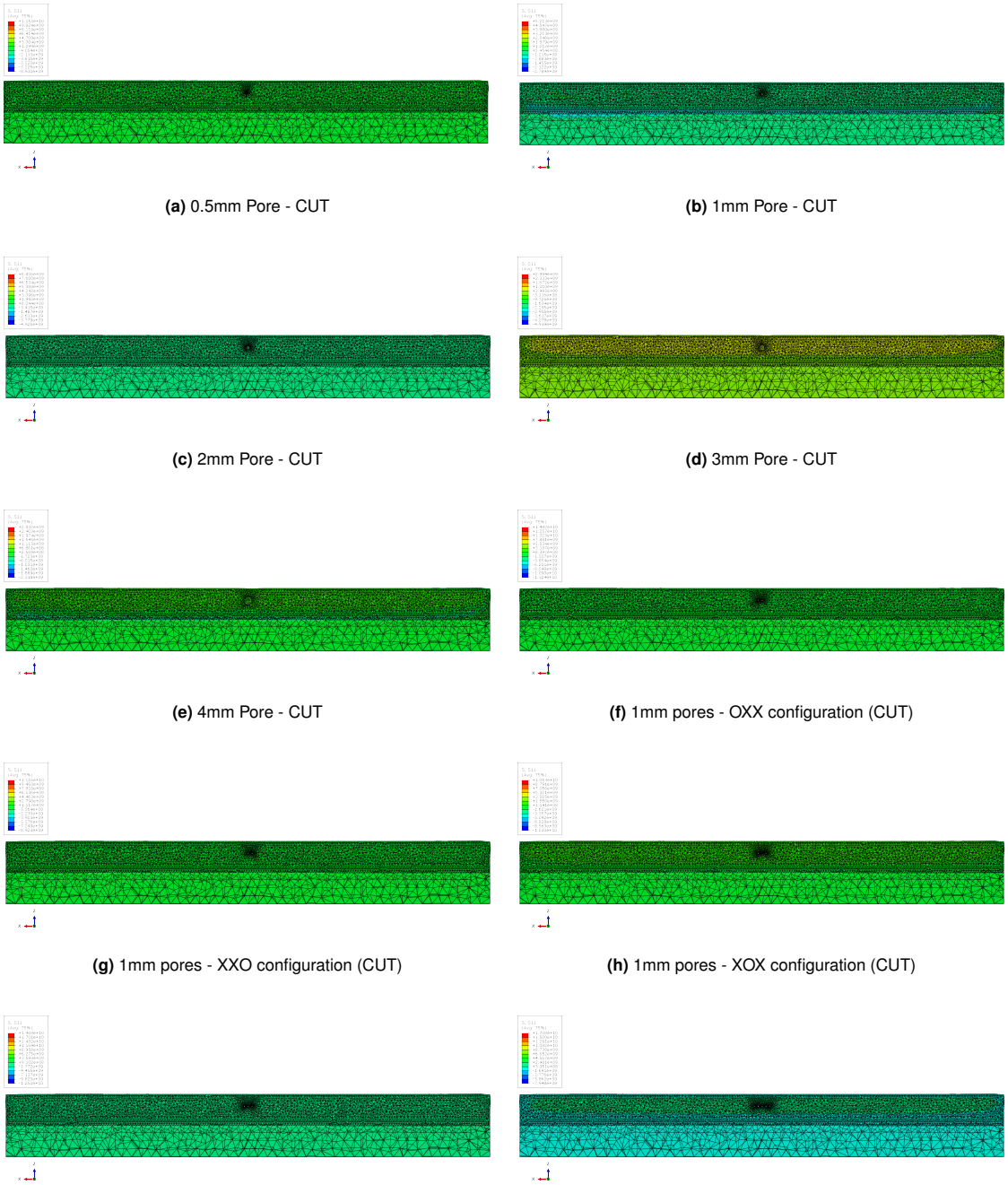

(a) 0.5mm Pore - CUT

(b) 1mm Pore - CUT

(c) 2mm Pore - CUT

(d) 3mm Pore - CUT

(e) 4mm Pore - CUT

(f) 1mm pores - OXX configuration (CUT)

(g) 1mm pores - XXO configuration (CUT)

(h) 1mm pores - XOX configuration (CUT)

(i) 1mm pores - XXX configuration (CUT)

(j) 1mm pores - XXXXX configuration (CUT)

Figure F.11: Longitudinal stresses, Mesh 2 (CUT)

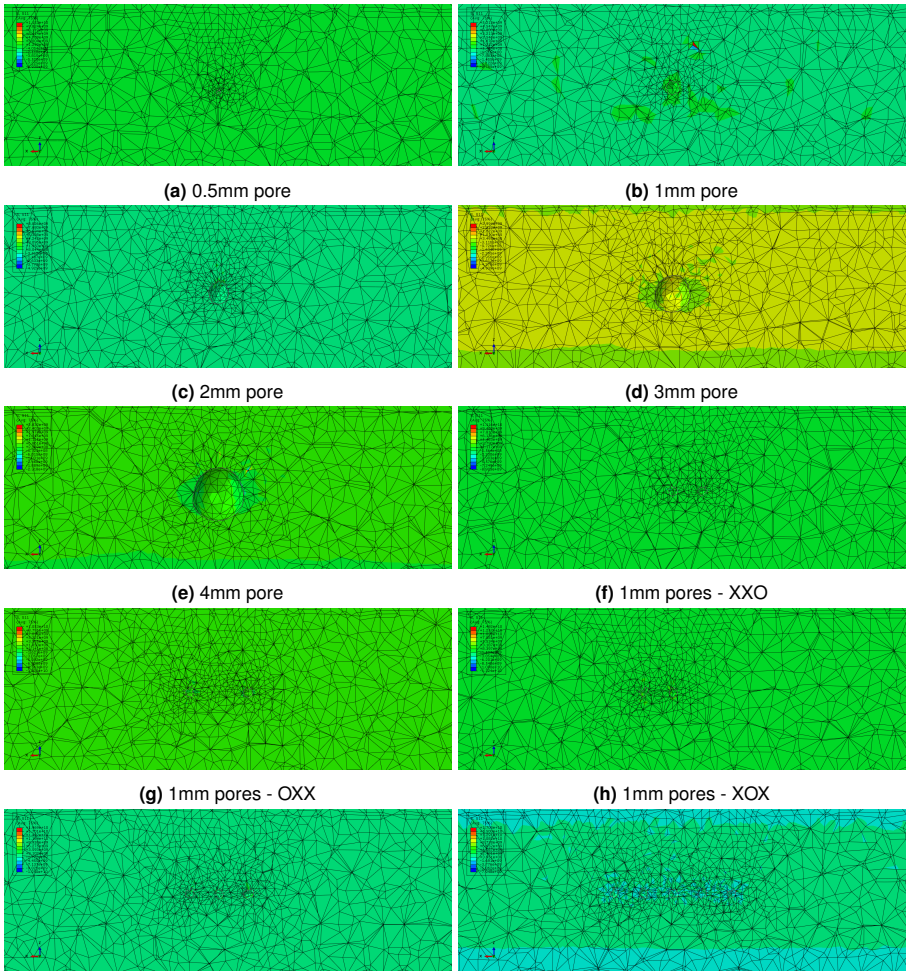

(a) 0.5mm pore **(b)** 1mm pore

(c) 2mm pore **(d)** 3mm pore

(e) 4mm pore **(f)** 1mm pores - XXO

(g) 1mm pores - OXX **(h)** 1mm pores - XOX

(i) 1mm pores - XXX **(j)** 1mm pores - XXXXX

Figure F.12: Longitudinal stresses, Mesh 2 (CUT - Zoom on the pores)

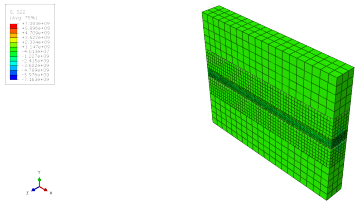

(a) 0.5mm Pore

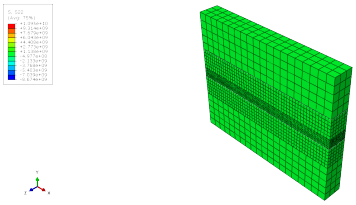

(b) 1mm Pore

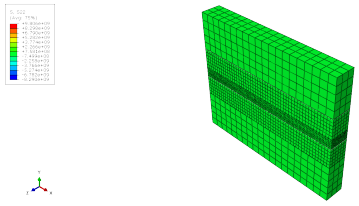

(c) 2mm Pore

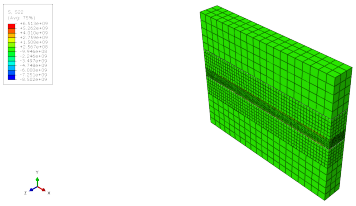

(d) 3mm Pore

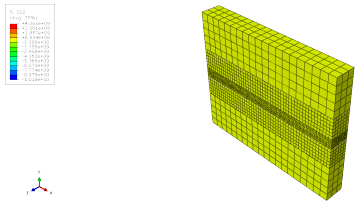

(e) 4mm Pore

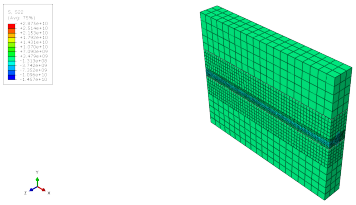

(f) 1mm pores - OXX configuration

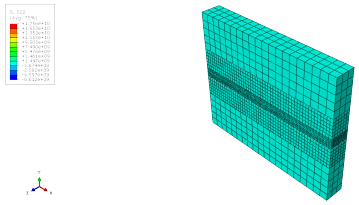

(g) 1mm pores - XXO configuration

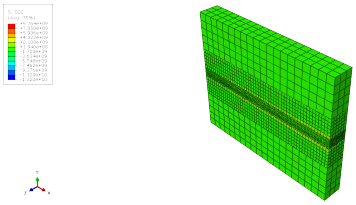

(h) 1mm pores - XOX configuration

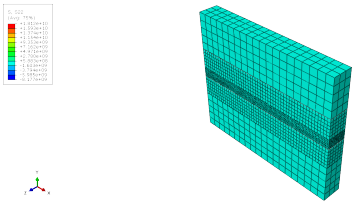

(i) 1mm pores - XXX configuration

Figure F.13: Transverse stresses, Mesh 1

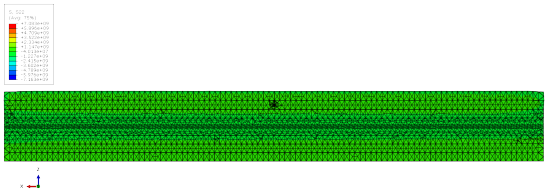

(a) 0.5mm Pore - CUT

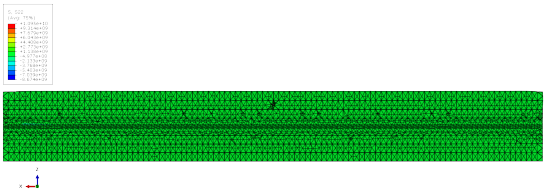

(b) 1mm Pore - CUT

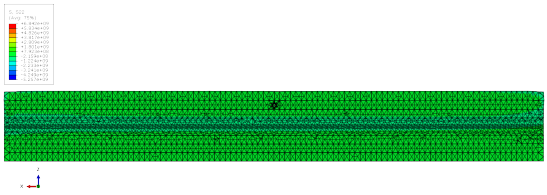

(c) 2mm Pore - CUT

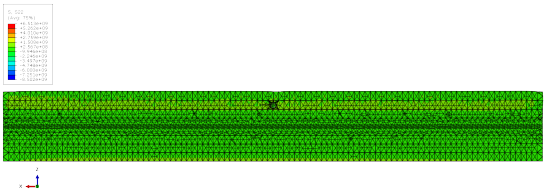

(d) 3mm Pore - CUT

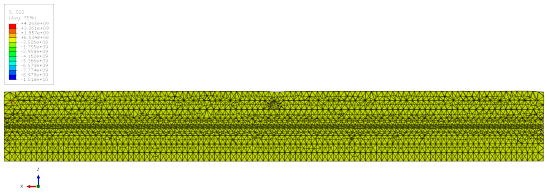

(e) 4mm Pore - CUT

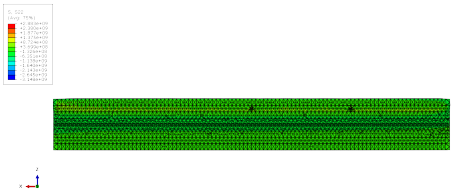

(f) 1mm pores - OXX configuration (CUT)

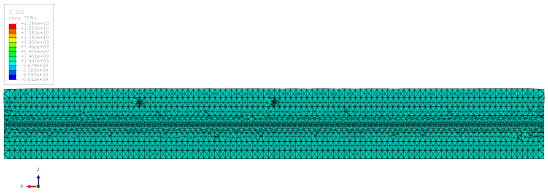

(g) 1mm pores - XXO configuration (CUT)

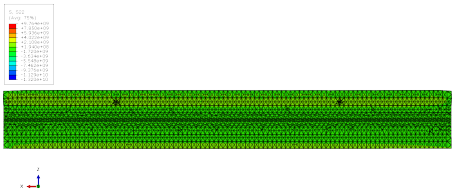

(h) 1mm pores - XOX configuration (CUT)

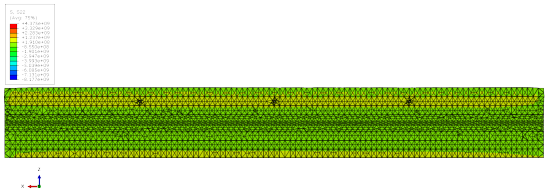

(i) 1mm pores - XXX configuration (CUT)

Figure F.14: Transverse stresses, Mesh 1 (CUT)

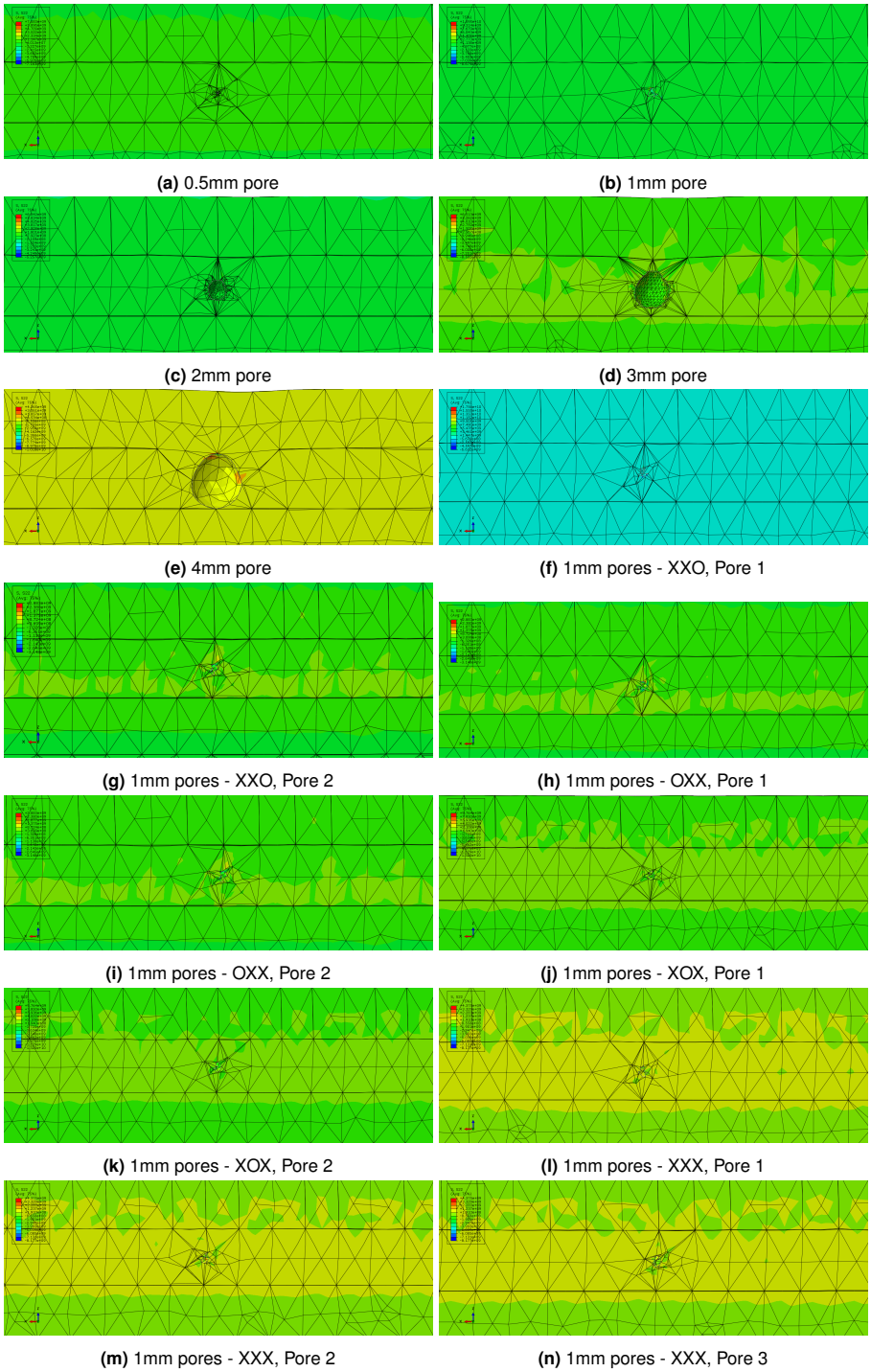

(a) 0.5mm pore **(b)** 1mm pore

(c) 2mm pore **(d)** 3mm pore

(e) 4mm pore **(f)** 1mm pores - XXO, Pore 1

(g) 1mm pores - XXO, Pore 2 **(h)** 1mm pores - OXX, Pore 1

(i) 1mm pores - OXX, Pore 2 **(j)** 1mm pores - XOX, Pore 1

(k) 1mm pores - XOX, Pore 2 **(l)** 1mm pores - XXX, Pore 1

(m) 1mm pores - XXX, Pore 2 **(n)** 1mm pores - XXX, Pore 3

Figure F.15: Transverse stresses, Mesh 1 (CUT - Zoom on the pores)

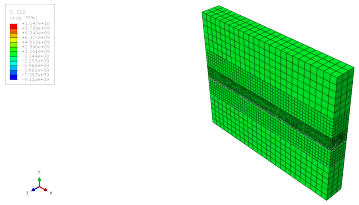

(a) 0.5mm Pore

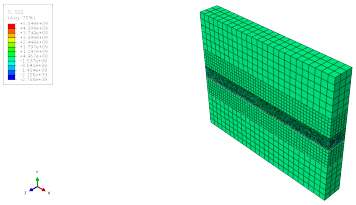

(b) 1mm Pore

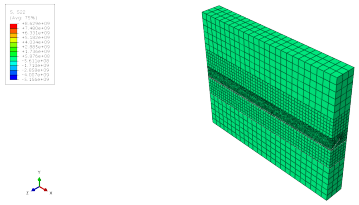

(c) 2mm Pore

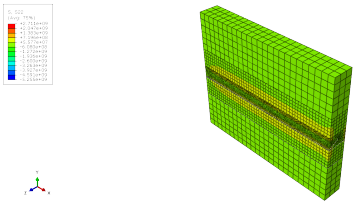

(d) 3mm Pore

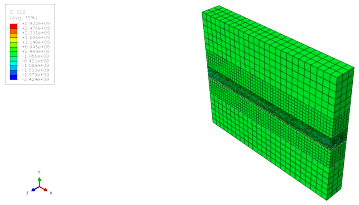

(e) 4mm Pore

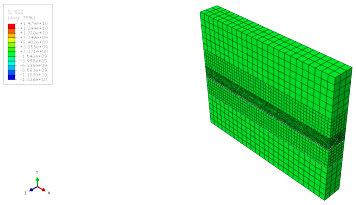

(f) 1mm pores - OXX configuration

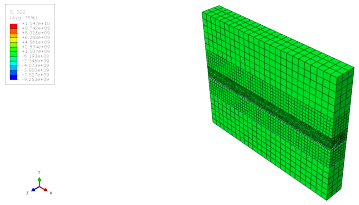

(g) 1mm pores - XXO configuration

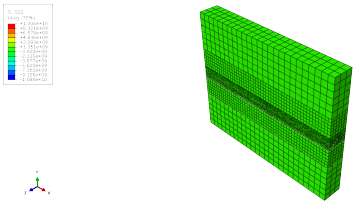

(h) 1mm pores - XOX configuration

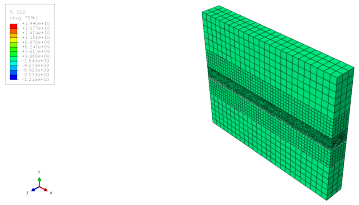

(i) 1mm pores - XXX configuration

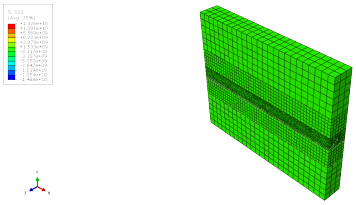

(j) 1mm pores - XXXXX configuration

Figure F.16: Transverse stresses, Mesh 2

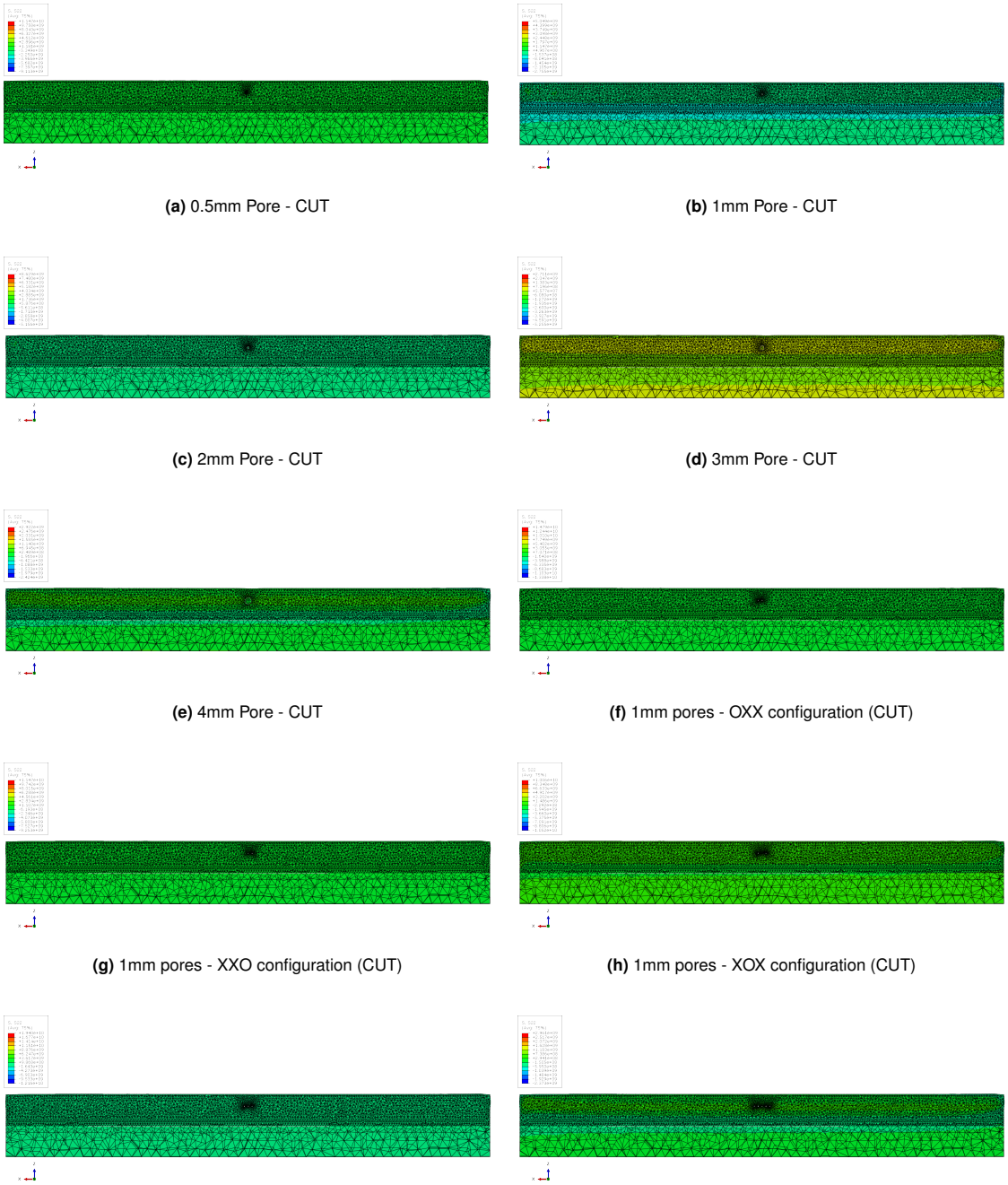

(a) 0.5mm Pore - CUT

(b) 1mm Pore - CUT

(c) 2mm Pore - CUT

(d) 3mm Pore - CUT

(e) 4mm Pore - CUT

(f) 1mm pores - OXX configuration (CUT)

(g) 1mm pores - XXO configuration (CUT)

(h) 1mm pores - XOX configuration (CUT)

(i) 1mm pores - XXX configuration (CUT)

(j) 1mm pores - XXXXX configuration (CUT)

Figure F.17: Transverse stresses, Mesh 2 (CUT)

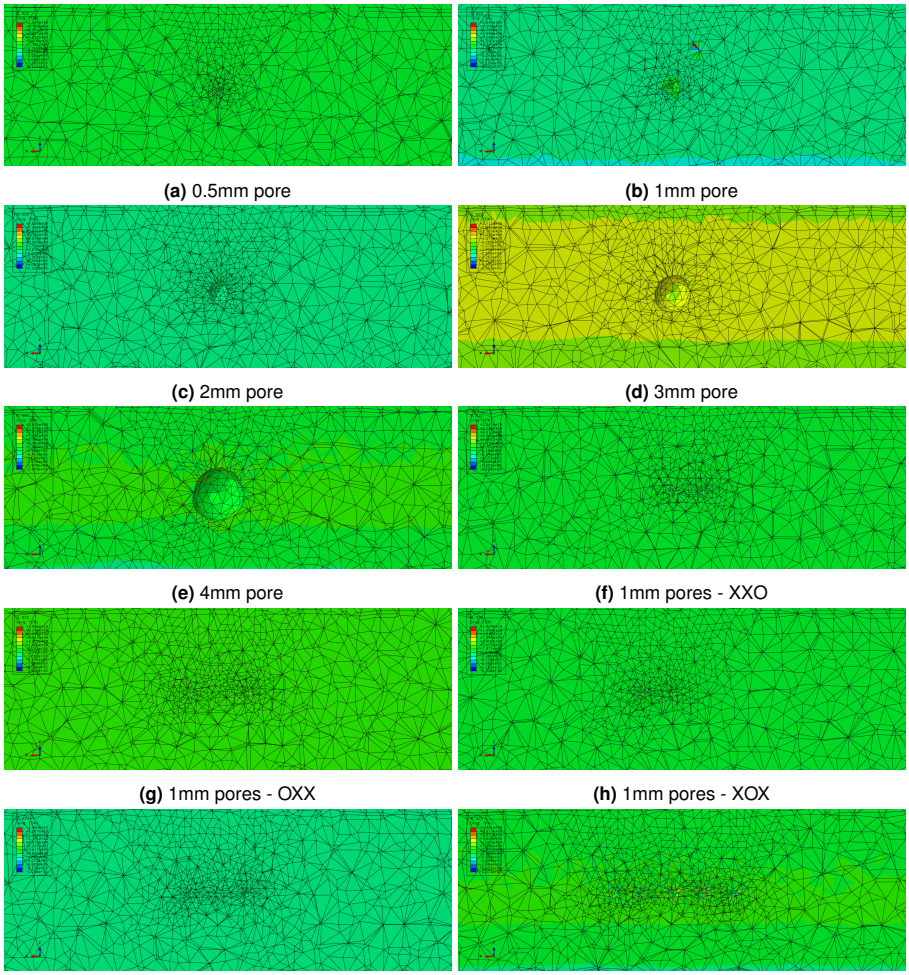

(a) 0.5mm pore **(b)** 1mm pore

(c) 2mm pore **(d)** 3mm pore

(e) 4mm pore **(f)** 1mm pores - XXO

(g) 1mm pores - OXX **(h)** 1mm pores - XOX

(i) 1mm pores - XXX **(j)** 1mm pores - XXXXX

Figure F.18: Transverse stresses, Mesh 2 (CUT - Zoom on the pores)